NASA Contractor Report 4006

Large Deformation Dynamic Bending of Composite Beams

E. J. Derian and M. W. Hyer

FOR REFERENCE

_____

NASA

NASA Contractor Report 4006

Large Deformation Dynamic Bending of Composite Beams

E. J. Derian and M. W. Hyer

Virginia Polytechnic Institute and State University
Blacksburg, Virginia

NASA

National Aeronautics
and Space Administration

Scientific and Technical
Information Branch

1986

This Page Intentionally Left Blank

SUMMARY

Studies were conducted on the large deformation response of composite beams subjected to a dynamic axial load. The beams were loaded with a moderate eccentricity to promote bending. The study was primarily experimental but some finite element results were obtained. Both the deformation and the failure of the beams were of interest. The static response of the beams was also studied to determine potential differences between the static and dynamic failure. Twelve different laminate types were tested. The beams tested were 23 in. by 2 in. and generally 30 plies thick. The beams were loaded dynamically with a gravity-driven impactor traveling at 19.6 ft./sec. and quasi-static tests were conducted on identical beams in a displacement controlled manner. For laminates of practical interest, the failure modes under static and dynamic loadings were identical. Failure in most of the laminate types occurred in a single event involving 40% to 50% of the plies. However, failure in laminates with 30° or 15° off-axis plies occurred in several events. All laminates exhibited bimodular elastic properties. The compressive flexural moduli in some laminates was measured to be 1/2 the tensile flexural modulus. No simple relationship could be found among the measured ultimate failure strains of the different laminate types. Using empirically determined flexural properties, a finite element analysis was reasonably accurate in predicting the static and dynamic deformation response.

This Page Intentionally Left Blank

TABLE OF CONTENTS

TABLE OF CONTENTS (continued)

TABLE OF CONTENTS (continued)

LIST OF TABLES

LIST OF FIGURES

LIST OF FIGURES (continued)

Chapter 1

INTRODUCTION

Fiber reinforced plastic composite materials have seen increased use in the aircraft industry in the past decade. These materials have found many applications in secondary and primary structures of military aircraft. Currently their use on commercial transport aircraft is limited to secondary structures. However, the use of composites in the primary structural design can significantly reduce the weight and improve the fuel efficiency of an aircraft. So it is likely that composite materials will see increase usage in the primary structural design of future commercial transport aircraft.

Much of the research in composite materials has been in determining the structural response and fatigue life under in-flight conditions. With commercial air transport an additional concern must be addressed. This additional concern is crashworthiness. Crashworthiness is concerned with preserving the well-being of the crew and passengers during crashes. The crashworthiness of a structure involves many issues. Fuel containment, seat design, peak deceleration, preservation of occupant space, body motion restraint, flammability, and smoke toxicity are just a few (ref. 1). However the main requirements of a crashworthiness structure are to maintain a protective shell for the occupants and to reduce their peak decelerations (ref. 2). Since crashworthiness deals with potentially survivable crashes, the impact velocities considered are relatively small (less than 40 ft/s). With impact velocities greater than this, the chances of surviving are

1

minimal.

Because of elastic-plastic behavior, aluminum absorbs energy when it yields and fails. On the other hand, fiber reinforced plastics fail in a brittle manner, thus, in general, reinforced plastics have less capacity to absorb energy. However, the total energy absorbed by the structure is not necessarily the crucial factor for crashworthiness. Crashworthiness is concerned with designing failure processes that maintain a constant load as a function of deformation during the impact event. The constant load minimizes decelerations, yet absorbs energy in a steady and progressive fashion (ref. 1). Much of the crashworthiness research of composite materials to date has been on testing the energy absorption capabilities of axially crushed tubes and specially designed honeycomb structures. It has been found that by changing the fiber orientations, material systems, and the structural geometry, the stability of the collapse can be controlled. Consequently the energy absorption can be significantly increased with a stable collapse. These tests give useful indications of the energy absorbing capacity for crushable parts of a structure. However, it is not entirely clear at this point in the development of composite structures that special crushable structures are necessary on all aircraft to meet crashworthiness criteria. Before designing special crushable structures it is necessary to know how a composite fuselage, designed for structural efficiency under in-flight conditions, will respond to crash loadings. Will the deceleration of the occupants be severe enough to cause death or injury? Will the integrity of the seat area be maintained? Will fuel leakage be a major problem? What, in general,

will be the dynamic response of a composite aircraft to crash conditions? Of course the dynamic response of a fuselage will vary greatly, depending on the attitude and the velocity of the airplane upon impact, and by changing the structural configuration of the fuselage. One way of understanding and predicting the response of the fuselage under the many ways a survivable crash could occur would be to perform large deformation dynamic analysis using a nonlinear finite element program. However, little is known about the load-deformation behavior of composite materials under dynamic loading and large deformations. Therefore, some of the basic input information for such an analysis is not available.

Very little research has been done on the large deformation response and failure of laminated composite structural elements, whether static or dynamic, let alone full composite structural assemblies. Understanding the response of simple structural elements is essential to being able to perform successful crash analyses of a complete composite fuselage. It is certainly the least expensive way to approach the problem, both experimentally and computationally.

Full scale aluminum fuselage sections of transport aircraft (Boeing 707) have been vertically drop-tested (refs. 3 and 4). The correlation of test data and the finite-element model was quite good for the global deformations and the decelerations. From the results of these studies, it appears that the large deformation dynamic bending response of aluminum structural elements is well understood. In addition, the vertical drop tests show that the majority of energy absorbed during a crash test is due to bending failure of skin, stiffeners and stringers

(ref. 5). Little or no energy is absorbed by the stable progressive crushing of components.

In this spirit, then, this study investigated the large deformation bending response of composite beams with a rectangular cross section. These beams could have represented the fuselage skin, or stiffener flange, or stiffener cap. The beams were loaded dynamically in bending to simulate the situations observed in the crash testing of aluminum fuselage sections. This study is considered to be a first step in understanding the dynamic response of composite structures. The overall goals of the study were to:

1. Design a simple test fixture to introduce crash-related bending loads in beams.

2. Determine any difference between large deformation static and large deformation dynamic response. Specific interest is in the failure mode.

3. Determine the influence of laminate stacking arrangements on the dynamic response and failure mode.

4. Predict the static and dynamic response, using an existing finite element program.

The majority of the effort in this study was experimental. To successfully simulate large deformations and failure under crash related loads, a suitable test fixture was designed and built. The fixture was built around the concept of a drop tower. The fixture is discussed in Ch. 2. Next, to determine the effects of dynamics on the large deformation response, the static response had to be understood, or at least observed. So, before any dynamic testing was done, three beams of a given laminate type were tested under quasi-static loads. The load, deflection, strain, and failure response were observed.

To determine the effect of laminate type on the response, twelve different laminate types were tested. After the static tests were completed, three more beams of each laminate type were tested dynamically. The results of the static and dynamic experiments are presented in Ch. 3. The differences in the dynamic and static tests, and the differences in the response and failure modes between the different laminate types are reported. An unexpected result in the surface strain response of the laminates was observed. Accordingly additional tests were conducted. In Ch. 4, this test procedure is presented and the results are reviewed to verify and further understand the phenomena.

Methods for predicting the response of the beams are explored in Chs. 5 and 6. Predicting the response of the beam involves both predicting the on-set of failure and predicting the global deformations to the applied load history. The strains at first failure in each laminate and the success of a strain-related failure criteria at predicting these failures are examined in Ch. 5. An existing finite element program was used in Ch. 6 to determine the success of predicting the deformation response of the composite beams. The predicted time histories of force and displacement response are presented and compared with experiment, as are the static and dynamic load-displacement response. In addition the spatial shapes of the dynamic response is presented at various times after impact. Finally, Ch. 7 presents conclusions and recommendations for further study.

Chapter 2

EXPERIMENTAL SET-UP AND PROCEDURE

The basic loading configuration used in the study is shown in fig. 2.1. The beam was loaded in a column fashion with a moderate amount of eccentricity to promote bending. The beams were oriented vertically as shown. The lower end of the beam did not move while the upper end moved vertically. A hinge on each end allowed free rotation of the beam ends. The static tests were conducted in a displacement controlled manner in a standard screw driven load frame. The dynamic tests were conducted in a specially designed drop tower and the dynamic loading, denoted by F(t) in fig. 2.1, was provided by a gravity driven impactor. In the unloaded position the hinge supports were 24.2 in. apart. The specimens were 23 in. long by 2 in. wide and generally 30 plies thick. At each end 1.5 in. of the specimen was clamped in the hinge, leaving the unsupported length of the beam at 20 in. In both the static and dynamic tests the deflection of the upper end of the beam was limited to 16 in. by a bumper. This limit on deflection was imposed so there would not be damage to the test fixture or related instrumentation due to the metal hinges impacting each other.

A 4 point bending configuration was originally considered. However, the eccentrically loaded column configuration was used instead. The primary reason was that to successfully model crash conditions, large deformations must be introduced into the beams. For large lateral deformations there are considerable axial deformations as well. With a 4-point loading system, the beam could easily deform to
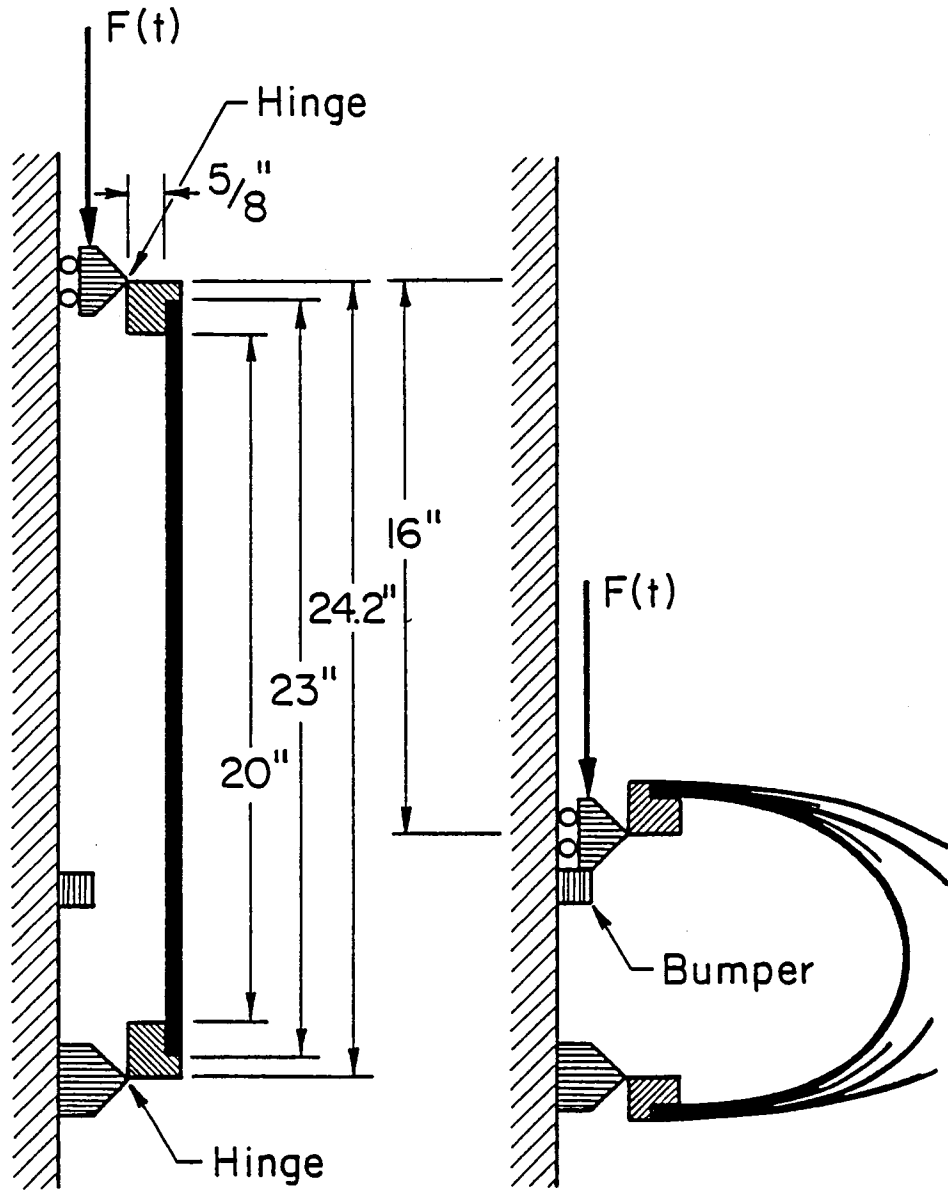
Figure 2.1   Basic Load Configuration

such an extent that it would slip through the supports without failure, as shown in fig. 2.2. With the eccentrically loaded column the beam deflections were limited only by the ends of the beam touching. In addition, with the 4-point loading systems the beam ends move relative to the simple supports. As the beam moves over the support, considerable friction forces can be generated. These forces are difficult to model analytically. On the other hand the eccentrically loaded column's simple support moves with the beam end. In this case the support can be attached to a low-friction linear bearing.

Another draw back of the 4-point loading system is that it can cause failure at the supports. With a four point bending configuration the supports impact on the surface of the beam in the regions of maximum bending moment. The impact can cause local damage and initiate failure. With the eccentrically loaded column the two support points are on the ends of the beams, regions of minimum bending moment. Consequently, failure always initiates at the center of the beam away from the end. With failure occurring in the center, the complicating effects of stress concentrations at the supports are not present.

2.1 Beam Specimens

Table 2.1 shows the lay-up and number of plies for each of the laminate types tested. The laminates were fabricated by the NASA-Langley Research Center using AS4/3502 graphite-epoxy pre-preg tape. For each laminate a 24 x 24 in. panel was fabricated. After curing, the panels were C-scanned to determine if any defects were present. Then, ten 2 x 23 in. beams were cut from each panel. Throughout this report
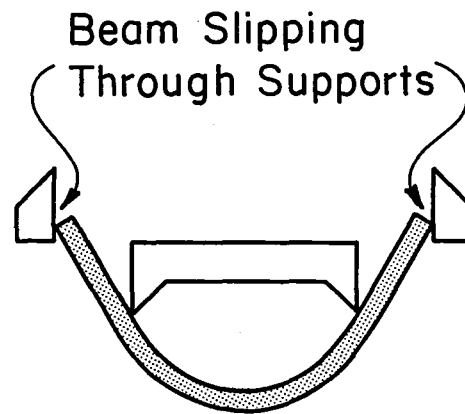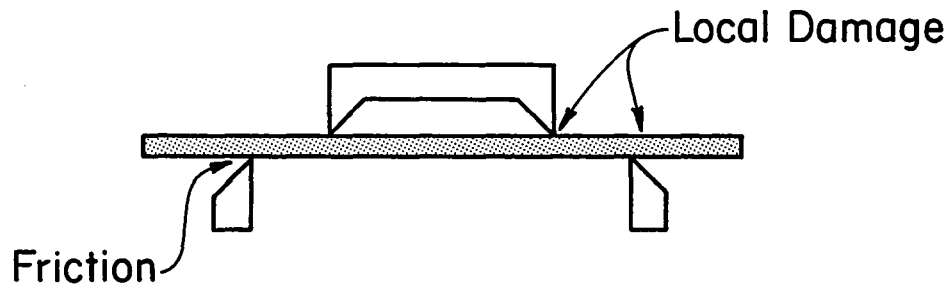
Figure 2.2   A Possible 4-Point Loading Arrangement

TABLE 2.1
SPECIMEN LAMINATE ORIENTATION

LAMINATE NUMBER	LAY-UP	NUMBER OF PLIES	IMPACTOR WEIGHT (LBS)
1	$[0]_{30}$	30	48.6
2	$[(15/0/-15)_5]_s$	30	36.1
3	$[(30/0/-30)_5]_s$	30	24.5
4	$[(45/0/-45)_5]_s$	30	24.5
5	$[(60/0/-60)_5]_s$	30	24.5
6	$[(75/0/-75)_5]_s$	30	24.5
7	$[(90/0/-90)_5]_s$	30	24.5
8	$[(0/90)_8]_s$	32	36.1
9	$[(0_8/90_8]_s$	32	36.1
10	$[(90_8/0_8]_s$	32	36.1
11	$[(45/-45/0/90)_4]_s$	32	24.5
12	$[(0/45/0/-45)_3/90/0/0_{1/2}]_s$	29	36.1

each beam specimen will be referred to by its designated number, e.g., specimen 2.1. The whole number portion refers to the laminate type, and the decimal portion refers to the particular beam cut from the panel. For example, specimen 2.1 is beam no. 1 cut from the $[(15/0/-15)_5]_s$ panel.

The laminate types were separated into three groups for study. In the first group, numbers 1 through 7, the laminates were all of the $[(\theta/0/-\theta)_5]_s$ family. The angle θ increased from 0° to 90° in steps of 15° to study the effect of increasing the angle of the off-axis laminae. The second group, numbers 8, 9 and 10, were orthotropic laminates which all had the same inplane stiffness. The plies were stacked differently to study the effect of clustering on the failure modes and response. In the final group, numbers 11 and 12, were laminates which, according to current design philosophies, might be found on a fuselage. Laminate 11 is a quasi-isotropic lay-up and laminate 12 had 52% 0's, 41% 45's and 7% 90's. Laminate 12 is much more orthrotropic than laminate 11.

2.2 Dynamic Test Fixture

Figure 2.3 shows a drawing of the drop tower fixture used for the dynamic testing. Two 10 ft. long vertically oriented hardened steel rods 1 in. in diameter spread 6 in. apart were fastened to C channels on either end. The channels were fixed to the floor and ceiling of the room used for testing. The slider, which supported the upper end of the composite beam, and the mass car, which provided the impact force, slid down the rods on low-friction linear bearings. The composite beam
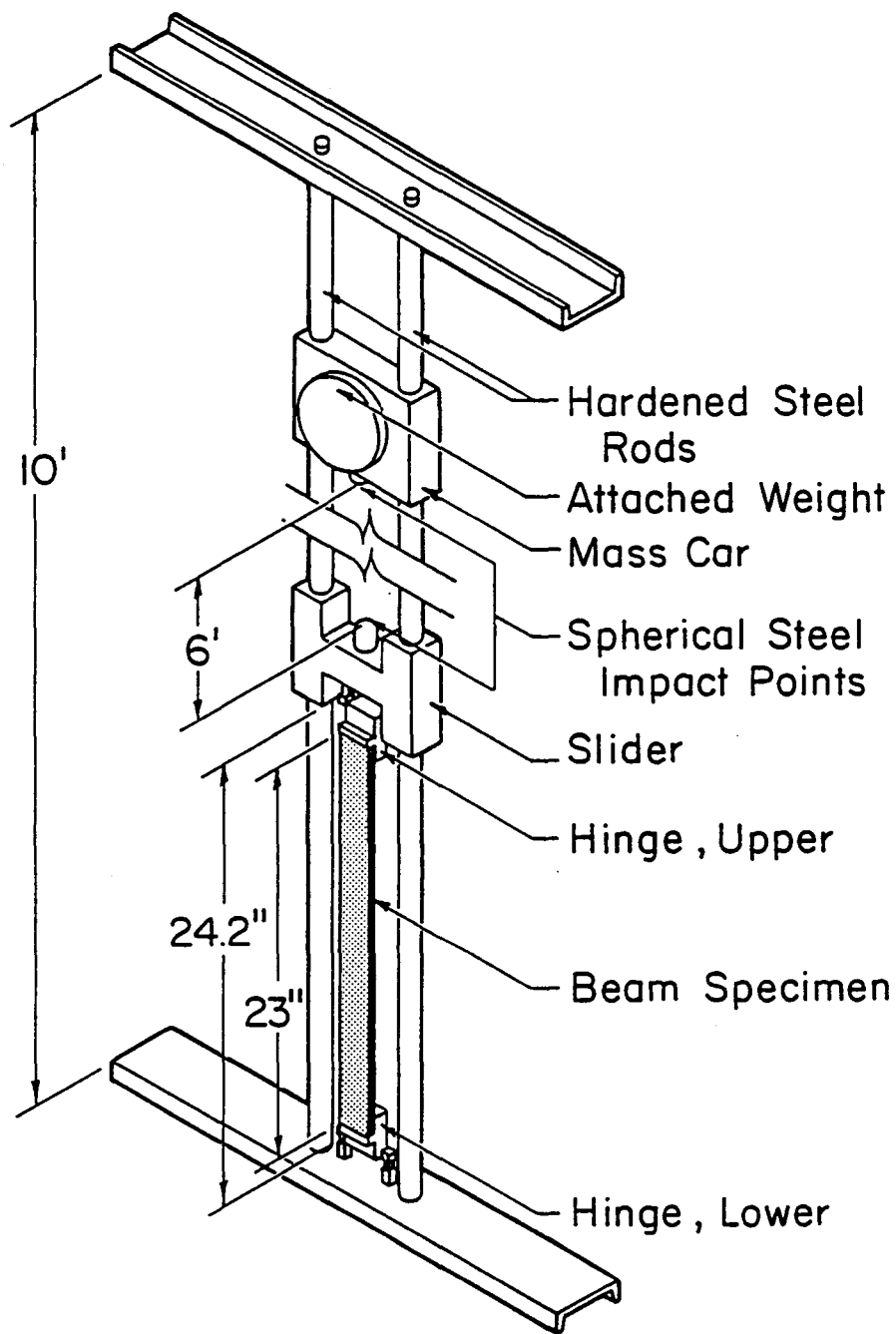
Figure 2.3   Schematic of Drop Tower

specimen was clamped to the top and bottom hinges which provided the simple supports. Figure 2.4 shows a detail drawing of the upper hinge. As shown in fig. 2.4, the rear surface of the specimen was offset 5/8 in. from the hinge pivot, or pin, which was in the plane of the vertical hardened steel rods. This offset provided the eccentricity which promoted the bending. The top hinge was attached to the slider whereas the bottom hinge, which was identical to the top one, was attached to the lower C channel. Weights were fastened to the mass car. The car was raised 6 ft. above the spherical steel impact point on the slider. A solenoid-activated release mechanism released the mass car. The mass car impacted the slider at 19.6 ft/s. As the slider and the mass car combination move downward, the specimen deflected axially and laterally. Figures 2.5 and 2.6 are photographs of the apparatus and instrumentation.

2.3 Static Test Fixture

To conduct the static tests, the top and bottom hinges from the dynamic test apparatus were attached to the heads of an Instron load frame. Figure 2.7 shows specimen 2.1 partially deflected and failed in the static test fixture. Again, the beam was clamped to the hinges and offset from the pivot points by 5/8 in. As can be seen in fig. 2.7, the hinges rotated with the ends of the beam. In the load frame the top hinge was attached to the load cell and was stationary. The bottom hinge was attached to the moving crosshead.

Force
Transducer

5/8"

Force
Transducer

Hinge
Pin

Beam Specimen

2"
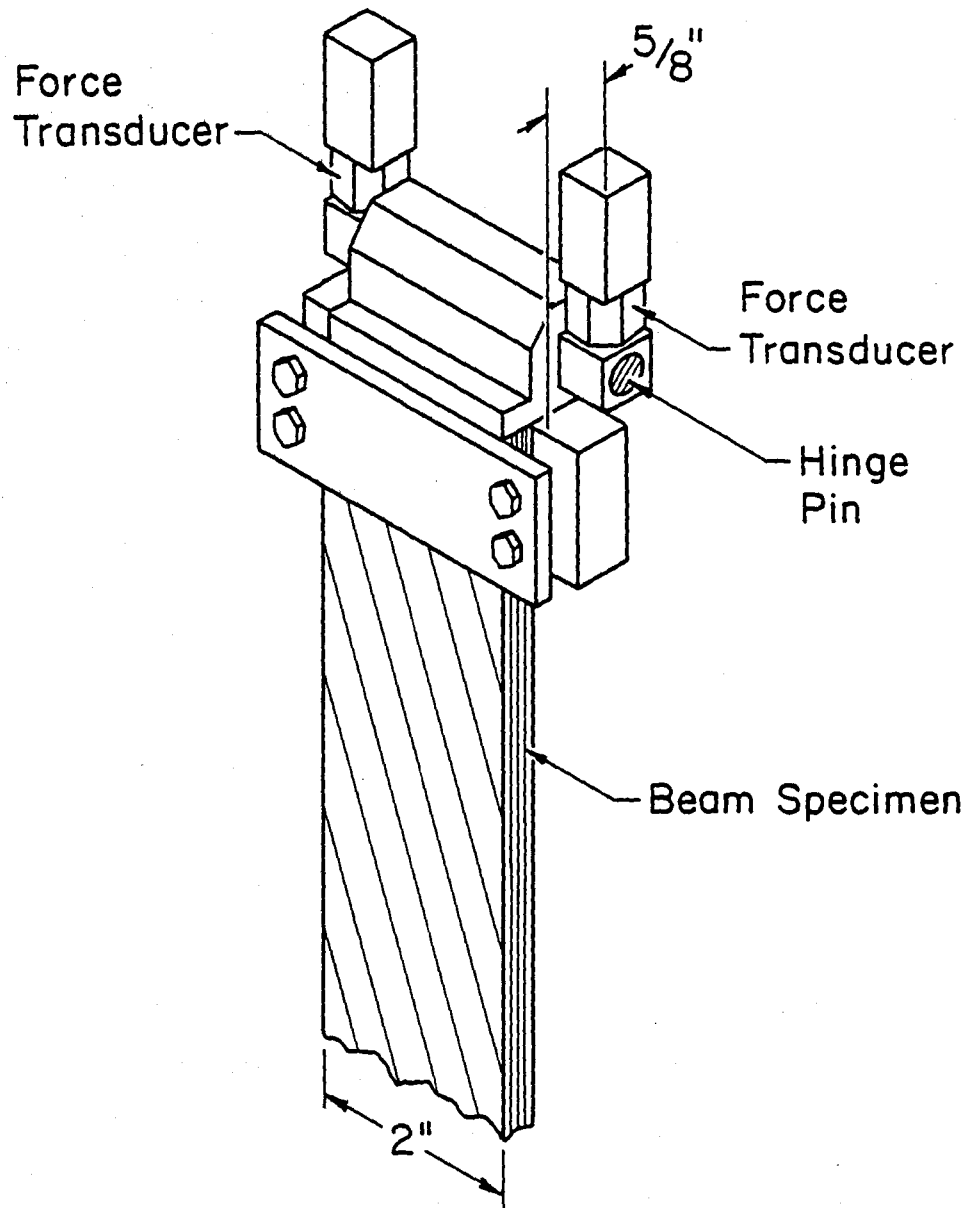
Figure 2.4   Schematic of Upper Hinge
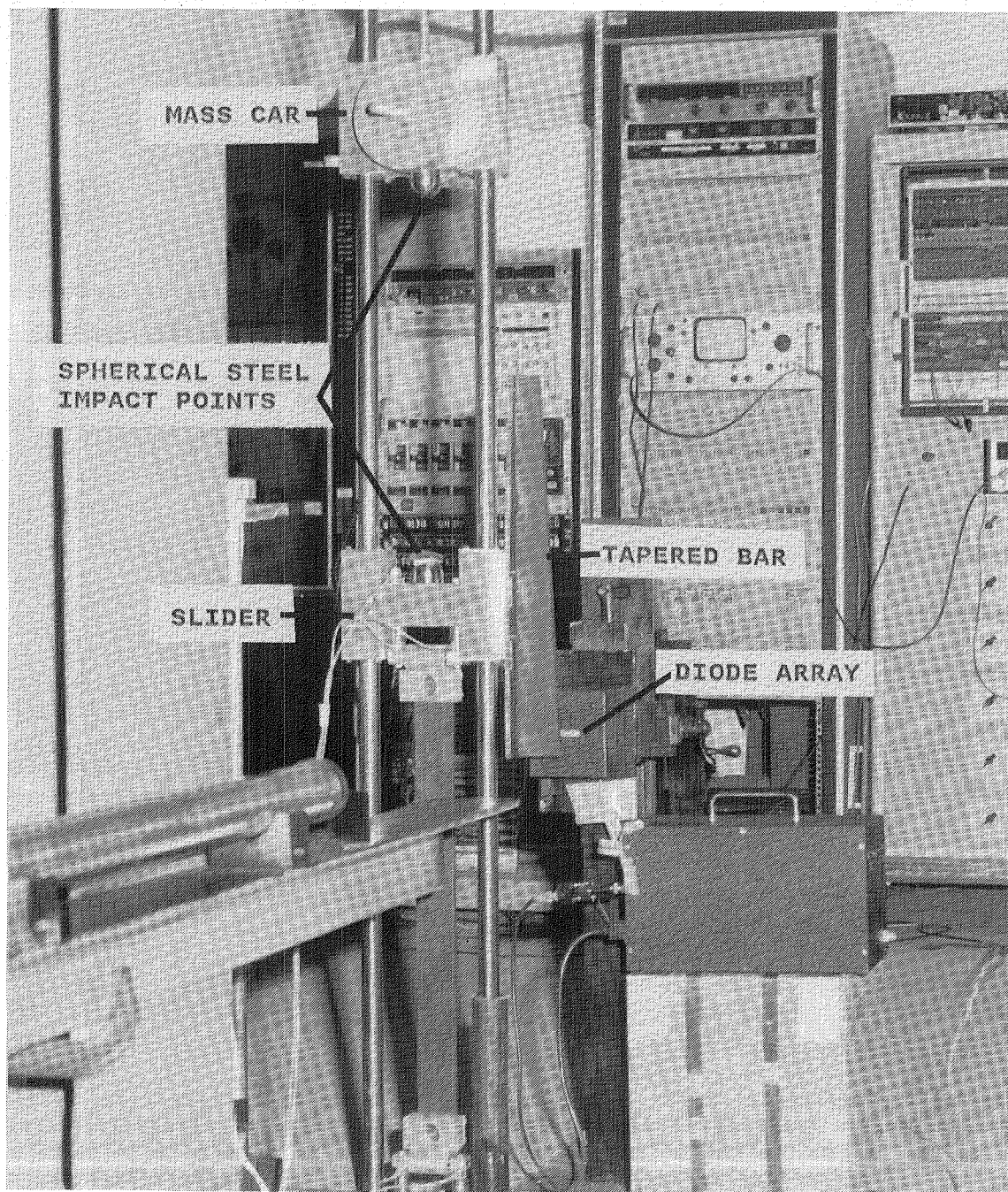
Figure 2.5   Photograph of Drop Tower
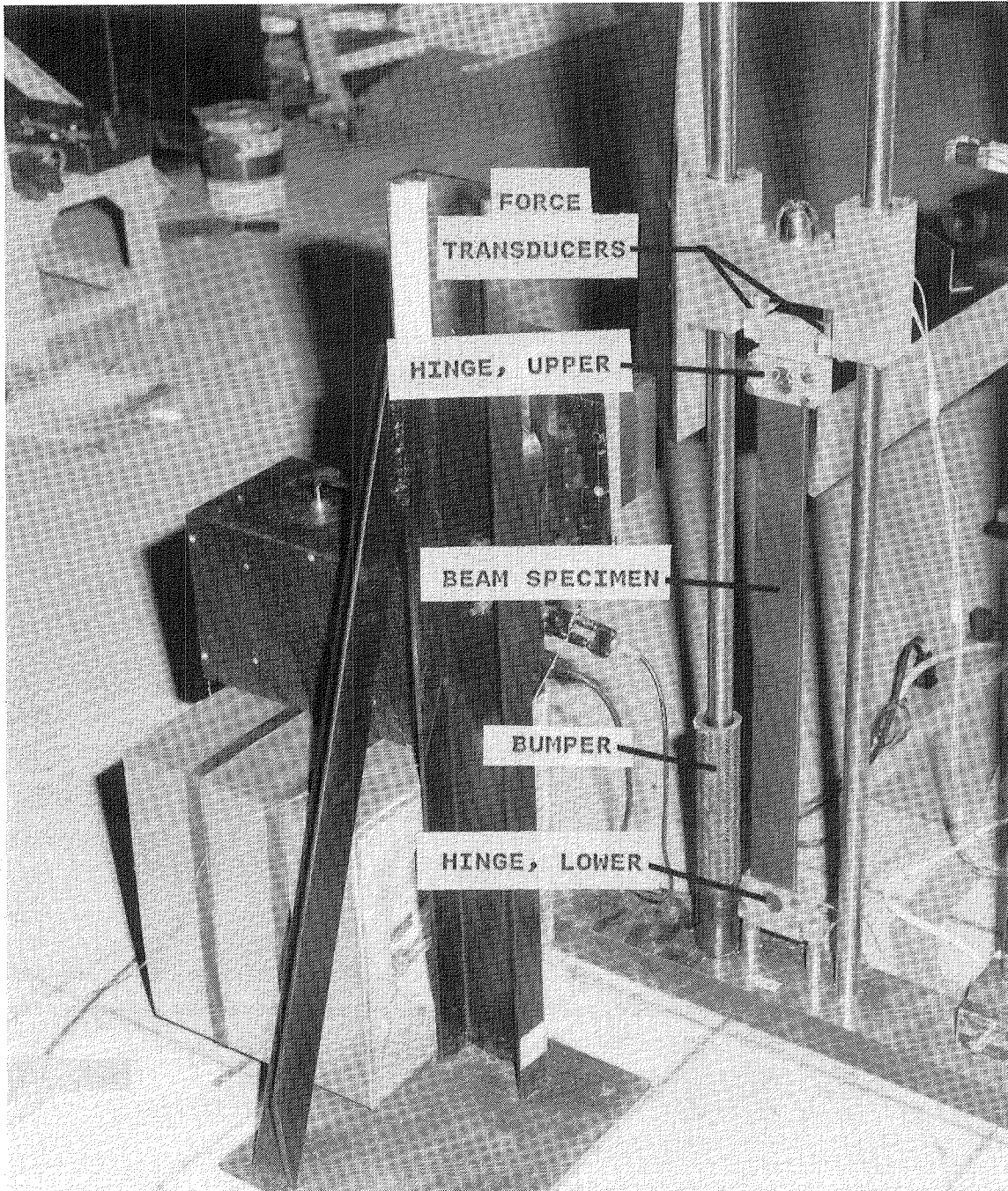
Figure 2.6   Photograph of Beam Holder
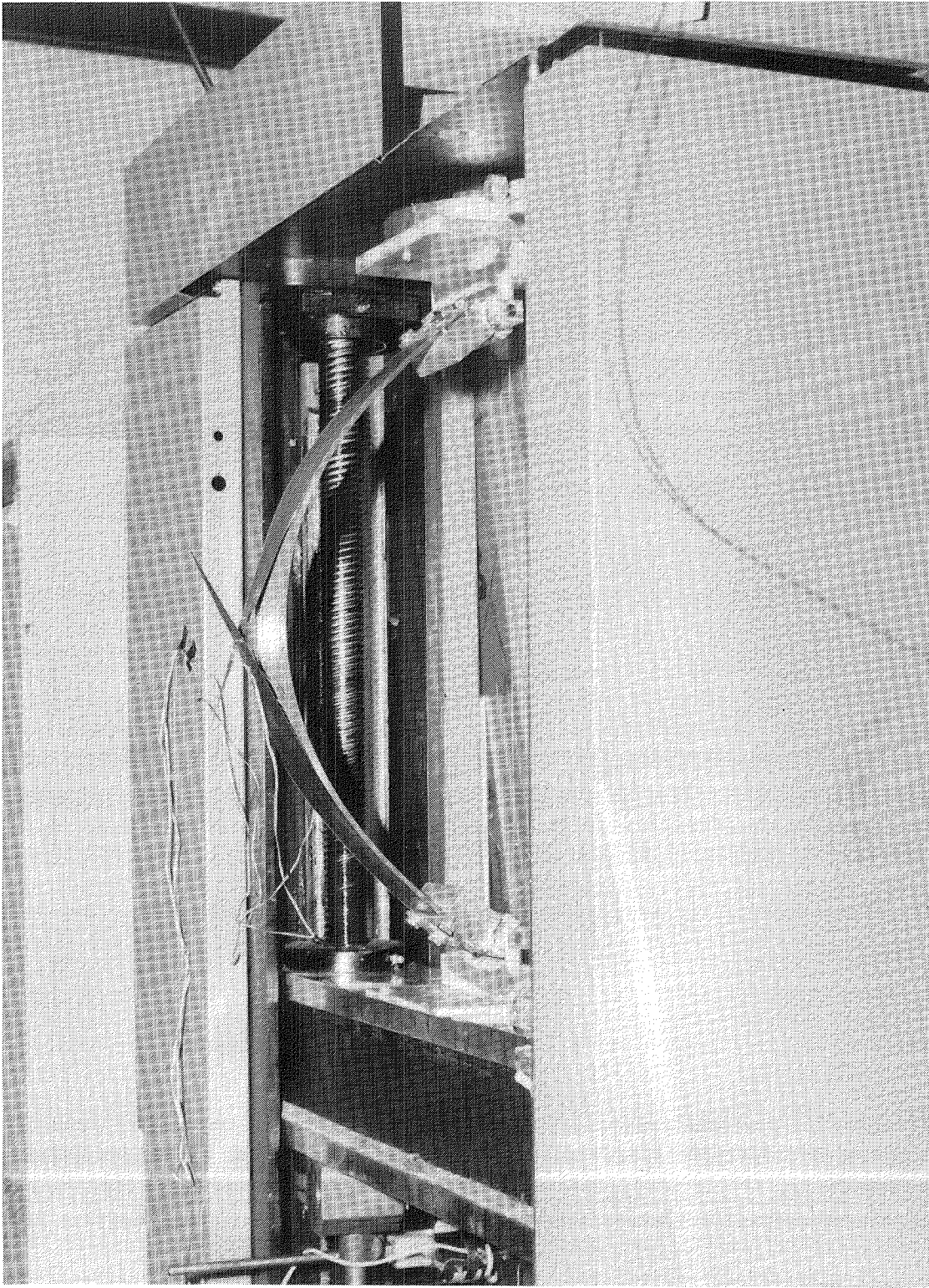
Figure 2.7   Photograph of Static Test Fixture

2.4 Data Aquisition

For both the static and dynamic tests, end load, end displacement, and surface strains at the center of the beam were recorded. The strains measured bending and axial compressive effects in the beam. Poisson strains were not measured. The manner in which these measurements were recorded differed in the static and dynamic tests. In addition to these measurements, for the dynamic tests high speed motion pictures of the edge view of the laminate were taken to record the overall deformations and the failure modes.

2.2.1 Static Tests

In the static tests the end axial load (F(t) in fig. 2.1) was measured using a 1000 pound load cell. The end axial displacement was measured and controlled with the crosshead speed which was set at 5 in. per min. The load - end displacement relation was recorded using the chart recorder. Back-to-back strain gauges measured the surface strains at the center of the beam and the signals were conditioned using amplifiers designed and built at the Langley Research Center. Strain-displacement relations from the two gauges were recorded using a X-Y plotter. All data were then digitized manually to facilitate data reduction.

2.2.2 Dynamic Tests

The dynamic tests were conducted at the NASA Langley Research Center's Impact Dynamics Research Facility. The data aquisition system there was designed to permit the simultaneous recording of 90 data

channels on one 28 track magnetic tape recorder using a constant bandwith FM multiplexing technique. This experiment required the use of 5 data channels. The channels were: two loads, two strains, and one displacement.

For the dynamic loading, the axial end load was measured by the two piezoelectric force transducers shown in fig. 2.4. The transducers were connected in parallel and placed on both ends of the hinge pin. This arrangement measured the sum of the slider forces acting on both ends of the hinge pin and therefore the total axial force time history at the upper end of the beam. An identical set of transducers were placed on the bottom hinge. The signals from the transducers were conditioned by charge amplifiers. These amplifiers produced analog signals that were recorded by the FM system. Again, two strain gauges were placed back-to-back on the center of the beam specimen. These signals were conditioned by amplifiers designed and built by Langley Research Center, but different from the ones used in the static tests.

The beam end displacement was measured by an optical displacement transducer. The optical device did not require any mechanical linkage fastened to the slider. The transducer was designed and built by Langley Research Center. The transducer worked as shown in fig. 2.8. A 16 in. long tapered bar was fastened to the slider. The outside edge of the bar tapered from a 1 in. width at the top to a 2 in. width at the bottom. A laser beam, which was diffracted into a horizontal line of light, shined on the front of the bar. Directly behind the tapered bar, a one-inch long array of 1024 light sensitive diodes was mounted horizontally. When the specimen was in the fully upright undeflected

Slider

Tapered
Bar

16"

Diode
Array

Beam
Diffracter

Laser
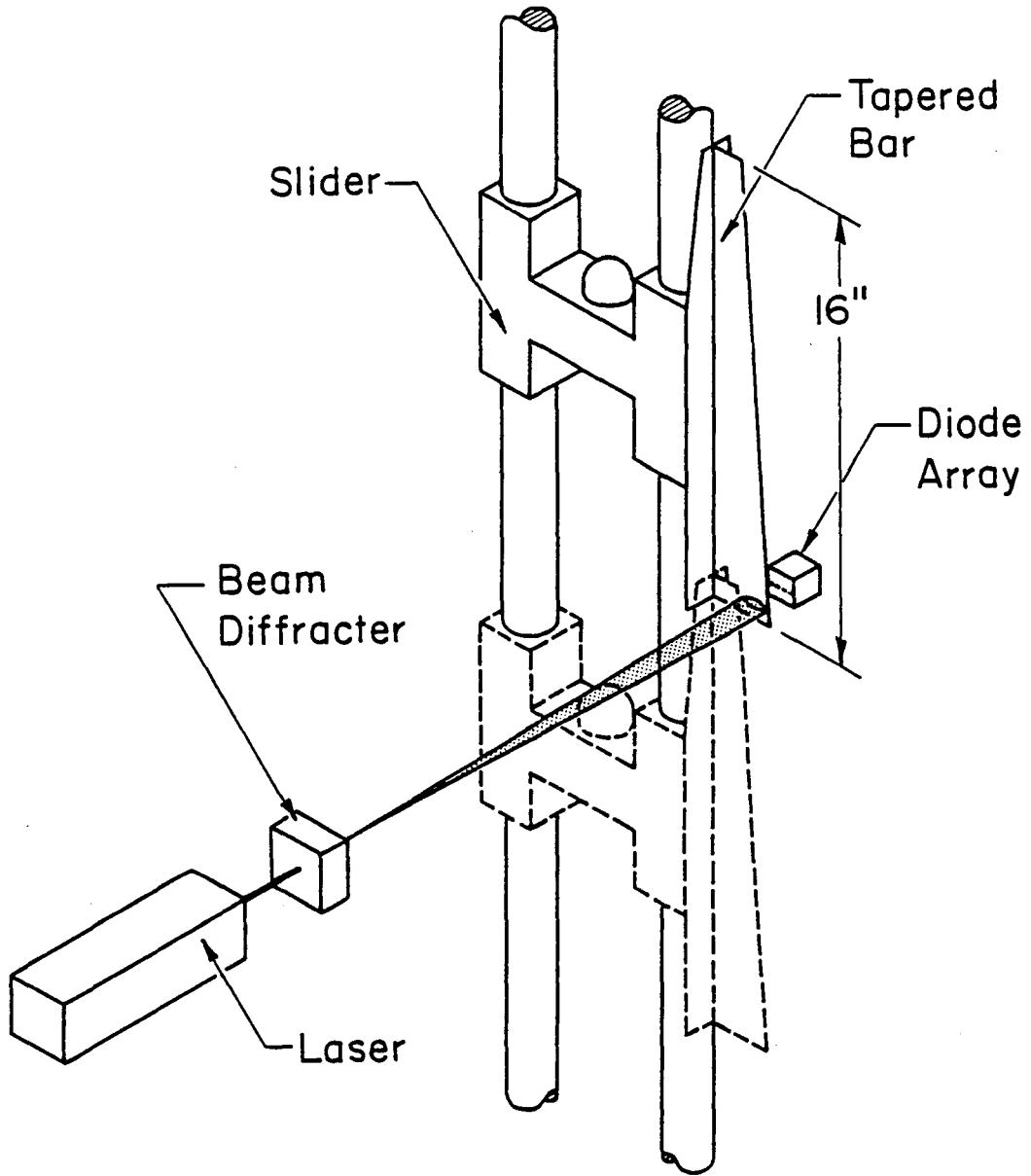
Figure 2.8   Schematic of Optical Displacement Transducer

position, the bottom of the tapered bar fully shadowed the diode array. As the top of the specimen deflected downward, more and more of the diodes became exposed to the light. When the specimen traveled its full 16 in. of axial displacement, the entire array was exposed to the laser light. An electronic circuit counted the number of diodes exposed to the laser light. The counter generated an analog signal proportional to the number of the activated diodes. With proper calibration, the optical transducer provided a signal proportional to the vertical end displacement of the beam.

As mentioned previously there were five time histories recorded during the dynamic event. These five dynamic signals were filtered at 1-KHz to remove spurious noise. The filtered signals were connected to voltage-controlled oscillators where they were converted into descrete FM signals. The FM signals were then recorded on magnetic tape. After the testing was completed the magnetic tape was played back through the voltage-controlled oscillators and the resulting analog signal was digitized at 4000 samples per second.

In addition to the digital data, a high speed movie camera was used to record an edge view of the laminate as it deformed and failed during the dynamic event. The edge of the laminate was painted white to facilitate viewing. The 16mm camera was set up to take 400 frames/sec. Movies were made for at least two specimens from each laminate type.

2.5 Initial Measurements

Some initial measurements were taken of the geometry of the beam

specimens. The results are shown in Table 2.2. From each laminate type the dimensions of 3 beam specimens were measured and then averaged. The length and width were measured to assure each was as specified. The thickness of each specimen was measured at the center and at each end of the beam with a micrometer. As can be seen, there was a variation in the thickness with length. The effect of the uncertainty in the thickness measurement on the response of the beams is examined in Appendix A. The beams were next placed on a flat surface and the camber, or deviation from prefect straightness, was measured with a ruler to determine the initial eccentricities in the beams. The eccentricity would add or subtract to the built-in 5/8" eccentricity of the test fixture. However, the initial eccentricities in the beams could not be measured with absolute certainty. The effect of the uncertainty in the eccentricity measurement is examined in Appendix B. Finally the beams were weighed. By knowing the Areal weight of the prepreg and the final weight of the beam, a good estimate of the fiber volume fraction could be made. As can be seen, the fiber volume fractions were within expectations. It should be mentioned that no tests were conducted on laminate 6.

TABLE 2.2
MEASURED SPECIMEN GEOMETRY

LAMINATE NUMBER	WIDTH	LENGTH	AVERAGE THICKNESS (in) ±0.002"			CAMBER ± 0.01" (in)	FIBER VOLUME FRACTION %
			TOP	MID	BOT		
1	2.00	23.00	0.162	0.168	0.162	0.03	69.8
2	2.00	23.00	0.162	0.165	0.162	0.02	69.2
3	2.00	23.00	0.158	0.160	0.159	0.02	69.6
4	2.00	23.00	0.160	0.165	0.106	0.02	69.7
5	2.00	23.00	0.160	0.167	0.160	0.04	69.6
6*	2.00	23.00	--	--	--	--	--
7	2.00	23.00	0.164	0.165	0.163	0.04	69.8
8	2.00	23.00	0.174	0.175	0.175	0.01	68.2
9	2.00	23.00	0.175	0.177	0.176	0.01	68.2
10	2.00	23.00	0.174	0.175	0.174	0.01	68.5
11	2.00	23.00	0.178	0.180	0.178	0.07	69.1
12	2.00	23.00	0.154	0.158	0.155	0.06	71.2

*not tested

2.6 Test Procedures

2.6.1 Static tests

Three specimens of each laminate panel were tested statically to failure. Three were chosen simply to determine the scatter in the data, particularly the failure data. The static test procedure was somewhat unique and is discussed here. First the load frame loadcell was calibrated. Next, the specimen was placed in the fixture such that the initial camber in the beams increased the load eccentricity. Then the load cell was zeroed, the strain gauges were connected to the amplifiers, and the amplifiers were balanced. The crosshead speed was set at 5 in./min. To determine if nonvisible damage like microcracking and fiber pullout was occurring as the beam specimens deformed, the axial end displacement was applied in stages. First the end of the beam was displaced axially 2 in. At the 2 in. displacement level, the crosshead motion was reversed and the displacement of the beam end was returned to zero. Next the end of the beam was displaced axially 4 in. At the 4 in. level the crosshead motion was reversed and the end of the beam was returned to zero displacement. This procedure was repeated in 2 in. increments until finally the beam was displaced axially 16 in. and then returned to zero. If the loading and unloading load-displacement curves coincided, then, within the sensitivity of the instruments, the specimen absorbed no energy during the cycle. Conversely, if the two curves did not coincide, then the area between the loading load-displacement curve and the unloading load-displacement curve was the energy absorbed by the specimen due to the failure mechanisms in that cycle.

2.6.2 Dynamic Tests

Three more specimens of each panel were tested to failure dynamically after the static tests were complete. The 6 ft. drop height selected for all the dynamic tests provided the same velocity of the mass car prior to impact for each test. However, since the stiffnesses of the 12 different laminate types were not the same, the decelerations of the mass at the top of the beam, and thus the dynamic force levels, would vary from one laminate type to the next. It was felt that it would be important for comparing the response of the different laminate types to have the dynamic force levels and the velocities somewhat similar. To keep the velocity and force levels similar from one laminate type to the next, the impactor mass was changed for each laminate type. To determine the impactor mass for each laminate type, the work required to deflect a beam 16 in. was calculated from the static load-displacement relation. An additional 20% of energy was added which more than accounted for energy lost due to friction and during impact of the slider and mass car. From this desired impact energy value, the impactor mass was computed. The impactor mass used for each laminate is given in Table 1.

Before any tests were attempted, calibration signals, corresponding to known levels of physical quantities, were recorded on each channel to facilitate digitization. With the impactor mass in place, the specimen was clamped into the hinges and the instrumentation was connected to the recorders. Next, all the transducers were balanced and zeroed. A 10 sec. countdown procedure was used wherein at 5 sec. the FM tape

recorder was activated and at 1 sec. the movie camera was started. Finally, at time zero, the mass was released and the dynamic load, strain, and displacement histories were recorded.

Chapter 3

RESULTS

As described in the previous chapter, beam specimens of each laminate type were tested quasi-statically and dynamically. The raw data from these tests were reduced and put in a common format so that easy comparisons of the test conditions and the beam specimen response could be made. Comparisons were made between the static and dynamic tests for each laminate type. Comparisons were also made among laminate types. This chapter presents a discussion of these experimental results and related observations.

3.1 Data Reduction

3.1.1 Static Data

The raw static data were recorded in graphic form, as mentioned previously, on an X-Y recorder. The graphic data were converted into numerical data by tracing the curves on a digitizing table. Then the digital data was stored in computer files to facilitate plotting and manipulation. Load-displacement and strain-displacement relations were generated from the data to analyze the tests.

3.1.2 Dynamic Data

The raw dynamic data were recorded on FM magnetic tape. The FM signals were played back through voltage-controlled oscillators to retrieve the original analog signal. Calibration signals were used to provide the proper relations between the analog signals and the physical

quantities measured by the transducers. The analog signals were then converted to digital data at a sampling rate of 4000 points per second. The five digitized dynamic data channels from each test were then placed in a computer file. Upon initial scrutiny of all the data, both systematic and random errors in the displacement channels were found. These data were enhanced to extract usable information as explained below.

The random errors were believed to be associated with noise from the electronic circuit which produced the analog displacement signal. Figure 3.1 shows the displacement time history from specimen 1.4. Note that in the raw, or unenhanced, signal, even before the impact occurred there was considerable noise. The noise level in fig. 3.1 corresponds to axial displacement fluxuations of up to 0.4 in. With the impactor not in contact with the slider, these displacements are not possible. Therefore this portion of the signal is noise. Unfortunately, this noise persisted after the impact and distorted the displacement signal. To improve this signal, the displacement data was passed through a digital filter. The filter used was a nonrecursive low-pass filter with a cut-off frequency of 500 hz. A description of the filter design and a review of its performance is given in Appendix C.

In addition to the random error, a considerable systematic error was observed as well. In fig. 3.1, in the raw signal, note the harmonic-like oscillation in the displacement history soon after the impact point. An interpretation of this signal would indicate that in the first 0.01 sec of the event the beam end displaced downward 4 in. and then upward 0.5 in. This behavior would not make physical sense.
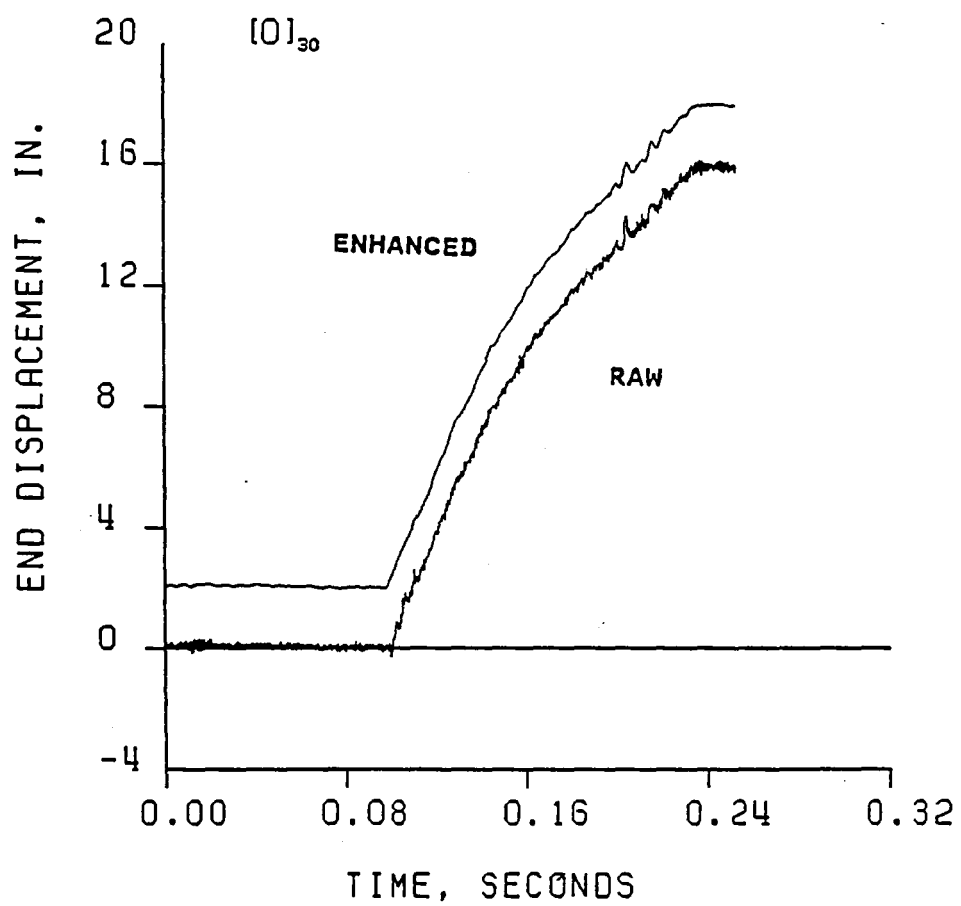
Figure 3.1   Raw and Enhanced Displacement Signal

The inertia of the impactor mass provided a monotonically increasing displacement. Upward displacement was not possible. To check this, the high speed films were closely scrutinized. No evidence of the top of the beam traveling upward soon after impact could be found in any of the films. The source of this error in the displacement signal is felt to lie in the displacement transducer design. Referring to fig. 2.8 and the tapered bar, in addition to up and down motion of the bar shadowing and exposing diodes, a small lateral displacement of the slider or the drop tower would also expose or shadow diodes. In fact, with lateral motions of the slider the transducer would record an apparent axial displacement 16 times the lateral displacement. A small rotation of the slider in the plane of the drop tower would have a similar effect. There were several probable causes of this unwanted motion of the slider: First, if the steel spherical impact points of the slider and mass car were not exactly aligned, a lateral component of force or a moment would be imparted to the slider. This would cause lateral motion and probably rotation of the slider. This motion would be the result of tolerance in the bearings or actual flexural motions of the drop tower. Also, after the tapered bar of the displacement transducer was attached to the slider, the impact force no longer passed through the center of mass of the slider. This would definitely cause a moment to be imparted to the slider. Unfortunately, during the design of the slider, the additional mass of the tapered bar was not taken into account.

To remedy the systematic error, the first 2 in. of each displacement history was replaced by a straight line segment. The

segment was faired in by hand for each test. Additional harmonic oscillations in the displacement curve after the failure point can be seen in fig. 3.1. These are of such a frequency content that they are felt to be caused by the same unwanted motions of the tapered bar. However, these oscillations were not removed as they had no major effects on the results. The upper curve in fig. 3.1 shows the altered displacement time history used for specimen 1.4. The enhanced time history incorporated both the digital filtering and the initial straight line segment.

Once the displacement data has been enhanced, relations between the load, displacement, strain, and time data could be meaningfully plotted. Specifically, for each dynamic test the load-displacement, strain-displacement, load-time, strain-time, and displacement-time relations are presented.

3.2 Experimental Results

To analyze each laminate type, seven relations were studied. These relations were:

        1) static load-displacement

        2) static strain-displacement

        3) dynamic load-displacement

        4) dynamic strain-displacement

        5) dynamic strain-time

        6) dynamic load-time

        7) dynamic displacement-time

In addition to these, the high speed movies were analyzed. The seven relations, the movies, and the post-test observations were used to characterize the test conditions and the beam response. The word 'response' as used here means both the spatial deformations and the failure modes.

By examining in detail the seven relations for laminate type 2, the $[(15/0/-15)_s]_s$ laminates, the method of characterization of the test conditions and the beam responses will be described. Due to the overwhelming amount of data from the tests, not all aspects of the testing of all the specimens will be described in detail. Laminate 2 will be discussed in detail and then a general description of the results common to all the tests will be given. Then a detailed description of the failure mode of each laminate type is presented. A comparison of the static and dynamic test results will be made. Finally, a summary of the observations of all the testing will be provided.

It should be noted, as previously stated, no tests were performed on laminate type 6. In addition, only two dynamic tests of laminate types 2, 3, 9, and 12 were completed because of equipment failure. Numerous strain guage failures were encountered on the static specimens. Typically only two static strain-displacement relations were recorded and in the case of laminates 5, 7, and 11 only one strain-displacement relation was recorded.

3.2.1 Experimental Characterization Method

To characterize the static tests and the static beam response, relations between the end load and end displacement and relations between the two surface strains and end displacement were plotted for each of the static beam specimens. As explained in the previous chapter, the displacements in the static tests were applied in increasing increments, and then returned to zero, to determine if nonvisible or nonaudible damage was occurring and dissipating energy. Figure 3.2 shows the load displacement relation for the specimen 2.2 from the $[(15/0/-15)_5]_S$ panel. The horizontal axis shows the end displacement and the vertical axis the end load. During the first cycle the beam was displaced 2 in., then unloaded. This process traced and retraced the top-most curve. Since the unloading relation retraced the loading relation within the resolution of the instrumentation, it was assumed that no energy was absorbed in the beam during this first 2 in. of displacement. Again for the second loading and unloading, to 4 in. axial displacement, the relation traced and retraced the top-most curve. During the third cycle, to 6 in. displacement, a sharp drop in the load occurred at about 5.8 in. of displacement. This sharp drop in the load corresponded to ply failures in the beam. These failures were definitely visible and audible. The ply failures reduced the flexural rigidity and thereby reduced the load required for that displacement. The displacement was continued to 6 in. and then unloaded back to zero load. With unloading, the load displacement relation followed the second curve from the top. As the loading-unloading cycles continued to increased lengths to 16 in., the loading-unloading curves coincided
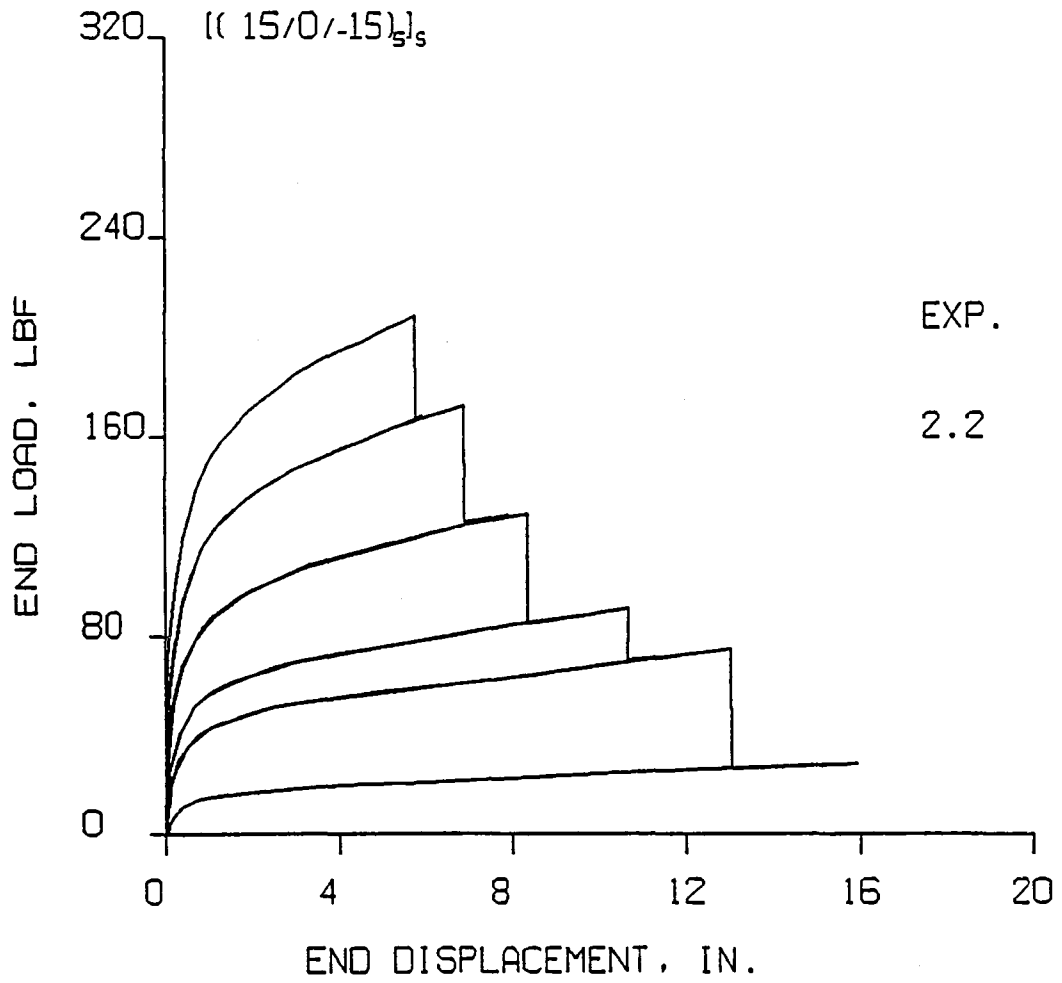
Figure 3.2   Static Load-Displacement Relation With Loading and
Unloading Curves for a [(15/0/-15)$_5$]$_s$ Laminate

except immediately after visible and audible laminate ply failures. This brittle failure-elastic response was typical for all the laminates except laminate 9. Therefore, it can be concluded that the dominate energy dissipation mechanism in the beams was associated with the ply failure events. This is not to say that there was no nonvisible damage or that it did not dissipate energy. It is to say that energy dissipated by nonvisible damage could not be detected. However, in the scale of energies associated with crash conditions, these nonvisible mechanisms absorbed negligible energy even if the mechanisms did exist. The unique static load-deflection behavior of laminate 9 is discussed later in section 3.2.3.

For the sake of clarity and simplicity no other loading-unloading curves are presented in the main text. However, the loading-unloading curves for each static test are presented in Appendix D. Instead, only the outer most locus generated by the loading-unloading procedure is presented in the main text for each test. Figure 3.3 shows on a common plot the outer locus of the static load-displacement relations for the three static specimens 2.1, 2.2, and 2.3. The finite element prediction for the deformation response is also displayed on fig. 3.3. That prediction will be discussed in a later chapter. Note the steep initial slope of the load-displacement relation as the stress state in the beam changed quickly from primarily column-like and compression to predominately bending. On the load-displacement relation, failure events are clearly indicated by sudden drops in the load. During a failure event several plies failed simultaneously on the tension side of the beam. The amplitude of the load drop gives a relative indication of
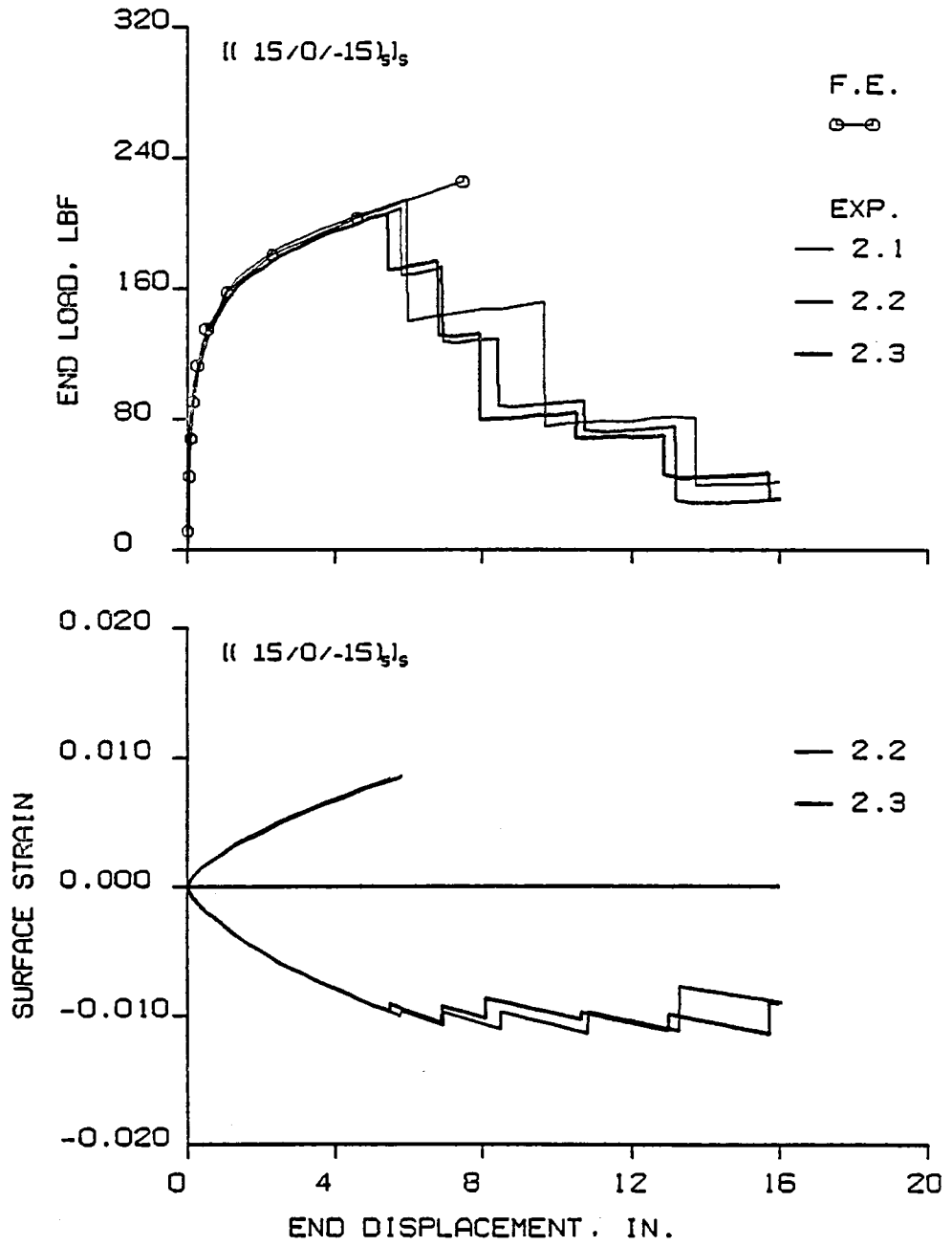
Figure 3.3 Static Load and Strain vs. Displacement for the $[(15/0/-15)_5]_s$ Laminates

the number of plies which failed during the event. The similarity of the response of the three replicate specimens should be noted.

Figure 3.3 also shows the static strain-displacement relations for the $[(15/0/-15)_5]_s$ specimens. (Strain gage problems prevented recording two of the results from the 3rd specimen.) Since it was destroyed when the surface ply failed, the gage on the tension side of the beam recorded strain only up to the first failure event. The compression side guage continued to record. Progressive failures in the beam are clearly visible in these relations. The compressive strains suddenly drop because the ply failures reduce the thickness of the beam and thereby reduce the strain required for the curvature corresponding to that end displacement. The magnitude of the strain levels should be noted; strains in the 1-2% level were common.

The high speed movies provided valuable visual information on the dynamic response of the beams. Figure 3.4 shows selected frames from the film of specimen 4.5, a $[(45/0/-45)_5]_s$ laminate. The approximate time, in seconds, after impact is indicated with each frame. The first frame shown, t = 0.0, was the last frame of the film taken before the impact. Shortly after impact, the shape of the beam is quite interesting, as shown in the second frame of the film, approximately 2.5 milliseconds after impact. In this frame the beam is deformed into a noticeable "W" shape. This shape occurs because the center of the beam has not yet responded to the impulsive loading. The third frame of film shows the center of the beam as it snaps through the "W". The frame of film after that shows an acute curvature at the center of the beam. The final frame of film shows a more obtuse curvature in the
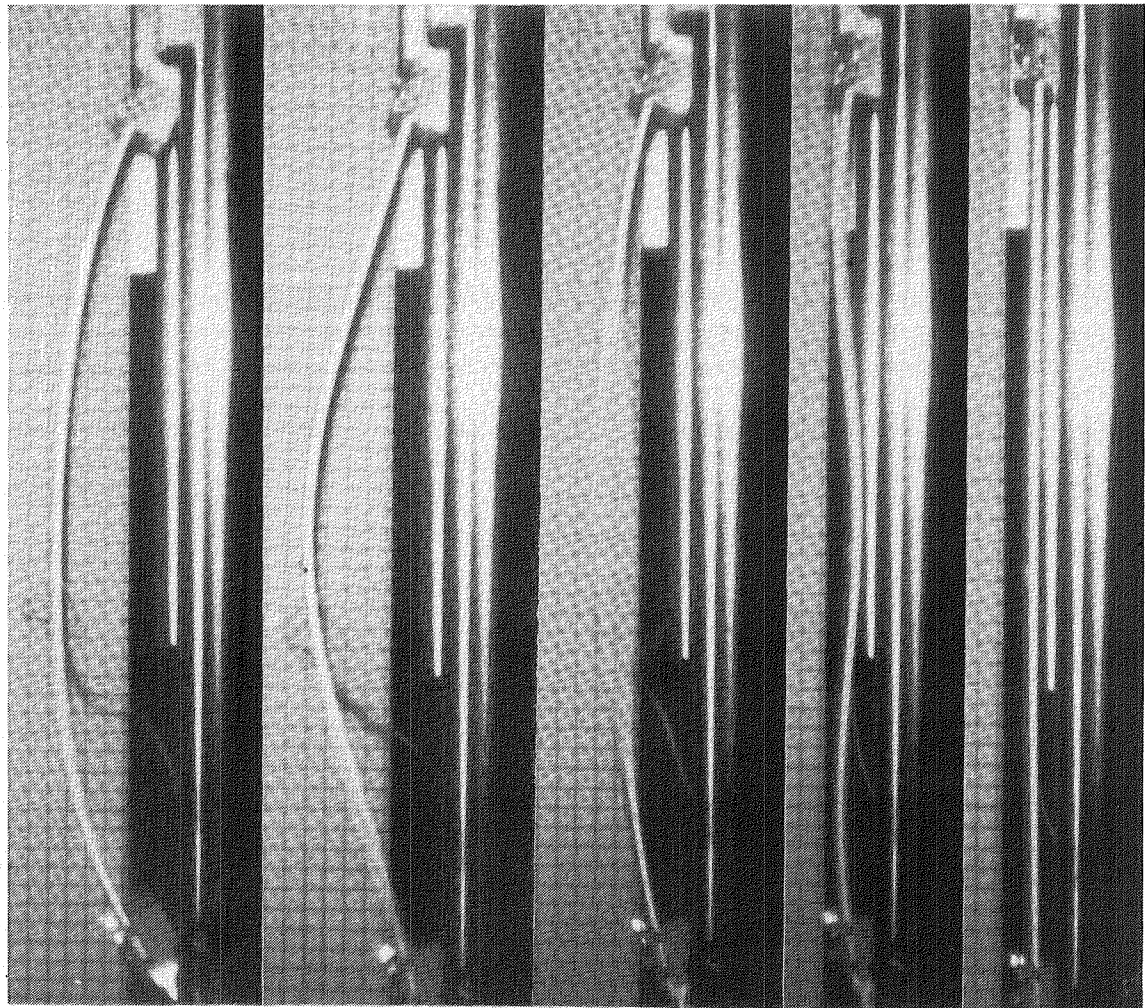
t=0.01   t=0.0075   t=0.005   t=0.0025   t=0.00

(seconds)

Figure 3.4   Third Mode Deformation Response

center as the beam snaps back. This "W" shape and snapping is associated with the third vibration mode of the beam. The movies show that in the test fixture the third mode vibratory response in the beams was excited and that this response was superimposed on the global deformation response which was similar to the static response. The film of specimen 4.5 was chosen for fig. 3.4 because it had the best visual information. However, the third mode response was seen in all the dynamic tests. In fact, for all specimens the spatial deformations up to first failure appeared similar.

The upper portion of fig. 3.5 illustrates the load-displacement relations for the two dynamically tested $[(15/0/-15)_5]_s$ specimens, specimens 2.4 and 2.5. The end displacement is shown on the horizontal axis and the end load on the vertical. The difference in scale between the dynamic and static load levels should be noted in figs. 3.5 and fig 3.3, respectively. The dynamic responses of the two beams were quite similar. The response curves up to failure are almost coincident, indicating the high repeatability of the dynamic experiments. Due to the statistical nature of failure in composites, there were some differences in the failure events. As with the static loading, failures are denoted by the sharp drops in the load. There is an initial high amplitude load spike in the response as the initial column configuration of the beam quickly decelerates the beam. As the beam begins to bend, the spike subsides. The third mode response, just discussed, is strongly evident in the load response. However, this vibratory response dampened as the beam deformed axially and laterally. This was evident in the films, as well as in fig. 3.5.
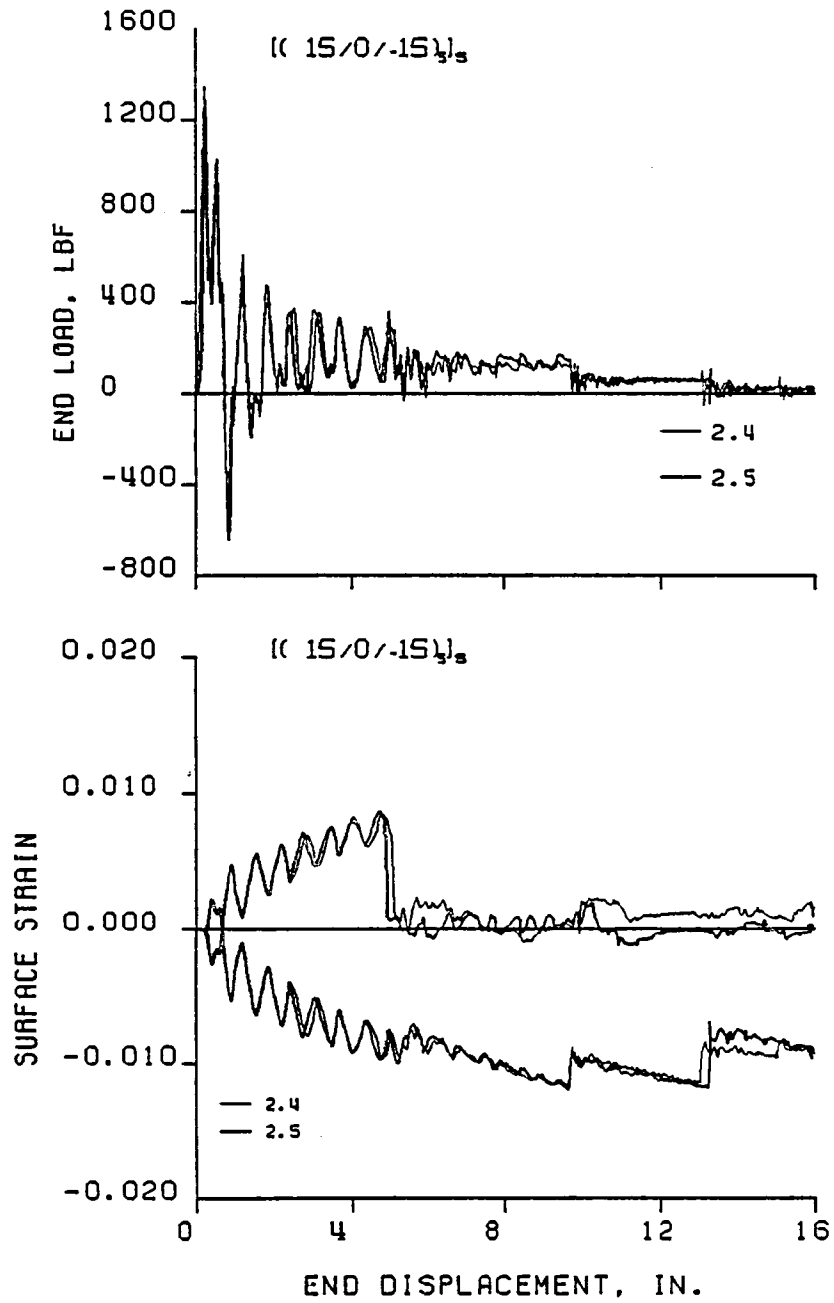
Figure 3.5   Dynamic Load and Strain vs. Displacement for the
$[(15/0-15)_5]_s$ Laminates

The lower portion of fig. 3.5 shows the surface strain-displacement relation for the two dynamic tests of the $[(15/0/-15)_5]_s$ laminate. The convex (tension) side strain is on the top and the concave (compression) side strain is on the bottom of that portion of the figure. Note that the concave side (bottom curve) initially starts out in tension and the convex side, (top curve) initially starts in compression. This initial reversal in strain is due to the initial "W" deformed shape of the beam. The failure events are clearly evident on this figure.

Figure 3.6 shows the load and strain time histories for the dynamic tests. The third mode oscillation can be further studied from this relation. The frequency of oscillation can be determined directly from this figure and compared to the computed 3rd mode natural frequency for the beam. As with the previous figure, failure events are clearly evident. As in the load-displacement relation, the load time history of the failure events are denoted by sudden drops in the load. No other load time histories are presented in the main text. The load time histories of all the other dynamic tests are presented in Appendix E.

The displacement time history for the two dynamic specimens tested is displayed in fig. 3.7. The displacement is given on the vertical axis and the time on the horizontal axis. The enhanced and raw data are plotted for each specimen and the results from each specimen are spaced vertically from each other in the figure. Note the straight line relation in the enhanced data near time zero. The end displacement-time relation characterizes the dynamic test. It provides information on the total duration of the event and the approximate change in velocity of the end of the beam during the event.
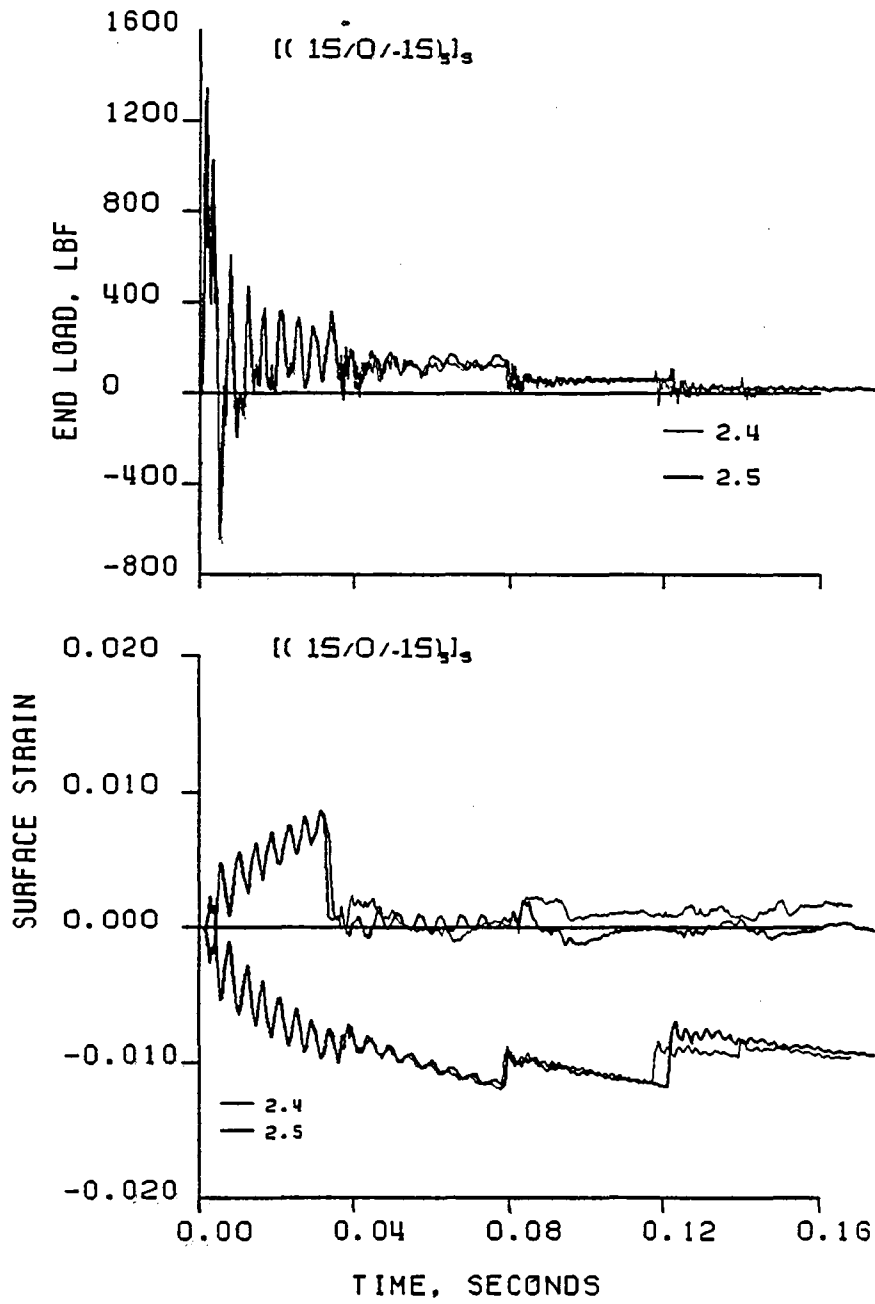
Figure 3.6   Dynamic Load and Strain vs. Time for the
[(15/0/-15)$_5$]$_s$ Laminates
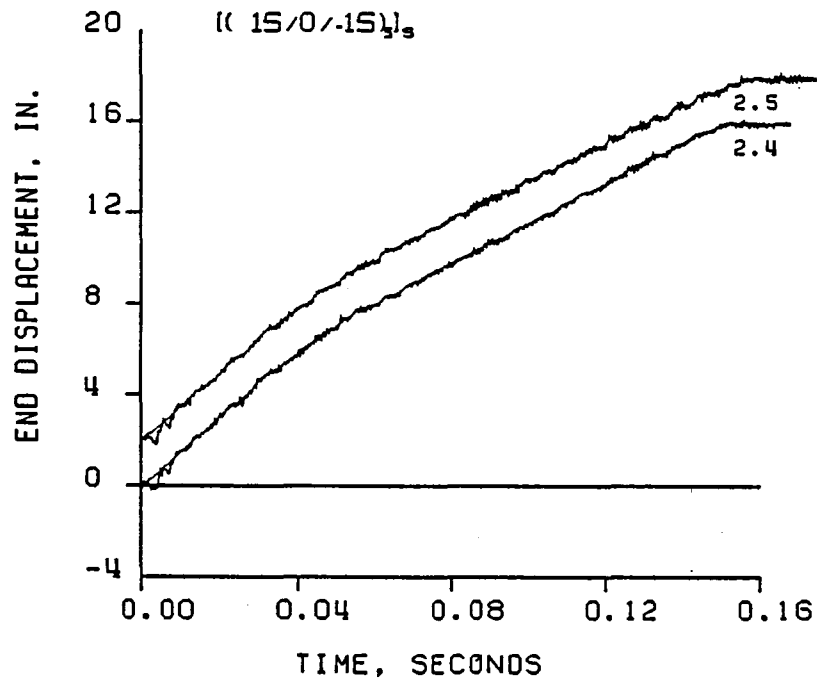
Figure 3.7   Dynamic Displacement vs. Time for the $[(15/0/-15)_5]_s$
Laminates

By examining these relations, combined with a post-test inspection of the specimens and examination of the films, much about the beam response and the failure modes can be determined. The next section discusses the features which were common to all tests.

3.2.2 Description of Characteristics Common to All Tests

Six of the relations just discussed for the $[(15/0/-15)_5]_s$ are plotted for each of the other 10 laminates tested in fig. 3.8 through fig. 3.37. Three main features of interest were common to all the tests. They are: (1) All the dynamic tests exhibited a third mode vibratory response; (2) With the exception of two laminate types, the static and dynamic failure modes of the laminates were identical, and; (3) All of the beams exhibited varying degrees of bimodular material behavior.

Third Mode Response

Analysis of the third mode vibratory response is best done through examination of the strain time histories. With the exception of laminates 9 and 10, all the laminates showed similar responses, qualitatively. All laminates showed the initial reverse value of strain associated with the initial "W" shape. Then a vibratory response was superposed on a monotonically increasing strain. The vibratory response dampened with time and severely dampened after ply failures. The frequency of the vibratory response was determined from the experimental data for each laminate type and is presented in table 3.1. The
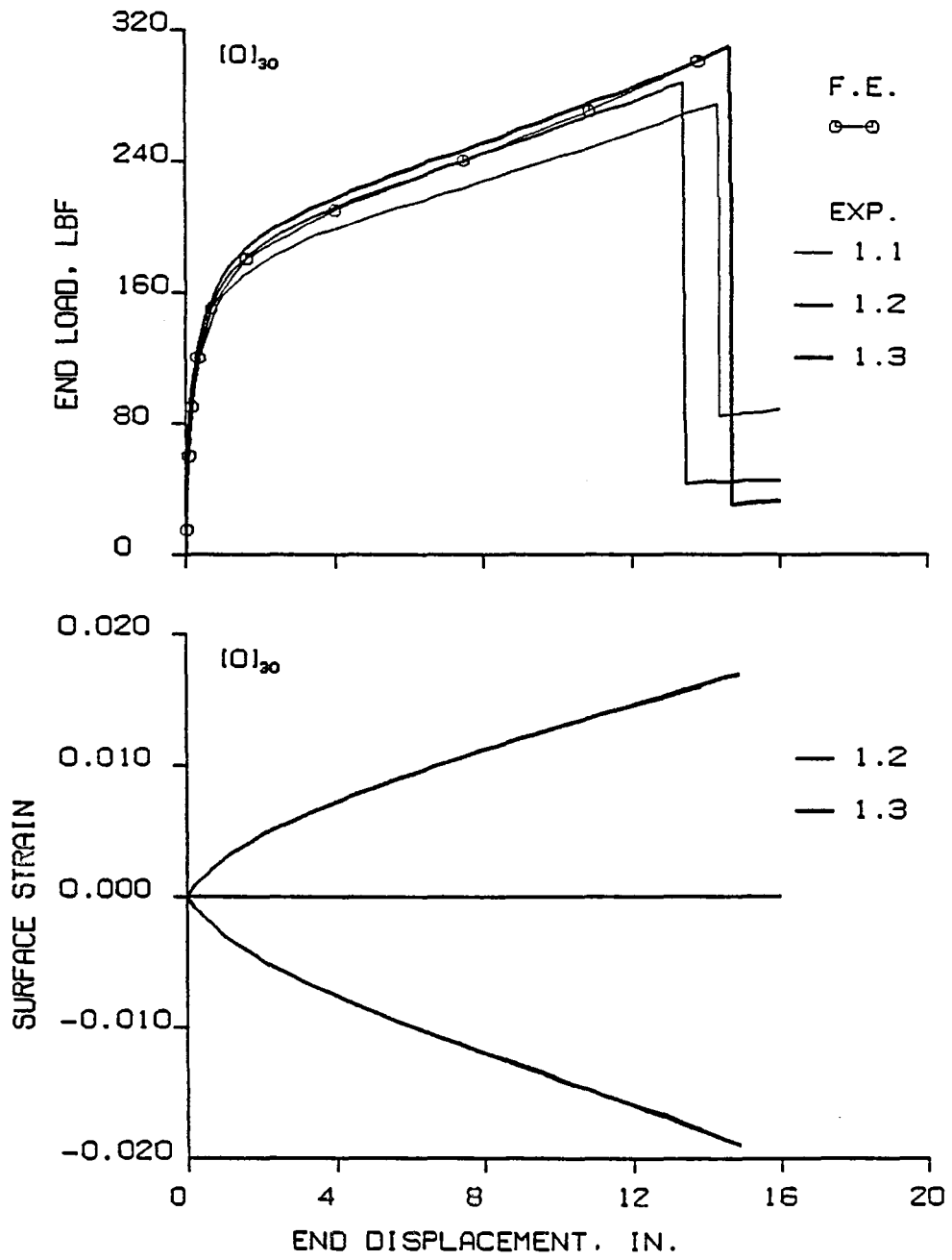
Figure 3.8   Static Load and Strain vs. Displacement for the $[0]_{30}$ Laminates
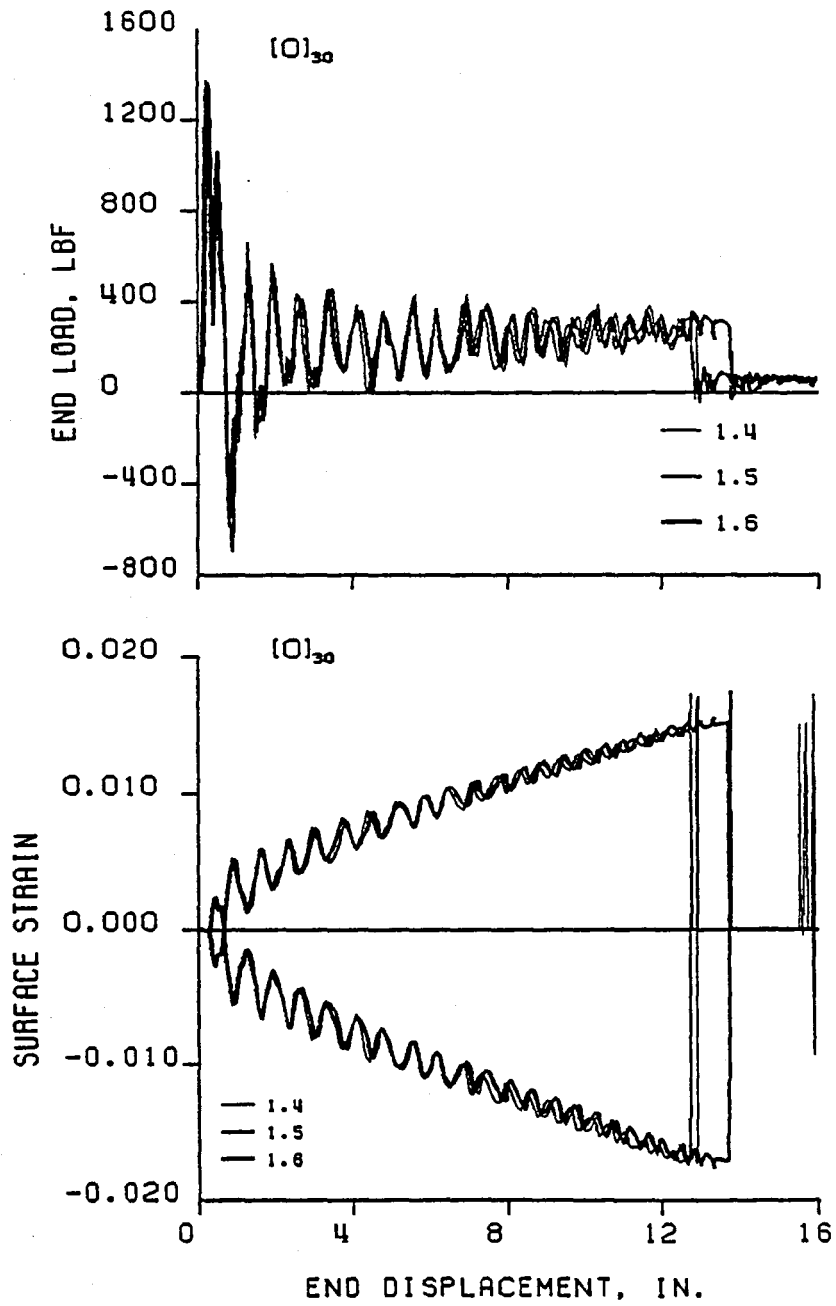
Figure 3.9   Dynamic Load and Strain vs. Displacement for the $[0]_{30}$
Laminates
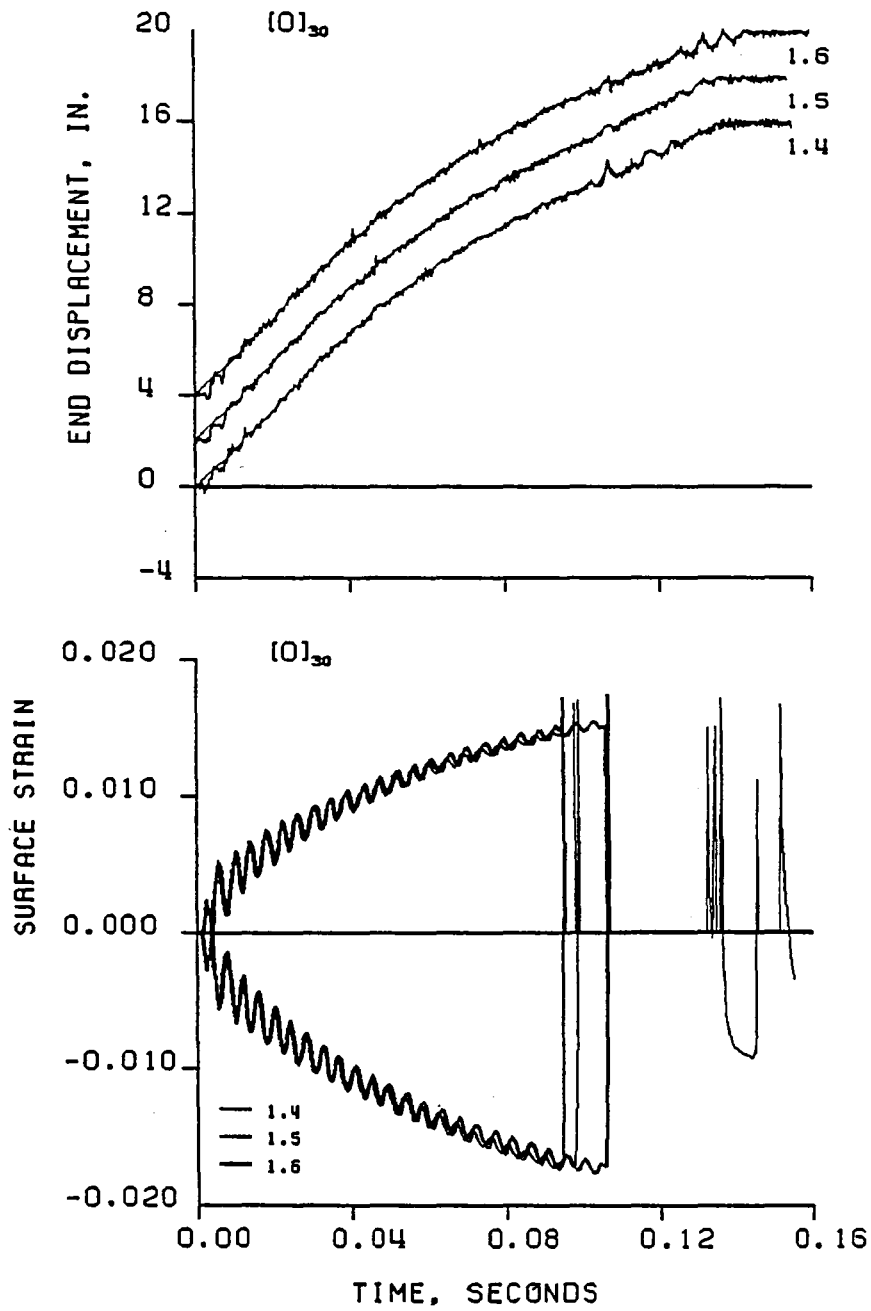
Figure 3.10   Dynamic Displacement and Strain vs. Time for the $[0]_{30}$ Laminates
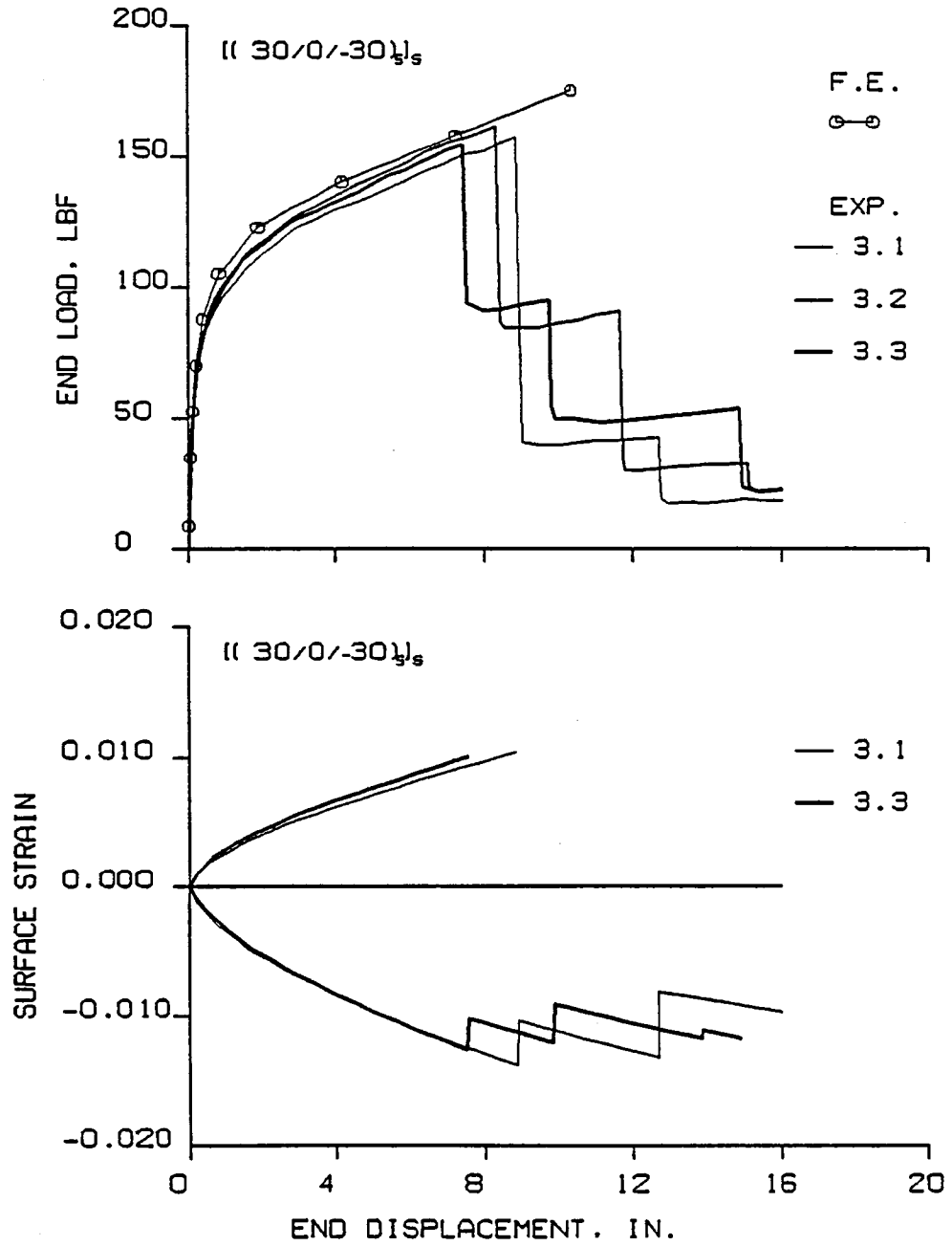
Figure 3.11   Static Load and Strain vs. Displacement for the
$[(30/0/-30)_5]_s$ Laminates
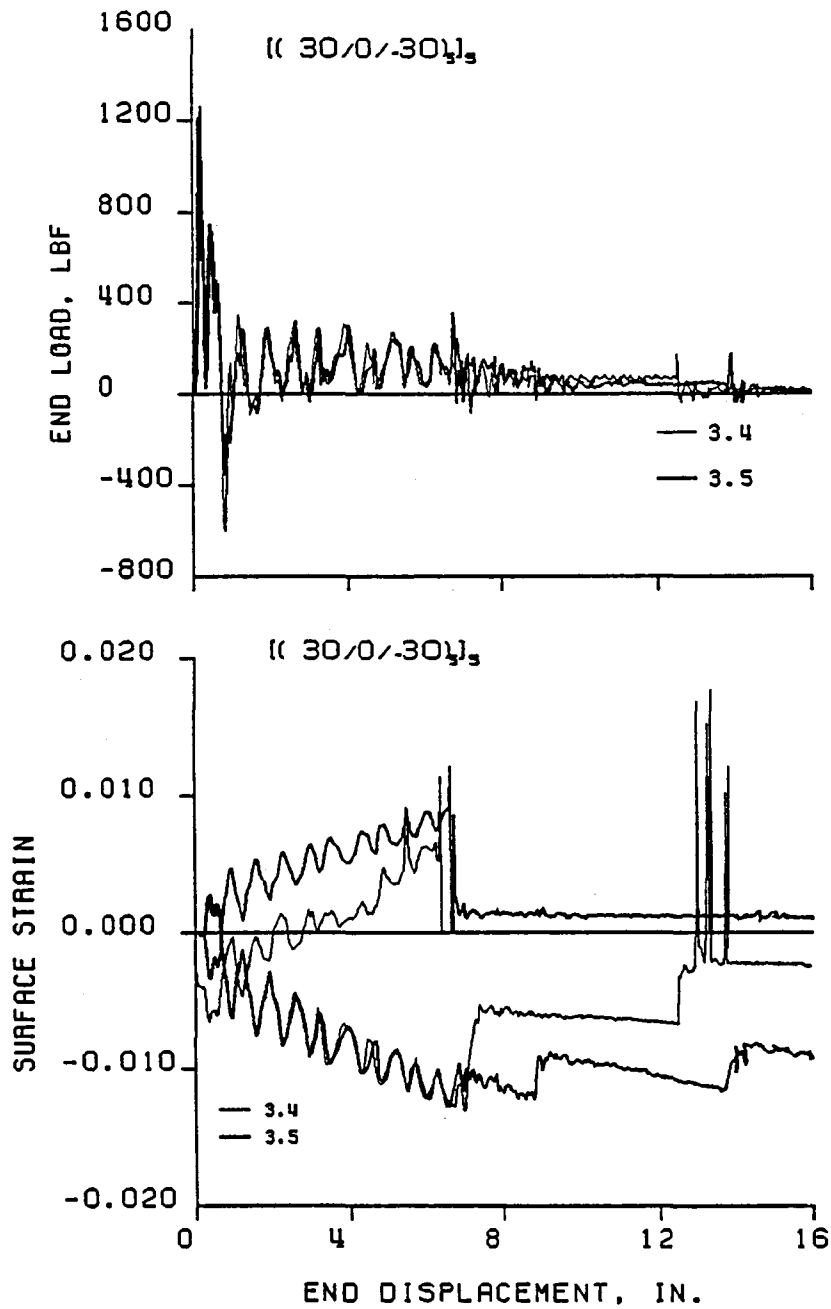
Figure 3.12   Dynamic Load and Strain vs. Displacement for the $[(30/0/-30)_5]_s$ Laminates
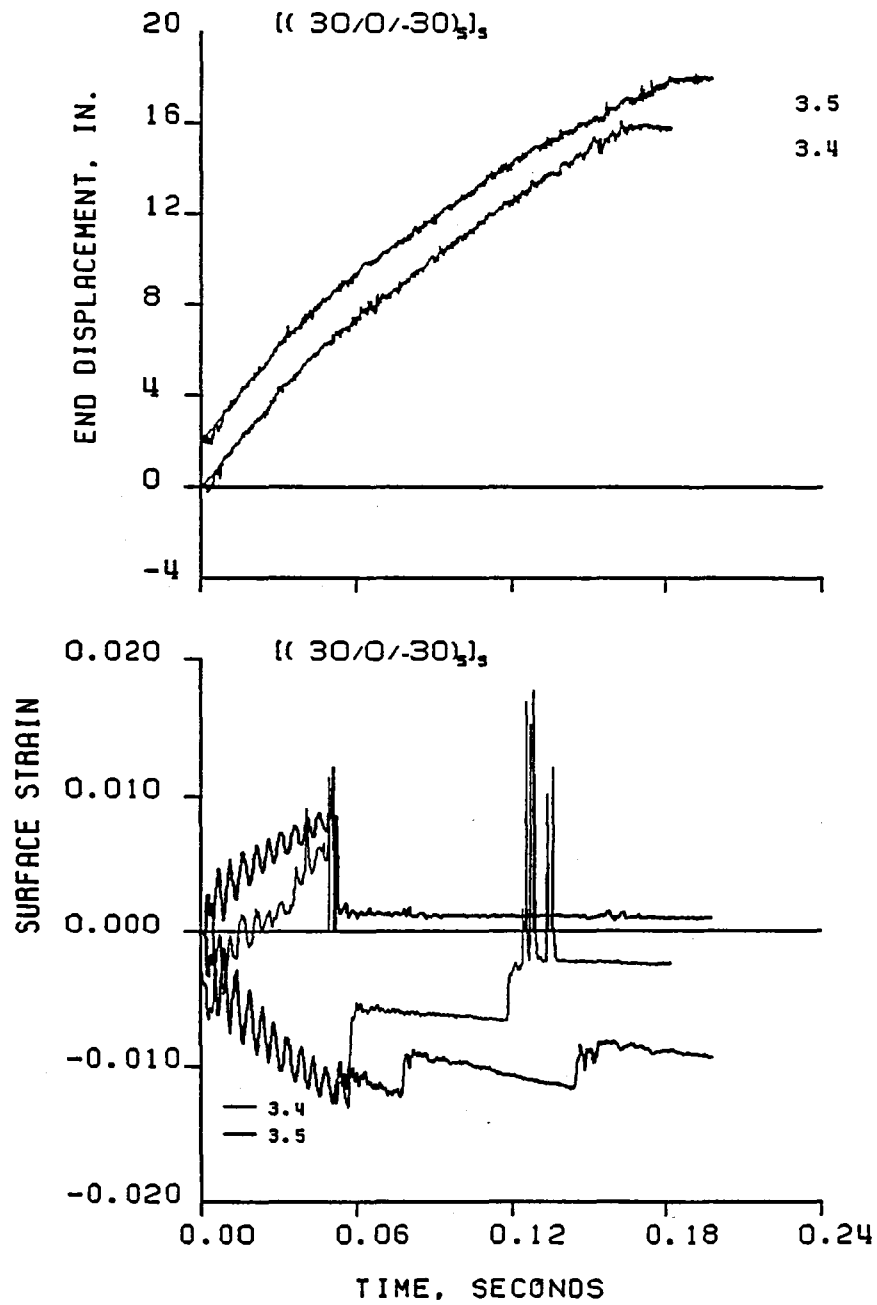
Figure 3.13 Dynamic Displacement and Strain vs. Time for the $[(30/0/-30)_5]_s$ Laminates
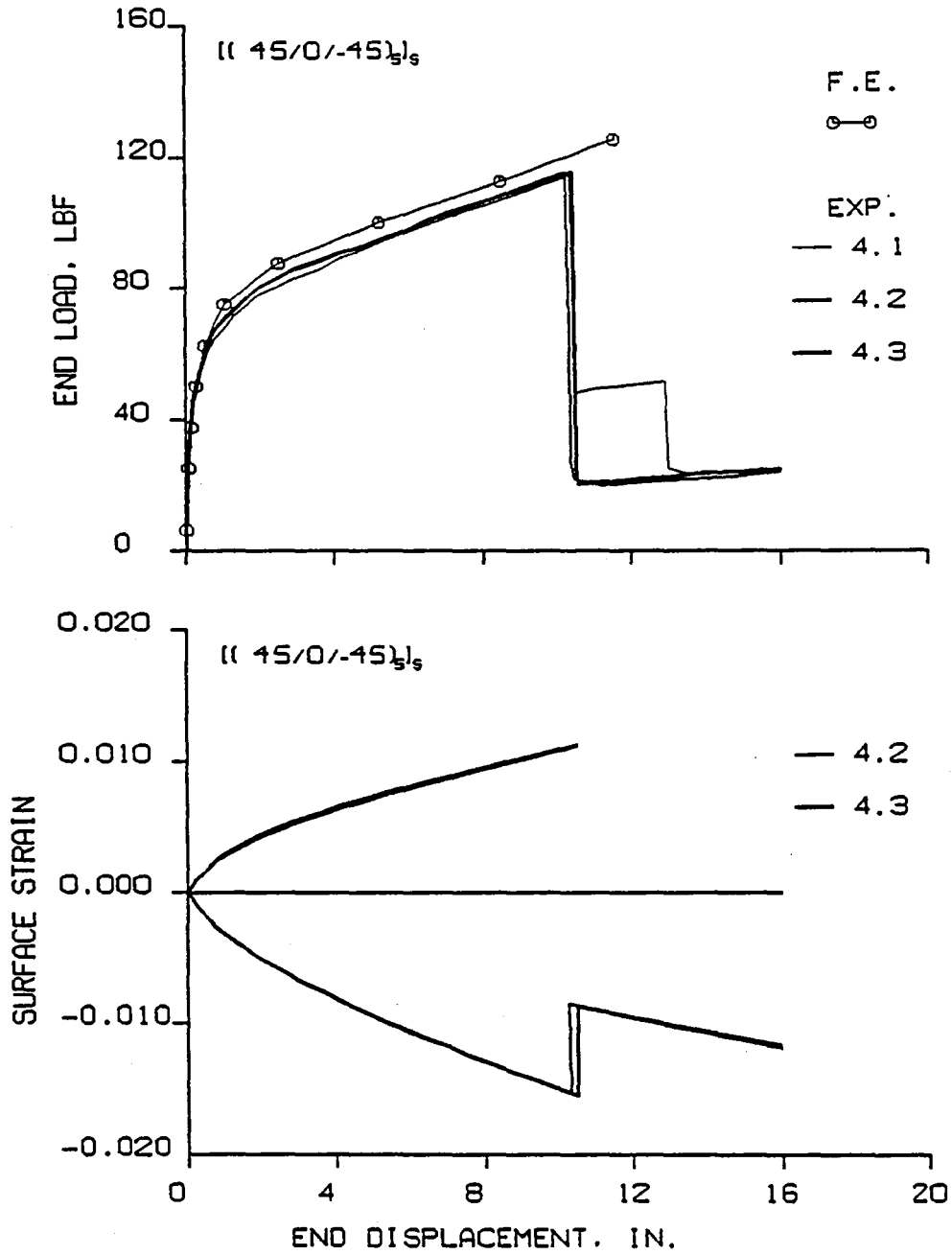
Figure 3.14   Static Load and Strain vs. Displacement for the
[(45/0/-45)₅]ₛ Laminates
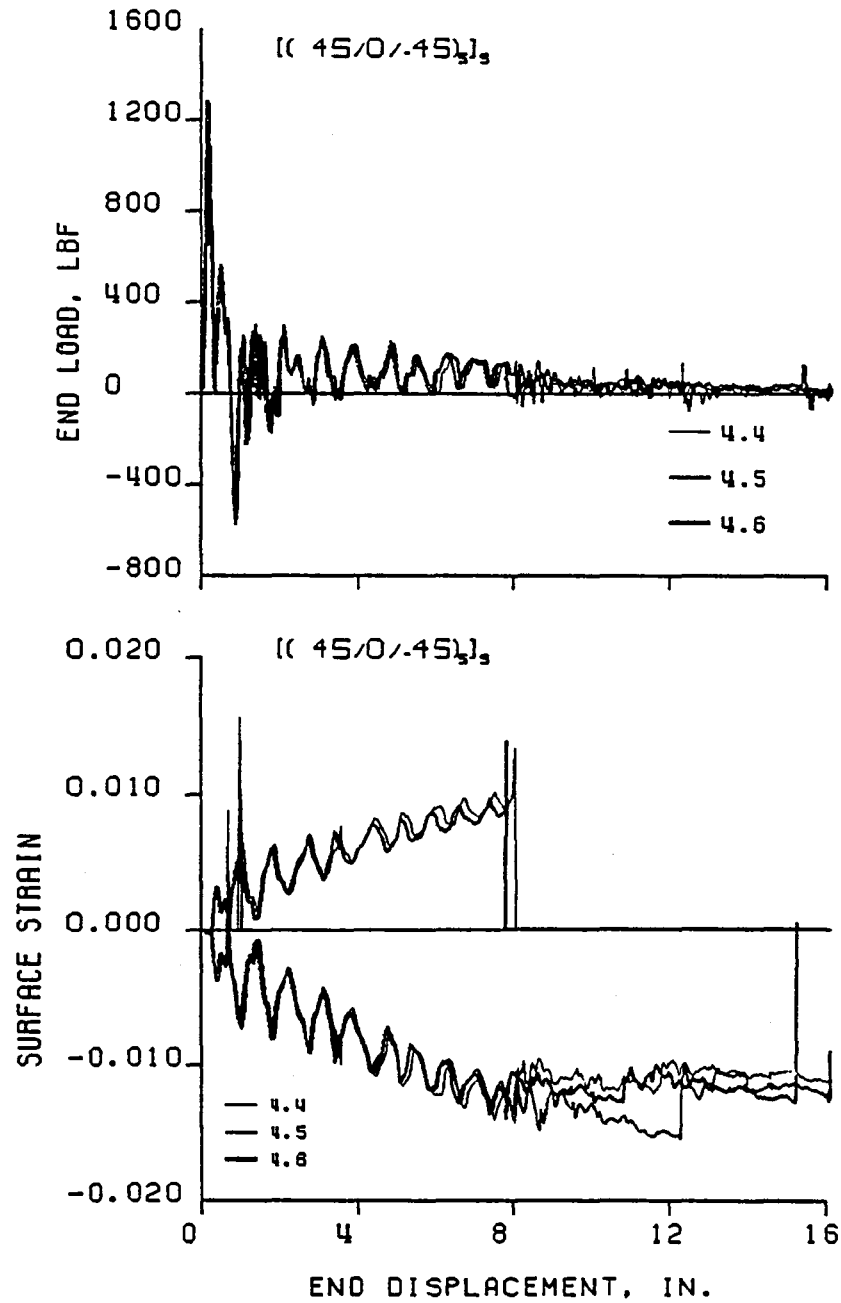
Figure 3.15 Dynamic Load and Strain vs. Displacement for the
$[(45/0/-45)_5]_s$ Laminates
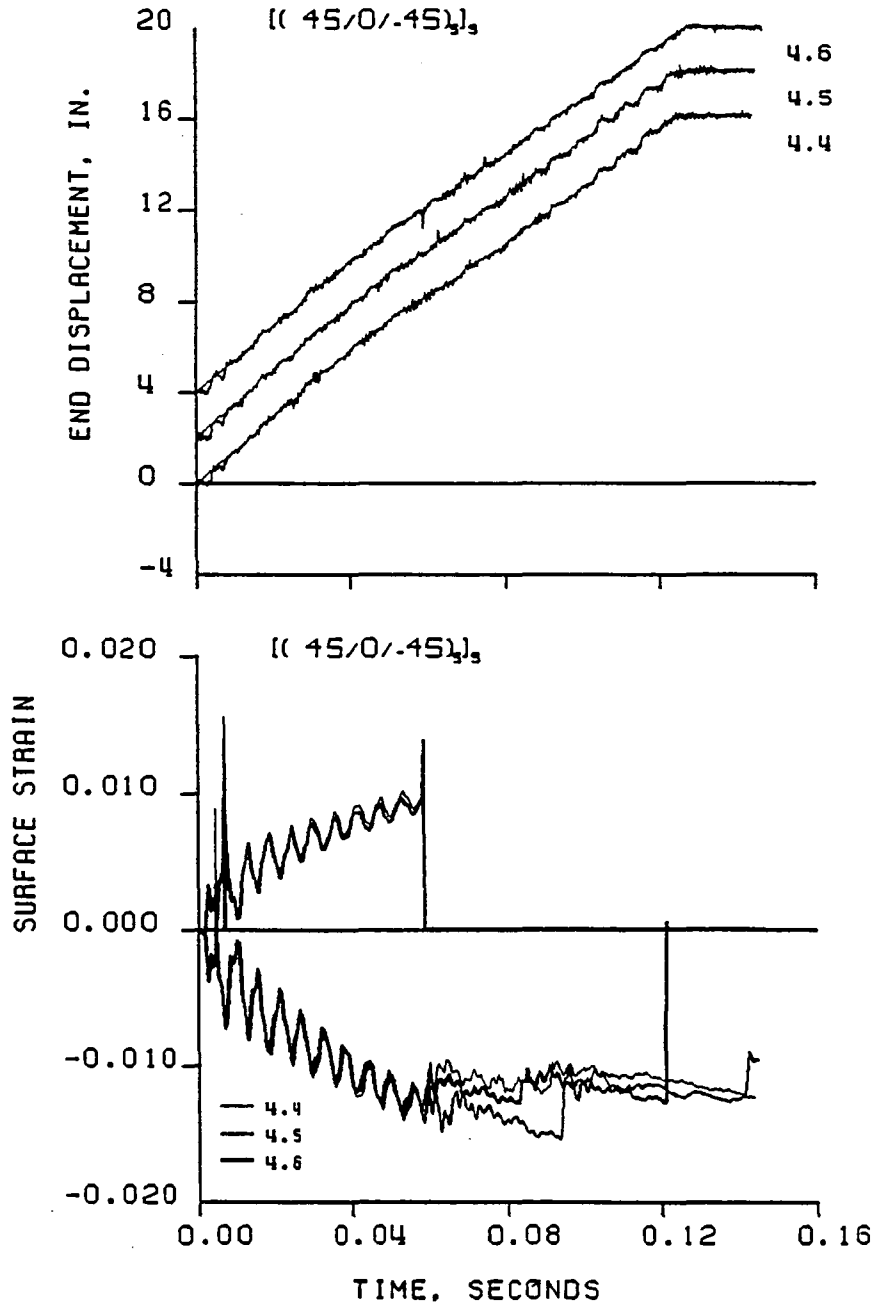
Figure 3.16   Dynamic Displaement and Strain vs. Time for the $[45/0/-45)_5]_s$ Laminates

54
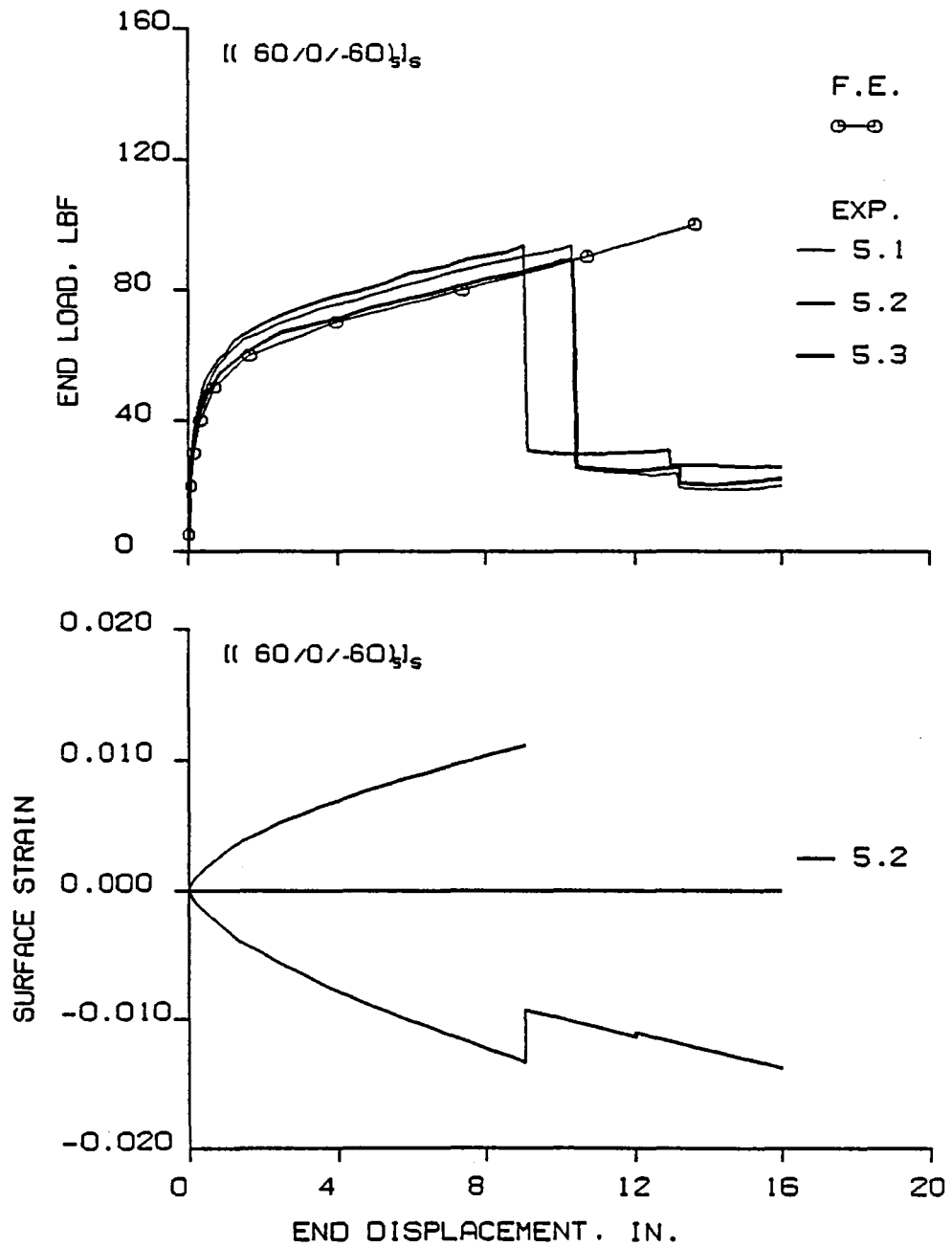
Figure 3.17   Static Load and Strain vs. Displacement for the
[(60/0/-60)₅]ₛ Laminates
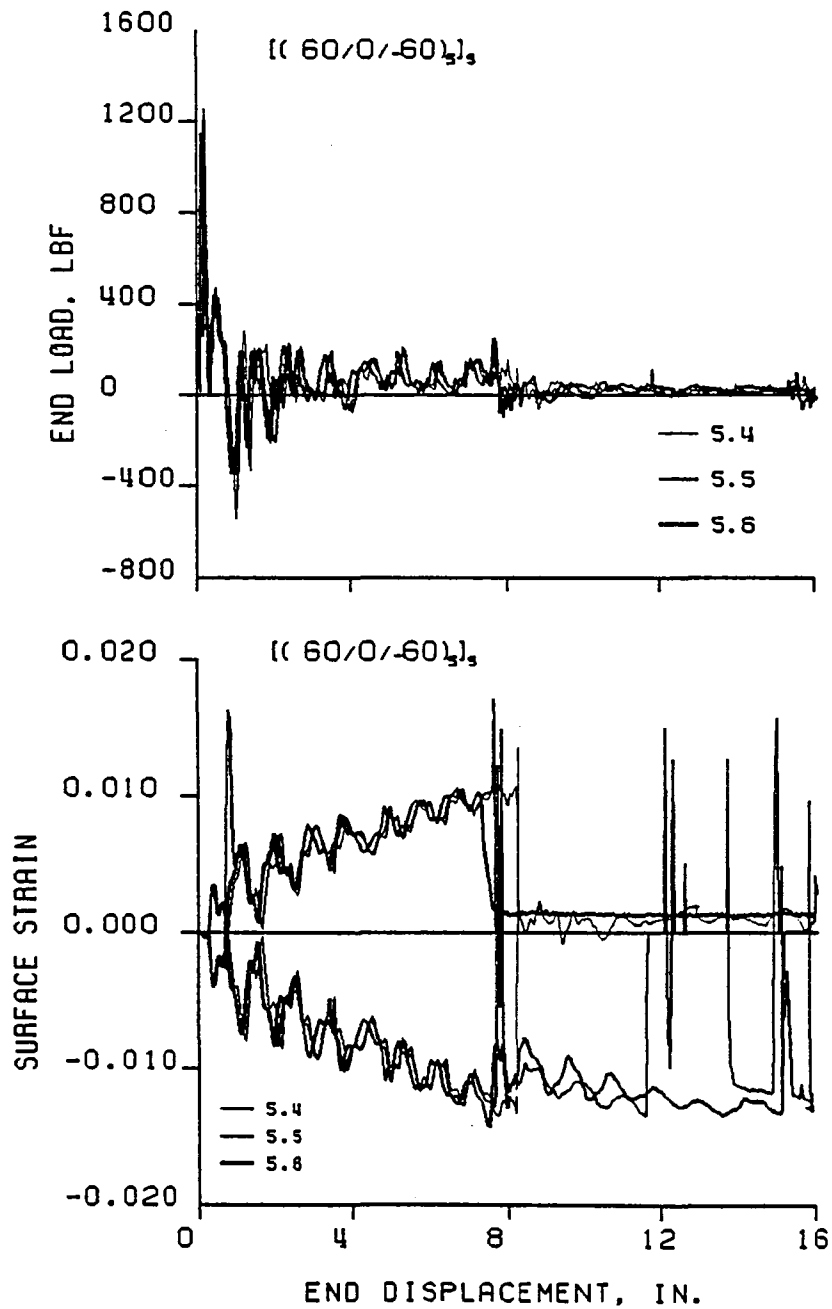
Figure 3.18   Dynamic Load and Strain vs. Displacement for the $[(60/0/-60)_5]_s$ Laminates
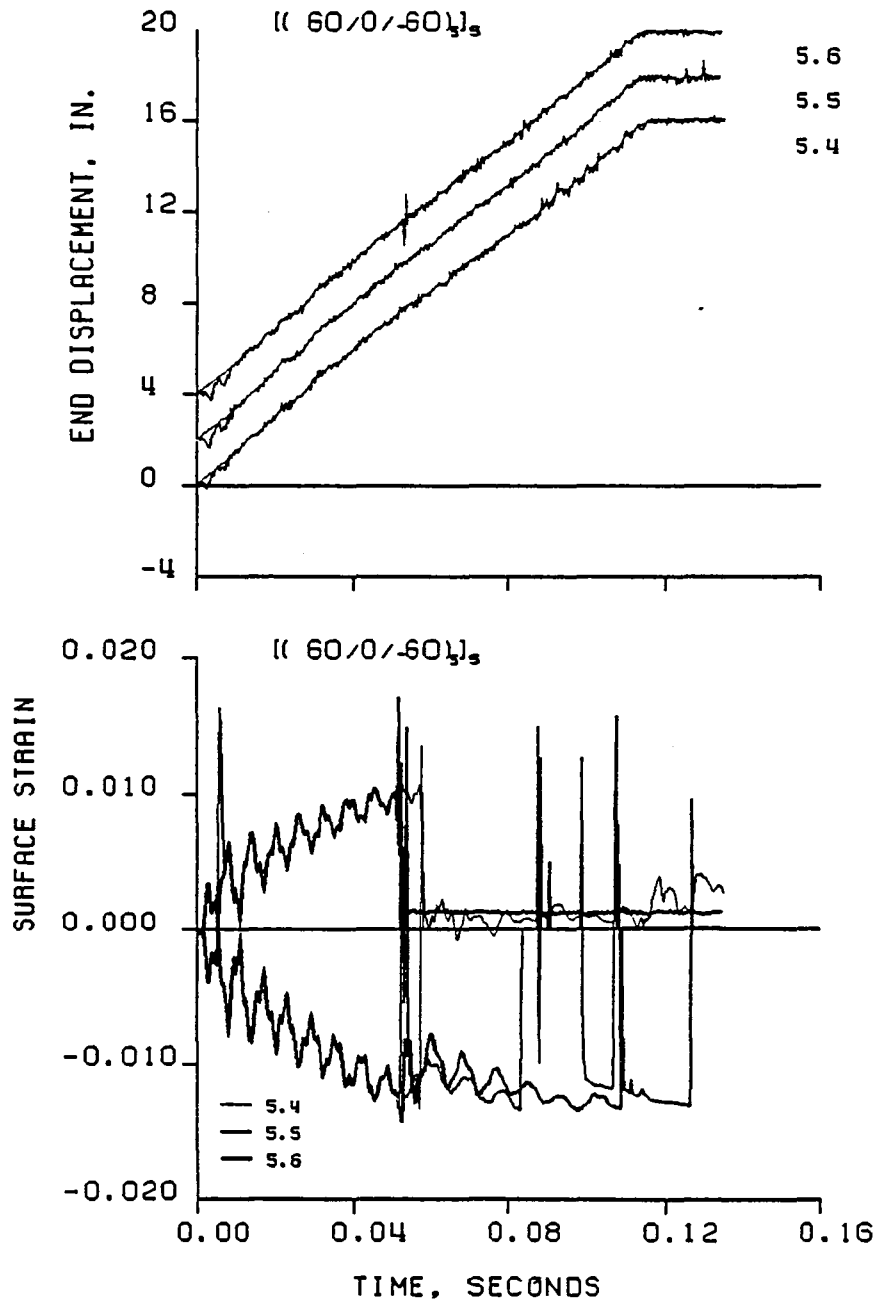
Figure 3.19   Dynamic Displacement and Strain vs. Time for the
[(60/0/-60)$_5$]$_s$ Laminates
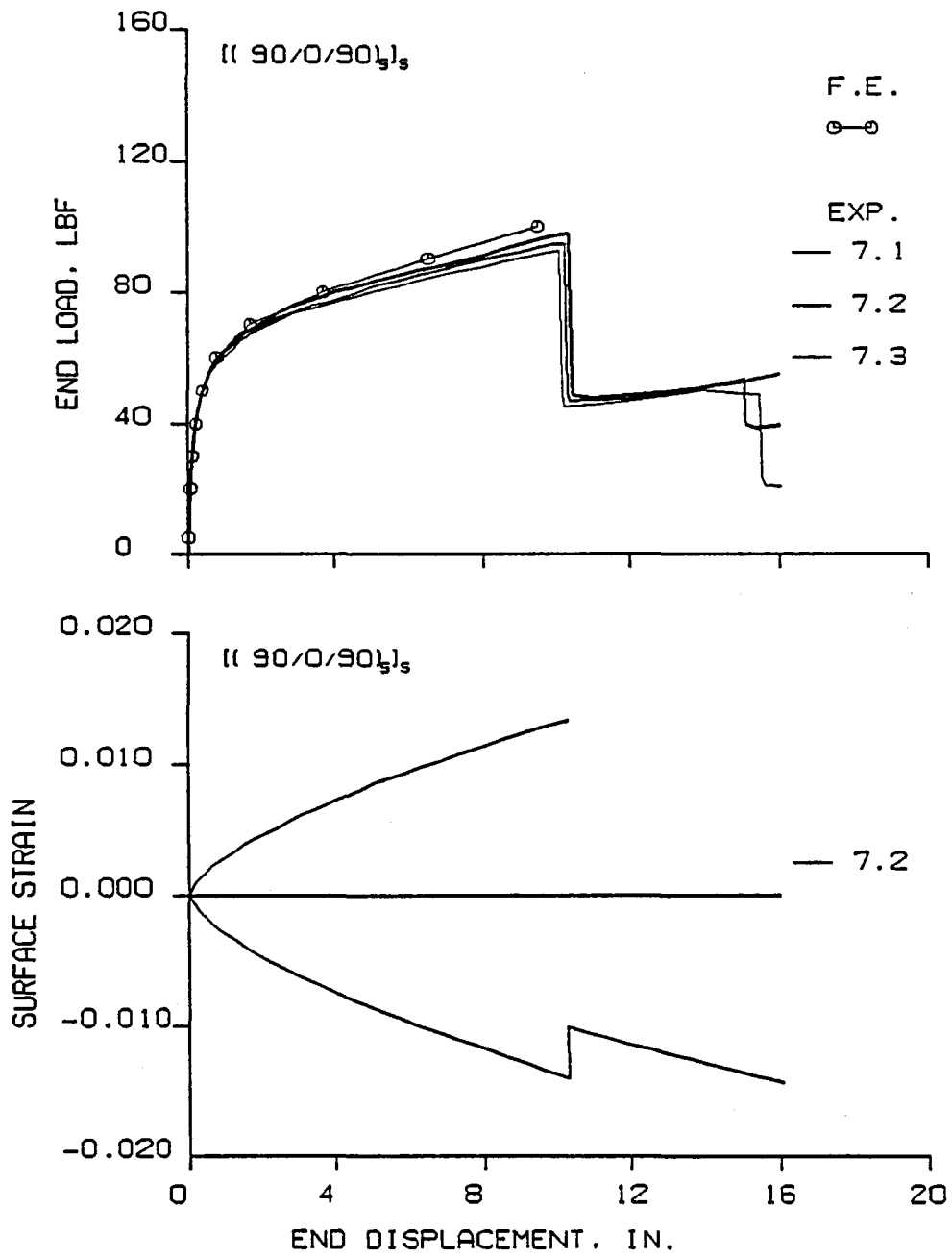
Figure 3.20   Static Load and Strain vs. Displacement for the
$[(90/0/-90)_5]_s$ Laminates
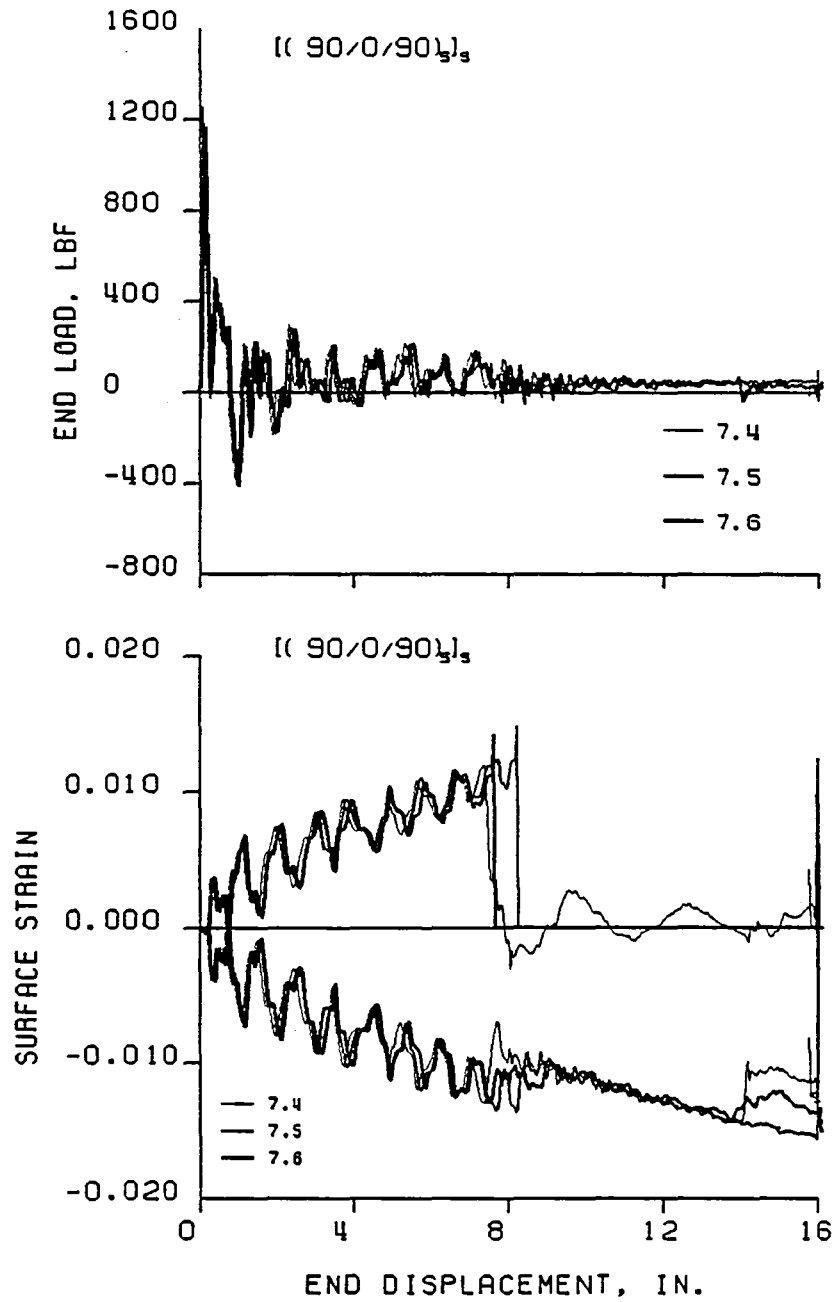
Figure 3.21   Dynamic Load and Strain vs. Displacement for the
$[(90/0/-90)_5]_s$ Laminates
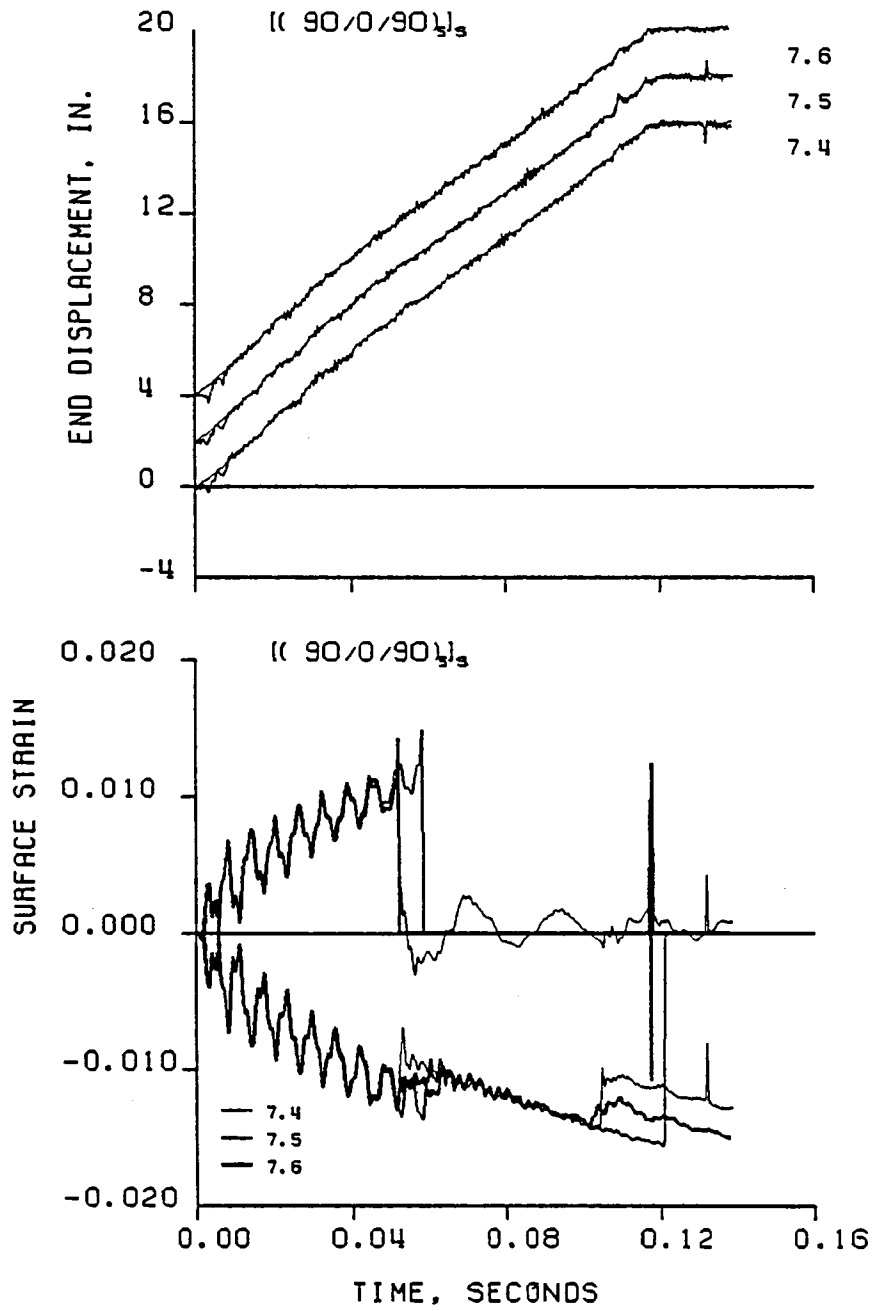
Figure 3.22 Dynamic Displacement and Strain vs. Time for the
$[(90/0/-90)_5]_s$ Laminates
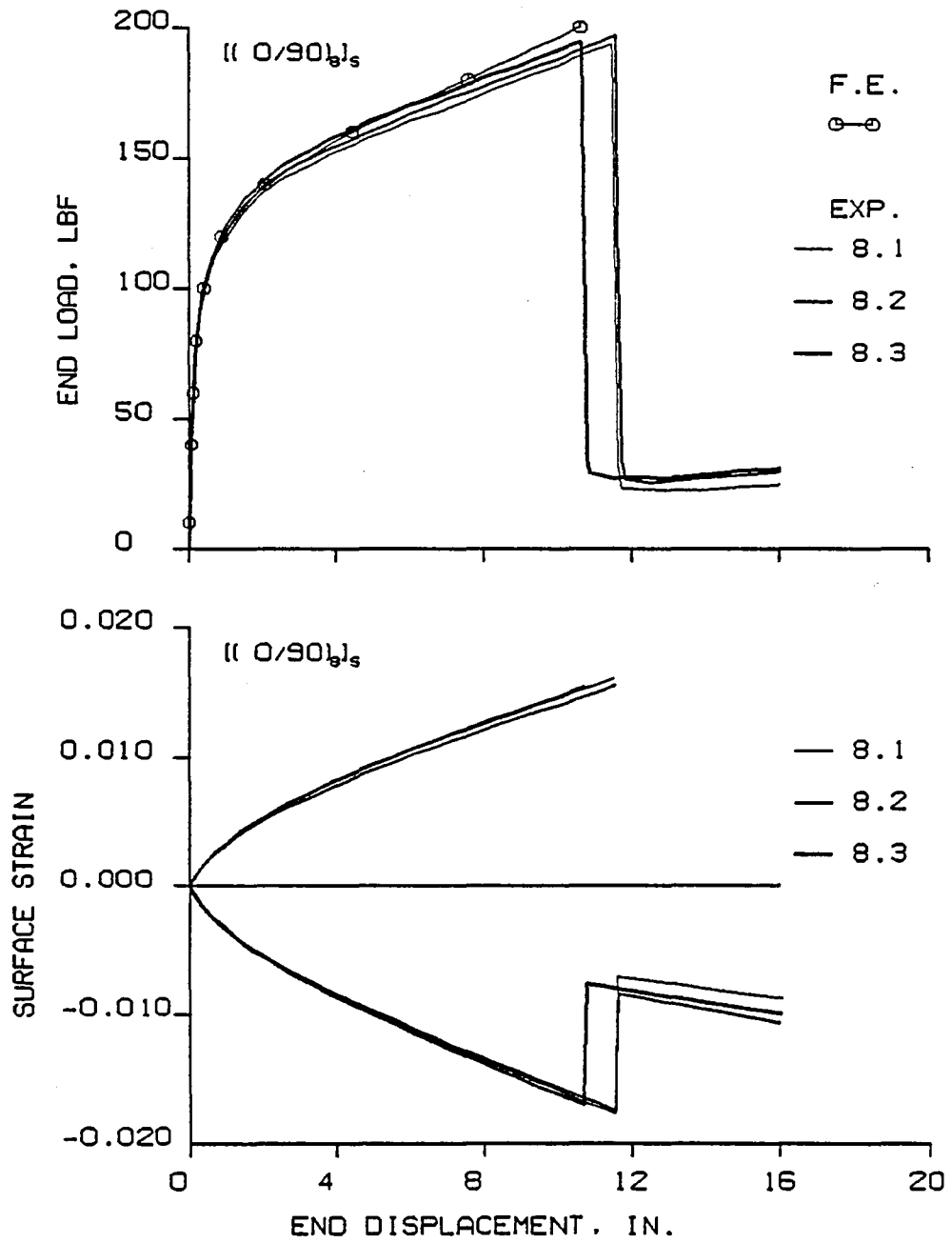
Figure 3.23   Static Load and Strain vs. Displacement for the
$[(0/90)_8]_s$ Laminates
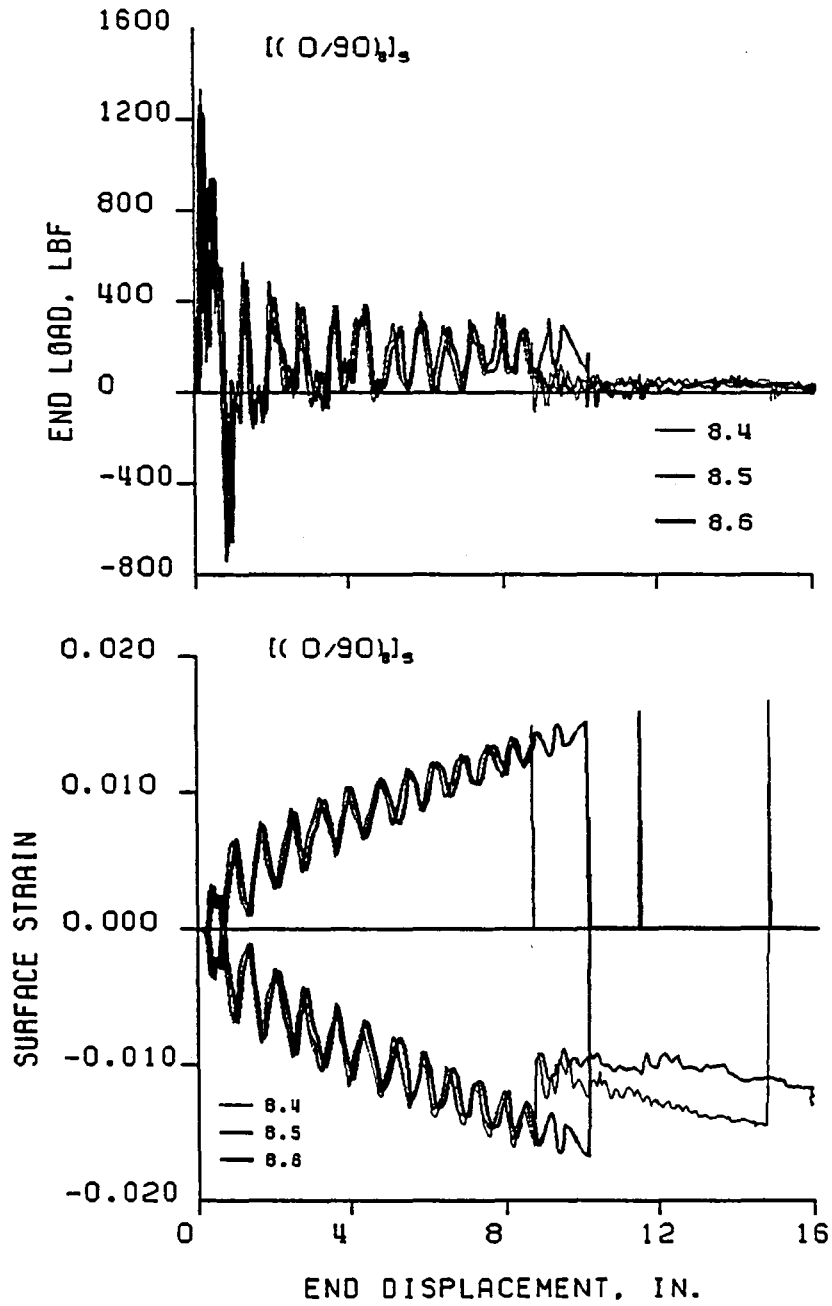
Figure 3.24   Dynamic Load and Strain vs. Displacement for the
$[(0/90)_8]_s$ Laminates
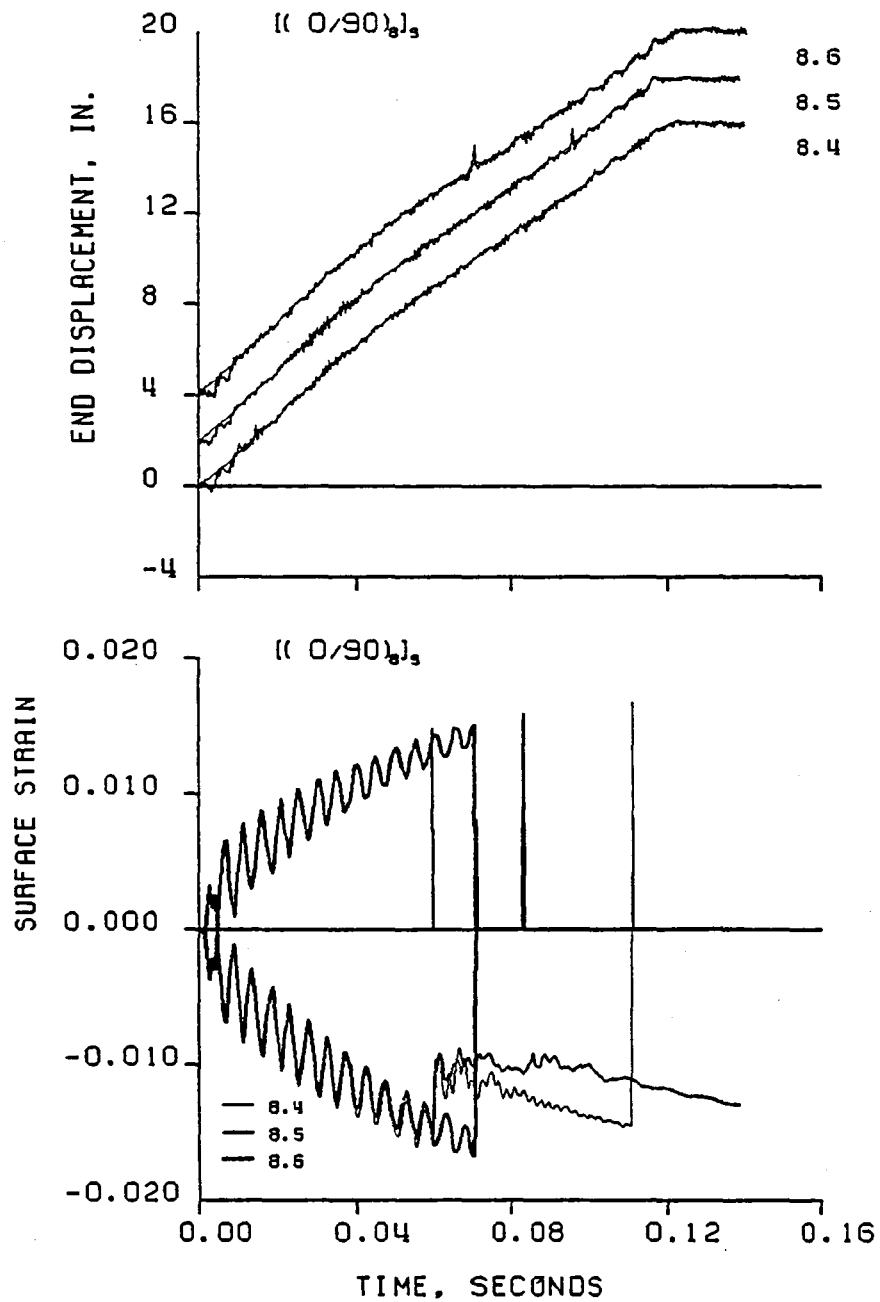
Figure 3.25   Dynamic Displacement and Strain vs. Time for the $[(0/90)_8]_S$ Laminates
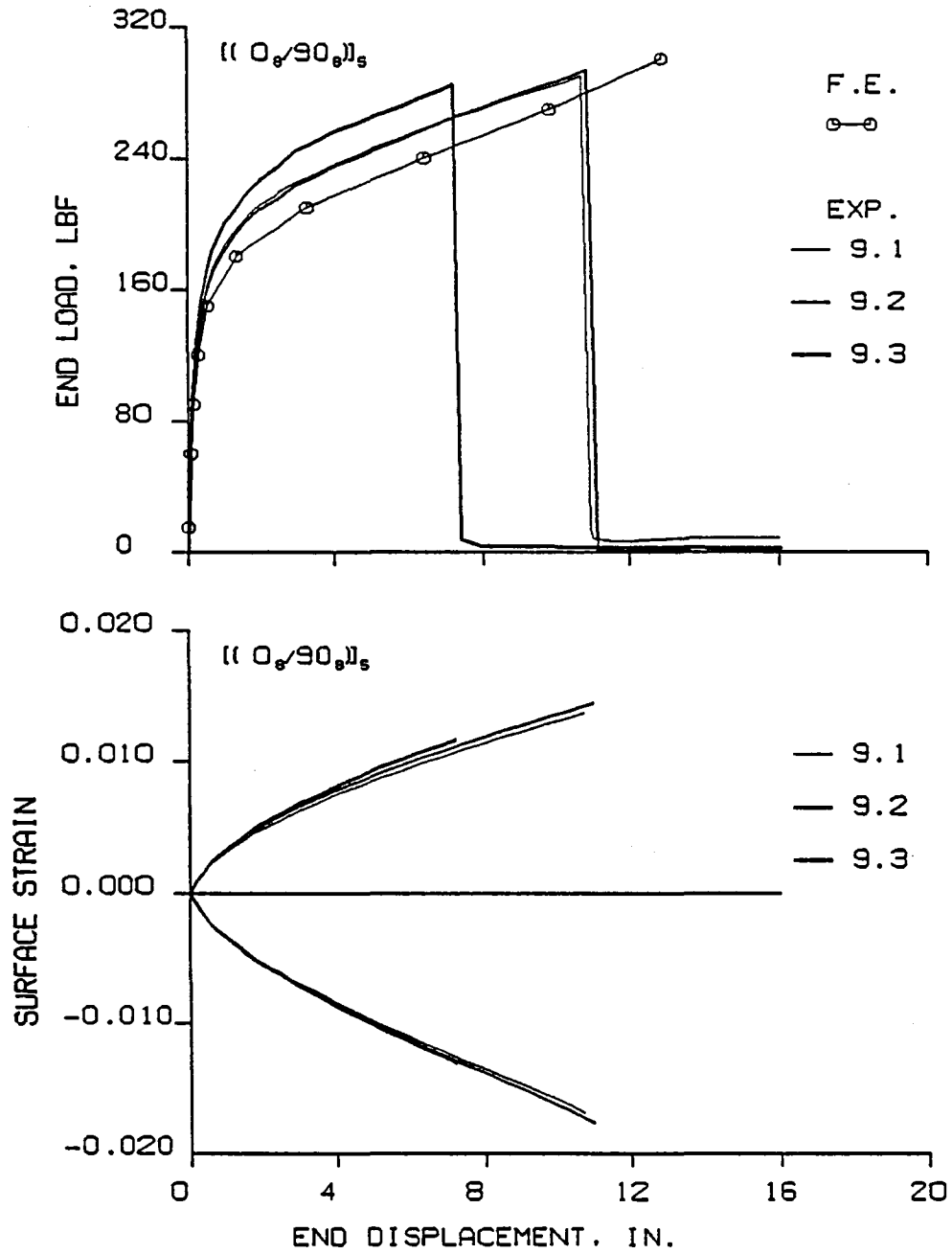
Figure 3.26   Static Load and Strain vs. Displacement for the $(0_8/90_8)_s$ Laminates
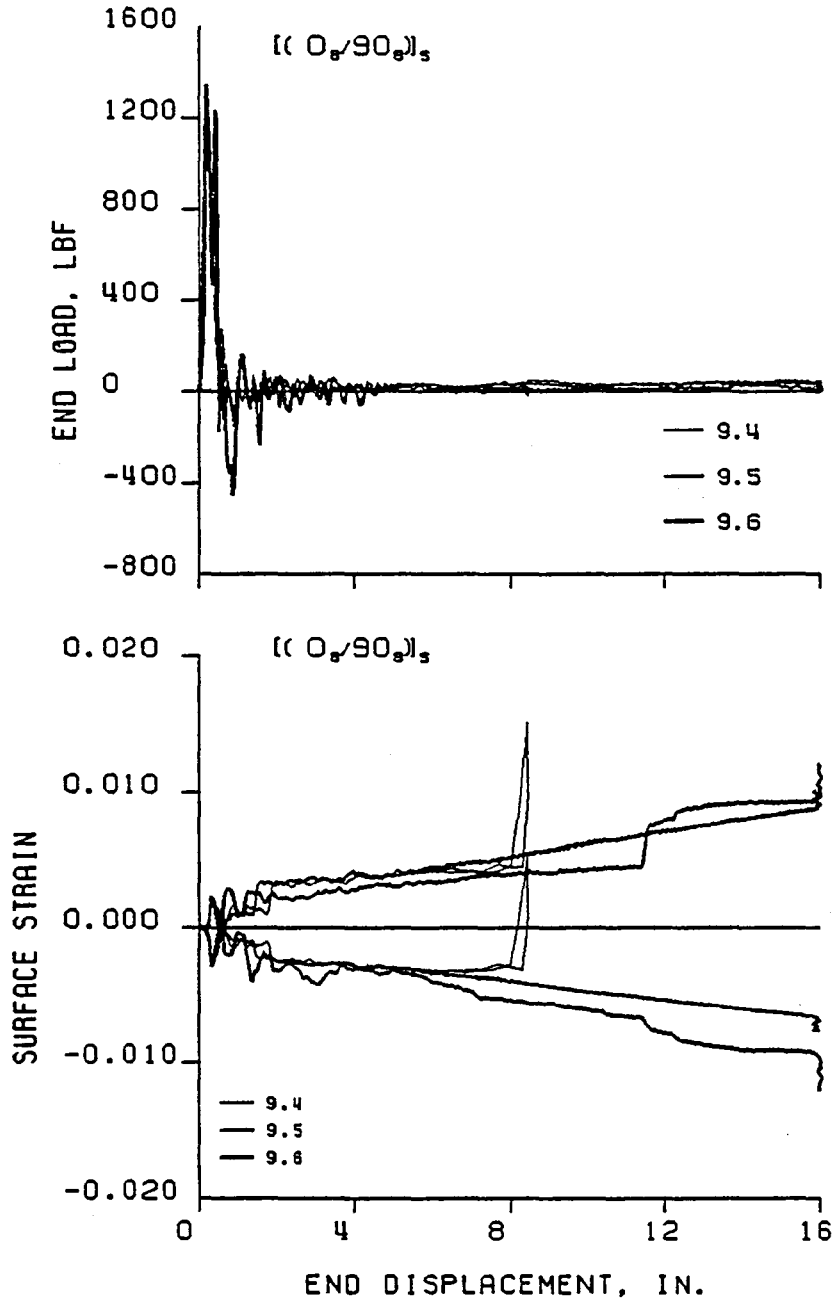
Figure 3.27   Dynamic Load and Strain vs. Displacement for the $(0_8/90_8)_s$ Laminates
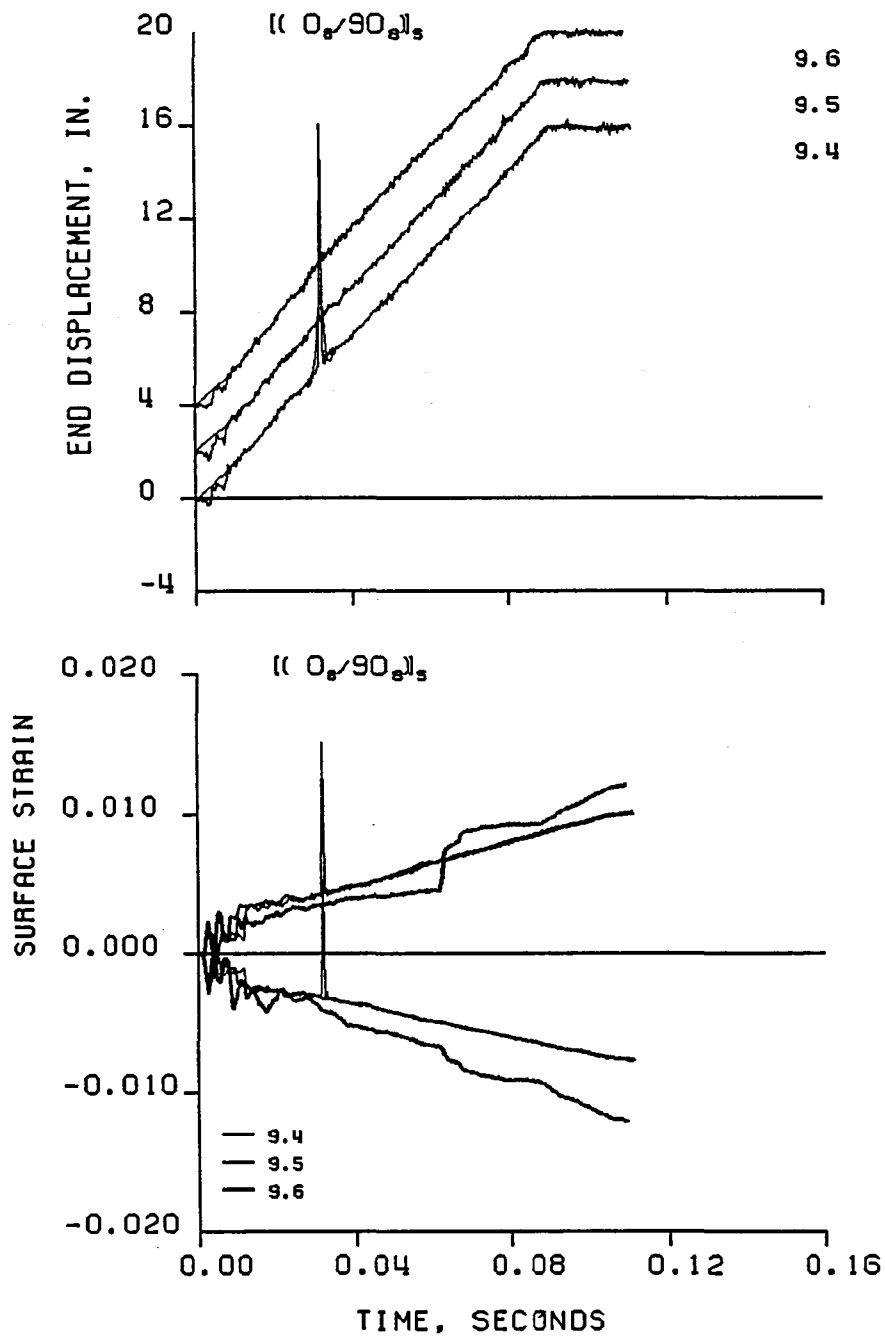
Figure 3.28   Dynamic Displacement and Strain vs. Time for the $(0_8/90_8)_s$ Laminates
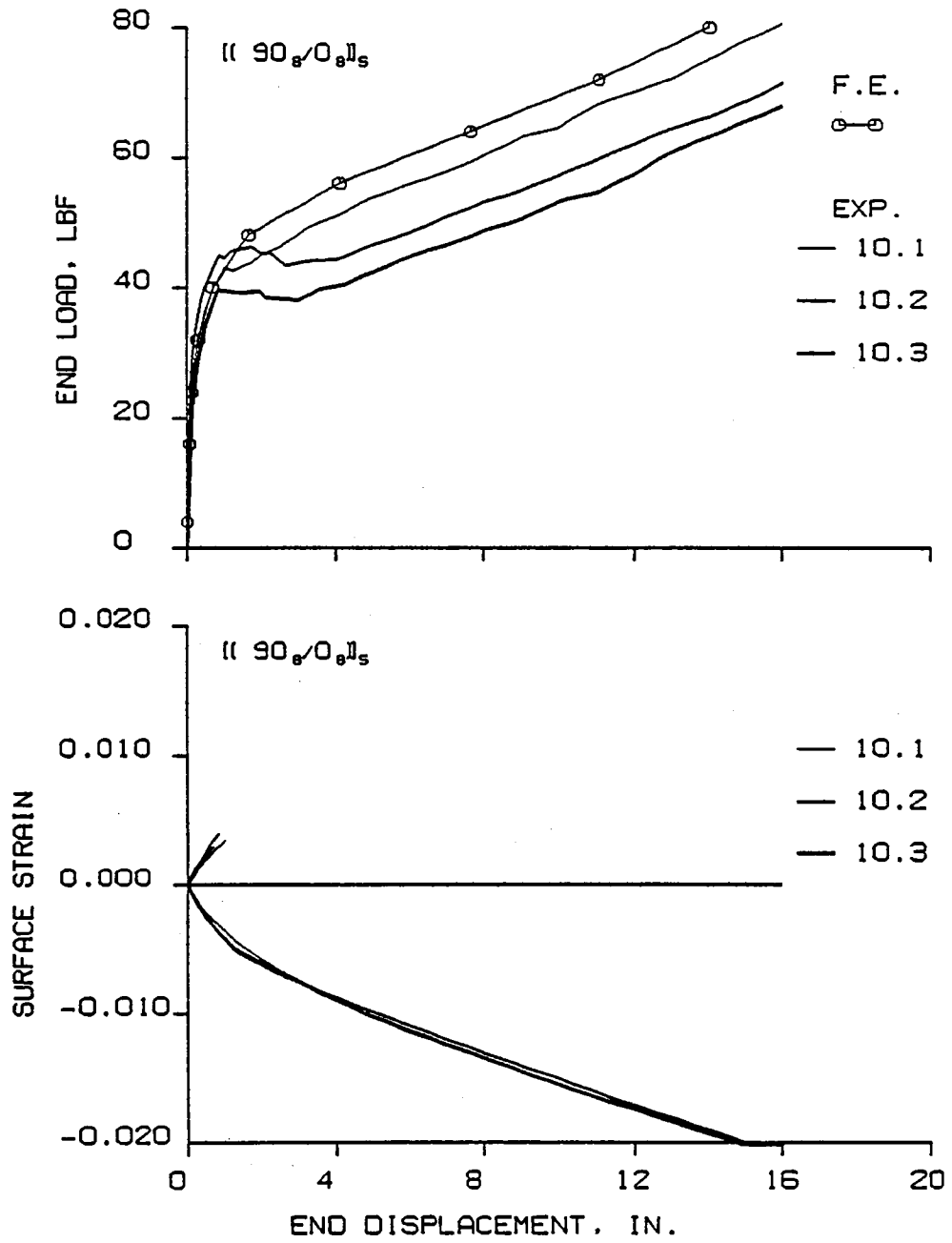
Figure 3.29   Static Load and Strain vs. Displacement for the $(90_8/0_8)_s$ Laminates
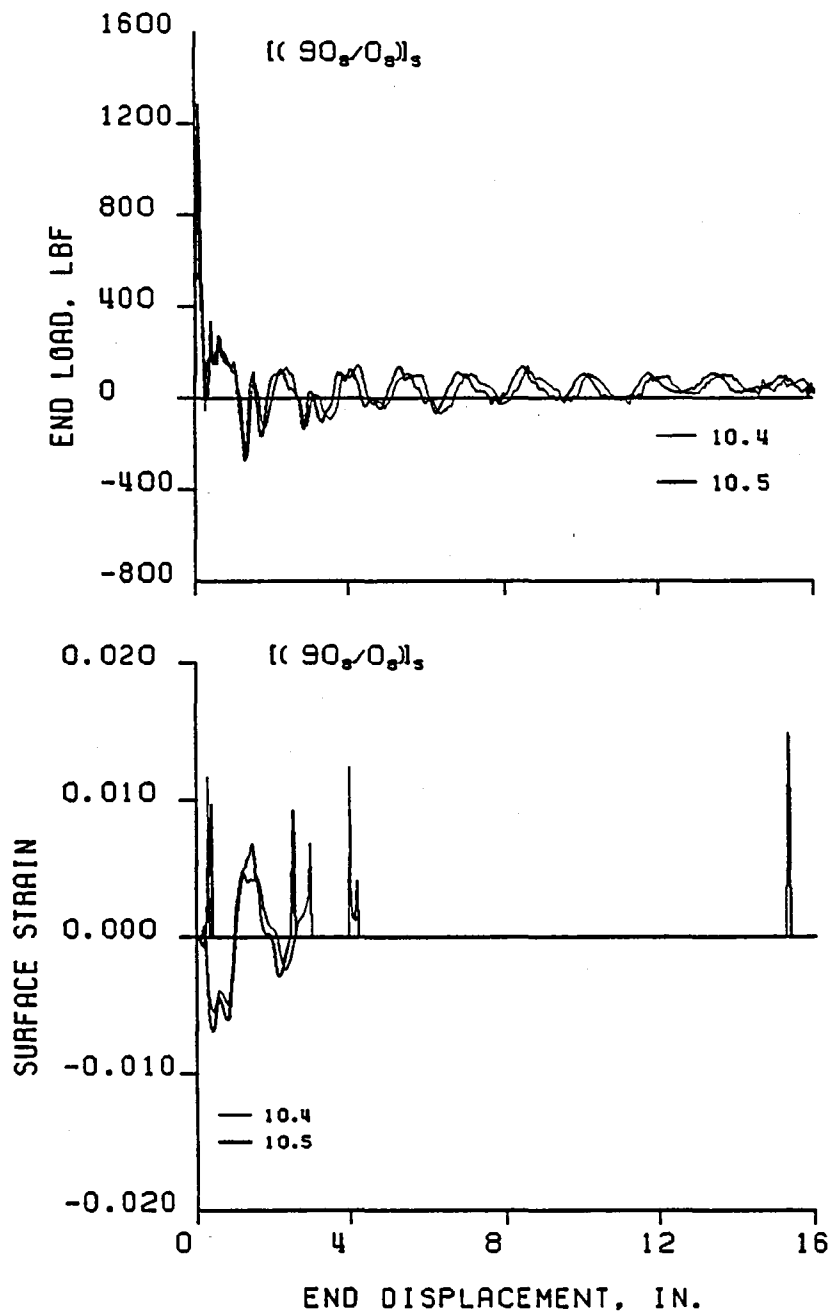
Figure 3.30   Dynamic Load and Strain vs. Displacement for the $(90_8/0_8)_s$ Laminates
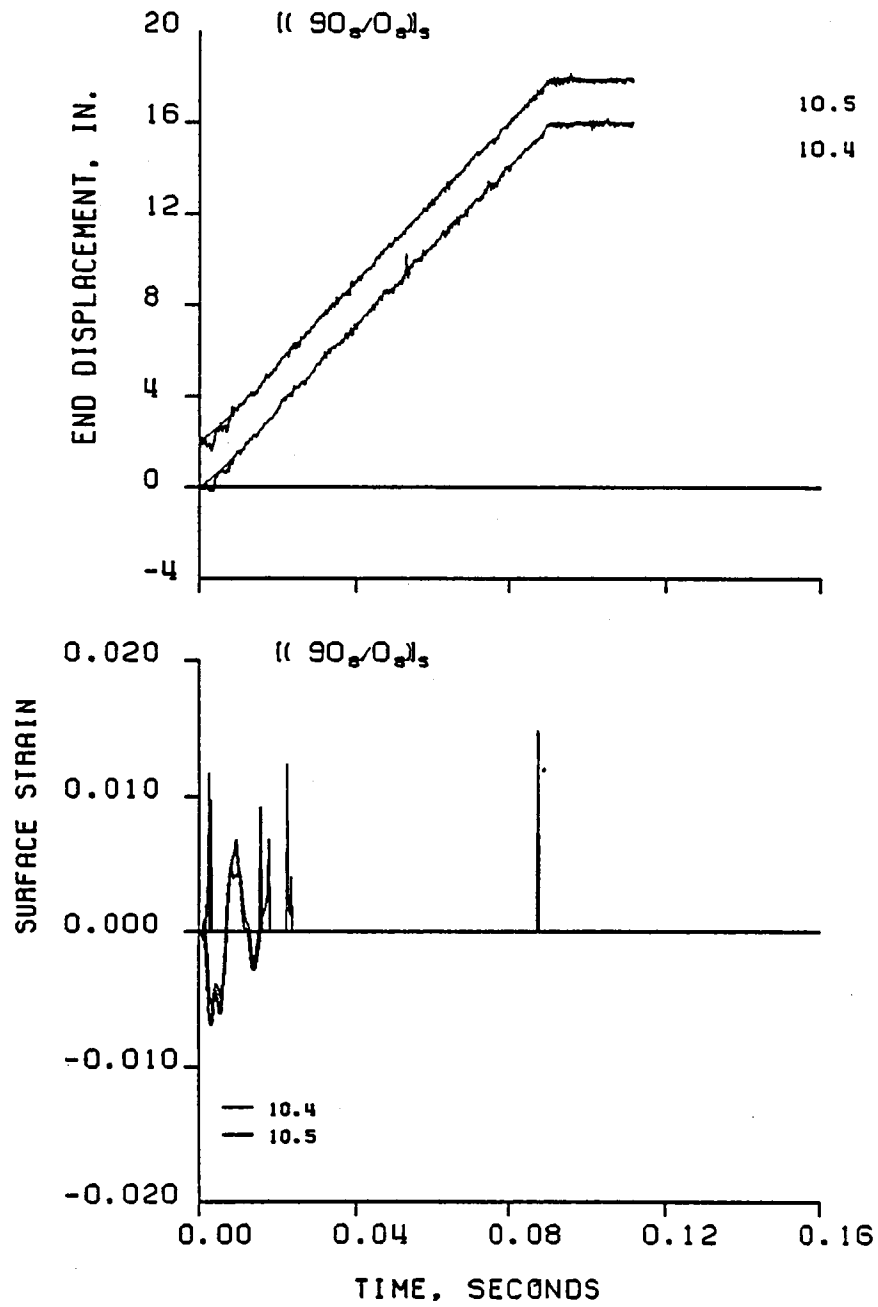
Figure 3.31   Dynamic Displacement and Strain vs. Time for the $(90_8/0_8)_s$ Laminates
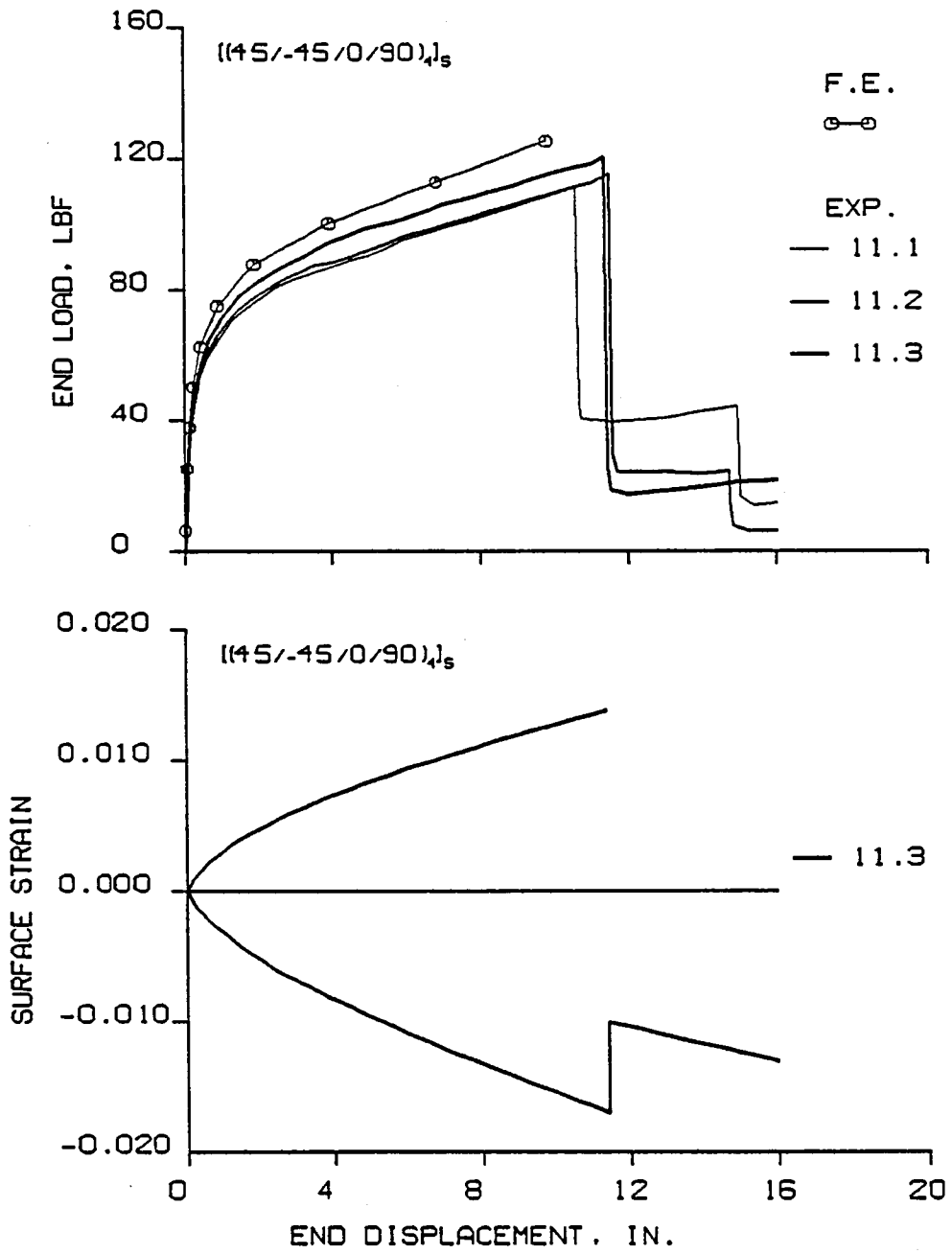
Figure 3.32   Static Load and Strain vs. Displacement for the
$[(45/-45/0/90)_4]_s$ Laminates
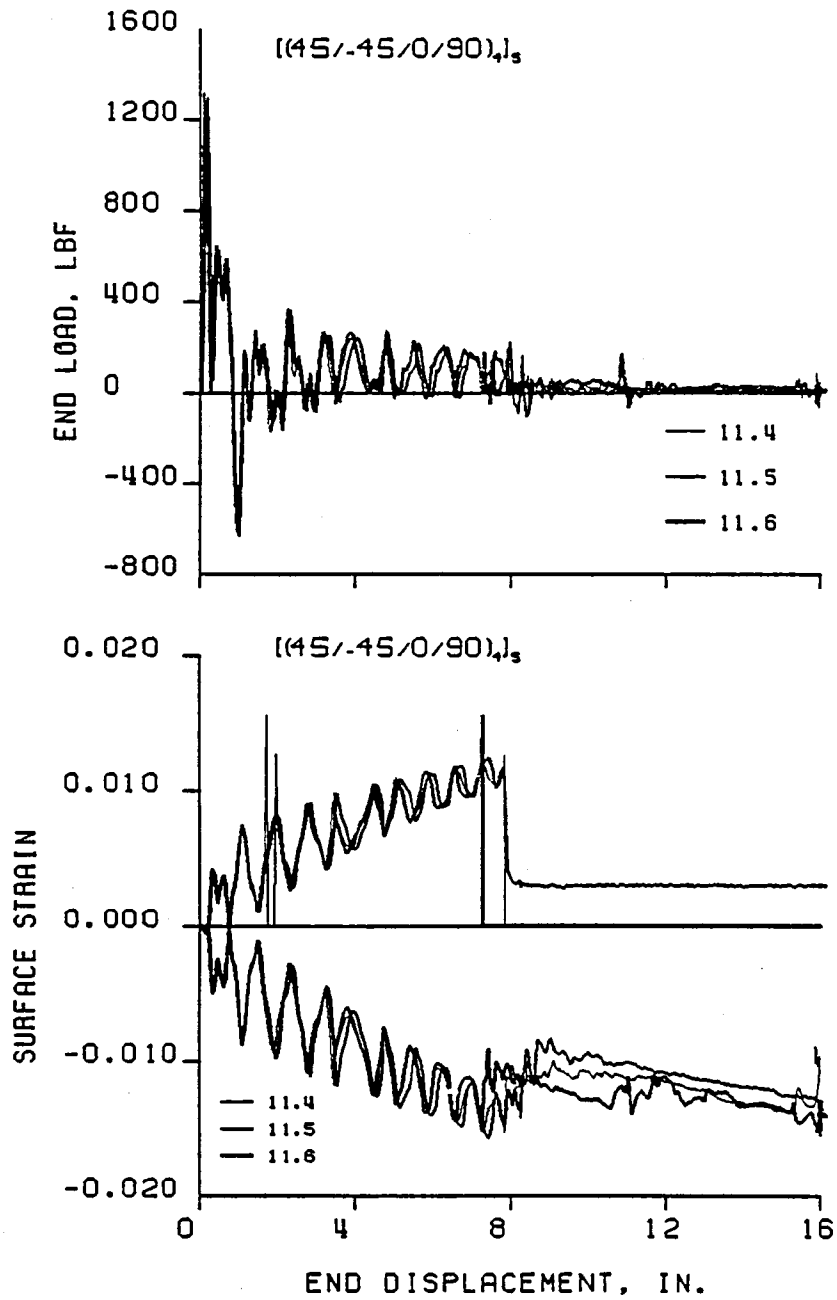
Figure 3.33   Dynamic Load and Strain vs. Displacement for the
$[(45/-45/0/90)_4]_s$ Laminates
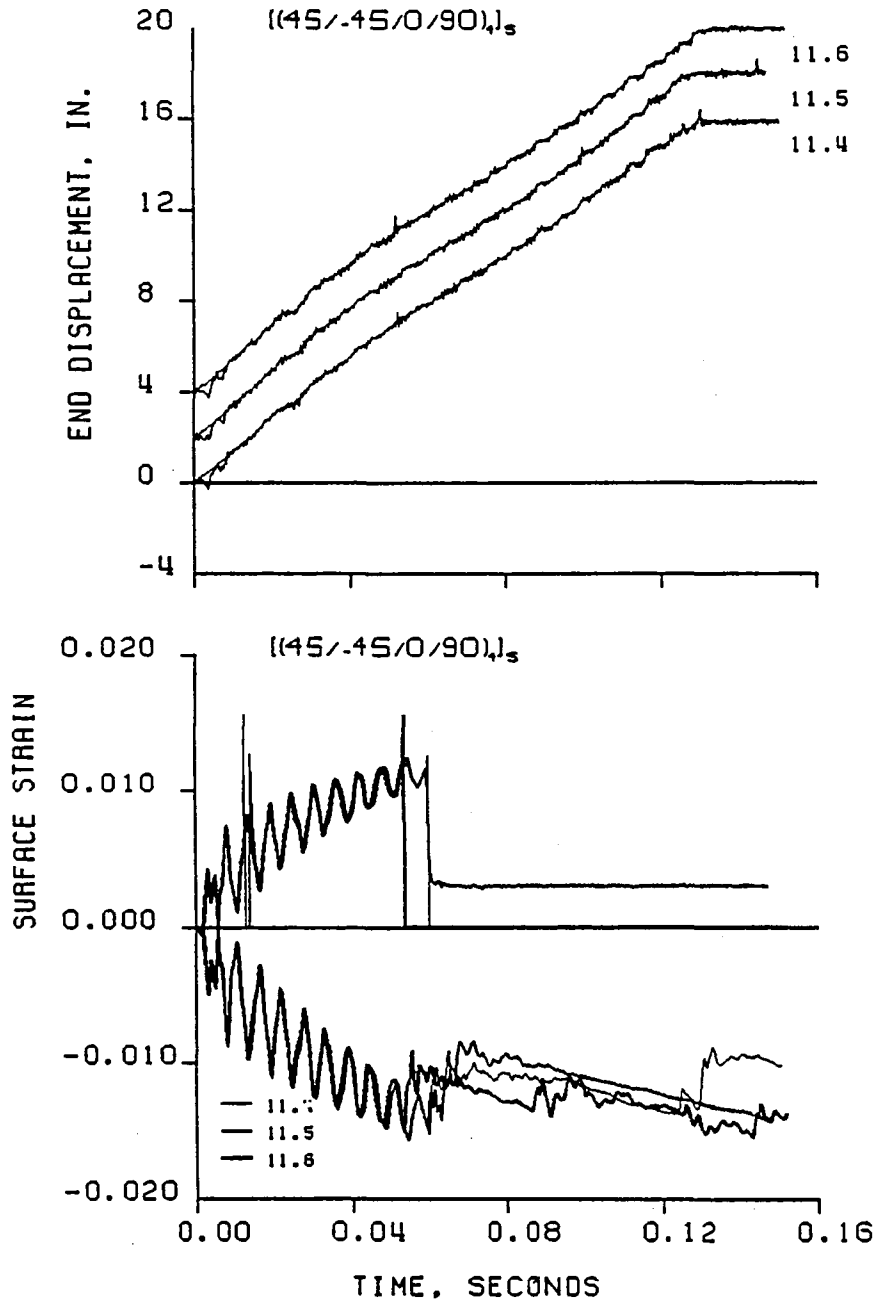
Figure 3.34   Dynamic Displacement and Strain vs. Time for the $[(45/-45/0/90)_4]_s$ Laminates
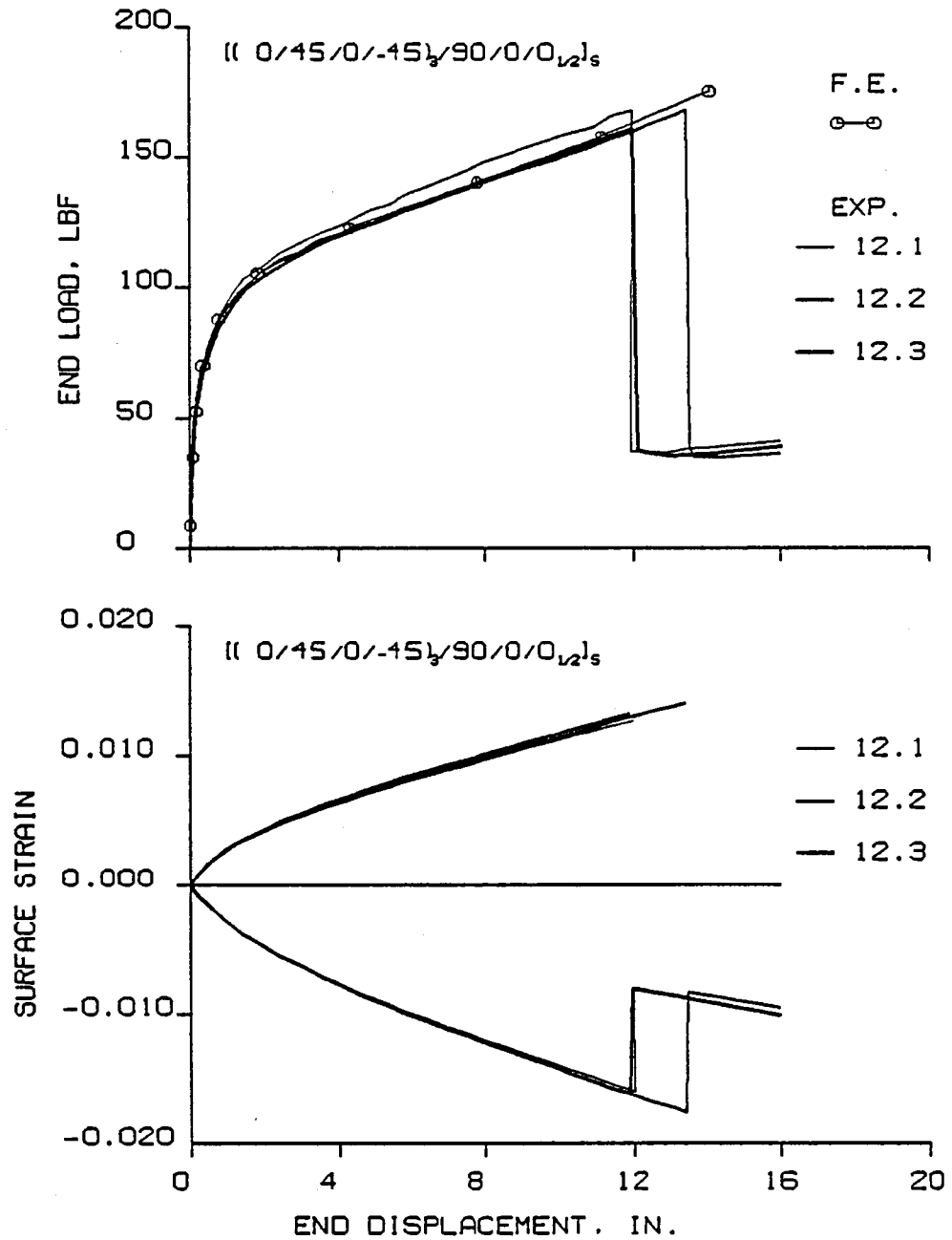
Figure 3.35   Static Load and Strain vs. Displacement for the $[(0/45/0-45)_3/90/0/0_{1/2}]_s$ Laminates
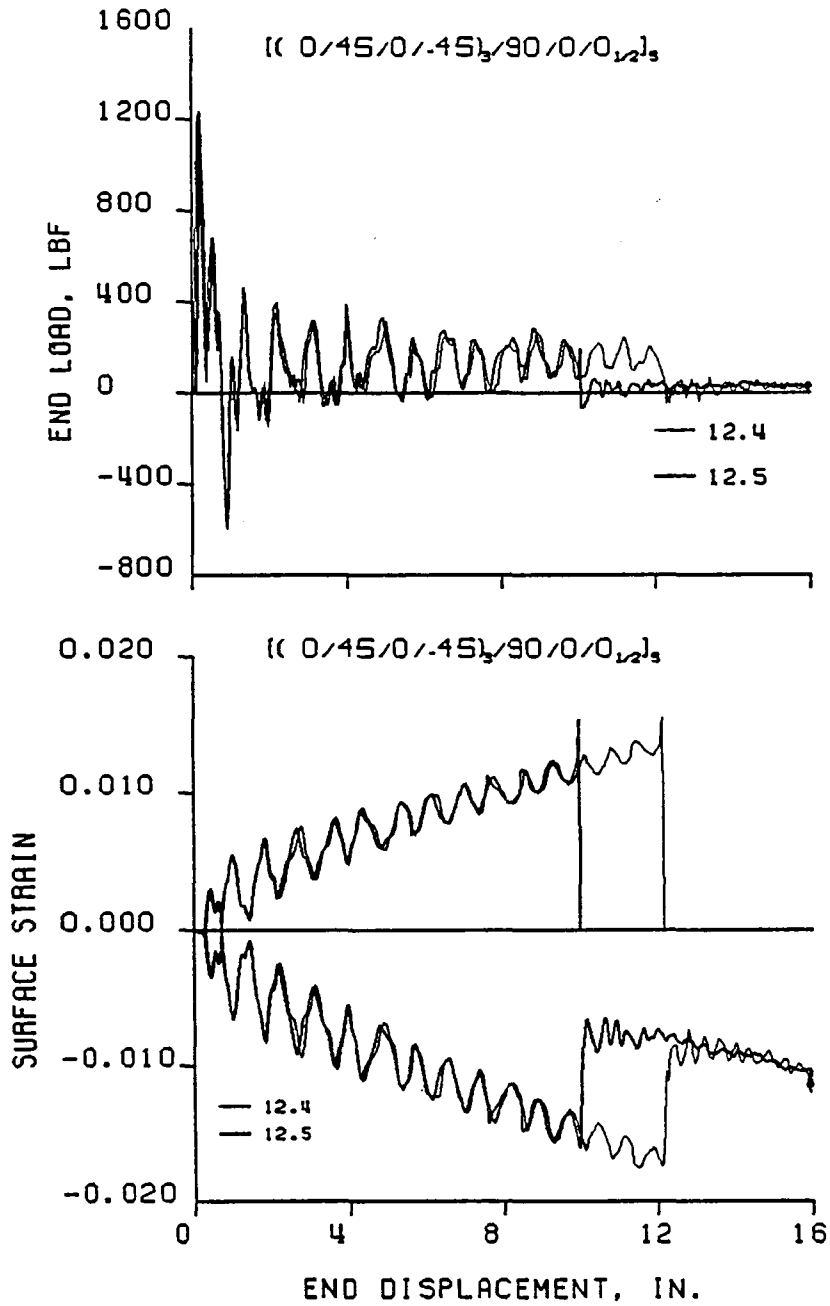
Figure 3.36 Dynamic Load and Strain vs. Displacement for the $[(0/45/0-45)_3/90/0/0_{1/2}]_s$ Laminates
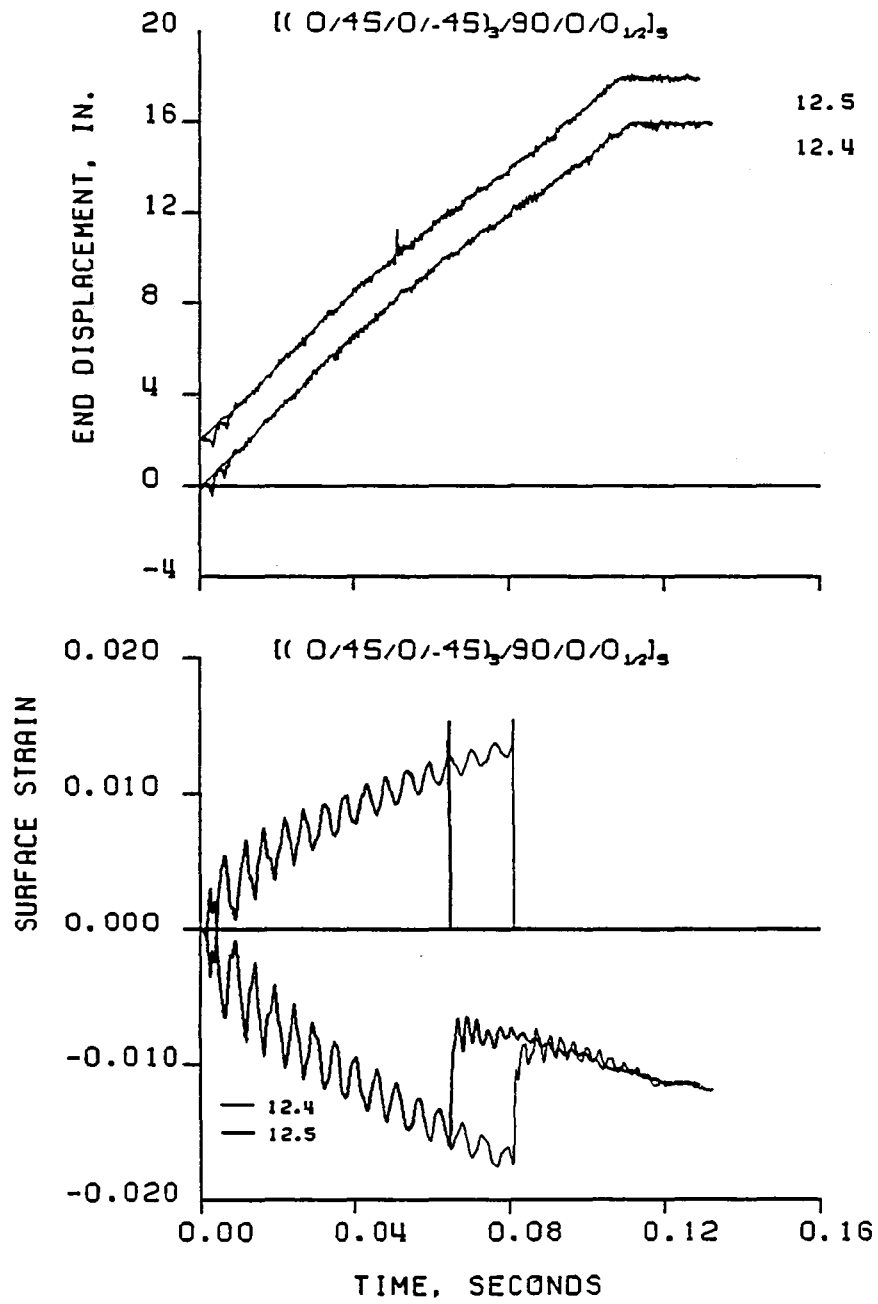
Figure 3.37   Dynamic Displacement and Strain vs. Time for the
$[(0/45/0-45)_3/90/0/0_{1/2}]_s$ Laminates

theoretical third mode natural frequency for a simply supported beam is also presented in table 3.1 for comparison. Reference 6 was used to compute the theoretical frequency. Table 3.1 demonstrates that the experimental and theoretical frequencies compared quite well. It is important to note that even though the initial impact velocities were only 19.6 ft/sec., the maximum strain rates were on the order of 5 in./in./sec. because of the third mode vibratory response. The maximum rate occurred during initial snap-through of the third mode "W" shape. If there had been no vibratory response, the maximum strain rate would have been less. Notice that the strain-time response of laminates 5 and 7 exhibit vibratory frequencies higher than the third mode, in addition to the third mode.

Laminate 9 failed very soon after impact in the dynamic tests and no sustained vibratory motion occurred. The failure mode was unusual and will be discussed in the next section. However, fig. 3.28 shows the characteristic initial reverse value of strain indicating that the vibratory response was excited. Due to early failure, it never fully developed. Laminate 10, figs. 3.30 and 3.31, actually did show the 3rd mode response. However, the surface plies failed soon after impact so the response was not measured by the strain gauges. The vibratory response is exhibited in the load-time history shown in fig. E.4 in Appendix E and it is quantified in table 3.1.

TABLE **3.1**
COMPARISON OF MEASURED VIBRATORY FREQUENCY
AND THEORETICAL THIRD NATURAL MODE

LAMINATE NUMBER	MEASURED FREQUENCY (HZ)	THEORETICAL NATURAL FREQUENCY (HZ)
1	227	237
2	223	231
3	205	207
4	176	178
5	155	158
6		
7	152	149
8	203	206
9	--*	254
10	112	120
11	172	177
12	187	185

*no oscillatory motion observed, immediate failure after impact.

Failure Modes

From examination of the static and dynamic load-displacement relations, and from the post-test examination of the specimens, it can be said that with the exception of two laminate types, the failure modes of the laminates under static or dynamic loading were identical. As had been indicated, the two exceptions to this were the $[0_8/90_8]_s$ and $[90_8/0_8]$ laminates, laminates 9 and 10. These laminates exhibited a different dynamic failure mode than was observed with the static loadings. A detailed description of the failure modes of each laminate will be presented in the next section.

Strain Response

Examination of the strain response of the laminates revealed that at a given load level, a given displacement level, or at a given time, the compressive surface strain was always greater in magnitude than the tension surface strain. Analysis shows that the compression strain due to the axial load should have been several orders of magnitudes less than the bending strains and effectively the beam was in a state of pure bending. With pure bending the magnitude of the tensile and compressive strains should have been the same. For example, in the $((90/0/-90)_5)_s$ beam, the compressive surface strain was only 5% greater than the tension strain, as shown in fig. 3.20 and fig.3.21. On the other hand, fig. 3.11 and fig. 3.12 show that for the $[(30/0/-30)_5]_s$ laminate, laminate 3, the compressive surface strain was more than 40% greater than the tension strain. Variation of the tensile and compressive

strains for the other laminates was somewhere between the 5% and the 40% levels. Understanding this phenomena will be important to developing a failure criteria. Additional tests were carried out to further understand this behavior of the beam specimens and the results will be discussed in the next chapter.

3.2.3 Failure Mode Description

By examining the static and dynamic load-displacement and load-strain relations, along with observing the movies and the failed specimens, the failure modes of each laminate can be described. In this section the static and dynamic failure modes will be assumed to be the same if no differences are indicated. Figure 3.38 shows a drawing of the coordinate system used in the description of the cracking, delamination, and failure of the laminates.

Laminate 1 $[0]_{30}$

The unidirectional laminate exhibited a single devastating failure event. Figure 3.39 shows a frame of the failure event under dynamic loading. Note the simultaneous failures on the tension and compression sides of the beam. A similar failure mode was observed in the static tests. This was the only laminate for which compression failures were observed. On the tension side a crack propagated perpendicular to the fibers (the y direction in fig. 3.38), across the entire width of the laminate, completely failing ten plies. On the compression side a crack propagated only partially across the width, in the y direction, and 10 plies deep. The center plies of the laminate, near the neutral surface,
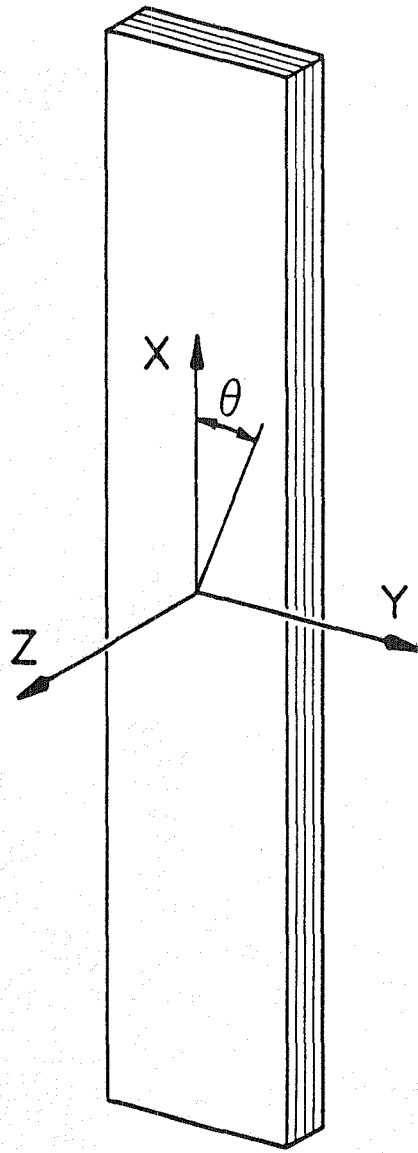
Figure 3.38   Beam Coordinate System
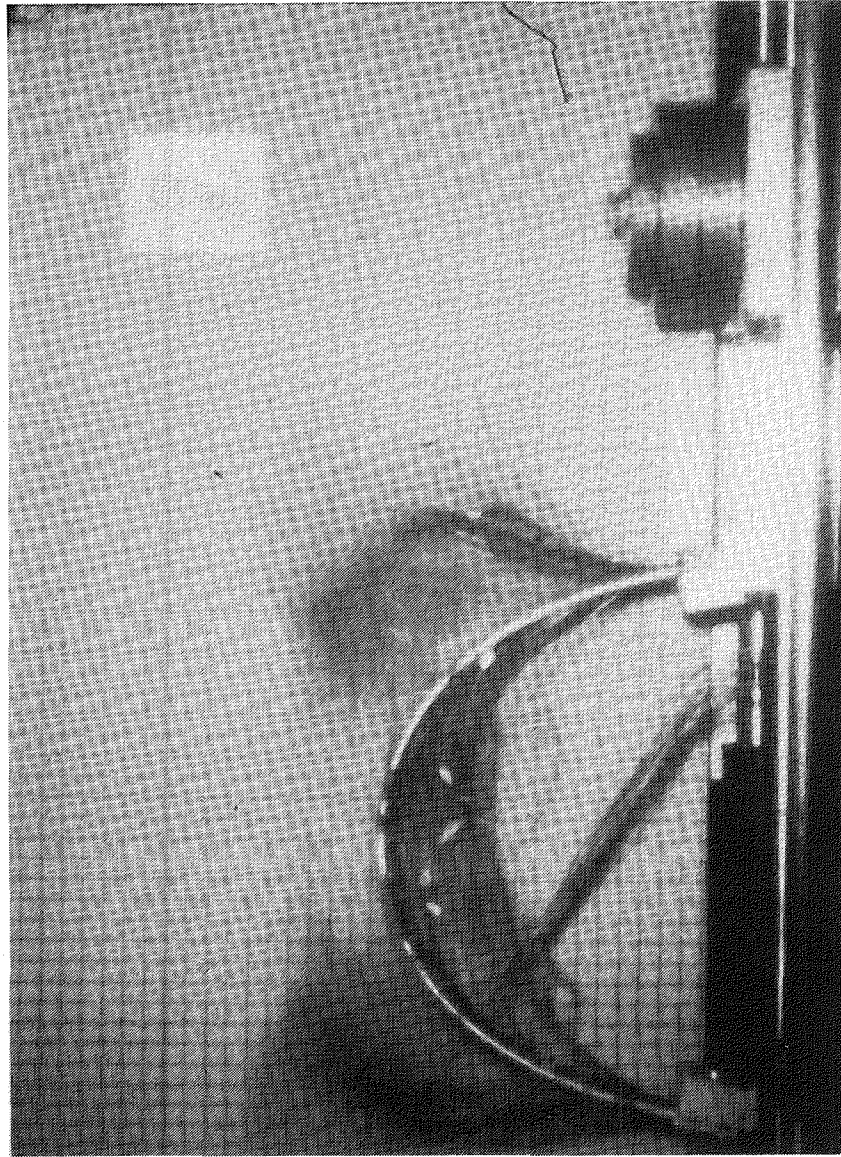
Figure 3.39 Failure Mode of Unidirectional Specimen

had no fiber failures. In the portion of the laminate which had fiber failures, the fibers broomed and splintered. In the portion of the laminate with no fiber failures, matrix cracks in the x-z plane propagated along the length, presumably initiating on the compression side of the laminate due to widthwise Poisson tensile effects.

Laminate 2 $[(15/0/-15)_5]_s$

The load-displacement and the strain-displacement relations show that $[(15/0/-15)_5]_s$ laminates exhibited from 3 to 6 failure events. A typical failure event consisted of the simultaneous failure of a group of 2 to 6 plies on the tension side of the beam. This group of failed plies would then delaiminate at least 8 in. along the length of the beam. By examining the failed specimens, it appeared that a crack initiated parallel to the fibers in the outer 15° ply. The crack propagated along the 15° direction from one edge of the beam to the other, and it propagated downward in the z direction, to a depth of 1 to 5 plies, before arresting. As the crack propagated downward, the fibers in the 0° plies and the -15° plies fractured. So, the 0° ply and the -15° ply failed on a 15° angle. Exactly how the other failure events initiated is not clear. However, it is felt they were similar to the first failure event. The remaining compression side (0.80 in., ≈50%) of the laminate was undamaged.

Laminate 3 $[(30/0/-30)_5]_s$

The $[(30/0/-30)_5]_s$ laminates exhibited 2 or 3 failure events, each event involving typically 5 to 10 plies. These ply groups then

delaminated at least 10 in. along the length of the beam. Again it appeared that a crack initiated parallel to the fibers in the outer 30° ply. The crack propagated along the 30° direction from one edge of the beam to the other. In some of the specimens the crack turned to propagate along the 0° direction (x direction in fig. 3.38) for a short distance and then turned back to the 30° direction. The crack propagated downward in the z direction from 3 to 5 plies, fracturing the fibers in the 0° and 30° plies before arresting. The remaining compression side of the laminate (.70 in. ≈45%) was undamaged.

Laminate 4 $[(45/0/-45/)_5]_s$

Although the post-failure inspection of the static and dynamic $[(45/0/-45/)_5]_s$ laminates revealed no differences in the failure modes, the strain responses shown in fig. 3.14 and fig. 3.15 indicated different behavior between the static and dynamic specimens. The post-failure inspection of the static and dynamic specimens showed many matrix cracks in both the 45° and the -45° lamina which surround the 0° lamina. Failure of the 0° lamina probably initiated near a matrix crack in a 45° lamina, but the crack direction in the 0° lamina followed no preferred direction. In some of the 0° laminae the crack alternately followed 45°, -45° and 0° directions. In others the crack followed a random jagged line across the width. Examination of fig. 3.16 indicates a unique dynamic strain response for this laminate. The unique response is especially evident in the response of specimens 4.4 and 4.6, and to a lesser degree in specimen 4.5. Notice that at the point of first ply failure, when the tensile strain response terminated, there is no sharp

drop in the compressive surface strain, as was seen in the other laminates. Instead, the compressive surface strain remained nearly constant for the rest of the event. This suggests that the failure mechanism for this laminate could be different from the ones described to this point. With this laminate, at the initiation of tensile side matrix cracks, which destroyed the tensile strain guage, the laminate did not fail and immediately lose load-carrying laminae. Instead the tensile side laminae yielded but remained intact and continued to carry some load as the laminae failed progressively throughout the remainder of the event. This type of failure mode for a 45° angle-ply laminate has been reported in the literature (ref. 7). This response was not evident in the static data. However, in the dynamic case, the yielding-progressive failure response lasted a mere 0.08 sec, from the initial tensile side matrix cracks, until the end of the dynamic event. During this time interval, the end of the beam displaced 8 in. It is possible that in the displacement controlled static tests, the failure event lasted for a similar finite time period, even though the beam would have displaced less than 0.01 in. at the quasi-static displacement rate. So, the mode of failure in the static and dynamic tests could have been the same, even though the recorded strain response was quite different. An identical static and dynamic failure mode is consistent with the information learned from the post-failure examination.

Laminate 5 $[(60/0/-60)_5]_s$

The $[(60/0/-60)_5]_s$ laminate exhibited an initial major failure event and a single minor subsequent event. From examination of the

strain responses, the failure events appear to be instantaneous. In the single major event, an outer group of plies failed. There were many parallel matrix cracks occurring in the 60° or -60° plies, and fiber failures on the 0° plies and some of the 60° plies. In the subsequent minor event the plies failed only partially. This failure mode is illustrated in fig. 3.40. A matrix crack occurred in the 60° direction and then the crack propagated downward only through the 0° lamina. The -60° lamina remained intact. The -60° fibers required the crack in the failed plies to open in extensional and shear modes. The -60° lamina delaminated near the crack but remained attached to the failed plies, bridging the crack.

Laminate 7 [(90/0/90)$_5$]$_S$

The [(90/0/90)$_5$]$_S$ laminate exhibited an initial major failure event and a subsequent single minor event. In the major event, the cracks initiated parallel to the fibers in the outer 90° ply. Then the crack propagated downward in the z direction, fracturing fibers in the 0° plies. The failed ply groups then delaminated 5 to 6 in. along the x direction.

Laminate 8 [(0/90)$_8$]$_S$

The [(0/90)$_8$]$_S$ laminate had only a single failure event. The crack propogated across the plies and downward, similar to laminate 7. One of the static and one of the dynamic specimens had some of the 90° plies near the neutral axis damaged with matrix cracks. There the adjacent 0° plies remained undamaged.
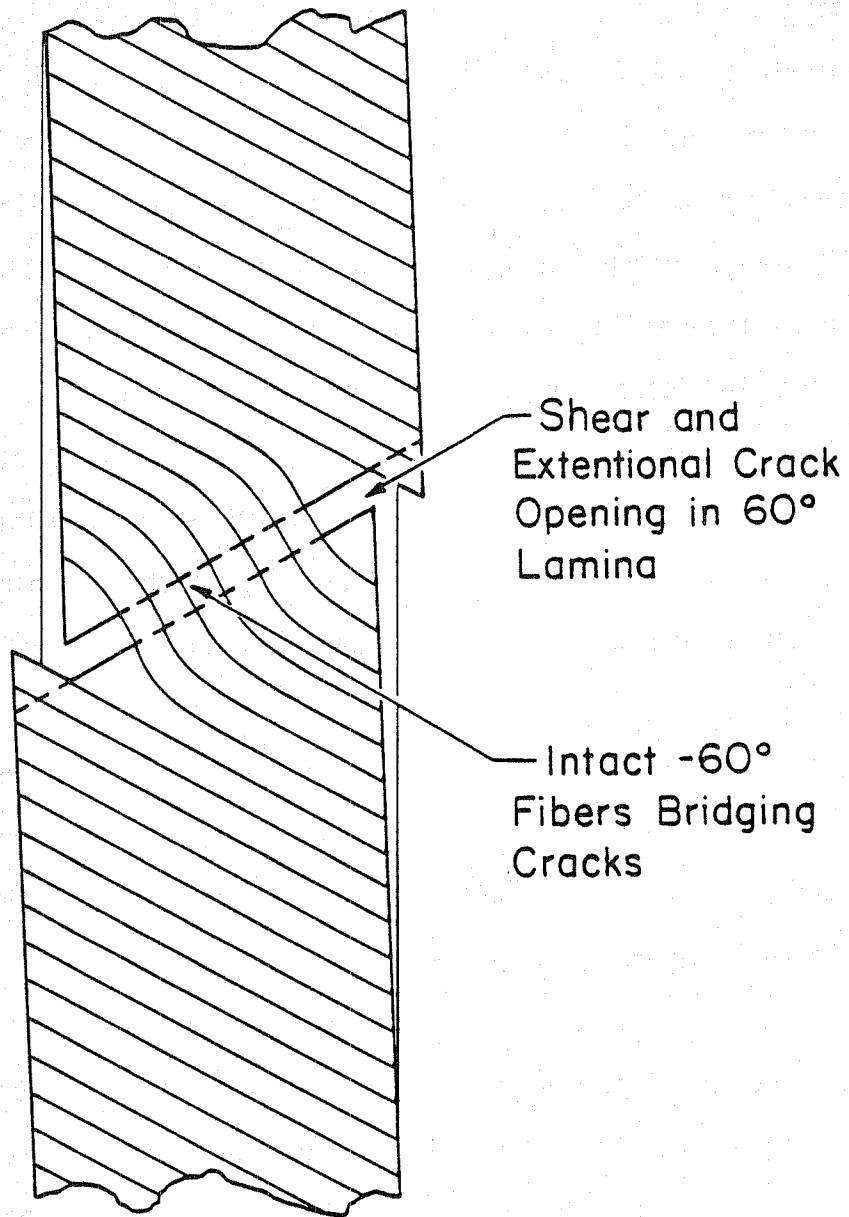
Figure 3.40   Sketch of Partial Failure Mode in $[(60/0/-60)_5]_s$ Laminates

Laminate 9 $[0_8/90_8]_s$

Laminate 9 had a completely different failure mode in the dynamic case than in the static case. Statically, specimen 9.1 and 9.2 exhibited fiber failures, and matrix cracks in the x-z plane, in the outer 0° lamina groups on the tension and compression sides of the beam. Even though this was a static test, as soon as the 0° fibers failed, the 90° core lamina immediately broke apart in chunks and scattered about the room. Specimen 9.3, which failed at an axial displacement level almost 4 in. less than the others, exhibited no fiber failures. However, there were matrix cracks, in the x-z plane, in the outer 0° lamina groups and the 90° lamina again dispersed about the room.

In contrast, under dynamic loads there was no failure in the outer 0° lamina groups. Soon after the impact event, a delamination initiated between the group of 0° lamina on the compression side of the beam and the 90° core laminae. The delamination propagated along the entire length of the beam. The 90° core laminae remained attached to the 0° lamina on the tension side of the beam. The laminate acted as two separate thin beams. Figure 3.41 shows a sequence of four frames at the initiation of the delamination. Notice that the delamination initiated between the center peak of initial "W" shape and the inflection point of that peak, i.e., about at the quarter span near the top of the beam. The construction of laminate 9 produces interlaminar tensile σ_z stresses at the free edge when the laminate is placed under tension. These are caused by the Poisson ratio mismatch of the 90° core and the 0° outer
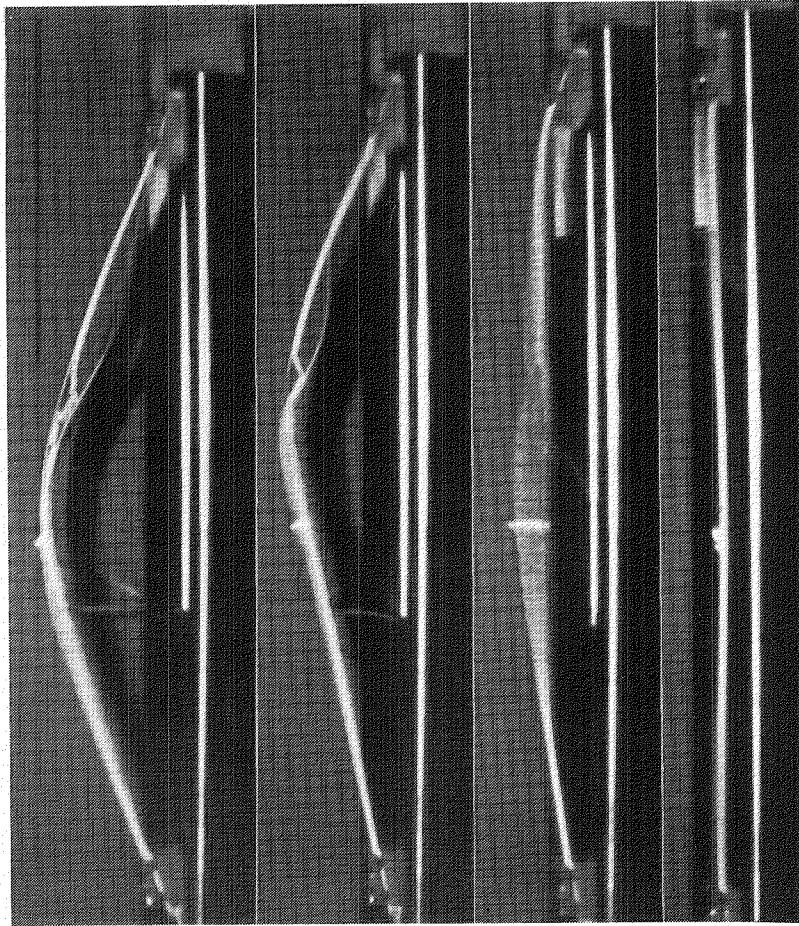
Figure 3.41   Dynamic Failure Mode of $(0_8/90_8)_s$

lamina group. The top half of the plies in the laminate were under tension in the center peak region. In addition, due to the deformed shape, the τ_{xz} stresses reach a maximum at the inflection point of the center peak. And due to the high amplitude load spike shown in fig. 3.27 the stresses are particularly high at this time in the event. Although the τ_{xz} stresses were similar for the other laminate types, laminate 9 had clustered plies. The interlaminar σ_z stresses are much greater in orthotropic laminates which contain clustered plies. Only in the dynamic testing of laminate 9 did large values of both the τ_{xz} and σ_z stresses occur simultaneously. Therefore it was thought that the combination of the σ_z and τ_{xz} stresses initiated the delamination in this particular laminate type.

Laminate 10 $[90_8/0_8]_s$

Laminate 10 exhibited differences in the failure modes between the dynamic and static loadings. Under static loading matrix cracks appeared in the 90° plys on the tension side with spacing of 1 to 2 inches. However, the 90° laminae remained attached to the 0° core. No matrix cracks appeared on the compression side. Thus the 90° laminae on the compression side contributed to the laminate stiffness. Notice the unusually high strain values of over 2% in fig. 3.29. This exceeded the range of the recording apparatus. However under dynamic loading both of the 90° outer lamina groups separated in chunks from the 0° core. Therefore the beam acted as a single thin undirectional beam. This 90° lamina separation was probably due to the inertial force and reverse curvature from the excited vibratory motion.

Laminate 11 $[(45/-45/0/90)_4]_s$

The strain-displacement relations for laminate 11 showed that it exhibited behavior similar to laminate 4. However with this laminate the failure mode was not as distinctive. Some of the dynamic specimens had several minor sharp drops in the compressive strain value, in addition to the plastic hinge behavior.

Laminate 12 $[(0/45/0/-45)_3/90/0/0_{1/2}]_s$

Laminate 12 failed with one failure event, exhibiting instantaneous ply failures and longitudinal delaminations. The ply failures propagated more or less in a perpendicular fashion across the beam, but with no preferred direction, similar to a paper tear. Figure 3.42 shows a frame from the failure event of this laminate type under dynamic loading.

3.2.4 Comparison of Static and Dynamic Tests

One of the most dramatic comparisons between the static and dynamic results concerns the end displacement at initial failure. For virtually all laminates, the value of end displacement at failure was less for the dynamic cases than it was for the static cases. Likewise, the strain level at failure was always lower in the dynamic cases than in the static cases. The strains are, of course, related to the end displacements. Even though inertia and the third mode oscillation make the relation less direct for the dynamic case than for the static case, it is felt to be significant that strain rate or displacement rate appears to influence failure strains.
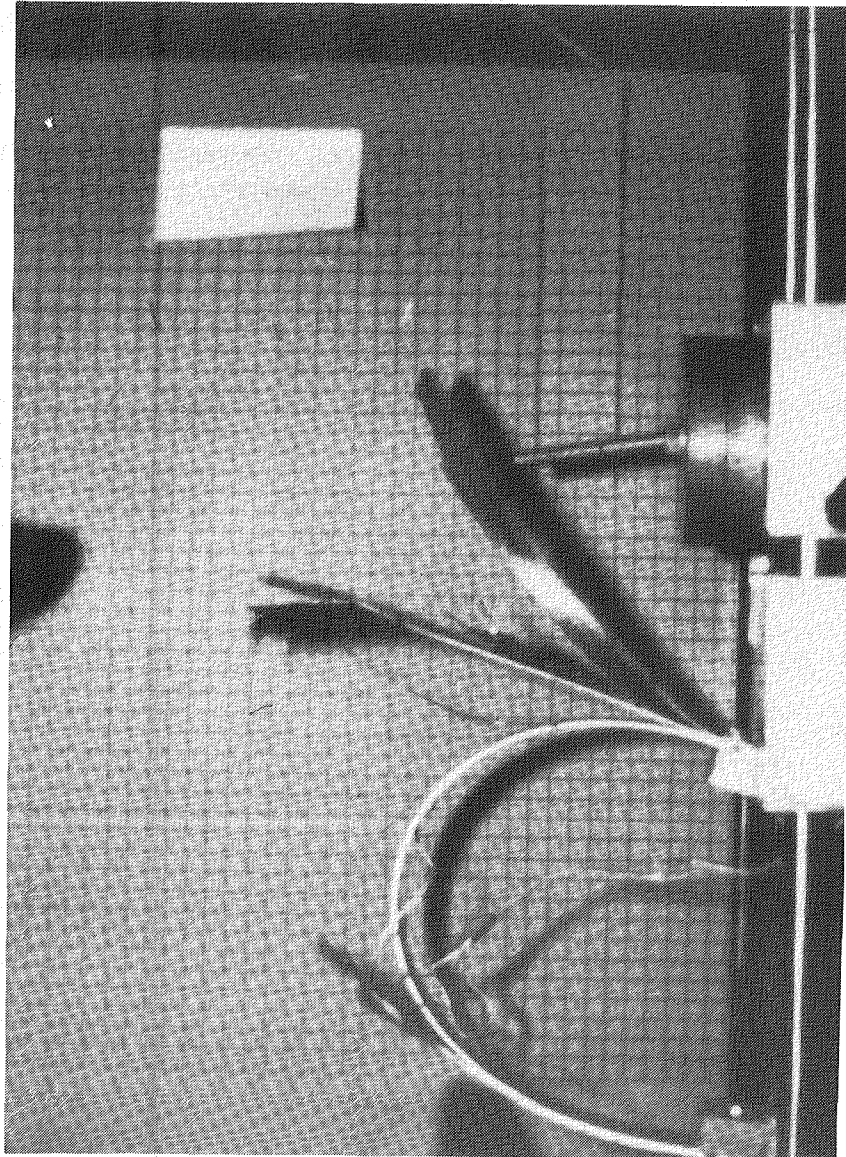
Figure 3.42   Failure Mode of $[(0/45/0/-45)_3/90/0/_{1/2}]_s$

To further compare the static and dynamic events, their end load vs. end displacement relations were integrated. These integrated relations are presented in fig. 3.43 through fig. 3.48. These integrals are associated with work done by the force at the top of the beam. This type of relation was explored as a method of determining if there were any energy absorbing mechanisms displayed in the dynamic response that were not evident in the static response. In addition, the integral effectively smoothed the dynamic load repsonse which allowed for comparisons to the already smooth static load-response.

On the figures the vertical axis gives the work required to displace the beam an amount given on the horizontal axis. The points on the work-displacement relation where the slopes abruptly change correspond to displacement values at which failure occurred. Again laminates 9 and 10 showed unusual differences in the static and dynamic responses and will be discussed separately.

As a group, all laminates except laminates 9 and 10 showed similar static and dynamic end load work vs. displacement relations. However, a close examination of the relations reveals there were some differences between the static and dynamic responses. This can be seen by examining fig. 3.43, for example. For the first inch of end displacement, the static and dynamic relations are divergent. The work required to displace the beam axially through the first 3/4 in. is greater in the dynamic tests than in the static tests as a result of the inertia of the beam resisting deformation more in the dynamic case. However, after the motion begins, it appears that overall, the work required to displace the beam dynamically a given increment is equivalent to the work
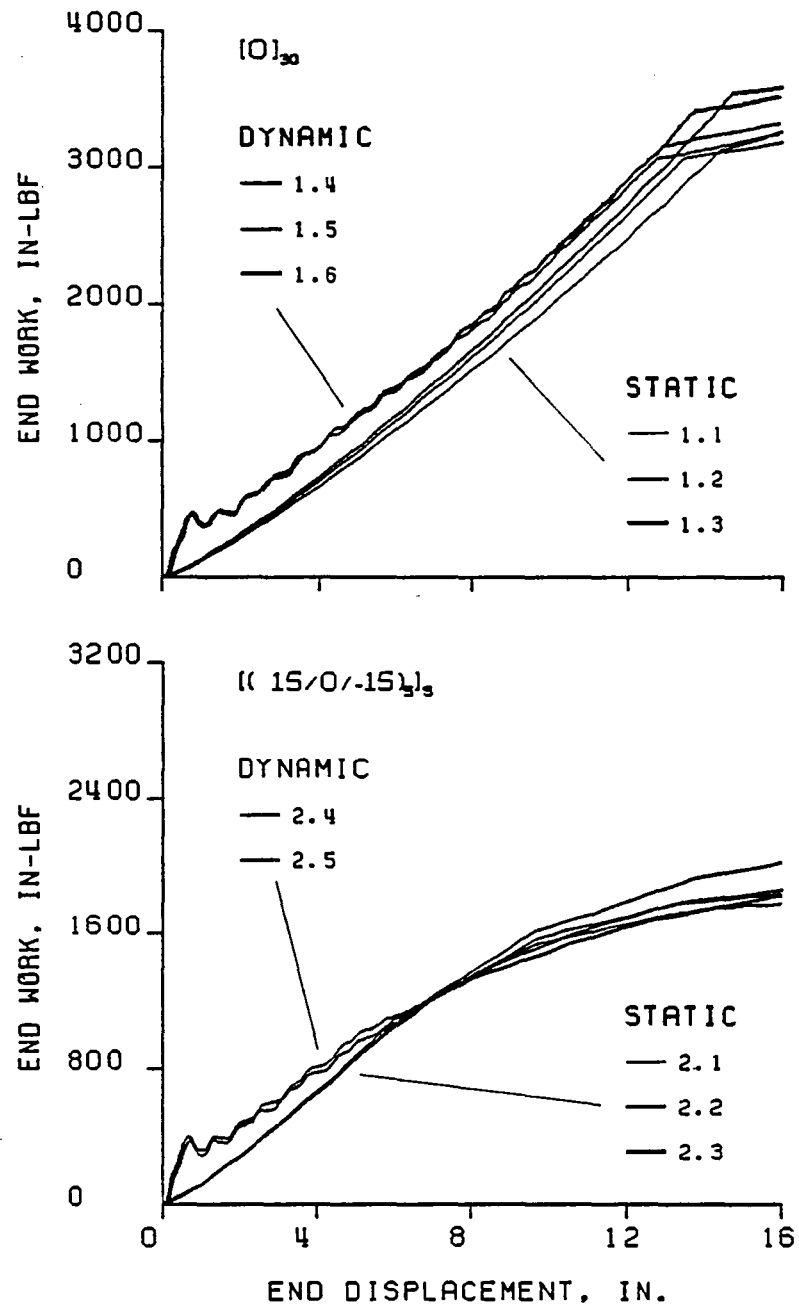
Figure 3.43   End Load Work vs. Displacement for the $[0]_{30}$ and $[(15/0/-15)_5]_s$ Laminates
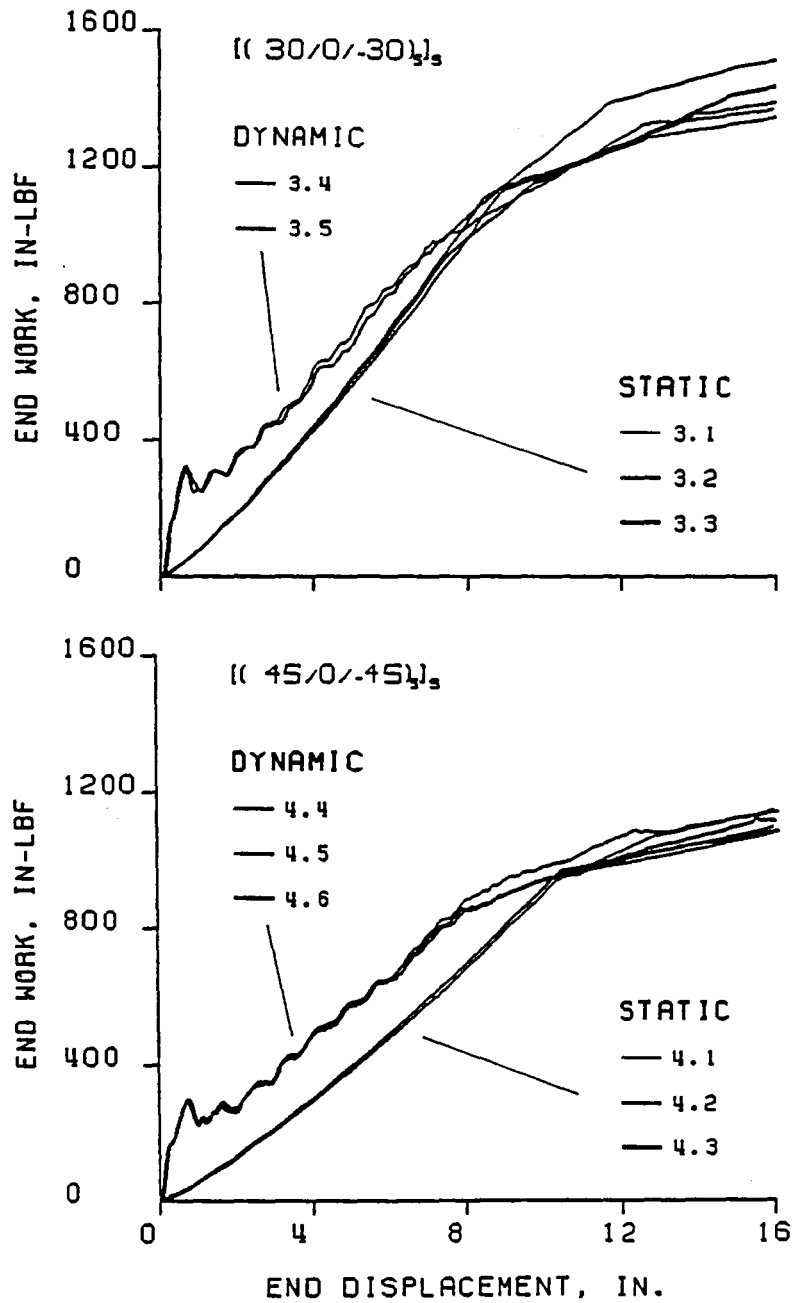
Figure 3.44   End Load Work vs. Displacement for the [(30/0/-30)₅]ₛ and [(45/0/-45)₅]ₛ Laminates
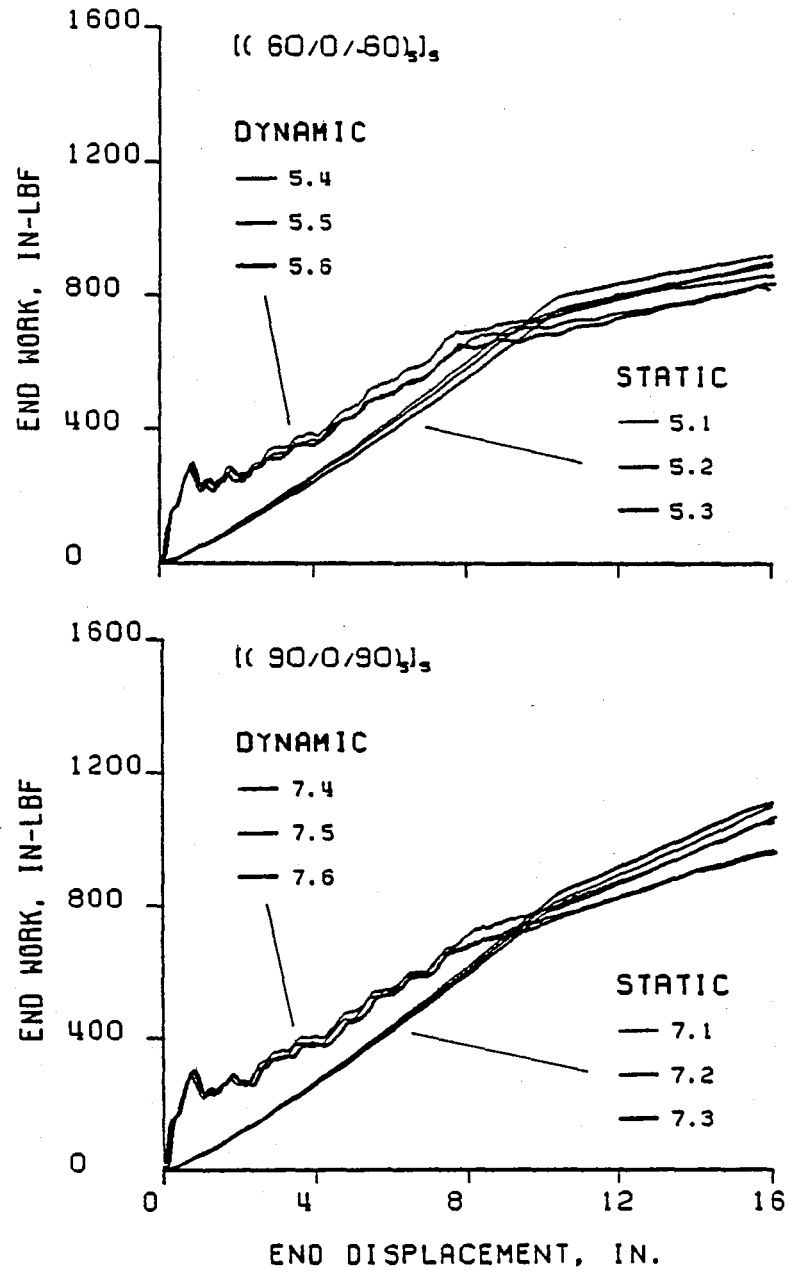
Figure 3.45   End Load Work vs. Displacement for the [(60/0/-60)$_5$]$_s$ and [(90/0/90)$_5$]$_s$ Laminates
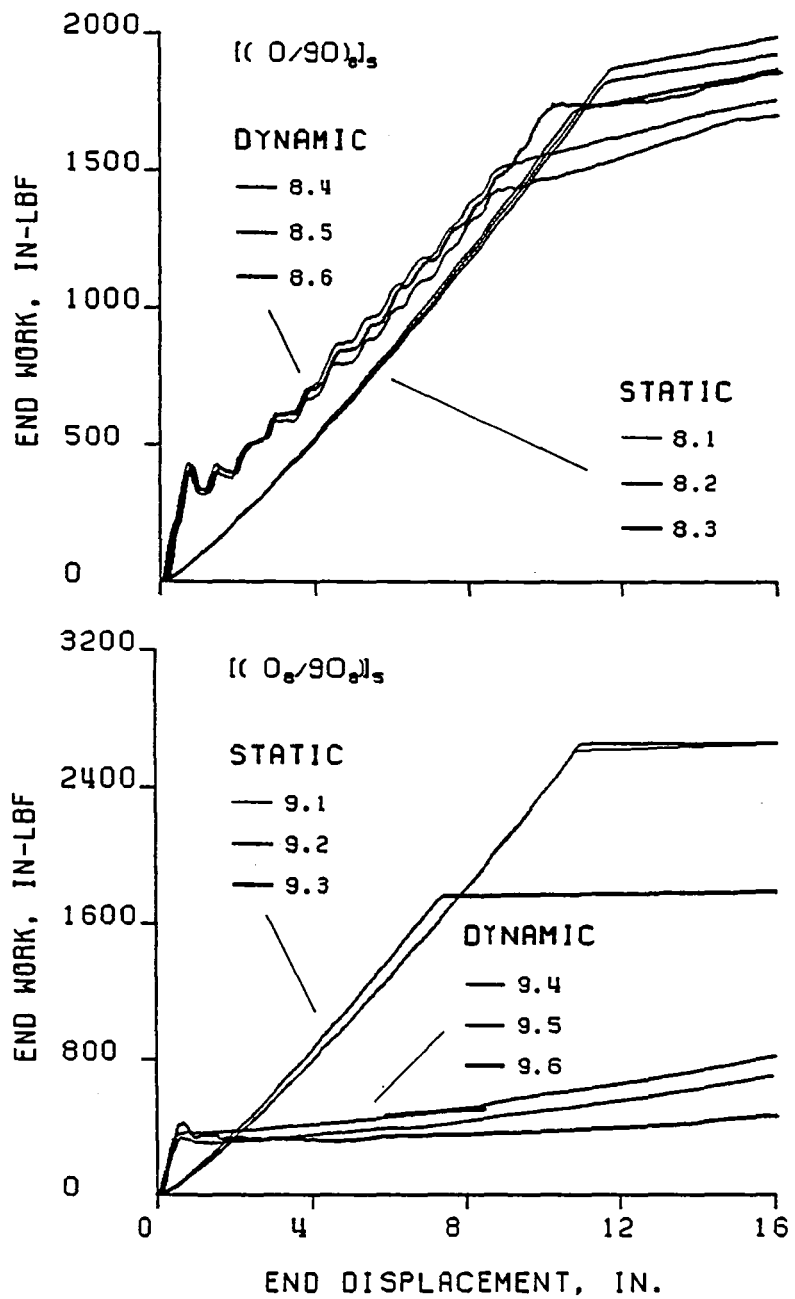
Figure 3.46   End Load Work vs. Displacement for the $[(0/90)_8]_s$ and $[(0_8/90_8)]_s$ Laminates
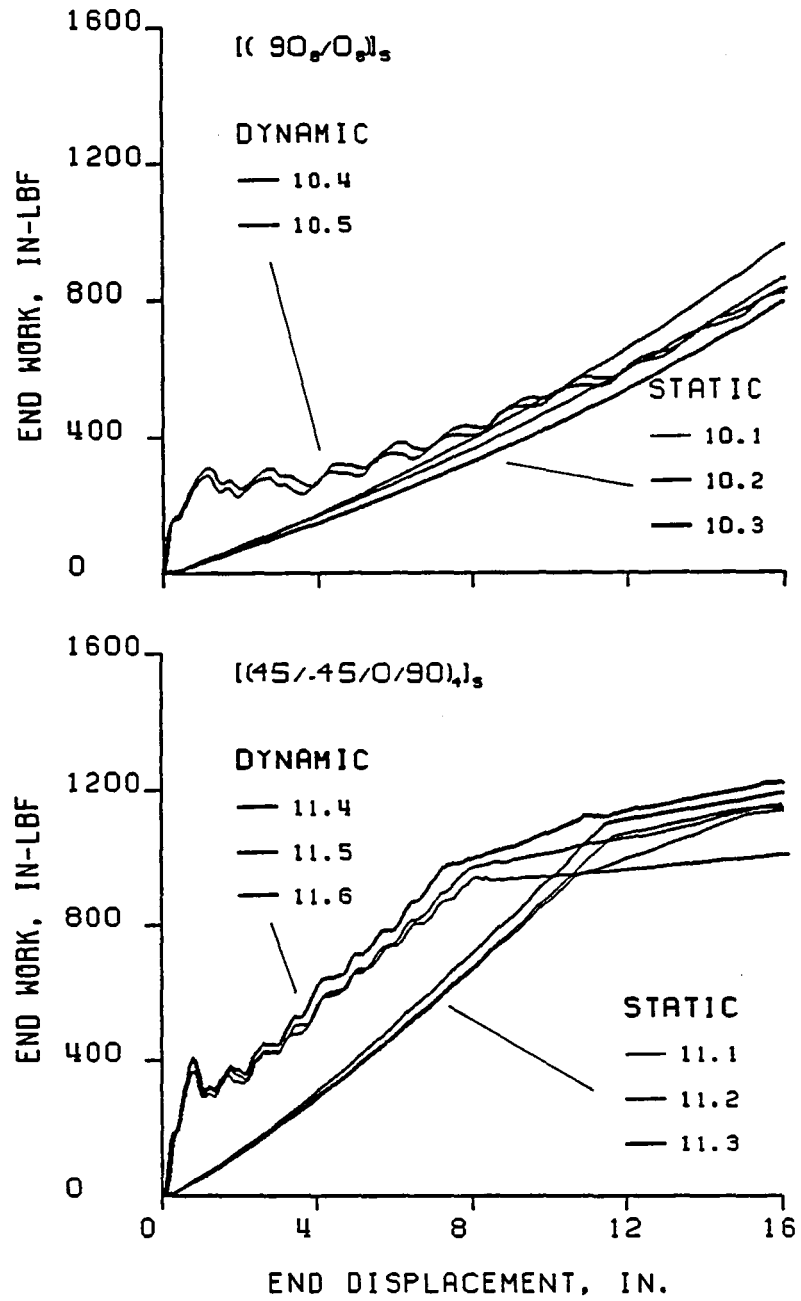
Figure 3.47   End Load Work vs. Displacement for the $[(90_8/0_80]_s$ and $[(45/-45/0/90)_4]_s$ Laminates
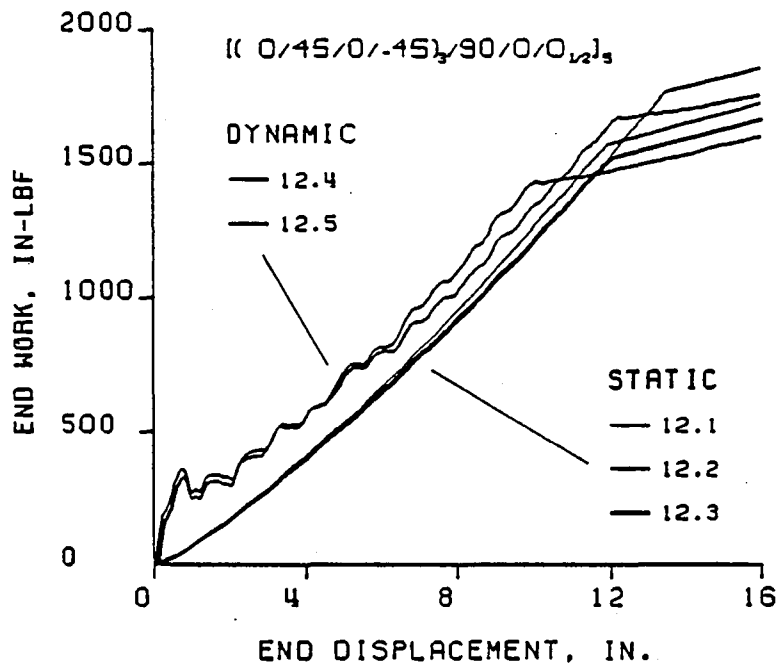
Figure 3.48   End Load Work vs. Displacement for the
               $[(0/45/0/-45)_3/90/0/0_{1/2}]_s$ Laminates

required to displace the beam statically the same increment. This indicates that the displacement rate of doing work is comparable for both the static and dynamic events. The other laminates in this group show comparable behavior up to first failure. The work required to displace the specimens dynamically 3/4 in. was fairly consistent from specimen to specimen and was about 400 in.-lbs. The work required to statically displace the beams 3/4 in. varied with beam stiffness. Therefore, the softer laminates, such as 5 and 7, showed greater divergence between the static and dynamic events, as can be seen in fig. 3.45.

An interesting general conclusion concerning work can be made by further comparing the work for the static and dynamic cases. As stated earlier, failure of the dynamic specimens occurred at a lower value of end displacement than failure of the static specimens. As a result, the static specimens required more work to displace the full 16 in. than the dynamic specimens did, even though the dynamic specimens required significantly more work to displace the first 3/4 in.

Finally, fig. 3.46 dramatically shows the differences in the static and dynamic failure modes for the $[0_8/90_8]$ laminates, laminate 9. The initial dynamic response of laminate 9 is comparable to the other laminates, i.e., requiring 400 in.-lb. of work to move the end 3/4 in. However, soon after the impact event the beams delaminated and separated into two thin beams. The two thin beams required considerably less work for deformation. There were moderate differences between the static and dynamic failure modes for laminate 10, the $[90_8/0_8]_s$ laminate. Shortly after impact, the outer plies separated from the beam and the beam acted

as a single thin unidirectional beam. In the static test, the outer plies cracked but remained intact and contributed to the stiffness of the laminate. Therefore, the slope of the static work-deflection relation was different for the static case than for the dynamic case.

3.3 Summary of Experimental Observations

Laminates 9 and 10 exhibited unusual and distinct failure modes under both static and dynamic loadings. However, because the laminae in these beams were clustered, these laminates are not of practical interest. In fact they were designed to nurture differences in static and dynamic loadings. In this they were successful. The rest of the laminates exhibited no differences between the failure modes under static and dynamic loading.

The progression of the failure, or the number of failure events, varied from six events, for specimen 2.3, to one event. Also, in general, the specimens that were tested dynamically failed at strain values and axial displacement values less than those of the static specimens. These results will be explored further in ch. 5.

Finally, variation between the tensile and compressive surface strains were observed in the static and dynamic tests. The variations ranged from an increase in compressive strain of from 5% above the tensile strain to increases of up to 40%. These phenomena will be investigated and discussed further in the next chapter.

Chapter 4

INVESTIGATION OF DIFFERENCE BETWEEN COMPRESSIVE

AND TENSILE MODULI

Examination of the static and dynamic strain response of the 12 laminate types showed that the compressive side surface strain at the center of the beam was greater than the tensile side strain. This difference in the surface strains varied from 5% for laminate 7 to 40% for laminate 4. At first it was felt that the greater compression strain was due to there being a net compressive axial force on the laminate. However, calculations show that these compressive strains can be effectively ignored since they are always at least 2 orders of magnitude less than the surface strains actually measured. In addition, there is no shear deformation at the center of the beam due to the symmetry of the loading. So, the center section of the beam is effectively in a state of pure bending. With pure bending and a linear elastic material, the magnitude of the tensile and compressive strains should be identical but this was not the case. The observed behavior was known to be elastic. Recall, it was found in the static tests that the loading and unloading strain response curves were coincident, unless there were ply failures. Therefore the difference in compressive and tensile strains was due to either a nonlinear elastic effect or the laminates were perhaps exhibiting bimodular elastic behavior.

To determine which of these two phenomena were occurring, laminates 1 through 7 and laminate 11 were selected for further study. Further tests were conducted to empirically determine the effective compressive and tensile bending moduli.

100

4.1 Experimental Set Up

Since the unusual material behavior was observed under static and dynamic loadings, for simplicity, these experiments were conducted in a static test apparatus. To measure the elastic properties, in addition to the strain data, knowledge of the internal bending moment is required. The bending moment at the center of the end loaded beam is equivalent to the end load times the distance between the line of action of the end load and the neutral surface of the beam at its point of maximum lateral deflection. The maximum deflection occurred at the center of the beam. This is illustrated in fig. 4.1, D being the distance of interest. To facilate measurement of the lateral deflection, a modification to the original static test apparatus was made. A rigid bar was mounted perpendicular to the moving crosshead and parallel to the undeformed beam. This bar provided a reference from which the lateral deflections could be measured. All other aspects of the set up were identical to the set up for the static tests performed earlier. However, different strain guage amplifiers and a different load frame were used.

4.2 Data Aquisition

As in the previous static tests the load was measured by the 1000 pound load cell and the end load-end displacement relation was recorded on a chart recorder. The strain guage signals were conditioned with signal amplifiers. Strain-load relations were recorded using an X-Y plotter. In addition, the axial end load, axial end displacement,
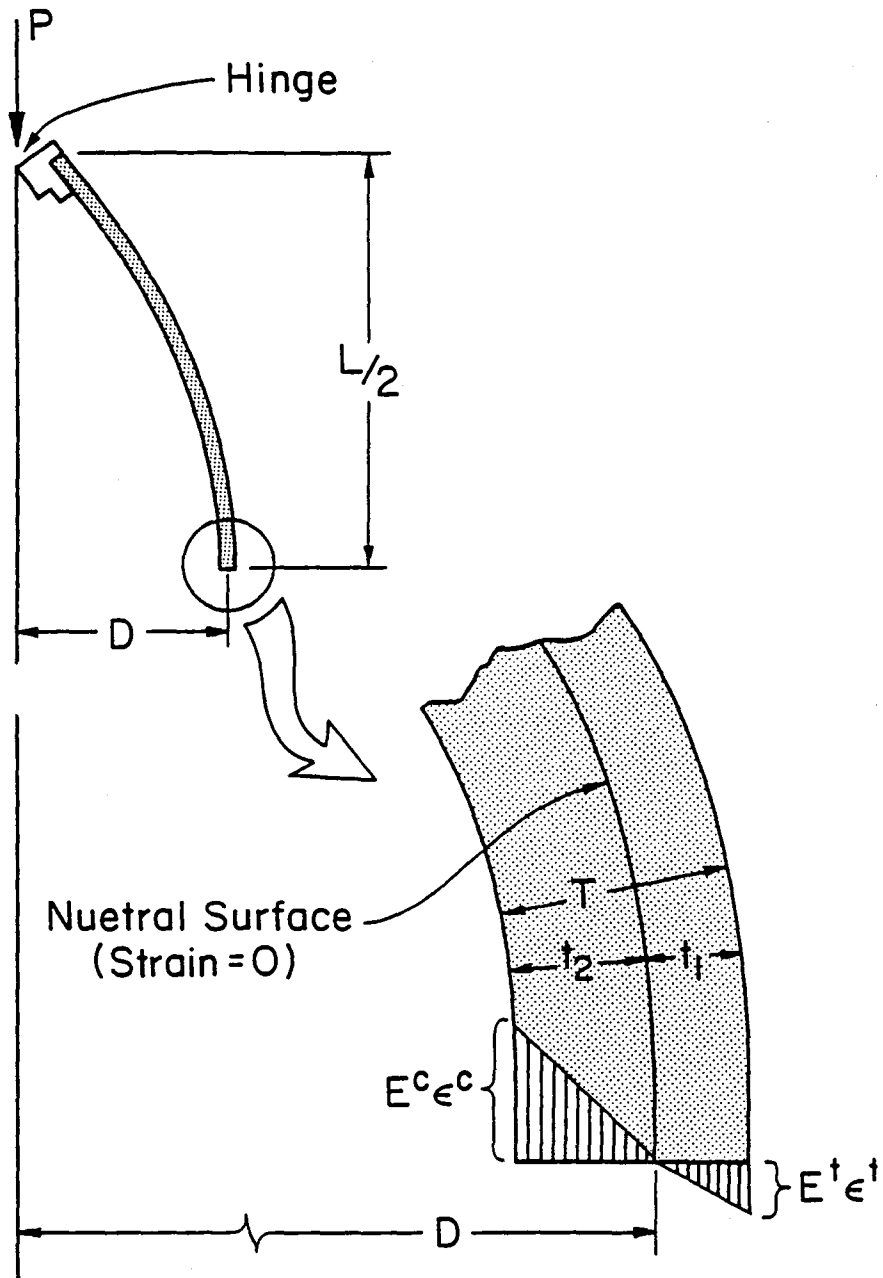
Figure 4.1   Stress Distribution and Moment Diagram

center lateral displacement, and the two strain values were manually recorded from digital voltmeters.

4.3 Test Procedure

First the beam specimen was placed in the load frame and the strain guages were connected. Then the load cell was zeroed and the strain guage amplifiers were balanced. The beam specimen was displaced axially and monotonically in 1/2 in. increments up to 85% of the axial displacement value at which failure was first seen in the previous static tests. At each 1/2 in. increment the lateral deflection was measured by hand with a ruler, then recorded. At this time the axial displacement, the end load and the two strain values were also recorded. This procedure was repeated until the predetermined axial displacement was reached. Then the displacement direction was reversed and the beam was unloaded until the beam reached the zero displacement point. The strain-load relation for unloading was checked to see if it was coincident with the loading relation.

4.4 Data Reduction

The data was reduced to determine the tensile and compressive moduli of the laminate. The reduction procedure utilized the fact that the beam was in static equilibrium. In addition, three assumptions were made. The first assumption was that the material properties could be smeared through the thickness. In other words, the stress was assumed to vary linearly from the outer surface to the neutral surface. The second assumption was that there was a linear variation of strain

through the thickness of the beam, i.e., the Kirchhoff assumption was valid. This assumption should be valid in that the beam was effectively in pure bending. Finally, the third assumption was that the laminate was bilinear elastic. This may or may not have been the case. If it were the case then the determined moduli should not vary with increasing curvature, load, or strain. If the moduli did indeed vary with curvature, load, or strain, then it could be concluded that the laminate was not bimodular but rather exhibited some other form of nonlinear elastic behavior. However, the precise nonlinear relation could not be determined from the analysis.

From the Kirchhoff assumption, knowledge of the total beam thickness and the empirical values of surface strain, the location of the neutral surface within the crosssection could be found. The location was given by

$$t_1 = \frac{\varepsilon^t T}{\varepsilon^t + \varepsilon^c} , \qquad (4.1)$$

and

$$t_2 = \frac{\varepsilon^c T}{\varepsilon^t + \varepsilon^c} , \qquad (4.2)$$

where

t_1 = distance from the neutral surface to the tension surface,

t_2 = distance from the neutral surface to the compression surface,

T = total beam thickness, (mid thickness, Table 2.2)

ε^c = strain at compressive surface, (absolute value)

ε^t = strain at tensile surface.

Figure 4.1 illustrates the geometric quantities involved. By assuming the net axial stress resultant could be set to zero, and by using the bimaterial assumption, a relation between the tensile and comressive moduli could be found. That relation is

$$\frac{1}{2} E^t \varepsilon^t t_1 b = \frac{1}{2} E^c \varepsilon^c t_2 b \; , \tag{4.3}$$

where

E^t = unknown tensile modulus

E^c = unknown compressive modulus

b   = beam width (= 2.00 in.).

Finally by enforcing moment equilibrium for the upper or lower half of the beam, it is found,

$$PD = (\frac{1}{2} E^t \varepsilon^t t_1 b) \, (\frac{2}{3} t_1) + (\frac{1}{2} E^c \varepsilon^c t_2 b) \, (\frac{2}{3} t_2) \tag{4.4}$$

where

P = end load

D = moment arm

The values of t_1 and t_2 can be determined from eqn. 4.1 and eqn. 4.2. Solving eqn. 4.3 and eqn. 4.4 for the moduli yields:

$$E^c = \frac{3PD}{\varepsilon^c(t_2^2 + t_1 t_2)b} \tag{4.5}$$

$$E^t = \frac{3PD}{\varepsilon^t(t_1^2 + t_1 t_2)b} \; . \tag{4.6}$$

Multiplying both sides of eqn. 4.5 and eqn. 4.6 by ε^c and ε^t, respectively, yields equations for the surface stresses, namely,

$$\sigma^c = \frac{3PD}{(t_2^2 + t_1 t_2)} \, , \tag{4.7}$$

$$\sigma^t = \frac{3PD}{(t_1^2 + t_1 t_2)} \, . \tag{4.8}$$

The beam curvature can be computed from

$$\kappa = \frac{\varepsilon^t}{t_1} \, . \tag{4.9}$$

Using this procedure the compressive modulus, the tensile modulus, the stress at the tensile surface, the stress at the compressive surface, and the beam curvature were computed at each displacement increment. The raw data used for the computations are presented in Appendix G.

4.5 Results

The moduli-curvature relations are plotted for each laminate tested and are given in fig. 4.2 through fig. 4.5. The horizontal axis shows the beam curvature and the vertical axis shows the empirically determined bending tensile and compressive moduli. All the laminates exhibited an elastic response. This was known because the graphically recorded load-strain relations were coincident for loading and unloading. The unidirectional laminate, fig. 4.2, showed the compressive modulus to be 23% less than the tensile modulus at high curvature levels. Published values for the fiber direction modulus
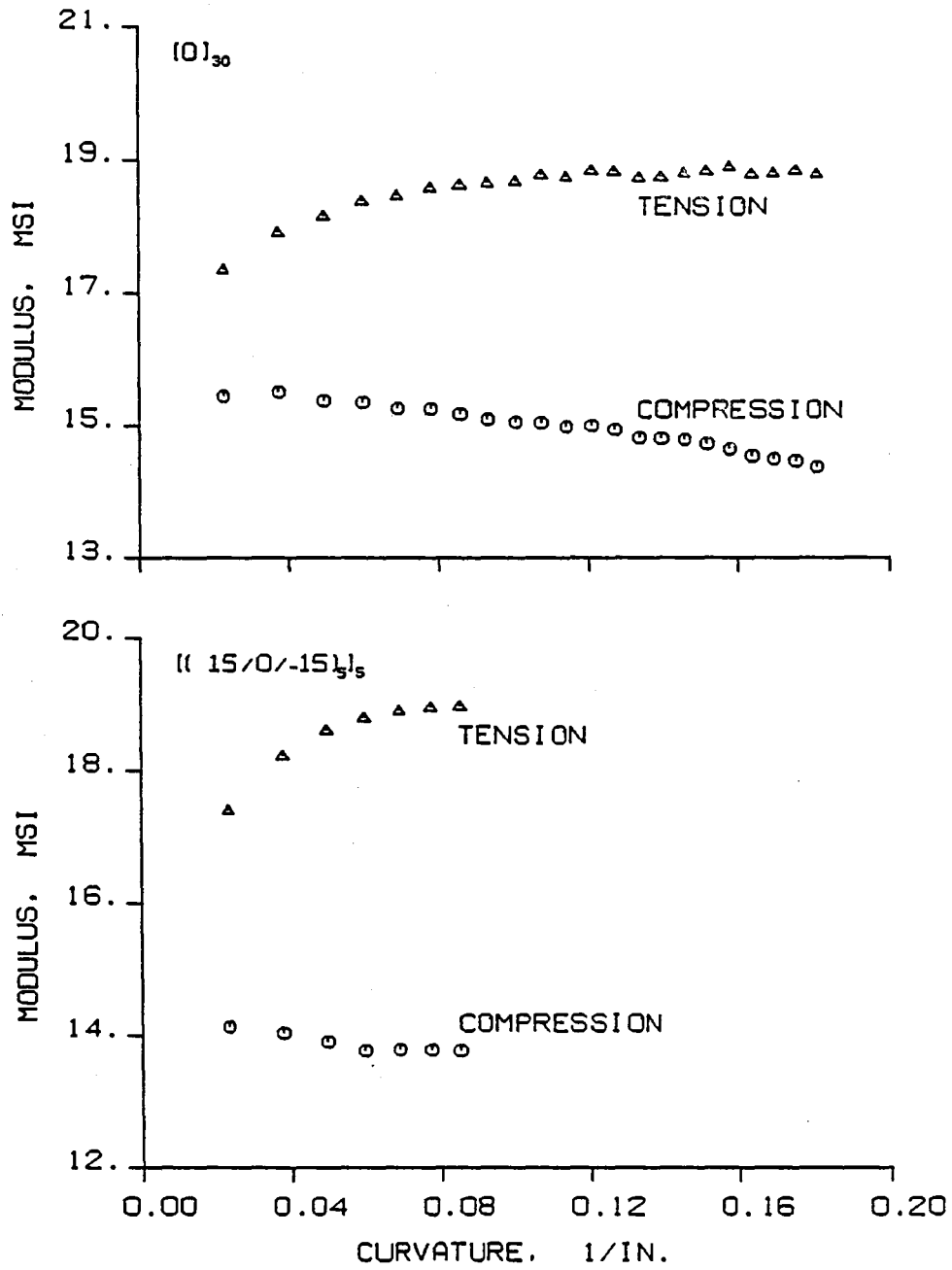
Figure 4.2   Moduli vs. Curvature for the $[0]_{30}$ and $[(15/0/-15)_5]_s$
Laminates
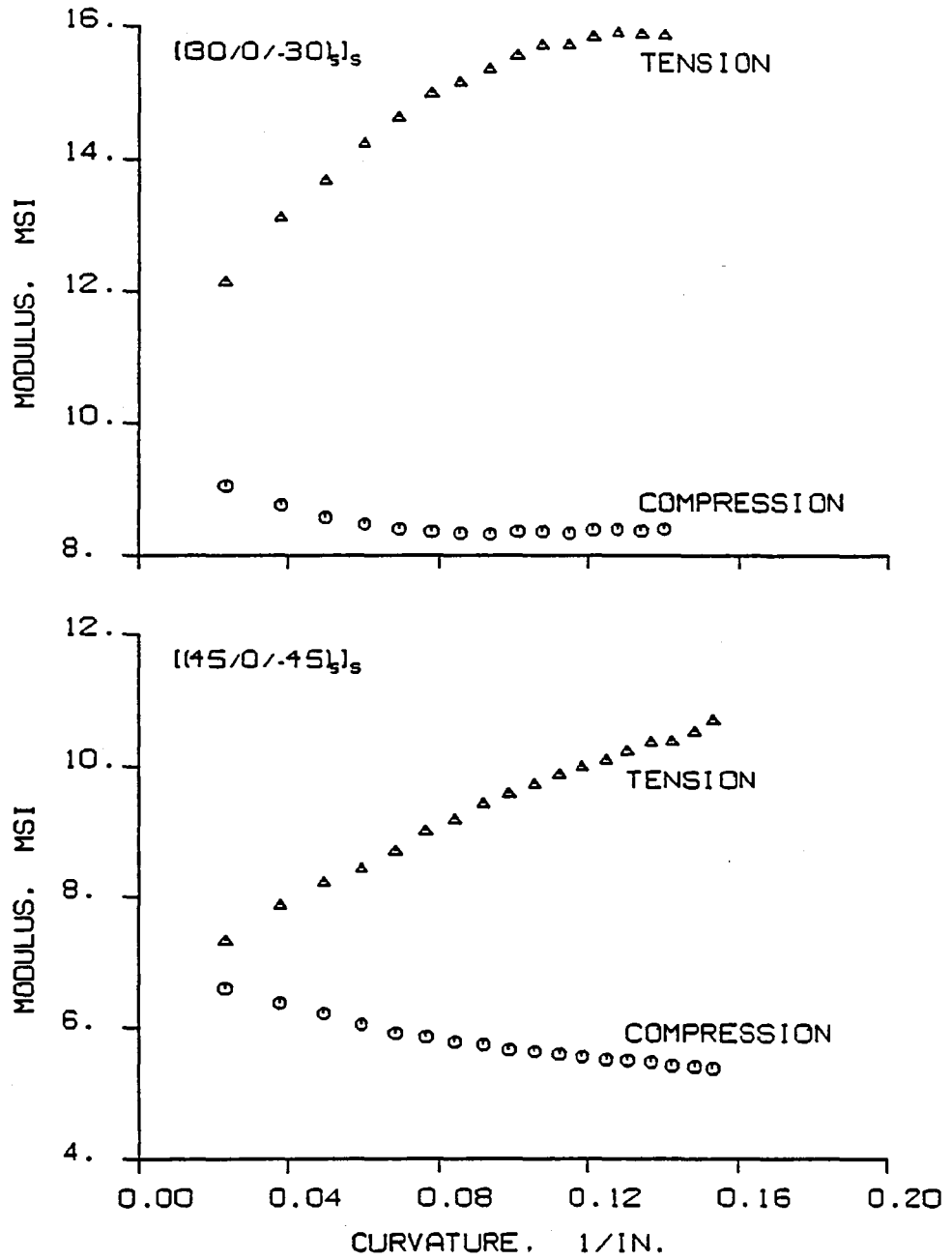
Figure 4.3   Moduli vs. Curvature for the $[(30/0/-30)_5]_s$ and $[(45/0/-45)_5]_s$ Laminates
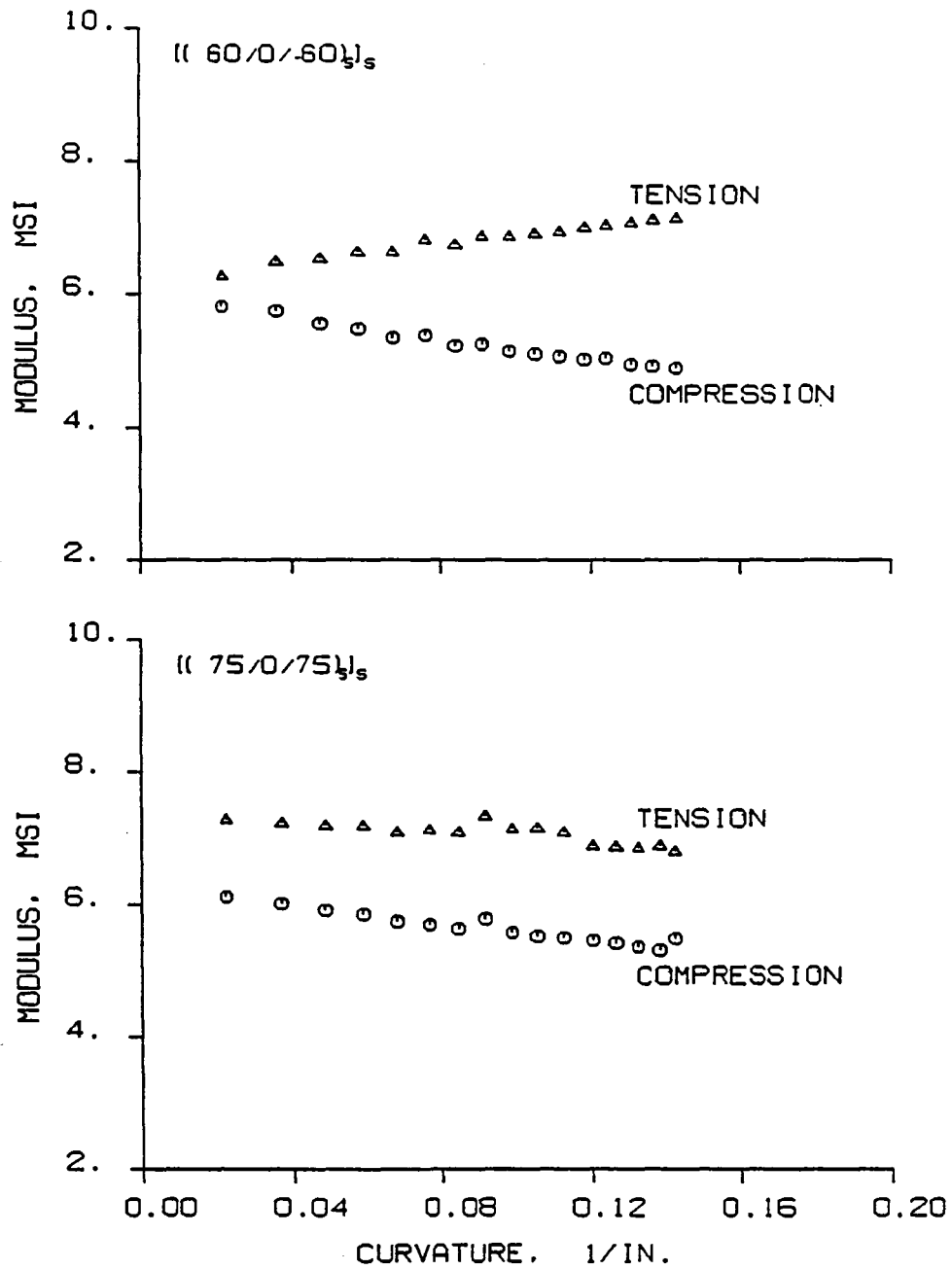
Figure 4.4   Moduli vs. Curvature for the [(60/0/-60)₅]ₛ and [(75/0/-75)₅]ₛ Laminates
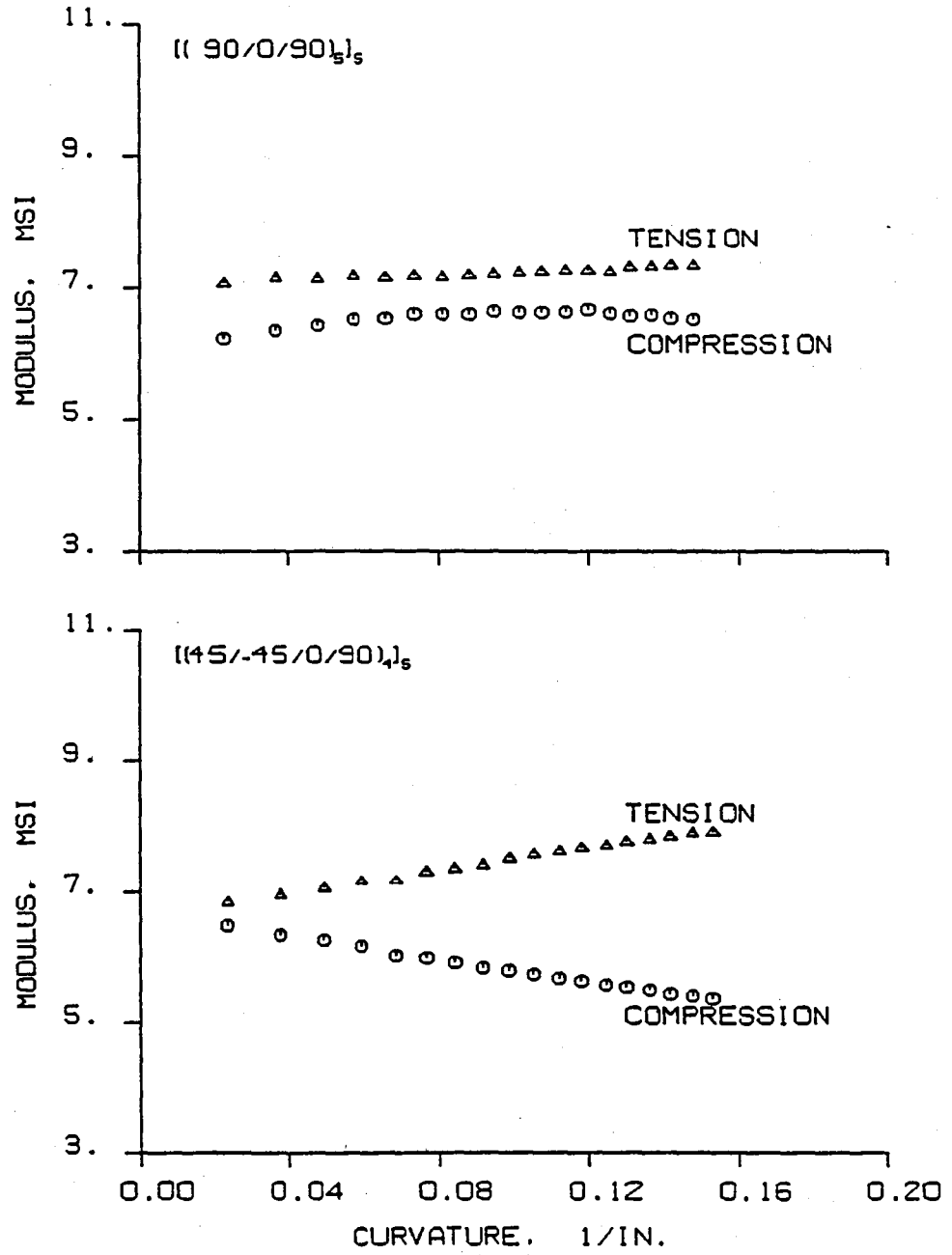
Figure 4.5   Moduli vs. Curvature for the $[(90/0/90)_5]_s$ and
$[(45/-45/0/90)_4]_s$ Laminates

indicate that compressive modulus should be only 9.75% less than the tensile modulus. As shown in fig. 4.4 and fig. 4.5, laminates 6 and 7 exhibited the least amount of bimodularity. Also, laminates 6 and 7 exhibited nearly constant values of the modulus with curvature, or more specifically, a linear response of stress with strain. In the other laminates the compressive modulus decreased with curvature and the tensile modulus increased with curvature. This is especially evident in laminates 4 and 11 shown in fig. 4.3, and fig. 4.5, respectively. Because the moduli were not constant with curvature there appears to be a nonlinear elastic stress strain response more complex than bimodular. Laminates 3 and 4, shown in fig. 4.3, exhibited a remarkable amount of bimodularity. Notice that for both of these laminates the compressive modulus was nearly 50% less than the tensile modulus at high curvature levels.

Effective stress-strain relations for the different laminates were also determined from the bending tests. Though it is known that the stresses change value dramatically from one lamina to the next (in contradiction to one of the assumptions used to reduce the data), a stress-strain relation for the laminate-as-a-whole in tension and a stress-strain relation for the laminate-as-a-whole in compression were computed. By using the measured values of ϵ^t and ϵ^c and the stresses from eqn. 4.7 and eqn. 4.8, effective stress-strain relations were empirically determined. Figures 4.6 through 4.9 show these stress-strain relations. It is important to review the derivation of equations in this chapter to put the stress-strain behavior shown in fig. 4.6 through fig. 4.9 into context. However, it appears that, to a first
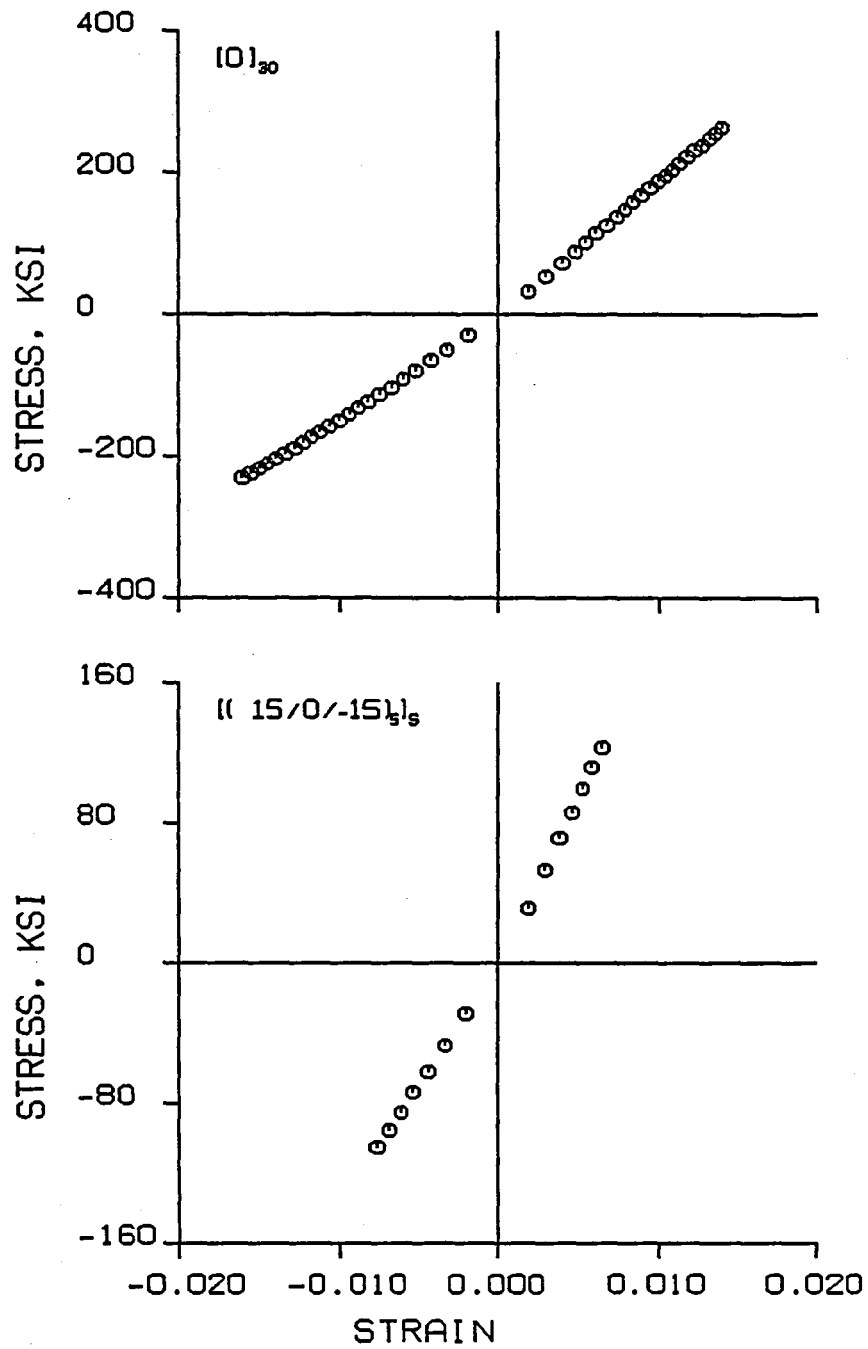
Figure 4.6   Stress vs. Strain for the $[0]_{30}$ and $[(15/0/-15)_5]_s$ Laminates
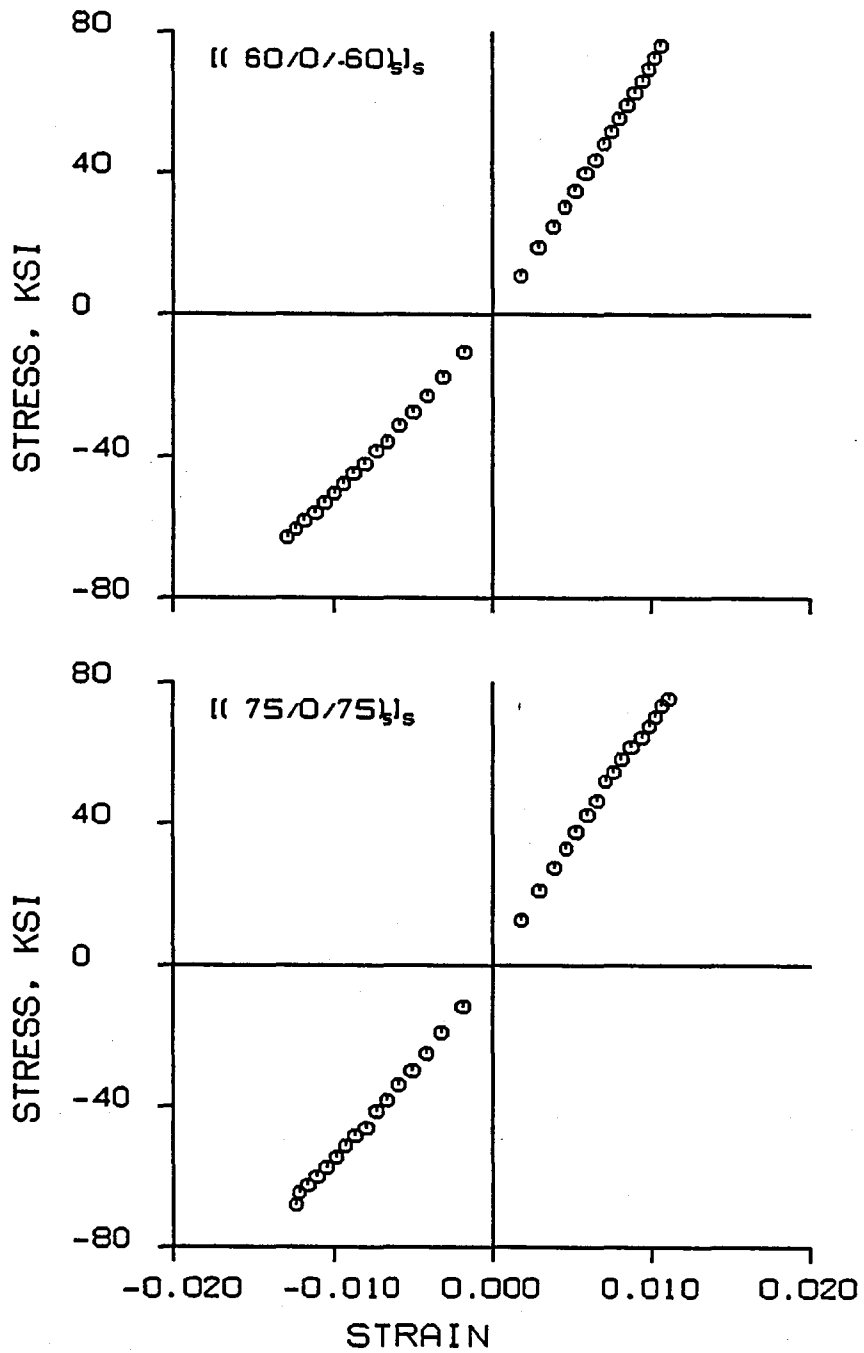
Figure 4.7   Stress vs. Strain for the $[(30/0-30)_5]_s$ and $[45/0/-45)_5]_s$ Laminates
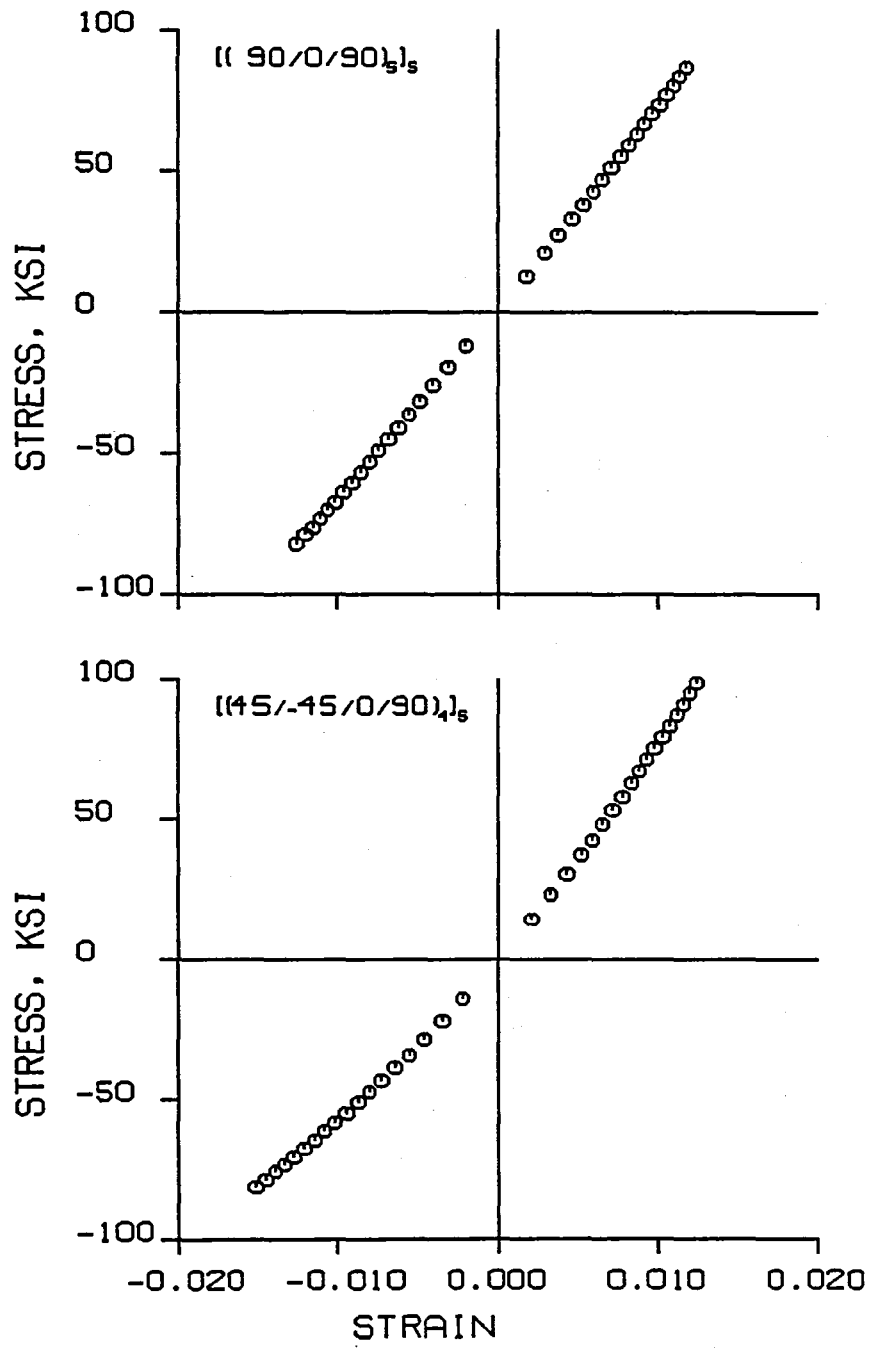
Figure 4.8   Stress vs. Strain for the $[(60/0/-60)_5]_s$ and $[(75/0/75)_5]_s$ Laminates
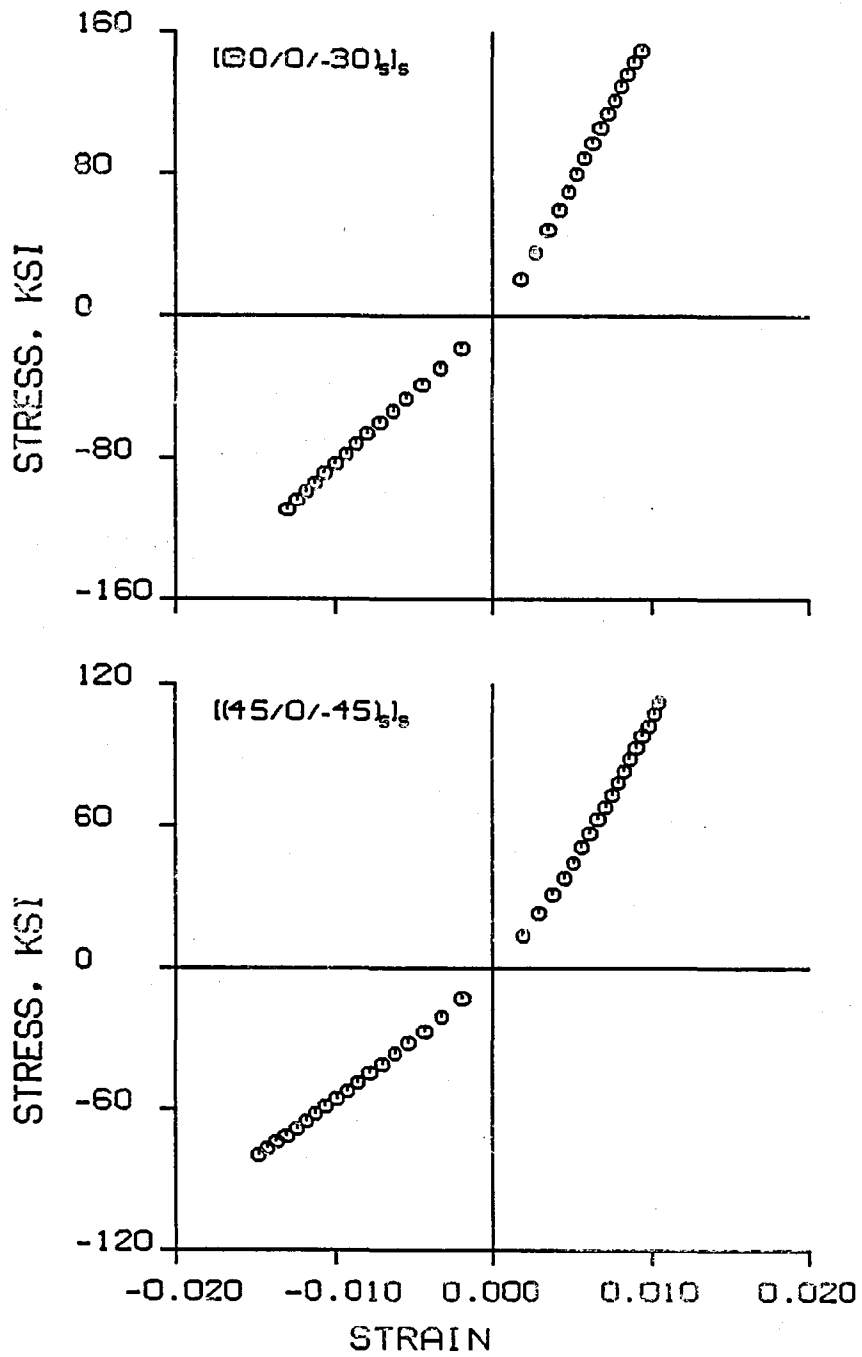
Figure 4.9   Stress vs. Strain for the $[(90/0/90)_5]_s$ and $[(45/-45/0/90)_4]_s$ Laminates

approximation, the laminates did exhibit bimodular behavior. A close examination of the figures reveals that the two portions of the stress-strain relation are not perfect straight lines. Therefore, a more complex nonlinear elastic behavior may be the case.

4.6 Error Analysis

The compressive and tensile moduli were determined from 5 measured quantities. From eqn. 4.5 and eqn. 4.6

$$E^C = E^C (P, D, \varepsilon^t, \varepsilon^C, T) \tag{4.10}$$

and

$$E^t = E^t (P, D, \varepsilon^t, \varepsilon^C, T) \tag{4.11}$$

Uncertainties in each one of the five independent variables contribute to the overall uncertainty in the moduli. The uncertainty in the load was 1% of the maximum value of the load cell, in this case 10 lbs. The lateral deflection, which was measured by hand, had an uncertainty of 0.05 in. There were many factors contributing to the uncertainty in the strain measurements. They were: (1) The finite distance between the foil grid of the strain guage and the surface of the beam; (2) Drift in the amplifiers, (3) The transverse sensitivity of the strain gauge, and; (4) Misalignment of the guages on the specimen. It was felt that all these errors together contributed to an uncertainty of .000100 in./in., or ≈1%, of the maximum strain measured. Finally the uncertainty in the thickness measurement was taken to be 0.0025 in. or 2%. This accounts

for the uncertainty in the measurement and the variation of thickness across the width of the specimen. The way in which each of these uncertainties contribute to the uncertainty in the computed moduli can be given by the relation

$$W_E = [(\frac{\partial E}{\partial P} W_P)^2 + (\frac{\partial E}{\partial D} W_D)^2 + (\frac{\partial E}{\partial \epsilon_c} W_\epsilon)^2 + (\frac{\partial E}{\partial \epsilon_t} W_\epsilon)^2 + (\frac{\partial E}{\partial T} W_T)^2]^{1/2} ,$$

(4.12)

where W_E is the uncertainty in the moduli and $W_P, \ldots, W_T$ are the uncertainties in the individual variables.

The uncertainty calculations were performed with each calculation of the compressive and tensile moduli. The results of the uncertainty analysis show that the uncertainty in the moduli calculations can be quite high, 2-3 MSI for the first data points taken at low values of axial displacement and load. However, the uncertainty in the moduli is much lower, 0.5-1.0 MSI, for the data taken at large values of axial displacement load. The uncertainty of the moduli were most sensitive to the uncertainty in the strain measurements. The uncertainty in the strain measurements were the most difficult to quantify. If a vertical error bar had been plotted with each data point in the moduli-curvature relations of fig. 4.2 through fig. 4.5, a horizontal tensile modulis vs. curvature relation and a different horizontal compressive modulus vs. curvature relation could have been drawn within the error bars. This would mean that the moduli did not vary with curvature, and hence load or stress level. Therefore, the apparent nonlinear behavior other than bimodular is not conclusive. However, it appears there is still substantial experimental evidence of a difference between the tensile and compressive moduli.

4.7 Observations

Reasons for the nonlinear behavior are not entirely clear. It is surmised that in tension the fibers align themselves with the principle stress directions and in compression the fibers buckle, or turn away from the principle stress directions. These two tendencies result in different stress-strain behavior in tension than in compression in a bending situation. This behavior was entirely unexpected and the thorough examination of it was not with in the overall goals of this study. However, the flexural moduli empirically derived here will be used in ch. 6 with a finite element program to predict the deformation response of the beams.

Chapter 5

INVESTIGATION OF THE FAILURE RESPONSE

Predicting the response of an aircraft fuselage to crash conditions involves both the prediction of the dynamic deformation response of the structure, and the prediction of the on set and extent of failure in the structural elements. This chapter focuses on the later by investigating the experimentally recorded ultimate surface strains in each of the laminates. Because of the uncertainty of the material behavior, i.e., bimodular vs. some other form of nonlinear elastic behavior, the onset of failure in the laminates was investigated using empirically measured strain values. This is in contrast to using stresses. The static data was studied to investigate the dependence of ultimate strain values with the laminate type. Then the static data were compared to the dynamic data to determine the effect of the dynamic response on the ultimate strain of the laminates. Since the failure modes for laminates 9 and 10 were significantly different in the static and dynamic tests, the ultimate failure strains could not provide a meaningful comparison for these laminate types. Therefore, the strengths of laminates 9 and 10 were not investigated in this chapter.

5.1 Data Reduction

The ultimate longitudinal tensile and compressive strains, ε_x^t and ε_x^c, were determined from the experimental strain-displacement response of the static and dynamic tests. The value of ε_x^t was taken to be the longtitudinal tensile strain value at the

displacement just prior to guage failure. The value of ϵ_x^c was the compressive strain at the same displacement. The ultimate strains for all of the static and dynamic specimens tested are presented in Appendix F. The average ultimate ϵ_x^t and ϵ_x^c were computed for the static specimens and the dynamic specimens of each laminate type. The strain transformations were used to transform the average values of longitudinal strain into the material princple strains ϵ_1, ϵ_2 and γ_{12}. Since all of the failures (except in the unidirectional laminate) occurred on the tension side, only the tensile ultimate strains were transformed. In addition, the maximum fiber strain in the 0° lamina closest to the tension surface was computed. This ply was of interest because it was the most highly stressed lamina, though not the most highly strained. A summary of all the computations is presented in table 5.1.

5.2 Quantitative Characterization of Failure

The mechanics of failure in a composite beam under bending loads is complex. For the laminate types selected for this study, failure was defined as the initial loss of load carrying capacity. This was usually associated with fiber failure in one or more lamina. As described in ch. 3, the failure events probably occurred in the following order. First, a matrix crack initiated in an angle ply lamina which was located on or near the tension surface of the beam. It is speculated that the crack then caused an axial and/or shear strain concentration in the fibers in the ply adjacent to the crack. This is depicted in fig. 5.1. The initiation of the matrix crack in the outer most angle ply and

TABLE 5.1
FAILURE STRAINS

Laminate Number	Avg ϵ^t Ult (%)	Avg ϵ^c Ult (%)	Tension ϵ_1 Ult (%)	ϵ_2 Ult (%)	γ_{12} Ult (%)	Tensor Poly	ϵ_1 in 0° lam. nearest ten. surface (%)	Strain Conc. Factor
Static 1	1.61±.11	1.81±.11	1.61	-.48	0.00	1.42	1.61	1.00
Dynamic 1	1.50±.04	1.70±.02	1.50	-.45	0.00	1.36	1.50	1.00
Static 2	0.85±.01	0.99±.04	0.75	-.50	-.72	0.85	0.79	2.04
Dynamic 2	0.75±.00	0.88±.00	0.66	-.44	-.64	0.66	0.70	2.14
Static 3	1.02±.02	1.37±.03	0.55	-.55	-1.81	1.58	0.94	1.71
Dynamic 3	0.93±.01	1.28±.01	0.45	-.55	-1.65	1.41	0.86	1.74
Static 4	1.11±.01	1.52±.03	0.17	0.17	-1.81	1.20	1.01	1.59
Dynamic 4	1.00±.01	1.40±.01	0.15	0.15	-1.69	0.98	0.92	1.63
Static 5	1.18±.06	1.43±.08	0.02	0.79	-1.33	2.93	1.09	1.48
Dynamic 5	0.99±.03	1.19±.04	0.02	0.67	-1.12	2.17	0.93	1.61
Static 7	1.33±.01	1.4±.01	0.05	1.33	0.00	6.47	1.24	1.30
Dynamic 7	1.22±.03	1.33±.03	0.04	1.22	0.00	5.51	1.14	1.32
Static 8	1.57±.04	1.74±.04	1.57	0.07	0.00	1.01	1.57	1.02
Dynamic 8	1.44±.05	1.60±.07	1.44	0.06	0.00	0.98	1.44	1.04
Static 11	1.38±.00	1.70±.00	0.48	0.48	-1.80	1.96	1.19	1.35
Dynamic 11	1.21±.02	1.51±.02	0.42	0.42	-1.58	1.56	1.03	1.46
Static 12	1.34±.07	1.66±.09	1.34	0.24	0.00	1.04	1.34	1.20
Dynamic 12	1.29±.08	1.67±.10	1.29	0.23	0.00	1.07	1.29	1.16
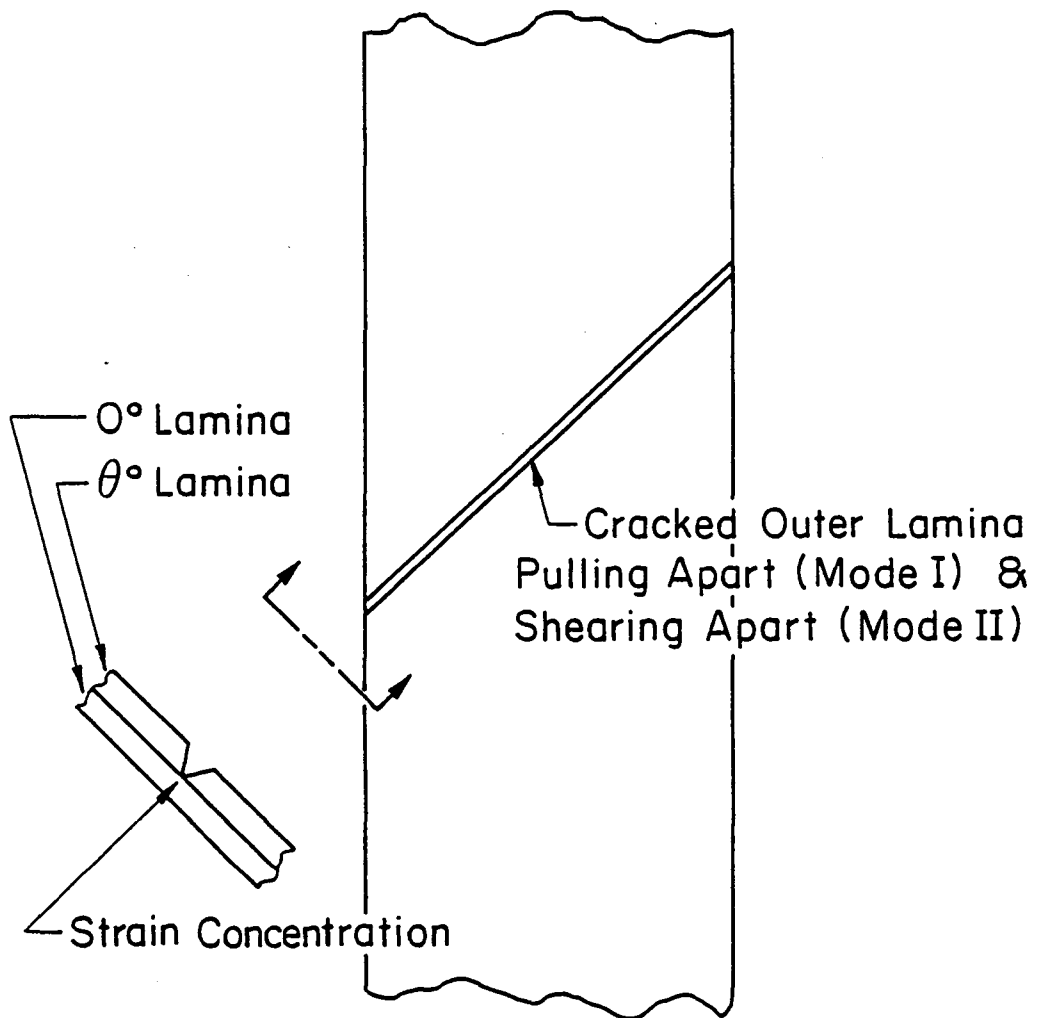
Figure 5.1   Strain Concentraton Near Matrix Crack

the failure of the fibers in the adjacent ply may or may not have occurred simultaneously.

To examine failure in the laminate, a phenomenological approach and a mechanistic approach were taken. The phenomenological approach taken was the strain tensor polynominal (ref. 8). This approach treats the composite as an anisotropic but homogenoeus material. The strain tensor polynominal interprets failure as the occurence of any definable discontinuity in the material response. This interpretation of failure may not correspond to loss of load carring capability. The mechanistic approach taken was to examine the strain in the 0° lamina on the tension surface, or the 0° lamina nearest to the tension surface. Because this was the most highly stressed lamina, failure of this lamina would initiate the loss of load carrying capability.

5.2.1 Strain Tensor Polynominal

The simplified plane-stress version of the strain tensor polynominal can be expressed as

$$\frac{\epsilon_1}{E_1 - E_1'} + \frac{\epsilon_2}{E_2 - E_2'} + \frac{\epsilon_1^2}{E_1 E_1'} + \frac{\epsilon_2^2}{E_2 E_2'} + \frac{\gamma_{12}^2}{G^2} = 1$$

where E_i and E_1' are the absolute value of the ultimate extension and compressive normal strains in the i direction, i = 1, 2, and G is the ultimate shear strain. The interaction term was taken to be zero. The values of E_1 and E_1' used for the static specimens were the ultimate static strain values of the unidirectional laminate, laminate 1. Likewise, the values of E_1 and E_1' used for the dynamic specimens were

the ultimate dynamic strain values of the dynamically tested unidirectional laminate. The other values used were: E_2 = 0.47%, E_2' = 0.67% and G = 1.93%. These were taken from published results for AS4-3502 and were used for both the static and dynamic specimens. The ultimate strain values were used in the tensor polynomial to predict failure. If the value of the tensor polynomial was less than 1 at failure, the polynomial would have been nonconservative in the prediction of failure. If the value of the polynomial was greater than 1, it would have been conservative in the prediction of the loss of load carrying capability. However, in the later case the polynomial may have accurately predicted the occurence of material failures, such as matrix cracks in the outer layer of the laminate, even though it conservatively predicted the occurance of the loss of load capacity. The results of the tensor polynomial calculations are presented in table 5.1.

5.2.2 Mechanistic Approach

For each laminate type, the maximum fiber strain in the 0° lamina nearest to the tension surface was calculated and is presented in table 5.1. The results show that this maximum fiber strain was not constant with laminate type. Thus this simple maximum fiber strain criteria could not be used as an indicator of laminate behavior for more general laminates. However, the fiber failures in these 0° lamina actually occurred in a region of strain concentration, under a matrix crack in an adjacent lamina. This was shown in fig 5.1. The ultimate tensile strain in the fiber direction for the material was known from the

statically and dynamically tested undirectional laminate. Therefore, for each laminate type, the strain concentration factor associated with the crack in the adjacent lamina could be determined. This was done by dividing the laminate ultimate strains (again as average strain) by the ultimate tensile strain of the material in the fiber direction. The strain concentrations computed this way are presented in table 5.1. The strain concentration factors for the static tests used the tensile strain at failure in the static tests of the unidirectional specimens, i.e., 1.61%. The strain concentration factors for the dynamic tests used the tensile strain at failure in the dynamic tests of the unidirectional specimens, i.e., 1.50%. Thus, for example, for laminate 4, the static strain concentration factor that the outer 45° ply caused the adjacent 0° ply to experience was 1.61%/1.01% = 1.59. Similarly, for the dynamic case, the strain concentration factor was 1.50%/0.92% = 1.63.

5.2.3 Results

Upon examination of the results it should be noted that there is a consistent difference between the static and dynamic results. The dynamic failure strains are always lower than the static failure strains. Except for laminate 12, the computed strain concentrations are always higher and the tensor polynomial value is always lower for the dynamic case. Reasons for this are discussed in the next section.

Examining the results of both the tensor polynomial and the strain concentration factor provides a qualitative understanding of the effect

of laminae orientation on the ultimate strain in the laminate. For the $[(\theta/0/-\theta)_5]_s$ family of laminates, laminates 2 through 7, both the static and dynamic 0° fiber concentration factors decrease with increasing off-axis angle. Also the tensor polynomial value increases with increasing off-axis angle. For example, in the static case of laminate 2 which has a 15% off axis fiber angle, the tensor polynomial had a value of 0.85 and the strain concentration factor was 2.04. The low value of the tensor polynomial could be contributed to the generation of interlaminar shear stresses near the free edge of the laminate which were not accounted for in the simplified plane-stress version of the tensor polynomial. The τ_{xz} shear stress is especially high in laminate 2 due to the large $\eta_{xy,x}$ missmatch between the 15° and 0° laminae, and the 15° and -15° laminae. The low value of the tensor polynomial suggests that the initial material discontinuity in the laminate and the loss of load carrying capacity of the laminate occurred simultaneously. This is consistent with the high value of strain concentration calculated for this laminate. The initial 15° matrix crack in the surface ply of the laminate might have caused high shear strains as well as high tension strains at the base of the crack in the adjacent 0° lamina. There is evidence, however, that the shearing effect causes higher strain concentrations than the tension effect. It is speculated that the amount of shear strain concentration is related to the $\eta_{xy,x}$ term of the angle ply lamina. For the $[(\theta/0/-\theta)_5]_s$ family, the computed strain concentration factor is a maximum for the 15° angle and so is the value of $\eta_{xy,x}$. The computed strain concentration reaches minimums at 0° and 90° as does $\eta_{xy,x}$. As stated above, laminate 7, with

off-axis angle plies of 90°, had the lowest value of strain concentration of laminates in the $[(\theta/0/-\theta)_5]_s$ family. It also had the highest value of the tensor polynomial. This suggests that the 90° outer ply cracked much before the load bearing 0° failed and a 90° crack had a less severe effect on the adjacent 0° than did an off-axis crack.

Comparing laminates 7 and 8 and also comparing laminates 4 and 12 shows that it is more severe for a 0° lamina to have cracked angle plies on both sides of it than if there is a cracked angle ply to one side only. Laminate 7 had 90° laminae on both sides of the 0° lamina nearest to the tension surface. The static strain concentration factor was 1.30. Laminate 8 had a 0° lamina on the surface with just one adjacent 90° lamina. There the strain concentration factor was 1.02. Laminate 4 had 45° laminae on both sides of the 0° lamina nearest to the tension surface. The strain concentration factor was 1.59. Laminate 12 had a 0° lamina on the surface with just one adjacent 45° lamina. The strain concentration was 1.20. These numbers indicate that cracks in the laminae on both sides of a 0° lamina are more detremental for the 0° lamina than if only one of the adjacent laminae is cracked.

5.3 Differences in Static and Dynamic Failure

As stated earlier, the results show that the ultimate strains in the dynamically tested specimens were lower than the ultimate strains of the statically tested specimens. Two reasons are speculated. First, the composite may have strain-rate dependent material properties. Second, the dynamic specimens undergo a more severe load history. The maximum strain rate in the dynamic tests was approximately 5

in./in./sec. A reduction in the ultimate strain of matrix dominated failures might be expected at this strain rate. However, a reduction in the ultimate strain was seen for fiber dominated failures as well. It is felt that strain-rate effects for fiber dominated failures are not likely. Therefore it was felt that other mechanisms must contribute to the lower ultimate strains in the dynamic tests. The dynamic specimens experienced different loading histories than the static ones. Recall that in the dynamic tests there was an initial high-amplitude load spike and an initial "W" deformation shape of the beam. The "W" deformation was such that the lamina which failed under tension were initially under compression. Also the dynamic specimens were subjected to a third mode vibratory response which could have fatigued the specimens. The dynamic loadings could have caused damage in the laminate on the micromechanical level early in the loading history and these could have contributed to the lower ultimate strain levels later in the loading history.

5.4 Prediction of the Extent of Failure

As a final note, this chapter has investigated the conditions which lead to the onset of failure. Failure was defined as the initial loss in load carrying capability. However, predicting the amount of drop in the load upon failure is as important as the prediction of the onset of failure. Recall from the load displacement relations discussed in ch. 3 that laminate 2 had from 3 to 6 failure events which resulted in relative small drops in load when a group of 2 to 6 plies failed simultaneously. Laminate 3 had 2 or 3 failure events, where 5 to 10 plies failed simultaneously. All the other laminates had 1 major

failure event, where 40% to 60% of the plies in the laminate failed simultaneously, producing a drop in the load of up to 80%. Further investigation is needed to determine the relation between the extent of failure and laminate type. Such studies are important if the collapse of a composite structure is to be predicted. During collapse, some structural members will fail, others will partially fail, and some will remain intact with load being transferred and retransferred throughout the structure. Knowing how to predict partial loss of load capacity of the individual elements would be important for predicting the collapse behavior.

Chapter 6

PREDICTION OF DEFORMATION RESPONSE

To predict the deformation response of the beam, an existing finite element program was used. The static load-deflection response was predicted for each of the laminates and was compared with the experimental results. For laminates 1, 4, and 7, the dynamic test conditions were modeled. The finite-element predictions for the load deflection, load-time, and the displacement-time were compared with the experimental results. Because of the expense in running the computer program, only 3 of the 12 laminates were selected for the dynamic analysis.

6.1 Finite Element Program

The finite element program used was capable of computing a nonlinear transient response of a structure subjected to time varying loads (ref. 9). The program allowed for large geometry changes by using a co-rotational coordinate system in the deformation model. The analysis is preformed by direct minimization of the scalar energy function.

6.2 Material Model

The program was written for crash analysis of aluminum structures. Therefore the material model was designed for isotropic linear elasto-plastic materials. Although nonlinear elastic materials cannot be modeled, linear bimodular materials can be modeled and were

used for the analysis. In addition, the program cannot model anisotropic materials. However, since the beam is one dimensional and the axial loads are insignificant compared to the bending loads, the compressive and tensile flexural moduli of the laminate was used in the material model, which raises another issue. Since the material was assumed bimodular, the neutral surface of the beam was not coincident with the midplane. The program has the capability to compute the position of the neutral surface at every position along the beam and at every time step. However to do so increased the computation time by a factor of ten. So this option was not evoked for the analysis performed in this chapter. However, the effect of tracking the location of the neutral surface on the static response is examined in Appendix H. As shown in the appendix, the error is significant, especially for laminate 3. However, for the dynamic case one computer run using the neutral surface computations would cost $1000. In addition, as will be seen shortly, there were other problems with the computer results. Thus the error was tolerated.

6.3 Material Properties Used

To perform a successful analysis, accurate material properties are required. Determining the properties of a laminated composite material is routinely done with classical lamination theory. Classical lamination theory uses the four independent material properties of the constituent lamina to determine the laminate properties. For a beam, the flexural modulus, E, can be computed by $E = 12 \, D_{11}/bh^3$, where h is the laminate thickness and b the laminate width. Using the material

TABLE 6.1
FINITE ELEMENT INPUT DATA

Laminate Number	Lay-Up	Lamination Theory Moduli		Moduli Used In Finite-Element Analysis		Dynamic Data For Finite-Element Analysis	
		E^t (MSI)	E^c	E^t (MSI)	E^c	Lumped Mass (Lbm)	Initial Velocity (in./sec.)
1	$[0]_{30}$	20.0	18.5	18.9	14.8	55.6	207.
2	$[(15/0-15)_5]_s$	19.05	17.22	18.8	13.7		
3	$[(30/0/-30)_5]_s$	15.24	13.82	15.9	8.4		
4	$[(45/0/-45)_5]_s$	11.31	10.31	10.9	5.5	32.3	179.
5	$[(60/0/-60)_5]_s$	8.88	8.13	5.2	7.1		
6	$[(75/0/-75)_5]_s$			7.1	5.9		
7	$[(90/0/-90)_5]_s$	7.95	7.27	7.2	6.85	32.3	179.
8	$[(0/90)_8]_s$	12.06	10.95	12.06	10.95		
9	$[(0_8/90_8]_s$	18.28	16.52	18.28	16.52		
10	$[(90_8/0_8]_s$	4.05	3.77	4.05	3.77		
11	$[(45/-45/0/90)_4]_s$	8.91	8.15	8.10	5.56		
12	$[(0/45/0-45)_3/90/0/0_{1/2}]_s$	14.34	9.18	14.34	9.18		

Material Properties Used In Laminate Analysis

E_1^t = 20.5 MSI E_1^c = 18.5 MSI

E_2^t = 1.67 MSI E_2^c = 1.64 MSI

G = 0.87 MSI

ν_{12} = 0.30

property data of table 6.1, the compressive and tensile flexural moduli were computed for each laminate type using classical lamination theory. These values are presented in table 6.1 and are labeled "lamination theory moduli". In addition, the flexural moduli of laminates 1 through 7 and 11 were empirically determined in ch. 4. The values of the moduli at the maximum curvature levels of each laminate type were compared with the lamination theory moduli. The comparisons showed poor agreement, particularly the compressive moduli. It was felt that the empirically determined moduli were more accurate. Thus the empirically determined moduli were used in the material model for the laminates. However, the moduli of laminates 8, 9, 10, and 12 were not determined empirically and the lamination theory moduli were used in the material model for those laminates. The flexural moduli used in the material model for each laminate type is presented in table 6.1 under the column "moduli used in finite element analysis". It is important to note that even though the assumptions of classical lamination theory were not violated, the lamination theory was poor at predicting the flexural moduli of the laminates. Therefore based on the evidence seen here, it appears classical lamination theory cannot be used with confidence for the prediction of the large deformation response of the laminated beams.

As stated in ch. 4, the uncertainty in the moduli at the high curvature levels was 0.5-1 MSI. The effect of this uncertainty on the response is examined in Appendix I.

6.4 Finite Element Mesh

Twenty elements were used to model the 20 in. unsupported portion of the specimen between the hinges. The element had a cubic transverse displacement field and a linear axial displacement field. The required beam thickness and widths were obtained from table 2. The total load eccentricity was equal to the 5/8 in. off-set introduced by the test fixture, plus the amount of measured beam camber from table 2. A single rigid element was used to model each hinge. Figure 6.1 shows the finite element mesh used.

6.5 Static Analysis

For the static analysis a vertical force was applied at node 1. Ten load steps, from 0 to the maximum load encountered in the experiments, were used to compute the static response of the beam.

6.6 Dynamic Analysis

To simulate the dynamic load, a lumped mass equal to the mass car plus the slider was assigned to node 1. Node 1 was given an initial velocity computed from the conservation of momentum of the mass car (which had an initial velocity of 235 in./sec.) impacting the slider. In addition, a constant force in the axial direction equal to the weight of the lumped mass was applied at node 1. Values of the lumped mass and initial velocities used for the three dynamic analyses are given in table 6. The starting time step size was 25 μ sec. Subsequent time steps were chosen by the program.

135
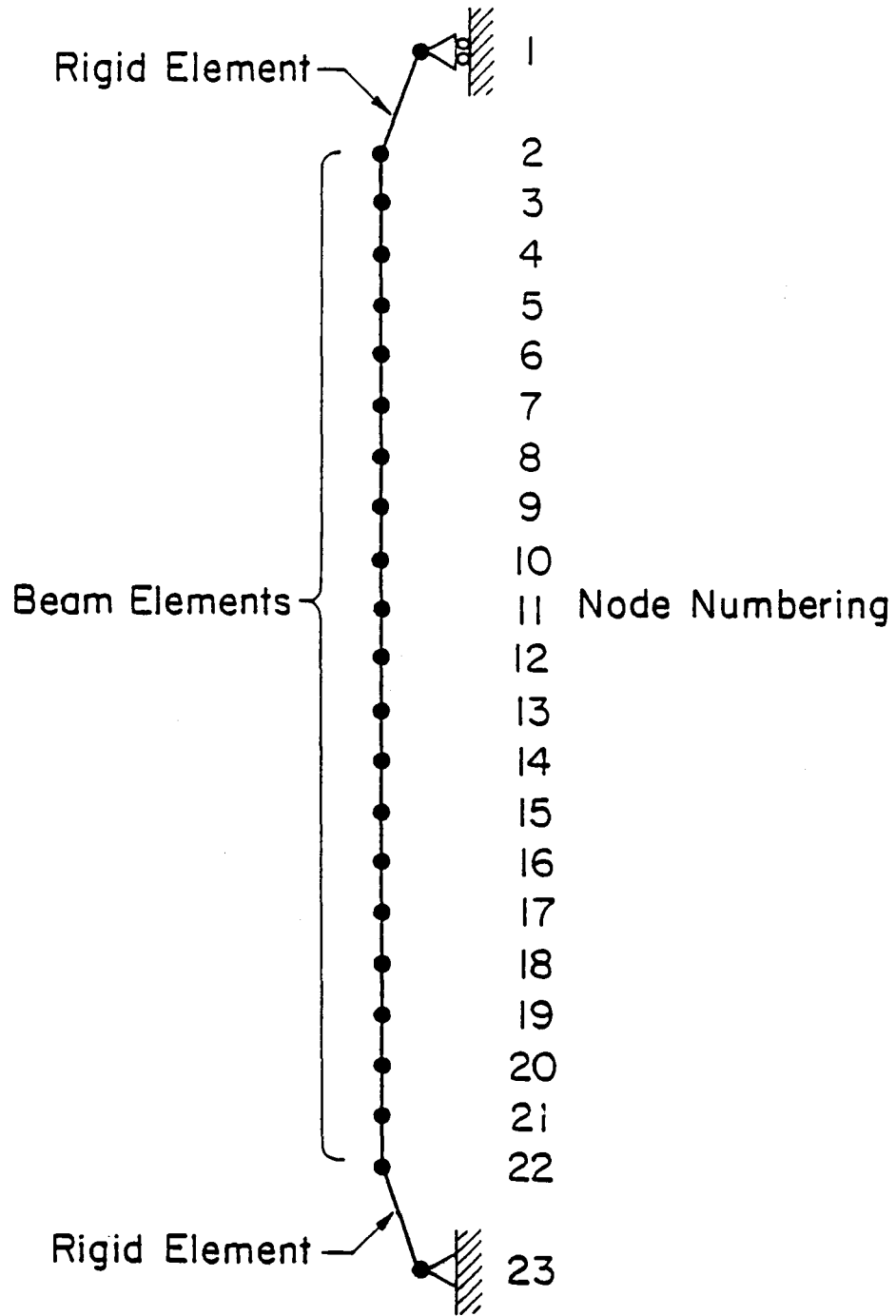
Figure 6.1   Finite Element Model

6.7 Static Analysis Results

The end load-displacement relation from the finite-element analyses are displayed with the experimental load-displacement relation in fig. 3.8 for laminate 1, in fig. 3.3 for laminate 2, in fig. 3.11 for laminate 3, in fig. 3.14 for laminate 4, in fig. 3.17 for laminate 5, in fig. 3.20 for laminate 7, in fig. 3.23 for laminate 8, in fig. 3.26 for laminate 9, in fig. 3.29 for laminate 10, in fig. 3.32 for laminate 11 and in fig. 3.35 for laminate 12. For laminates 1 through 8 and 12, the finite element analysis agrees well with the experiment up to initial failure. However, notice from table 6 the significant difference in the flexural moduli computed from laminate analysis compared with the empirical flexural moduli used in the analysis. For the $[(\theta/0/-\theta)_5]_s$ laminates, if the theoretical flexural moduli had been used in the finite element analysis, there would not have been good agreement with the experimental load-displacement relation. The finite-element program would have underpredicted the deflections for a given load.

Despite using theoretical moduli, the finite-element comparison for laminate type 8 was good. Unlike the previous comparisons, using the theoretical moduli in laminate 9 results in an overprediction of the deflections. For laminate 11 the finite element analysis underpredicts the deflections of the static specimens, even though the empirically-derived flexural moduli were used in the analysis.

6.8 Dynamic Analysis Results

Dynamic analyses was performed for laminates 1, 4, and 7.

Comparisons of the analyses and the experimental data were made for three relations: load-displacement, load-time and displacement-time. Analyses were performed up to the initial failure point in the beam.

Figure 6.2 shows the comparison of the analytical and experimental load-time relation for laminate 7. The relations are qualitatively similar but there are some obvious quantitative differences. In the first 0.01 sec. of the load response, much higher frequency components of structural vibration are predicted by the analysis than were recorded in the experiments. The initial load spike predicted by the analysis had an amplitude of 9845 lbs, more than eight times that which was recorded in the experiments. (The load response from the analysis was clipped at 4000 lbs. for display in Fig. 6.2), the amplitude of the third mode vibratory response was approximately twice that recorded in the experiments. However, the frequency of the third mode response was predicted quite accurately. Figure 6.3 shows the displacement time relations for laminate 7. Correlation between the experiment and analysis is good. When the load-time relation and the displacement-time relation are cross plotted in figure 6.4 to show the load-displacement relation for laminate 7, the oscillations in the analysis become slightly out of phase with the oscillations in the experiments.

The same three relations are shown in fig. 6.5 thru fig. 6.7 for laminate 4 and in fig. 6.8 thru fig. 6.10 for laminate 1. Comparisons similar to those above can be drawn for the correlation of the analysis and the experiment for laminate 4 and laminate 1.

Figure 6.11 shows 5 deformed meshes from the dynamic analysis of laminate 4. These deformed meshes were selected for comparison with the
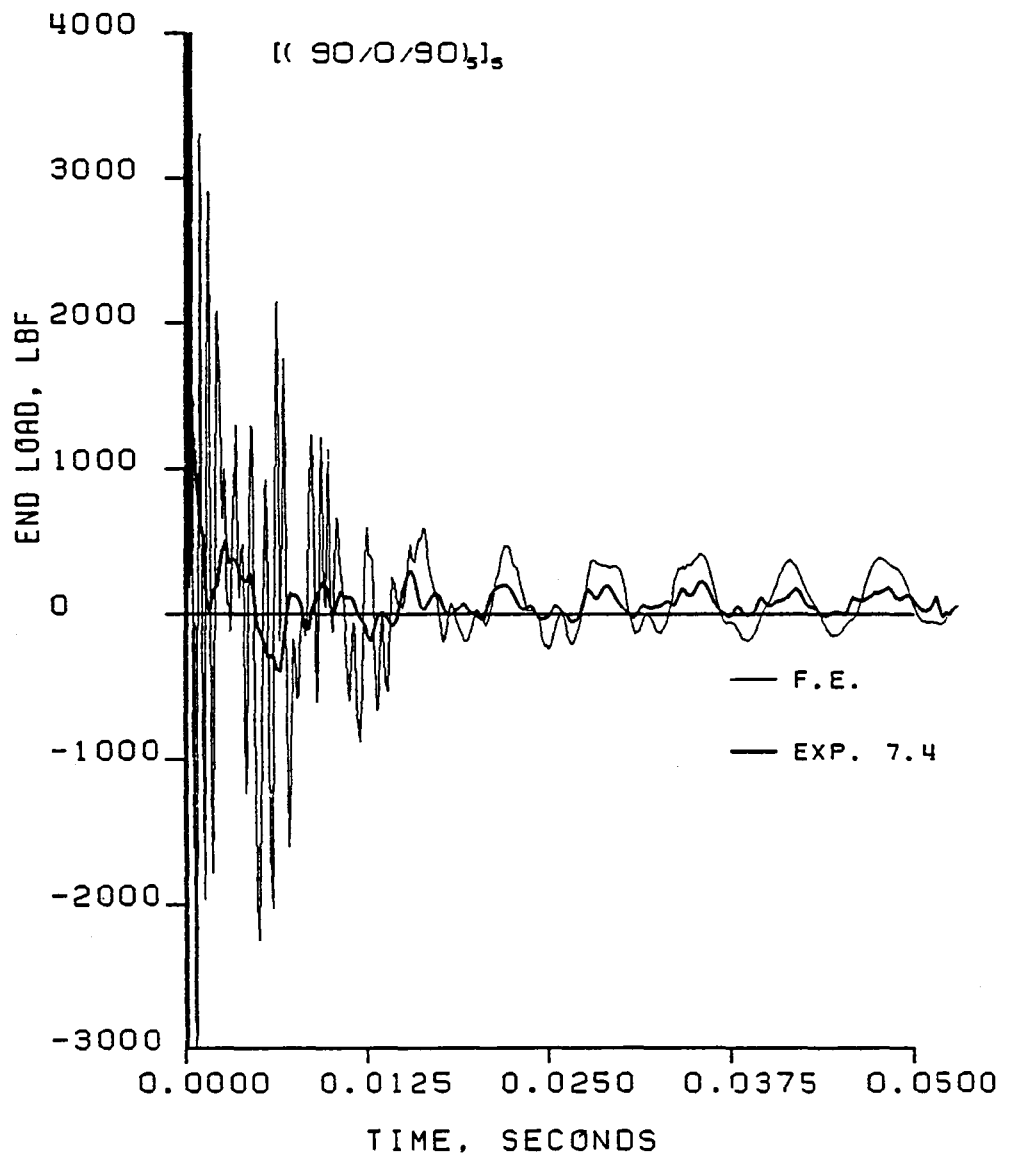
Figure 6.2   Dynamic Load vs. Time: Experimental and Finite
Element Results for a $[(90/0/90)_5]_s$ Laminate

Figure 6.3   Dynamic Displacement vs. Time: Experimental and Finite
Element Results for a $[(90/0/90)_5]_s$ Laminate
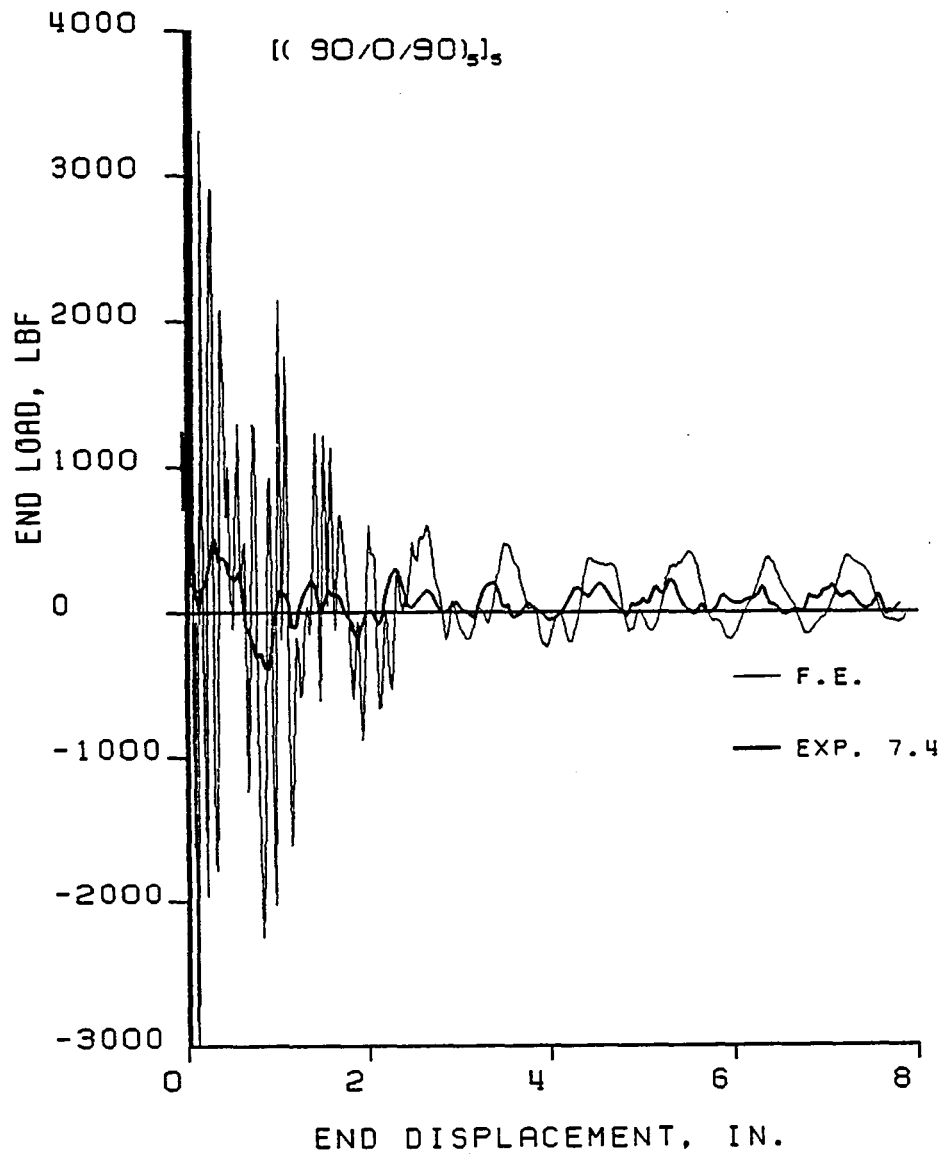
Figure 6.4   Dynamic Load vs. Displacement: Experimental and Finite Element Results for a $[(90/0/90)_5]_s$ Laminate
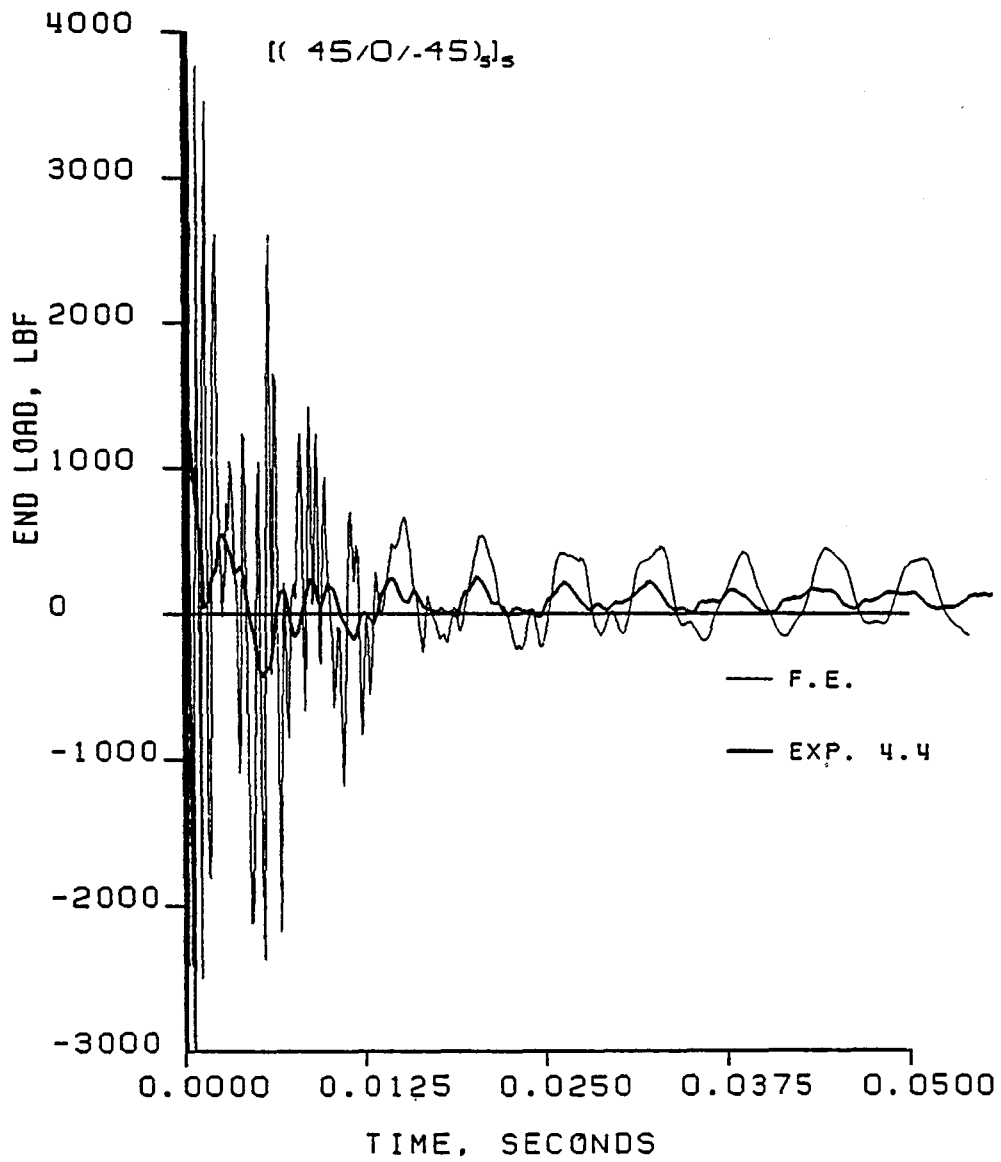
Figure 6.5   Dynamic Load vs. Time: Experimental and Finite
Element Results for a $[(45/0/-45)_5]_s$ Laminate
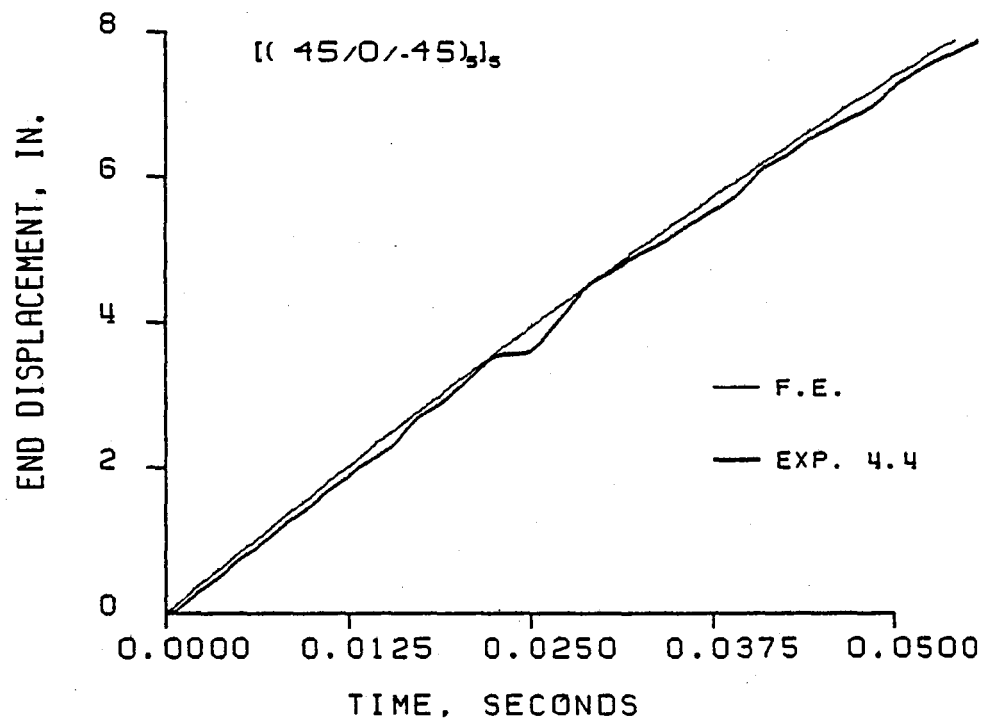
Figure 6.6   Dynamic Displacement vs. Time: Experimental and Finite Element Results for a $[(45/0/-45)_5]_s$ Laminate
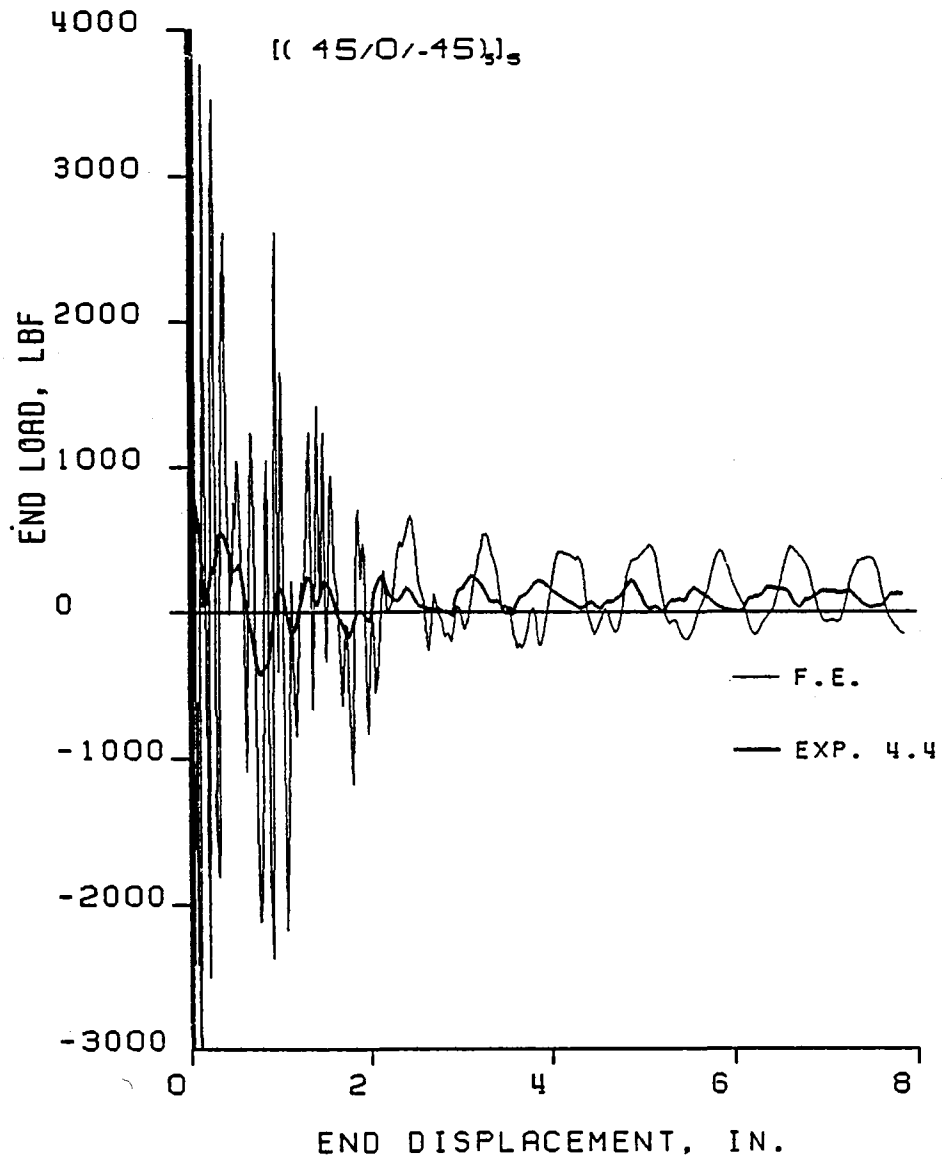
Figure 6.7   Dynamic Load vs. Displacement: Experimental and Finite
              Element Results for a $[(45/0/-45)_5]_s$ Laminate
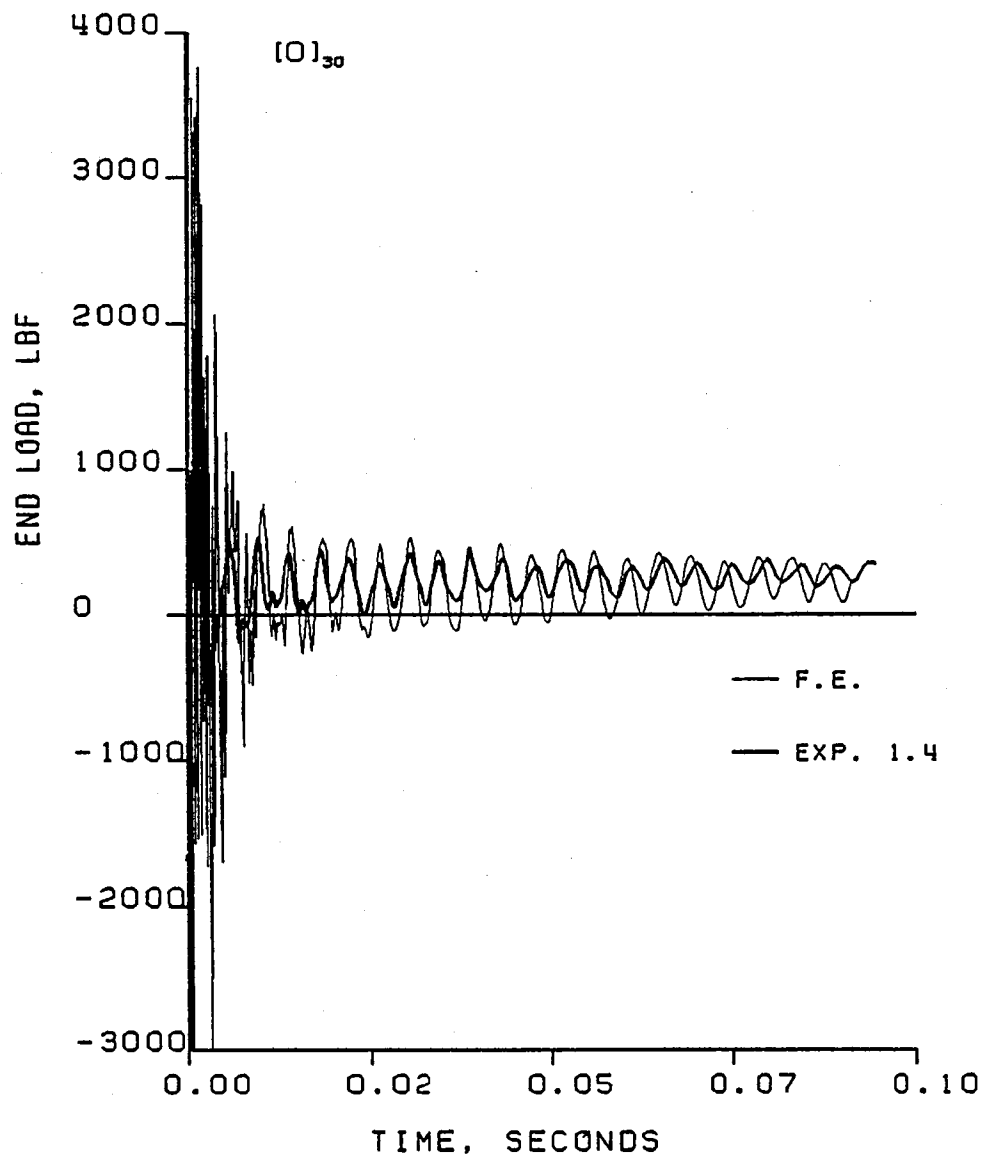
Figure 6.8   Dynamic Load vs. Time: Experimental and Finite
Element Results for a $[0]_{30}$ Laminate
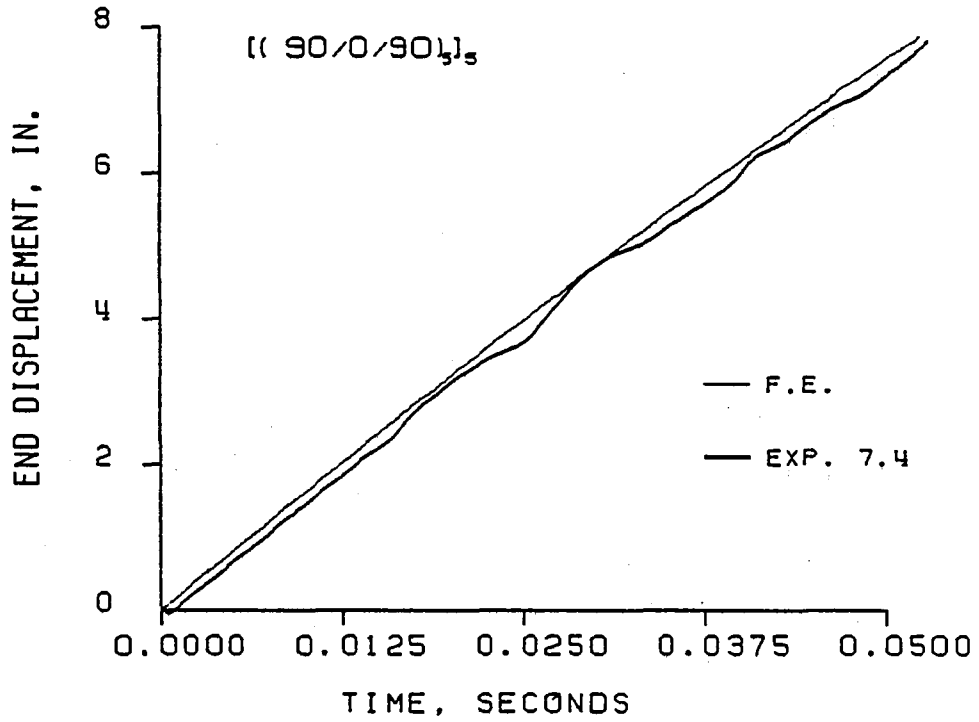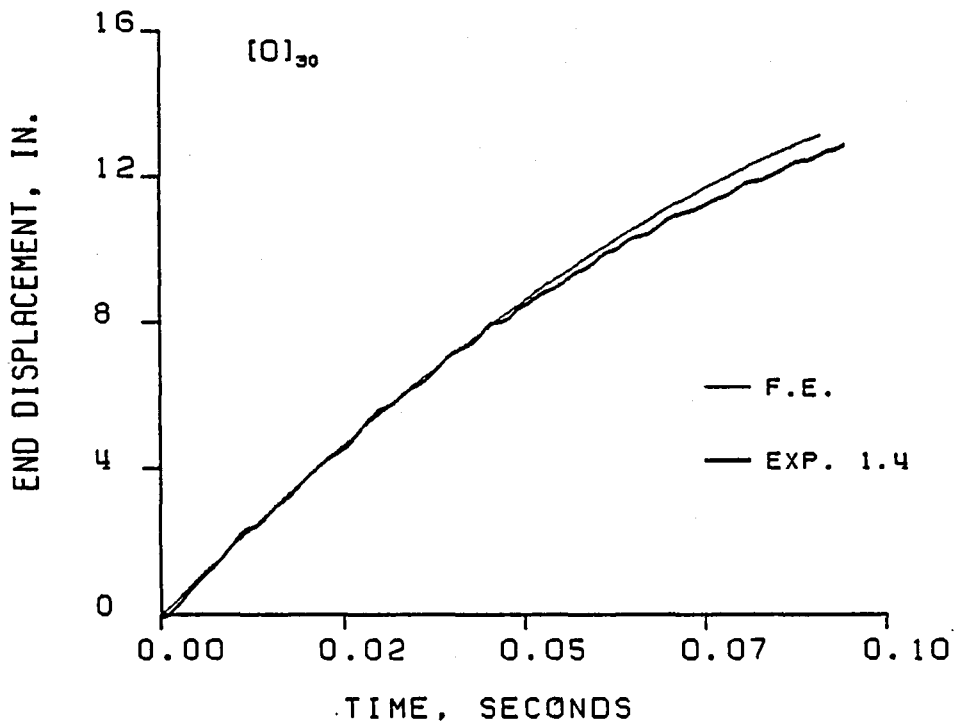
Figure 6.9   Dynamic Displacement vs. Time: Experimental and Finite
               Element Results for a $[0]_{30}$ Laminate
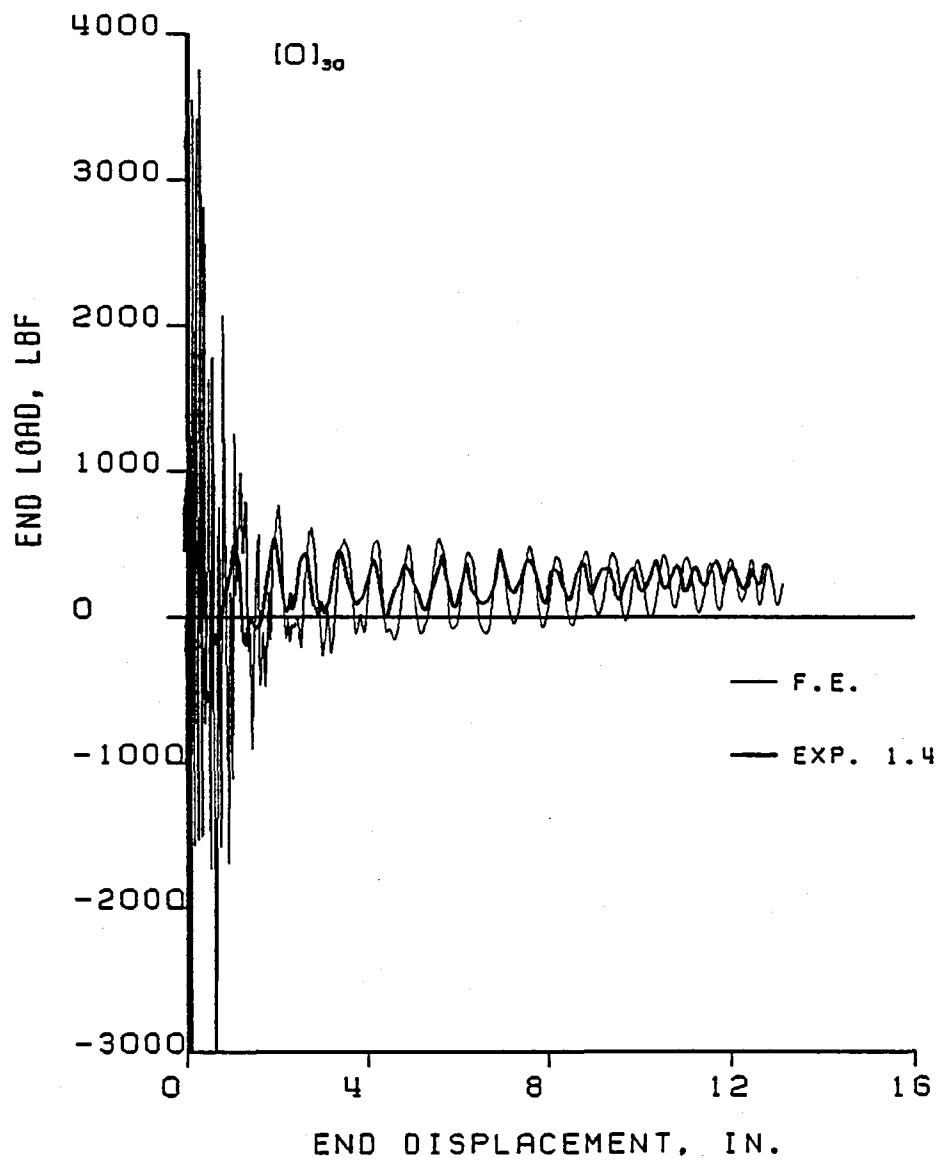
Figure 6.10   Dynamic Load vs. Displacement: Experimental and Finite
Element Results for a $[0]_{30}$ Laminate

t=0.0087   t=0.0063   t=0.0037   t=0.0013   t=0.00

(seconds)
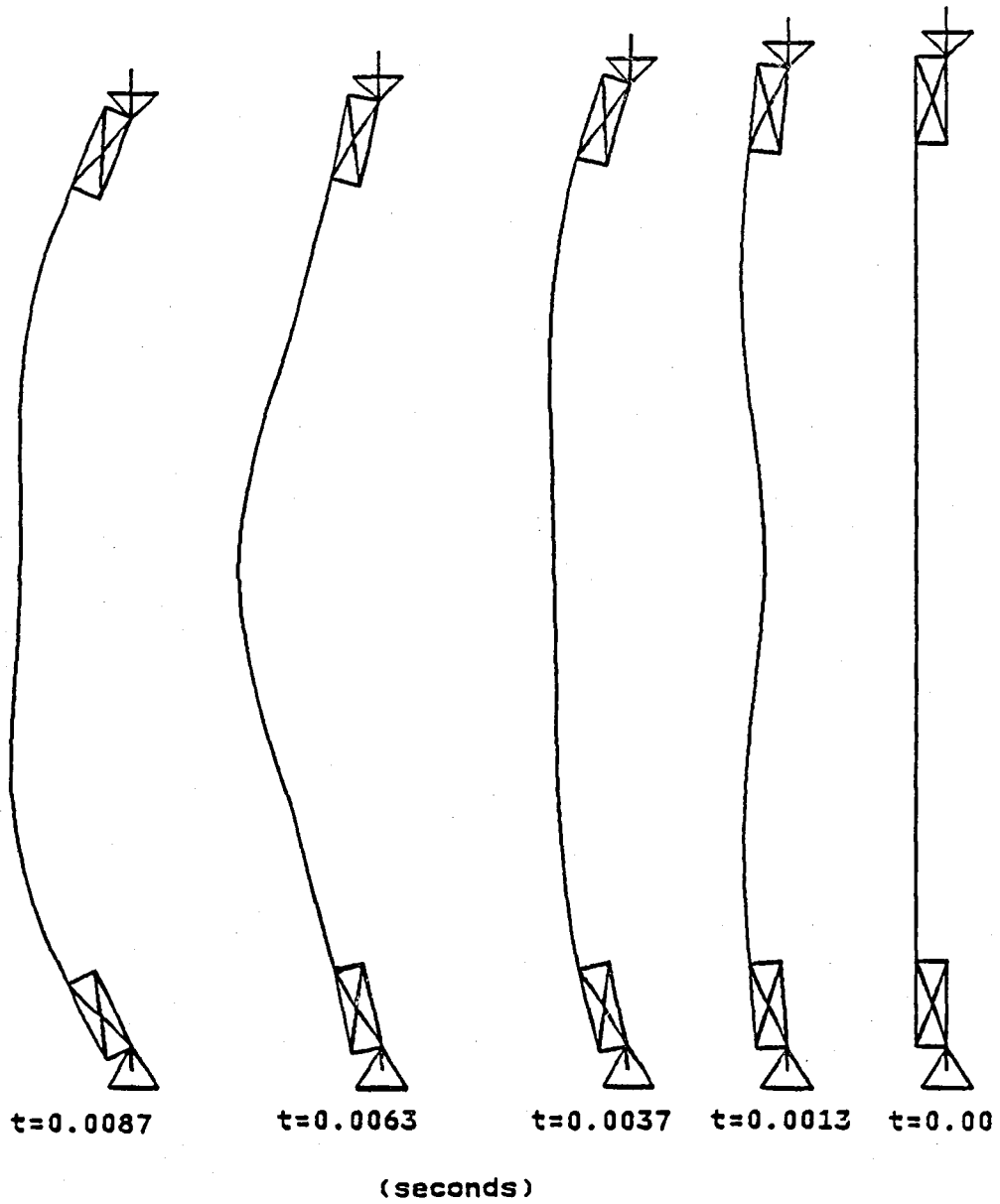
Figure 6.11   Spatial Shapes of a $[(45/0/-45)_5]_s$ Laminate Under Dynamic Loading

5 frames of film shown in fig. 3.4. The time after impact is indicated with each frame. The spatial shapes of the deformed meshes in fig. 6.11 agree quite well with the spatial shapes shown in the film. The times after impact are different in figs. 3.4 and 6.11 because there was no control in the time increment in the finite element analysis.

In summary, the analysis qualitatively predicts the nonlinear large deformation resonse of the dynamic tests but quantitatively overpredicts the amplitude of the initial load spike and the subsequent vibration. In addition, the analysis predicts much higher frequencies in the initial 0.01 sec. of the dynamic event. The discrepancies between the analyses and the experiments might be due to the lack of structural damping in the finite element model. In the experiment there is some material damping in the composite specimen, and there is damping of the high frequency components of the load as it is transmitted from the slider, to the load transducer, to the hinge, and finally to the composite specimen. The analysis assumes these load transfers are perfectly linear elastic. Also, recall from ch. 2 that the analog signal from the force transducer was filtered at 1000 hz before it was recorded. To make reasonable comparisons between the experimental data and the analysis, the analytical results should have been filtered at the same 1000 hz. Filtering analytical output to make comparisons with experimental data is a practice which has been reported by others researching crash behavior (ref. 5).

Chapter 7

CONCLUSIONS AND RECOMMENDATIONS

This study investigated the large deformation bending response of simple rectangular cross section composite beams. The study was seen as the first step in analyzing the crashworthiness of a composite fuselage structure. The overall goals of the study were to:

1. Design a simple test fixture to introduce crack-related bending loads in beams.

2. Determine any difference between large deformation static and large deformation dynamic response. Specific interest is in the failure mode.

3. Determine the influence of laminate stacking arrangements on the dynamic response and failure mode.

4. Predict the static and dynamic response, using an existing finite element program.

Conclusions

From this study the following conclusions may be drawn:

1. The eccentrically loaded column test fixture proved to be successful in introducing large deformation dynamic bending loads in to structural elements. The instrumentation recorded the deformation and failure response of the beam specimens with a minimum of problems. The configuration of the loading fixture was such that, under dynamic loading, a high amplitude initial load spike and a third mode vibratory response was excited in the beam. This more severe dynamic load environment is desirable for determining the dynamic load-deflection behavior of specific structural elements. Such

149

crash conditions will indeed introduce a severe load environment.

2. Laminate 9, a $[(0_8/90_8)]_s$ laminate and laminate 10, a $[(90_8/0_8)]_s$ laminate exhibited unusual and distinct failure modes under both static and dynamic loadings. However because these laminate had clustered laminae, they are not of practical interest.

3. The rest of the laminate types tested were of some practical interest. These laminate types exhibited no differences between the failure modes under static and dynamic loading.

4. The displacement levels at failure and, relatedly, the strains levels at failure were greater for the static tests than the dynamic tests. Strain-rate related material properties were not thought to be the cause of this result. Instead, the more severe load environment experienced by the dynamically tested specimens was felt to have been the cause.

5. The progression of failure, i.e., the number of distinct failure events during the 16 in. axial end displacement of the beam, varied with laminate type. Laminate 2, the $[(15/0/-15)_5]_s$ laminate, had from 3 to 6 failure events with associated small drops in the end load. Laminate 3, the $[(30/0/-30)_s]$ laminate, had from 2 to 3 failure events with moderate drops in the load. All other laminates had 1 major failure event, producing a drop in the load of up to 80%.

6. Neither phenomenological (strain tensor polynomial) nor mechanistic (maximum fiber strain) failure criteria as

successful in predicting the onset of failure. Failure was defined as the initiation of a reduction of load carrying capability. The strain tensor polynomial is designed to predict the onset of any failure such as matrix crack. The initiation of a matrix crack did not always coincide with the reduction of load carrying capability. The fibers failed in the presence of a matrix crack in an adjacent lamina. The matrix crack caused a strain concentration in the fibers and it is felt this initiated failure. Since it does not accurately measure the fiber strain in the region of failure, the strain measured by a strain guage cannot successfully be used to predict failure.

7. Because composite materials are heterogenous, when a crack initiates under bending loads in a lamina, it seldom propagates completely through the thickness of the laminate. Instead, the crack often turns at a lamina interface, and causes delaminations. This leaves part of the lamina undamaged and able to carry a portion of the original bending load. Failure critera do not address this issue of the prediction of the extent of failure.

8. The compressive side surface strain at the center of the beam was always greater than the tensile side surface strain, even though the beam was nearly in a state of pure bending. Further investigation revealed that the laminates had bimodular flexural properties. For laminate 4, the $[(45/0/-45)_8]_s$ laminate, the compressive flexural modulus was

measured to be nearly 50% less than the tensile flexural modulus. For the unidirectional laminate the compressive flexural modulus was measured to be 23% less than the tensile flexural modulus. Because of this, classical lamination theory was not successful in accurately predicting the flexural moduli of the laminates.

9. With empirically determined material properties used in the material model, the finite element analysis predicted with reasonable accuracy the static load-deflection relation, and the dynamic load-time, displacement-time and load-displacement relations.

Recommendations

The state of the art in finite element analysis is such that the dynamic structural response can be predicted accurately. However, the program must have available an accurate material model which characterizes the flexural rigidity, failure initiation, and failure extent. Unfortunately the state of the art in the mechanics of composite materials cannot provide such a material model. Thus, only empirically determined information can be used with confidence.

Therefore further research in the area of crashworthiness of composite structures should be directed in two main areas:

1. Basic research in the mechanics of composite materials needs to be conducted to being able to predict the material response. The bimodular behavior of a laminate, the

initiation of failure in a laminate, and the extent of failure once it has initiated need to be studied.

2. Further research should be conducted toward empirically characterizing the load-deflection behavior of practical structural elements, such as hat stiffeners or sections of a stiffened panel, under both static and dynamic loads. The test procedures used in this study would be suitable for such a characterization.

REFERENCES

1. Foye, R. L.; Swindlehurst, C. W.; and Hodges, W. T.: A Crashworthiness Test for Composite Fuselage Structure, in Fibrous Composites in Structural Design, ed., E. M. Lenoe, D. W. Oplinger and J. J. Burke, Plenum Press, New York, 1980.

2. Dorey, G.: Impact and Crashworthiness of Composite Structures, in Structural Impact and Crashworthiness, Vol. I, ed. G. A. Davies, Applied Science Publisher, London, N.Y., 1984.

3. Williams, M. Susan; and Hayduk, R. J.: Vertical Drop Test of a Transport Fuselage Section Located Forward of the Wing, NASA Technical Memorandum 85679, August 1983.

4. Williams, M. Susan; and Hayduk, R. J.: Vertical Drop Test of a Transport Fuselage Center Section Including the Wheel Wells, NASA Technical Memorandum 85706, October 1983.

5. Fasanella, E. L.; Hayduk, R. J.; Robinson, M. P.; and Widmayer, E.: Analysis of a Transport Fuselage Section Drop Test. Research in Structures and Dynamics - 1984, Robert J. Hayduk and Ahmed K. Noor, Compilers NASA CP-2335, June 1984, pp. 347-368.

6. Thompson, W. T.: Theory of Vibrations with Applications, Prentice-Hall Inc., Englewood Cliffs, N. J., 1981.

7. Rotem A.; and Hashin, Z.: Failure Modes of Angle Ply Laminates, J. Comp. Mats., Vol. 9, 1975, 191-205.

8. Wu, E. M.: Phenomenological Anisotropic Failure Criterion, in Composite Materials, Vol. 5, Fracture & Fatigue ed. Lawrence S. Broutman, Academic Press Inc., NY, 1974.

9. Kamat, M. P.: Nonlinear Transient Analysis of Aircraft Like Structures by Direct Energy Minimization-Theory and Validation, VPI-E-79,10, Virginia Polytechnic Institute and State University, Blacksburg, VA, March 1979.

10. Ackroyd, M. H.: Digital Filters, Butterworths & Co., London, 1973.

Appendix A
EFFECT OF VARIATION IN THICKNESS MEASUREMENT ON THE
PREDICTED END LOAD-DISPLACEMENT RELATION

During the cure cycle of the laminated composite plates, excess resin from the pre-preg tape flows out of the laminate. The flow of resin is not uniform throughout the plate. This results in a variation of plate thickness. When specimens are cut from the plate, the specimens are of various thickness. The thickness measurements for the specimens used in this study were presented in table 2.2. The variation in thickness from the end of the specimens to the center was fairly consistent and was accounted for in the analytical model. However, there was a significant variation in the thickness at the center of each beam, from specimen to specimen, and a random variation in the thickness across the width of any given specimen. The uncertainty in the thickness measurement was taken to be ± 0.002 in. This was one of the factors which could account for the deviation in the load-displacement relation from specimen to specimen.

To determine the effect of the variation in thickness on the load-displacement relation, the finite element analysis discussed in ch. 6 was employed. Figure A.1 shows the load displacement relation for 3 unidirectional beams. The center curve is from the beam with the average center thickness of t = 0.168 in. taken from table 2.2. The top and bottom curve represent the beams with the maximum variation from the average center thickness, t = 0.166 in. and t = .170 in. respectively. With the uncertainty of ±0.002 in. in the thickness there is an uncertainty in the displacement at 300 lbs of end load, of ±0.94 in. So with a variation in thickness of less than 1%, the variation in

155
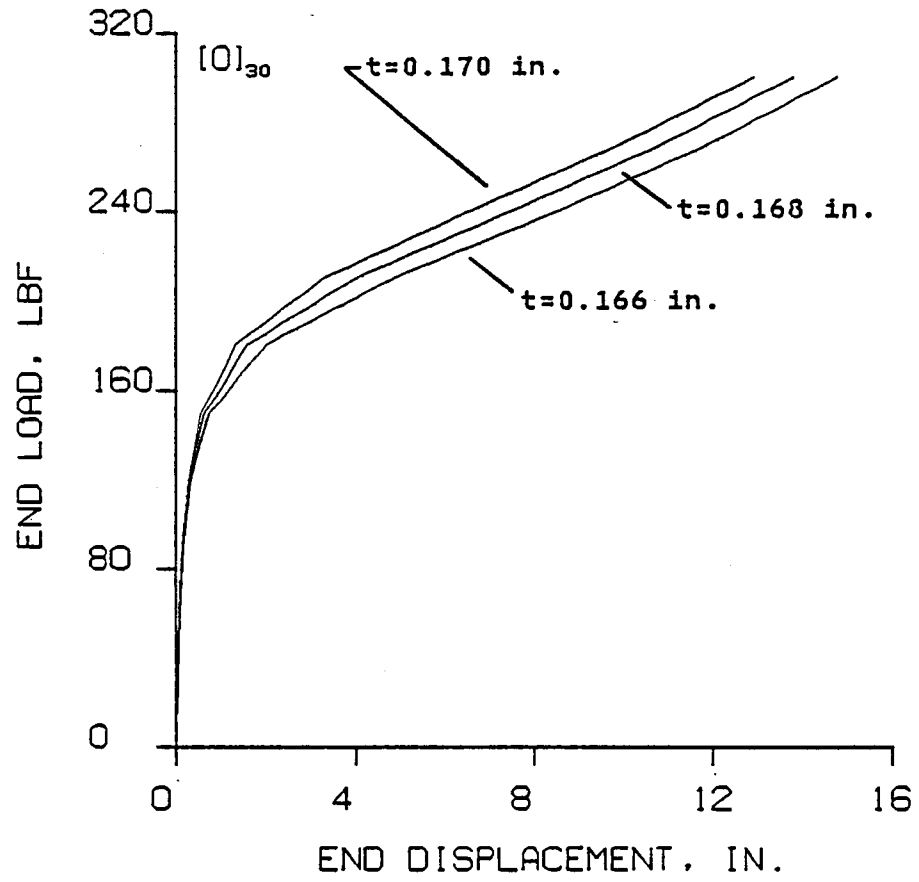
Figure A.1   Effect of Beam Thickness on Static Load-Displacement
Relation

displacement was about 8%. Such a variation in thickness could account for scatter of the data from the three replicate specimens.

Appendix B

EFFECT OF ECCENTRICITY ON THE LOAD-DISPLACEMENT RELATION

In the manual construction of a laminated plate, the orientation of the lamina can be placed with an accuracy of, at best, $\pm 2°$. Less than perfect placement of the lamina results in a slightly unsymmetric laminate. After the cure cycle the laminate becomes warped by the resulting unsymetric residual thermal stresses. The warp of the specimens contributes to the eccentricity of the load. The amount of warp in the beams of each laminae type was measured as the camber, or deviation from perfect straightness, with an uncertainty ± 0.01 in. The results of these measurements were presented in table 2.2. The amount of camber in each laminate type was included in the analytical model. However the uncertainty in the camber measurement, taken to be ± 0.01 in., was one of the factors effecting the deviation in the load-displacement relation from specimen to specimen.

To determine the effect of the minor variations in the eccentricity on the load-displacement relation, the finite element analysis discussed Ch. 6 was employed. The eccentricity due to the camber of the beams was added to the eccentricity from the loading configuration which was 5/8 in. Figure B.1 shows the load-displacement relation for three unidirectional beams. The one beam was the average camber, from table 2.2, of 0.03 in. The other two curves represent the beams with the maximum variation from the average camber, 0.02 and 0.04 in., respectively. As can be seen in the figure the three curves are essentially
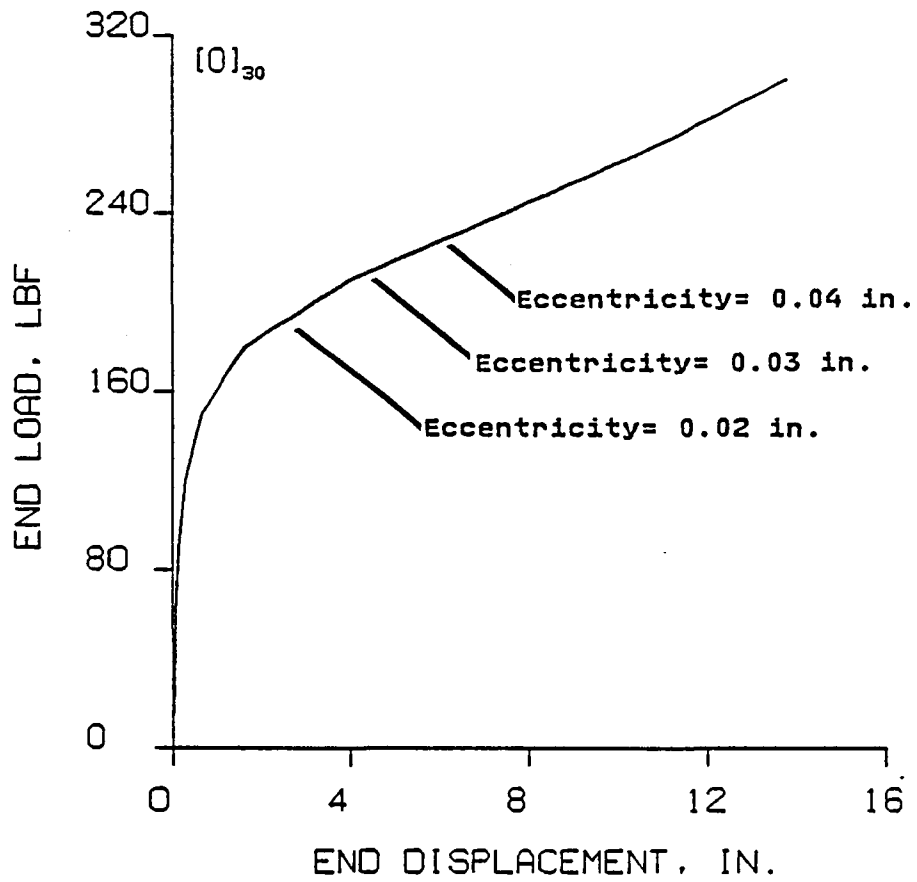
Figure B.1   Effect of Beam Eccentricity on Static Load-Displacement
Relation

coincident. Therefore minor variations ($\approx$1%) in the eccentricity of the load do not significantly effect the load displacement relation.

Appendix C

DIGITAL FILTER ROUTINE

The random noise in the displacement signal, which was subsequently digitized at 4000 samples per second, was smoothed by a digital filter routine. A low-pass filter with an ideal cut-off frequency of 500 hz. was designed and then programmed in FORTRAN. To design the filter, a fast Fourier transform routine transformed a filter gain function in the frequency domain to a smoothing function in the time domain (ref. 10). Then a window routine computed an optimal weighting sequence from the smoothing function. The weighting sequence used was 31 clock periods long, i.e., 31 sample points long.

Table C.1 shows the positive portion of the weighting sequence used. The table gives the gain characteristics, in decibels, and the phase characteristics, in degrees, as a function of frequency. The negative portion, i.e., clock period -1 to -15, is the same as the positive portion. Thus the filter is symmetric.

161

TABLE C
FILTER CHARACTERISTICS

Clock Period	Weight Sequence	Freq (HZ)	Gain dbs	Phase Shift (Deg)
0	0.12500	0	-0.00000	0.00000
1	0.12142	250	-0.00001	-0.00003
2	0.11109	500	-6.02061	-0.00001
3	0.09518	750	-120.00000	0.00000
4	0.07544	1000	-120.00000	0.00000
5	0.05401	1250	-120.00000	0.00000
6	0.03307	1500	-120.00000	0.00000
7	0.01457	1750	-120.00000	0.00000
8	0.00000	2000	-120.00000	0.00000
9	-0.00981	2250	-120.00000	0.00000
10	-0.01476	2500	-120.00000	0.00000
11	-0.01543	2750	-120.00000	0.00000
12	-0.01294	3000	-120.00000	0.00000
13	-0.00876	3250	-120.00000	0.00000
14	-0.00440	3500	-120.00000	0.00000
15	-0.00118	3750	-120.00000	0.00000

Appendix D
STATIC LOAD-DISPLACEMENT DATA

In this appendix the static load-displacement relation for each specimen tested is displayed. The figures show the loading and unloading load-displacement relations. Specimen 10 shows unusual behavior because it began to crack immediately upon loading.

Figure D.1   Static Load-Displacement Relation for Specimens
              1.1 and 1.2
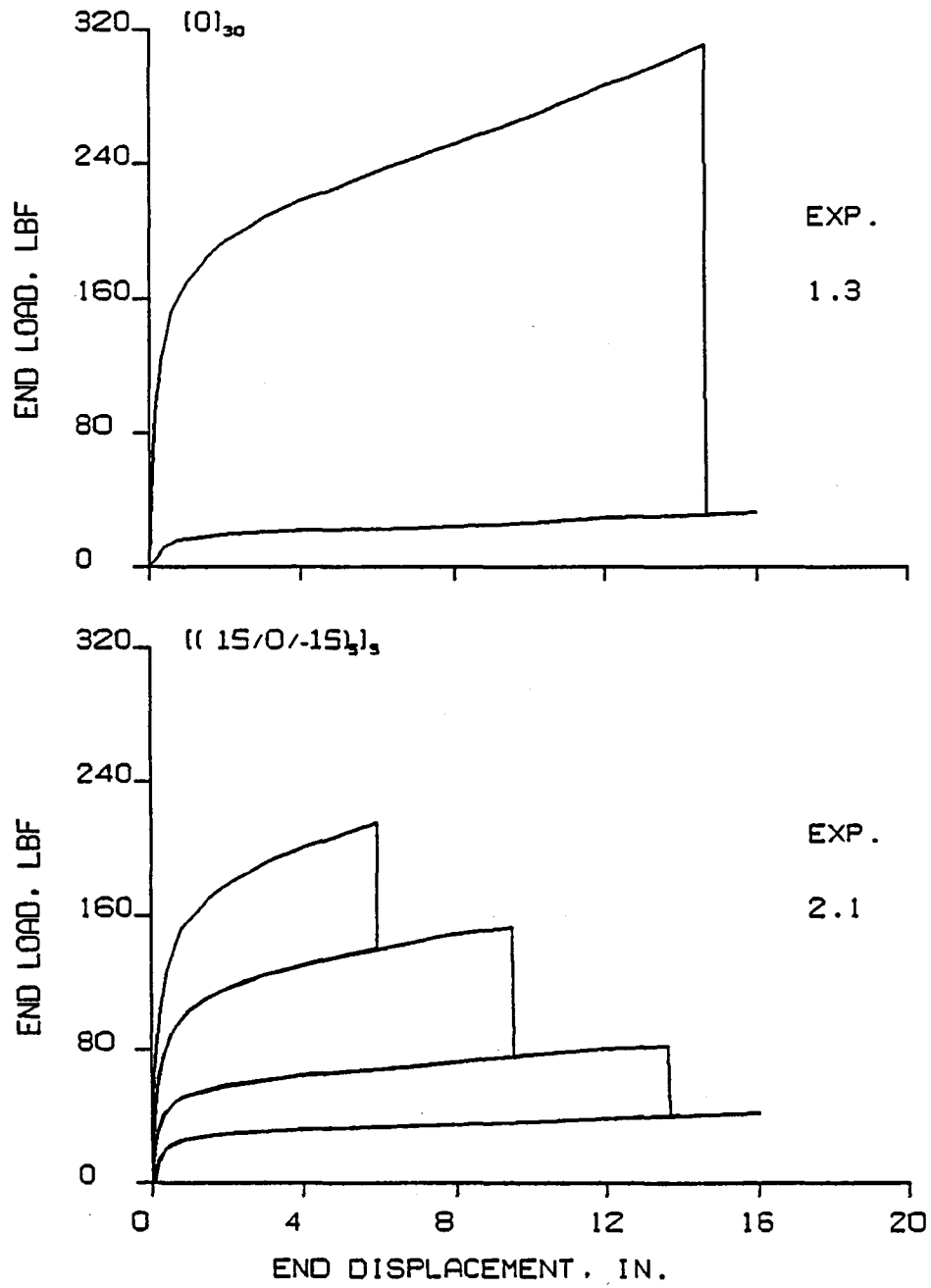
Figure D.2   Static Load-Displacement Relation for Specimens
1.3 and 2.1
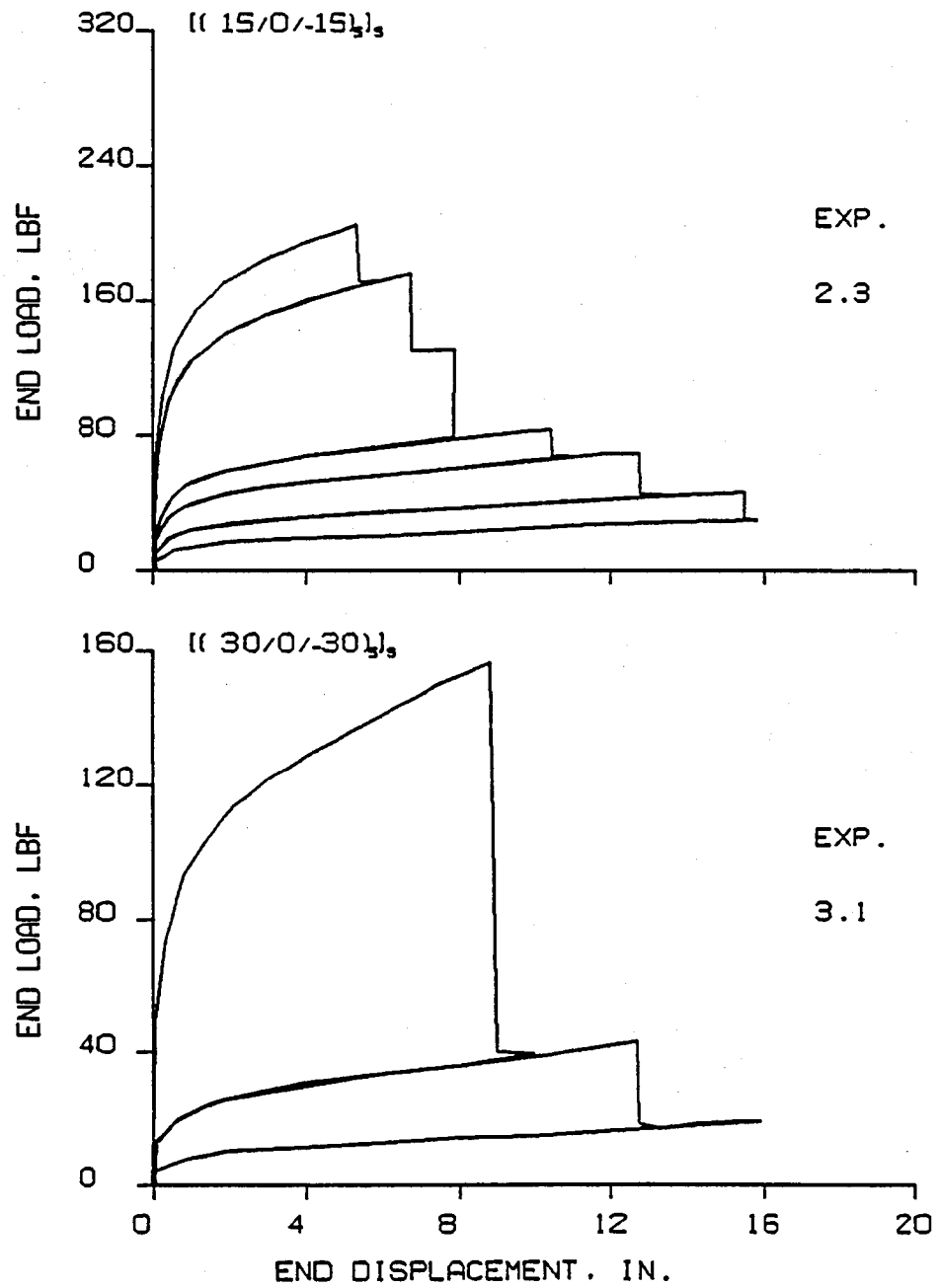
Figure D.3   Static Load-Displacement Relation for Specimens
             2.3 and 3.1
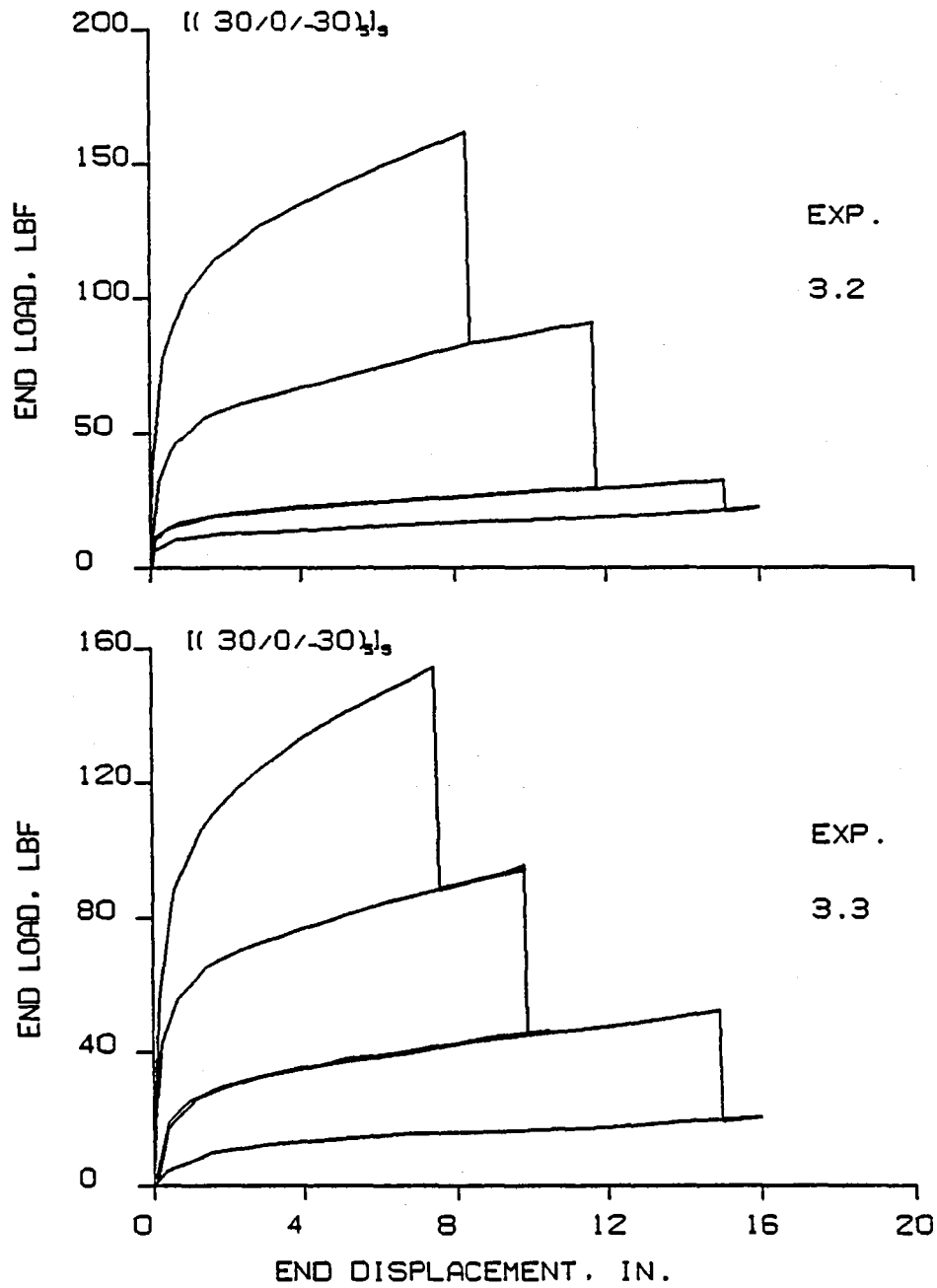
Figure D.4   Static Load-Displacement Relation for Specimens
             3.2 and 3.3
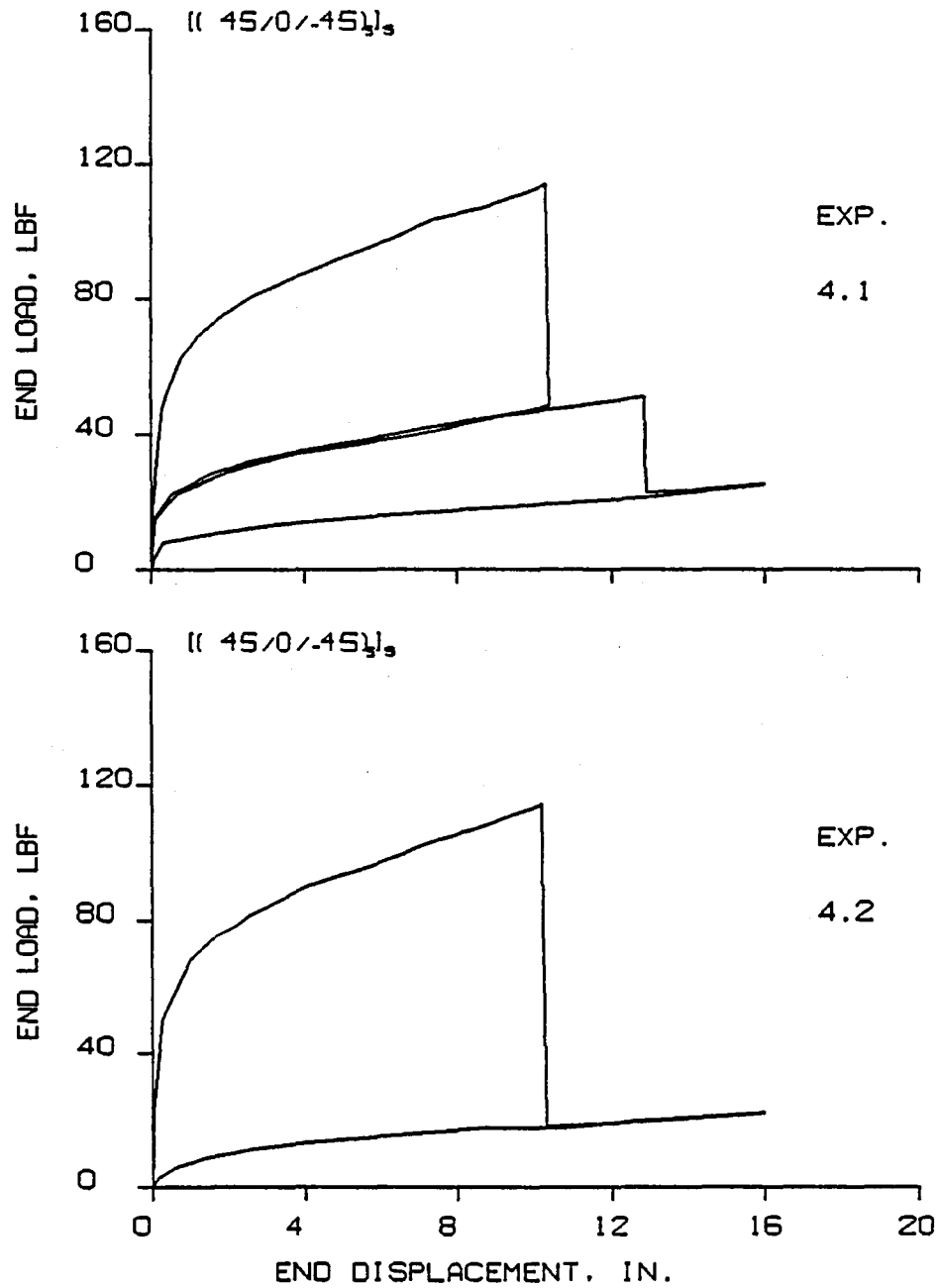
Figure D.5   Static Load-Displacement Relation for Specimens
             4.1 and 4.2
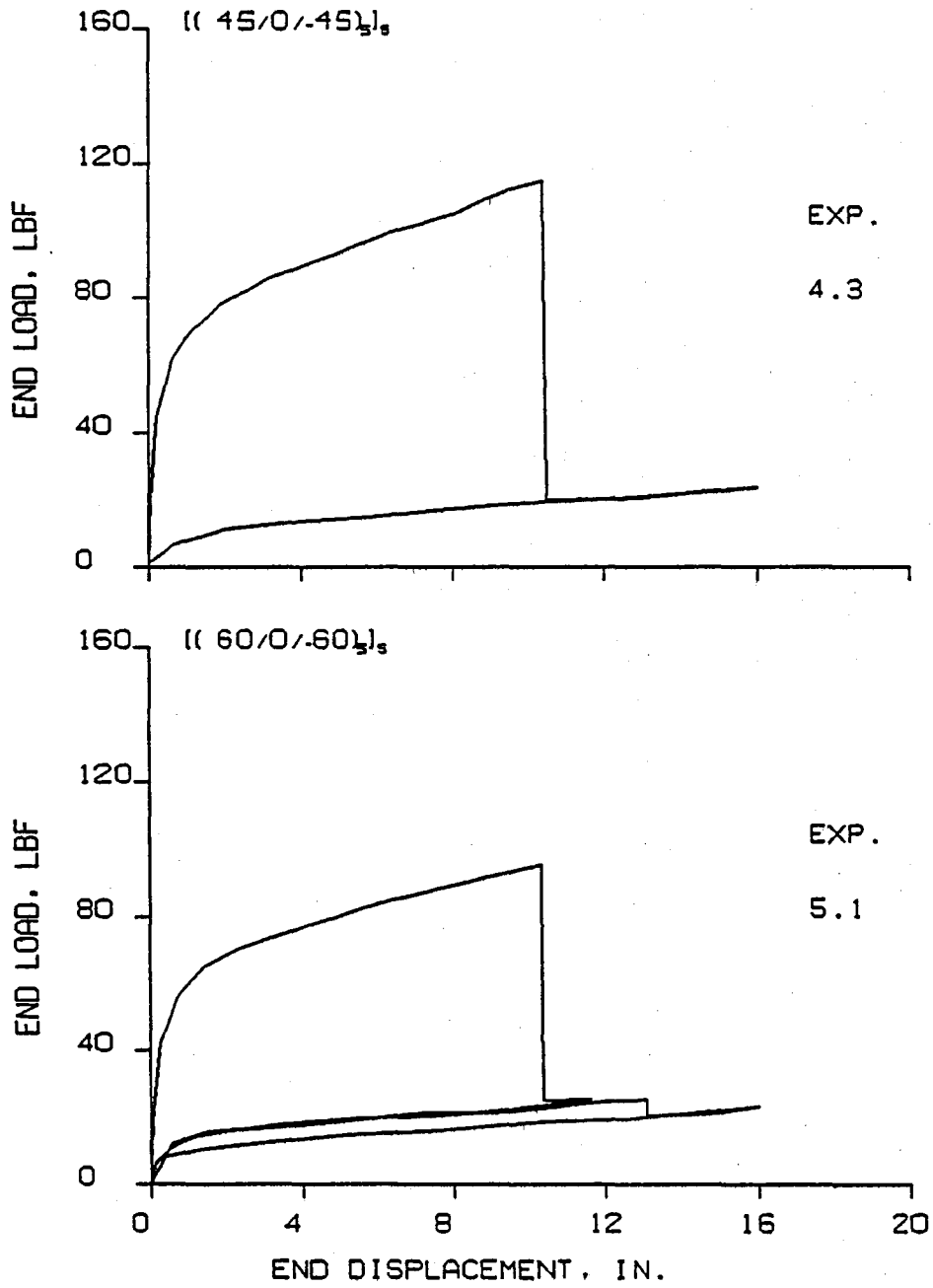
Figure D.6   Static Load-Displacement Relation for Specimens
            4.3 and 5.1
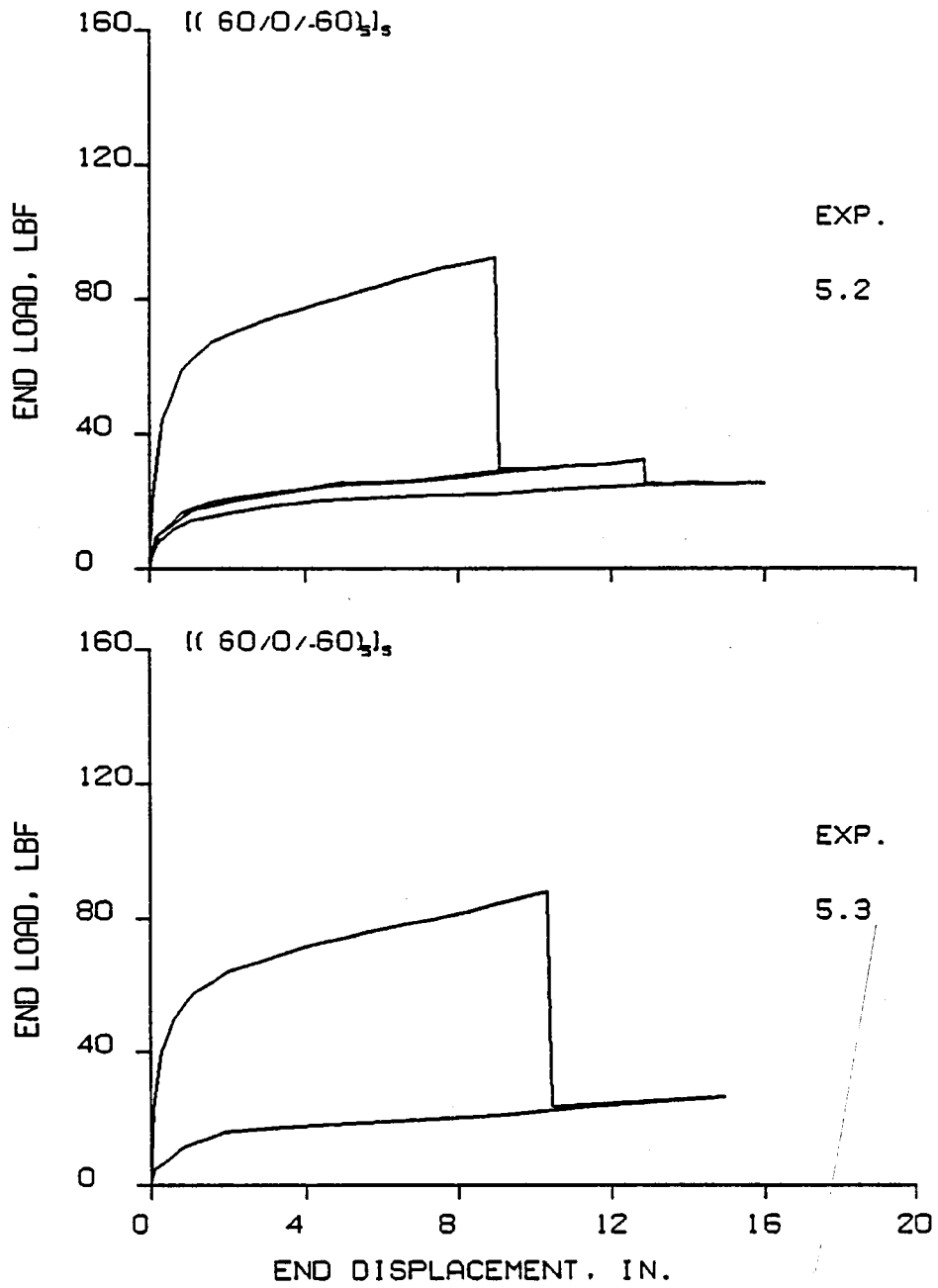
Figure D.7   Static Load-Displacement Relation for Specimens 5.2 and 5.3
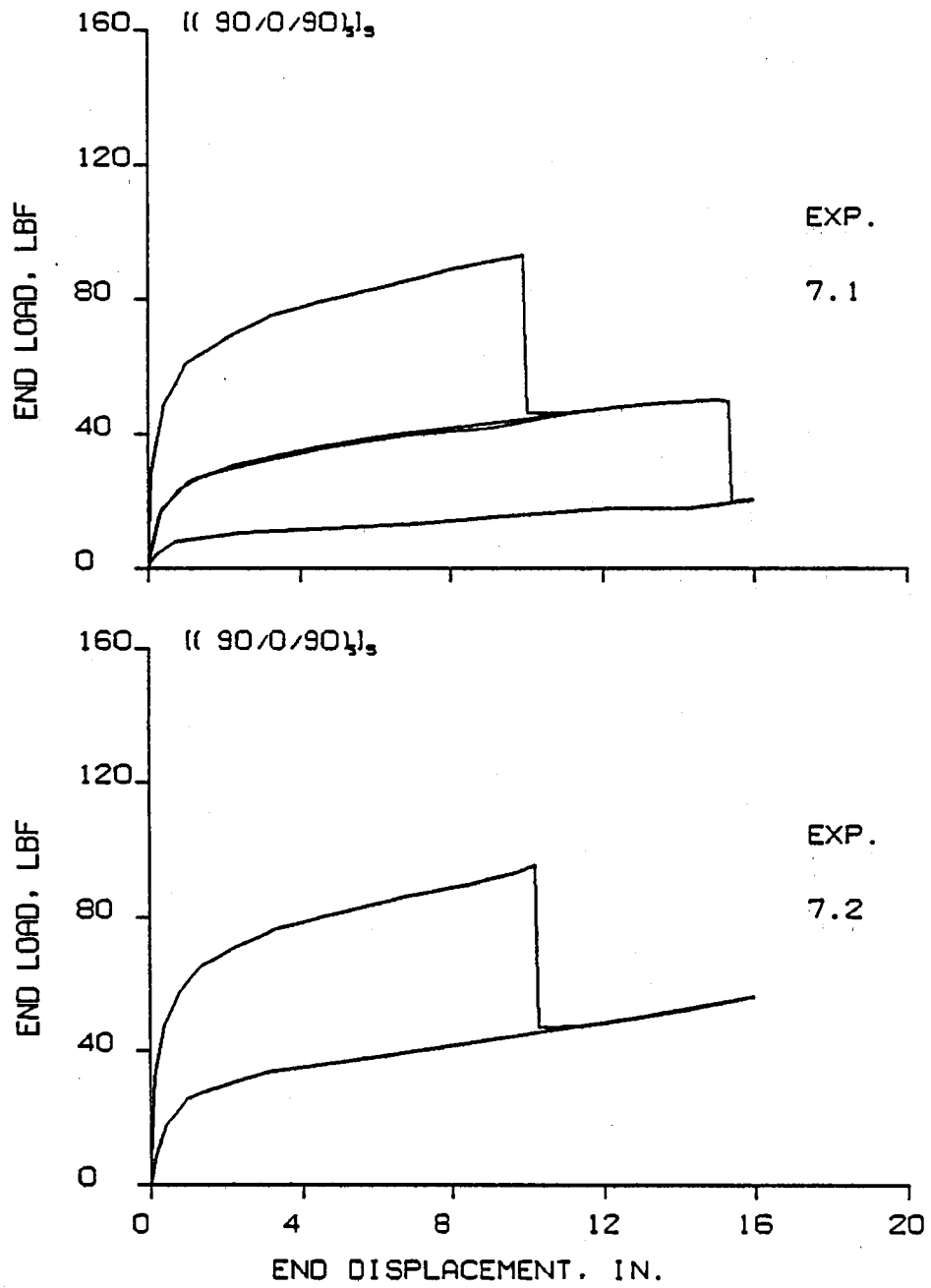
Figure D.8   Static Load-Displacement Relation for Specimens
             7.1 and 7.2
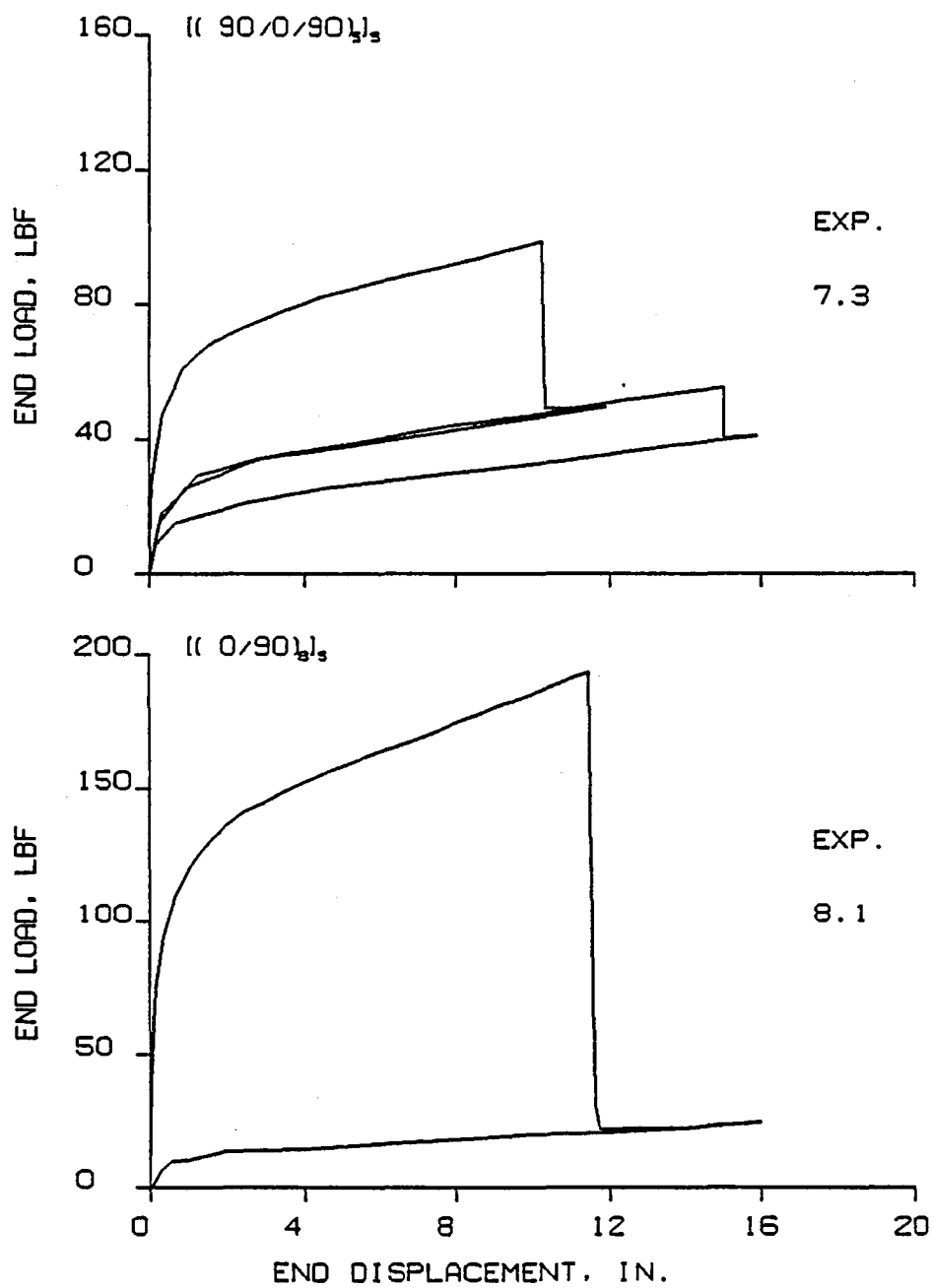
Figure D.9   Static Load-Displacement Relation for Specimens 7.3 and 8.1
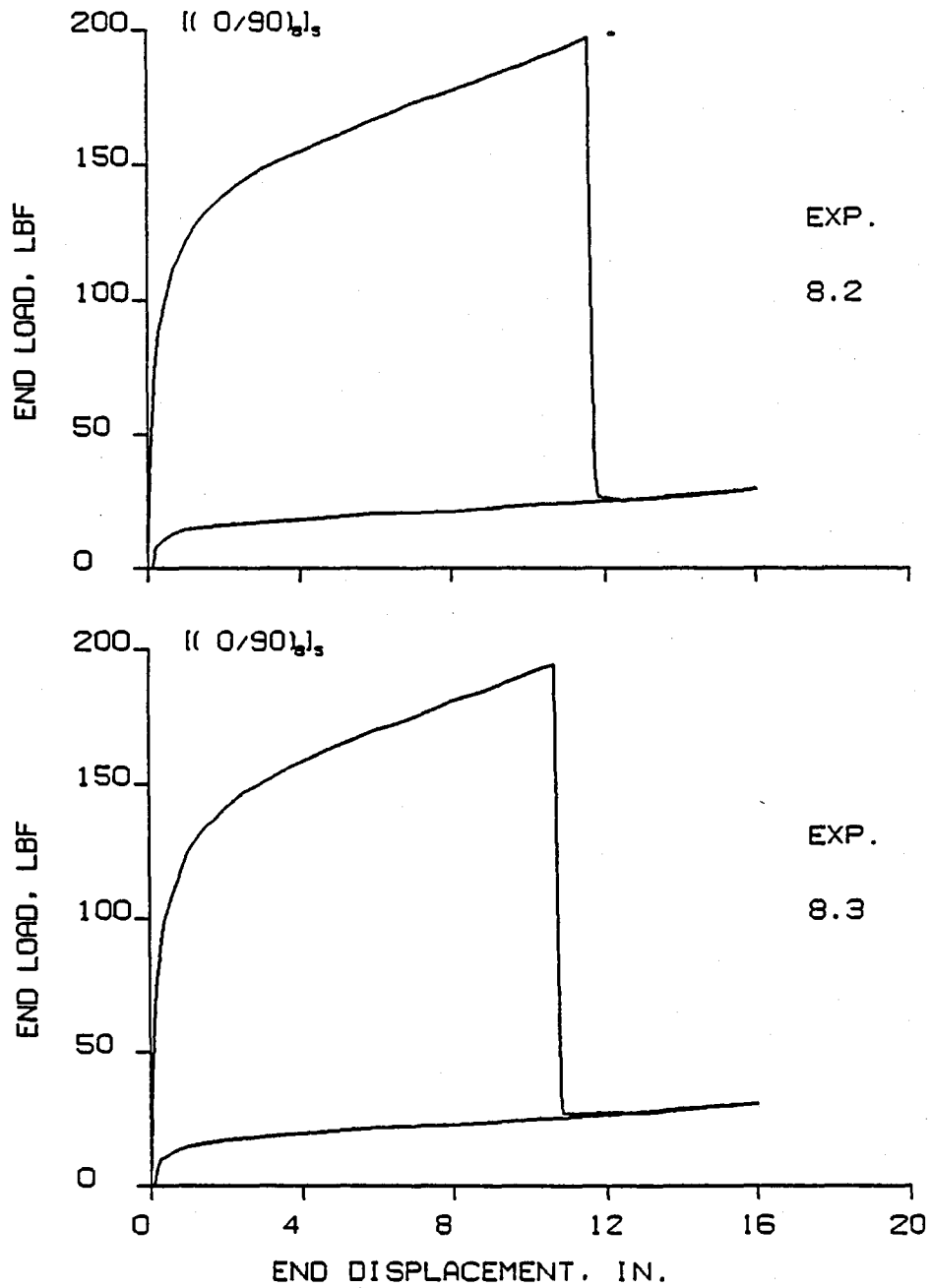
Figure D.10   Static Load-Displacement Relation for Specimens
8.2 and 8.3
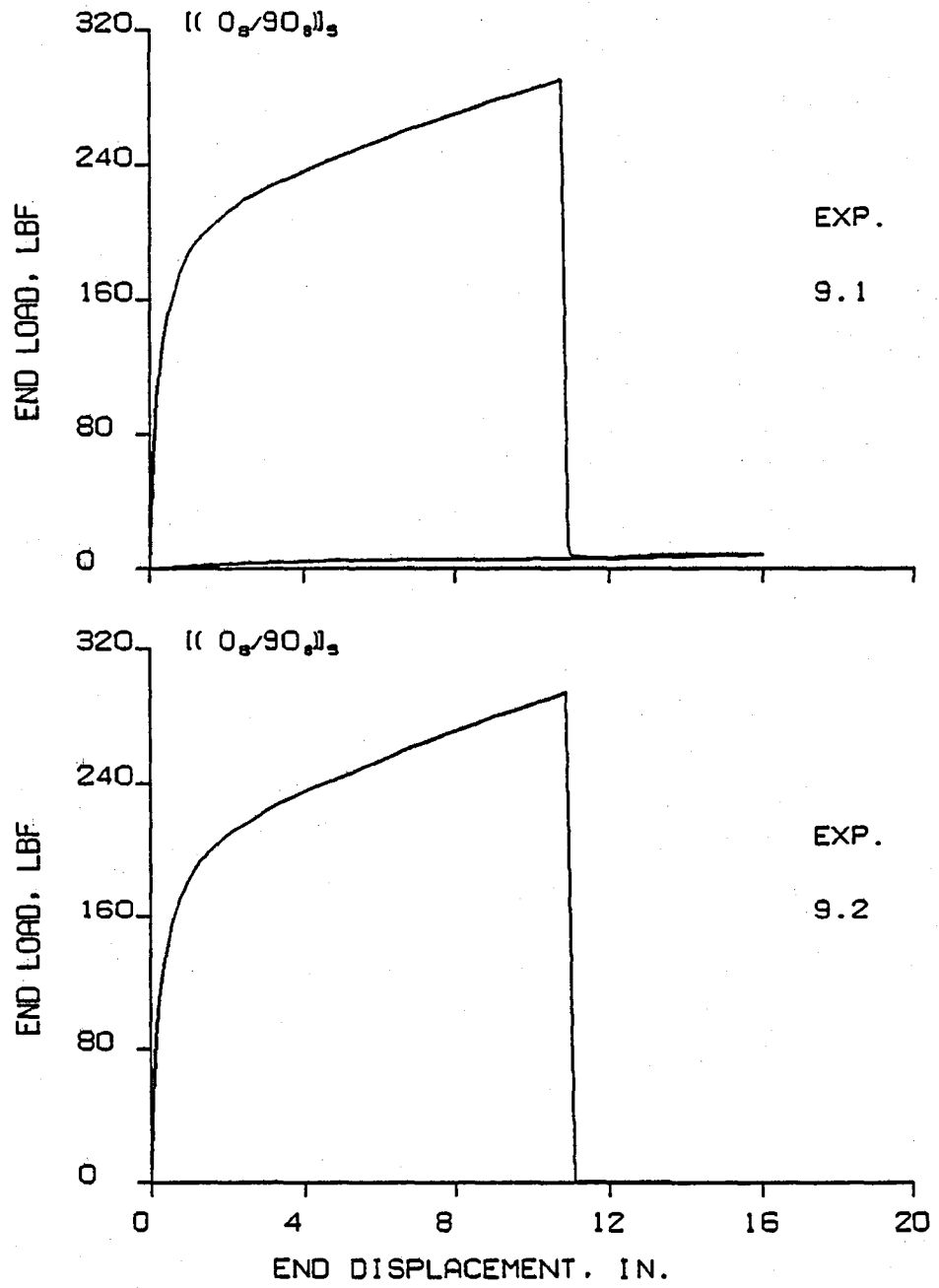
Figure D.11   Static Load-Displacement Relation for Specimens
9.1 and 9.2
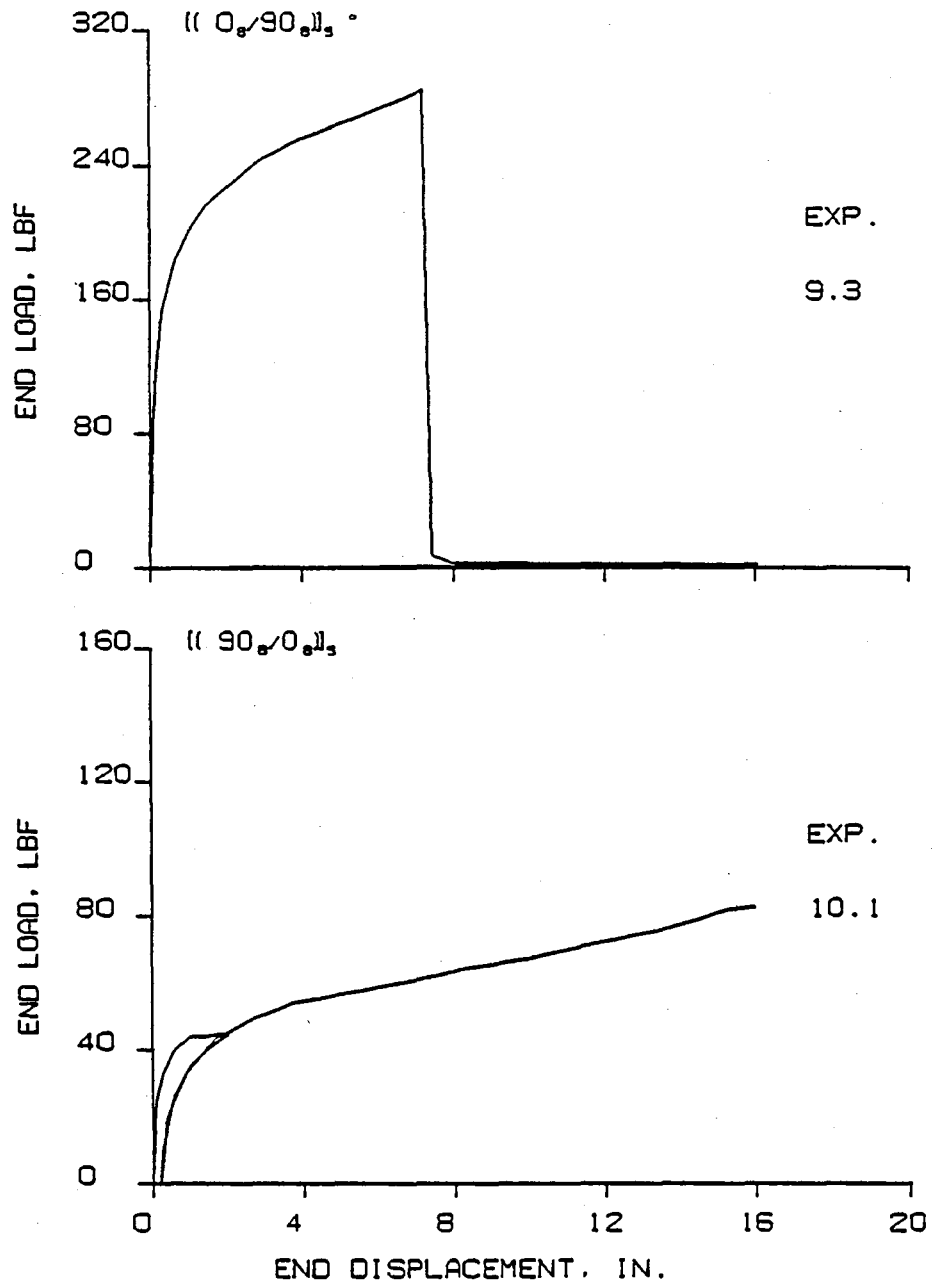
Figure D.12   Static Load-Displacement Relation for Specimens
9.3 and 10.1
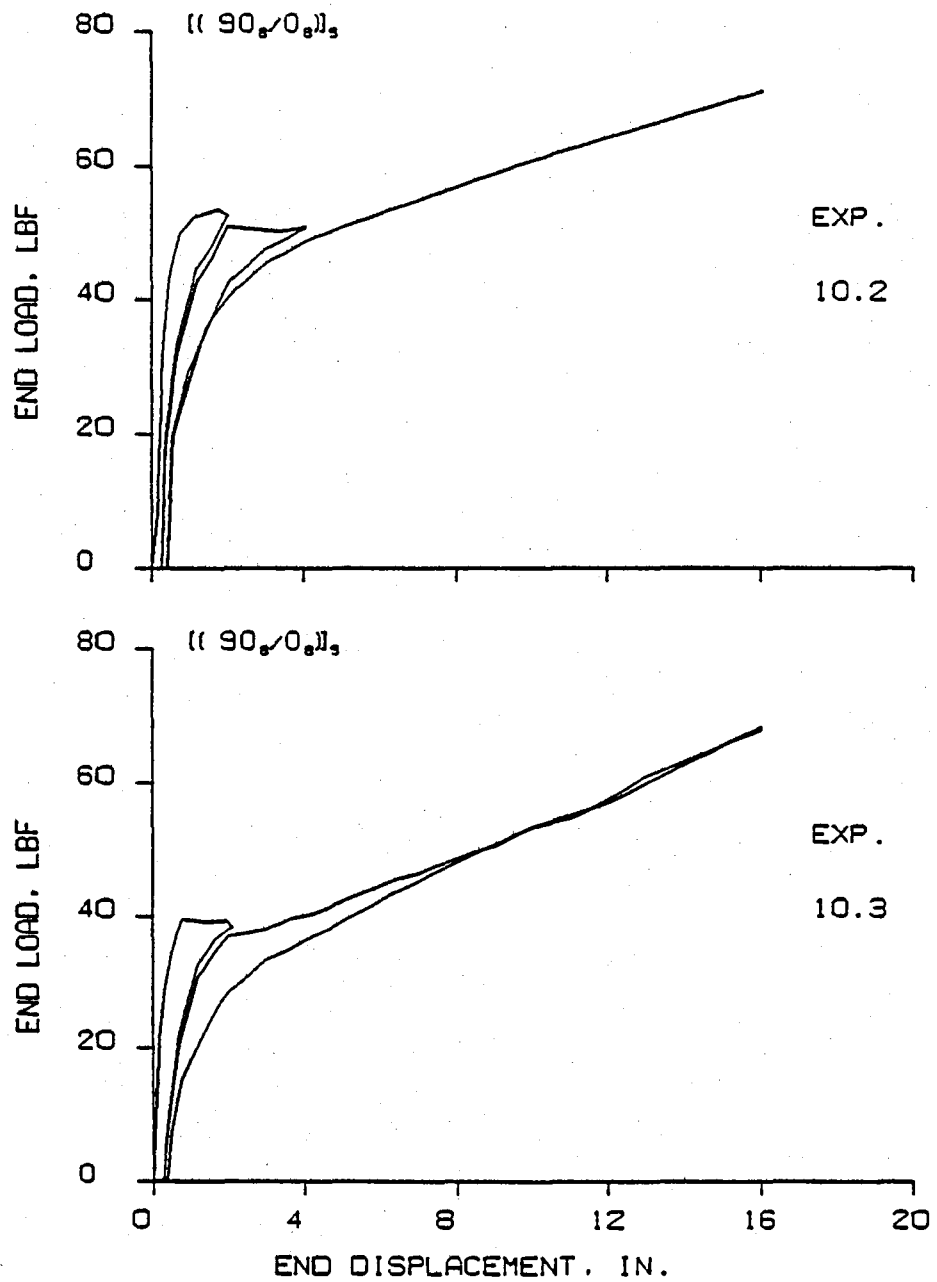
Figure 0.13 Static Load-Displacement Relation for Specimens
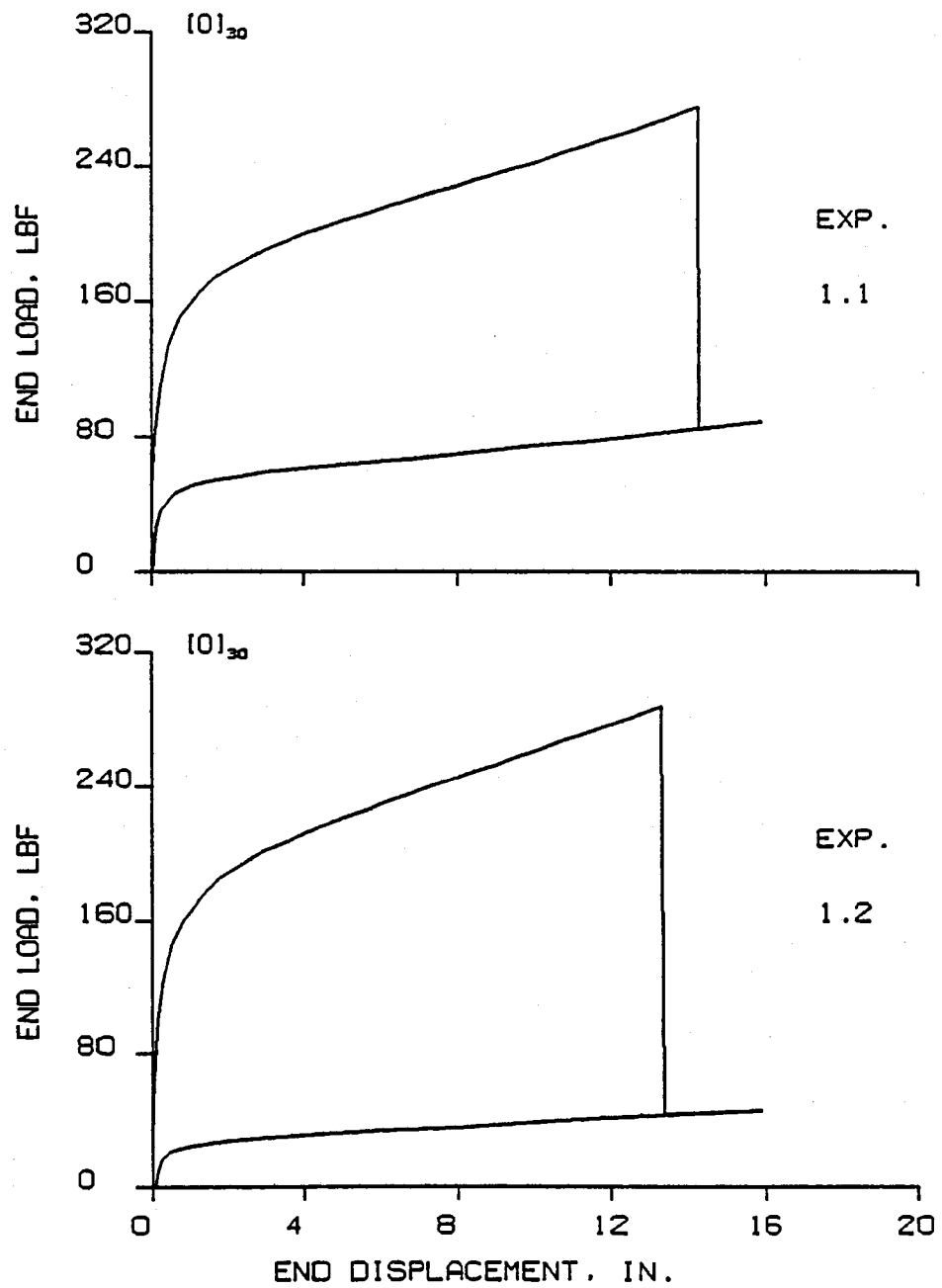10.2 and 10.3
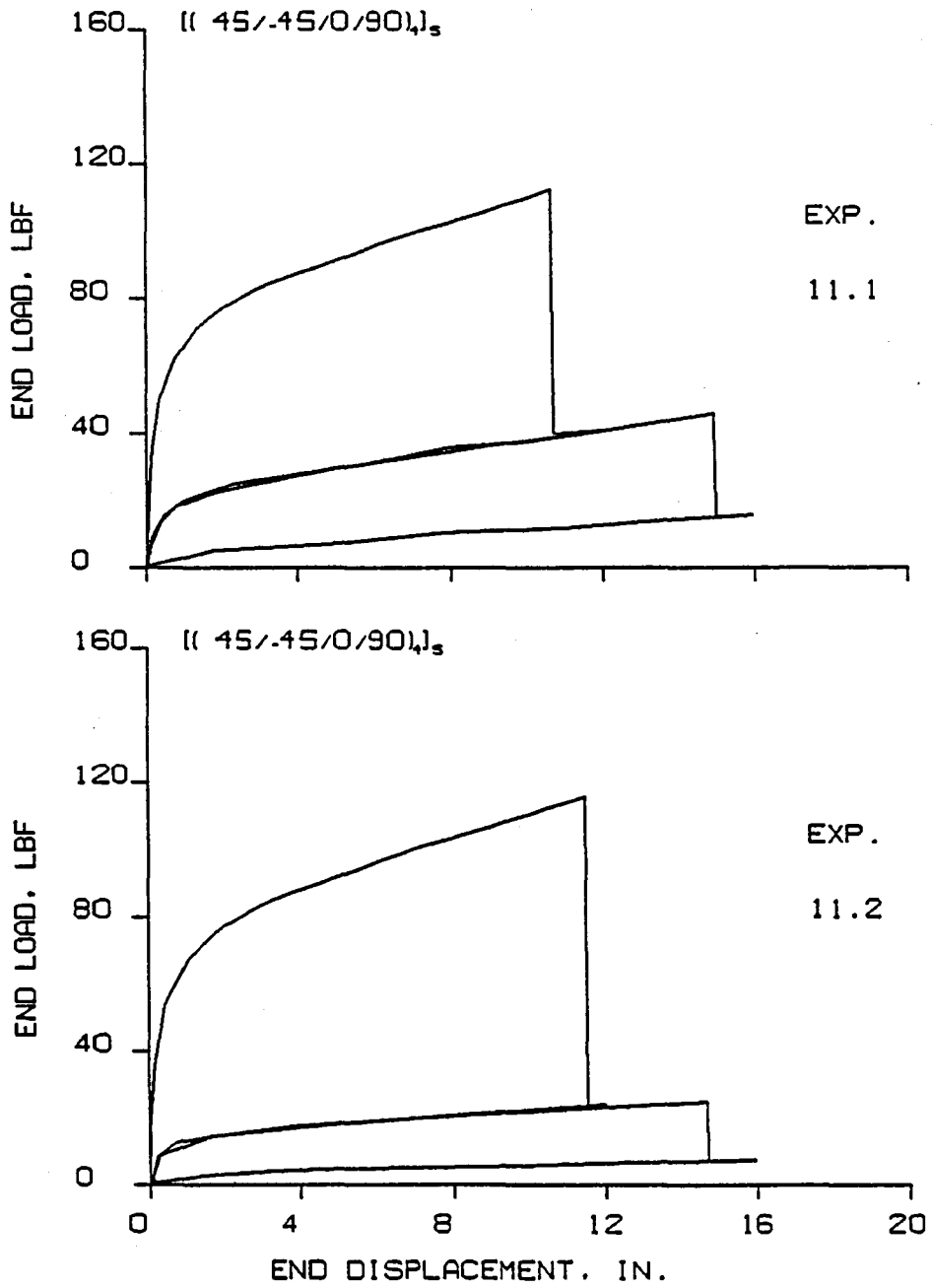
Figure D.14   Static Load-Displacement Relation for Specimens
               11.1 and 1.2
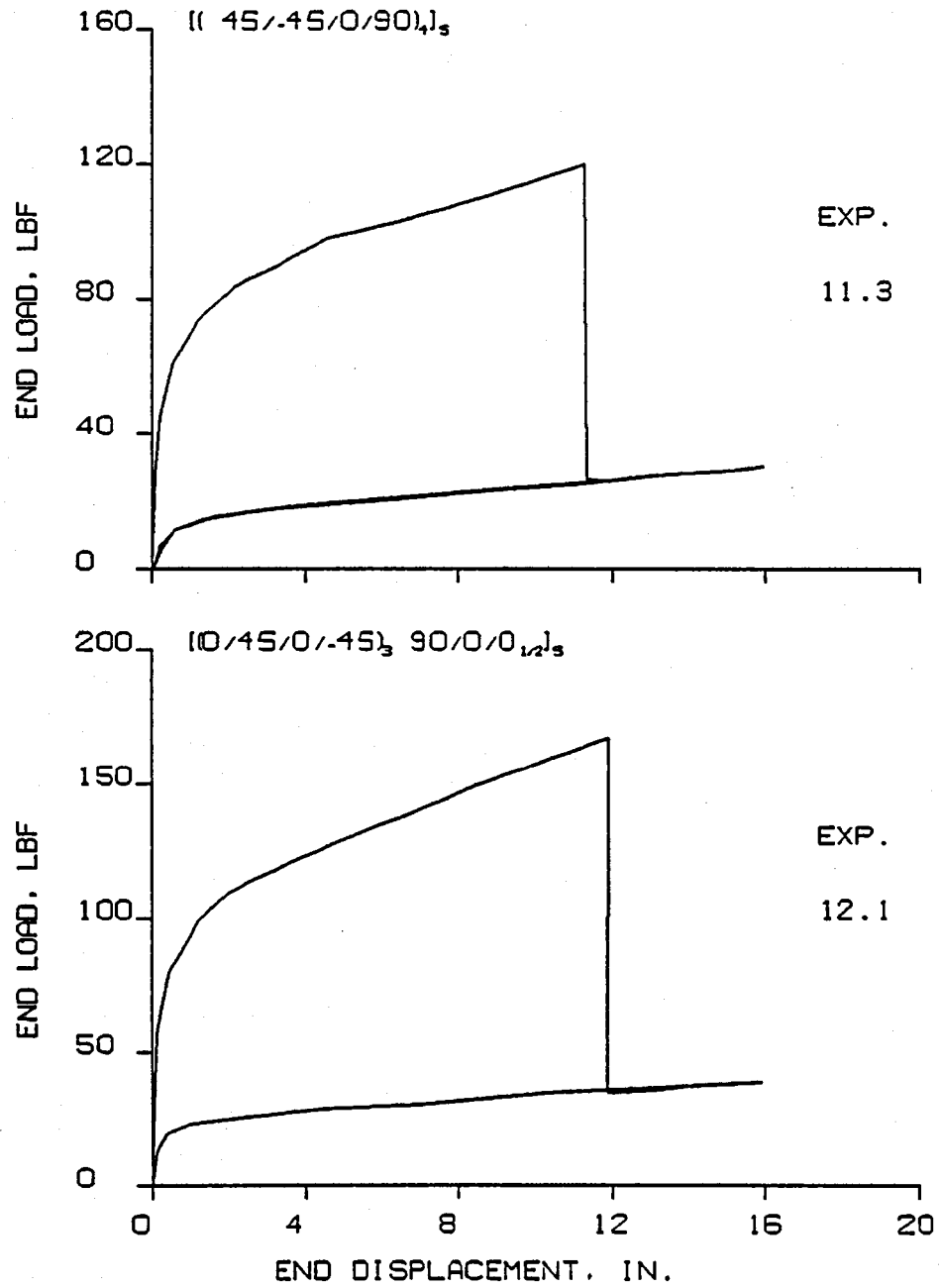
Figure D.15   Static Load-Displacement Relation for Specimens
11.3 and 12.1
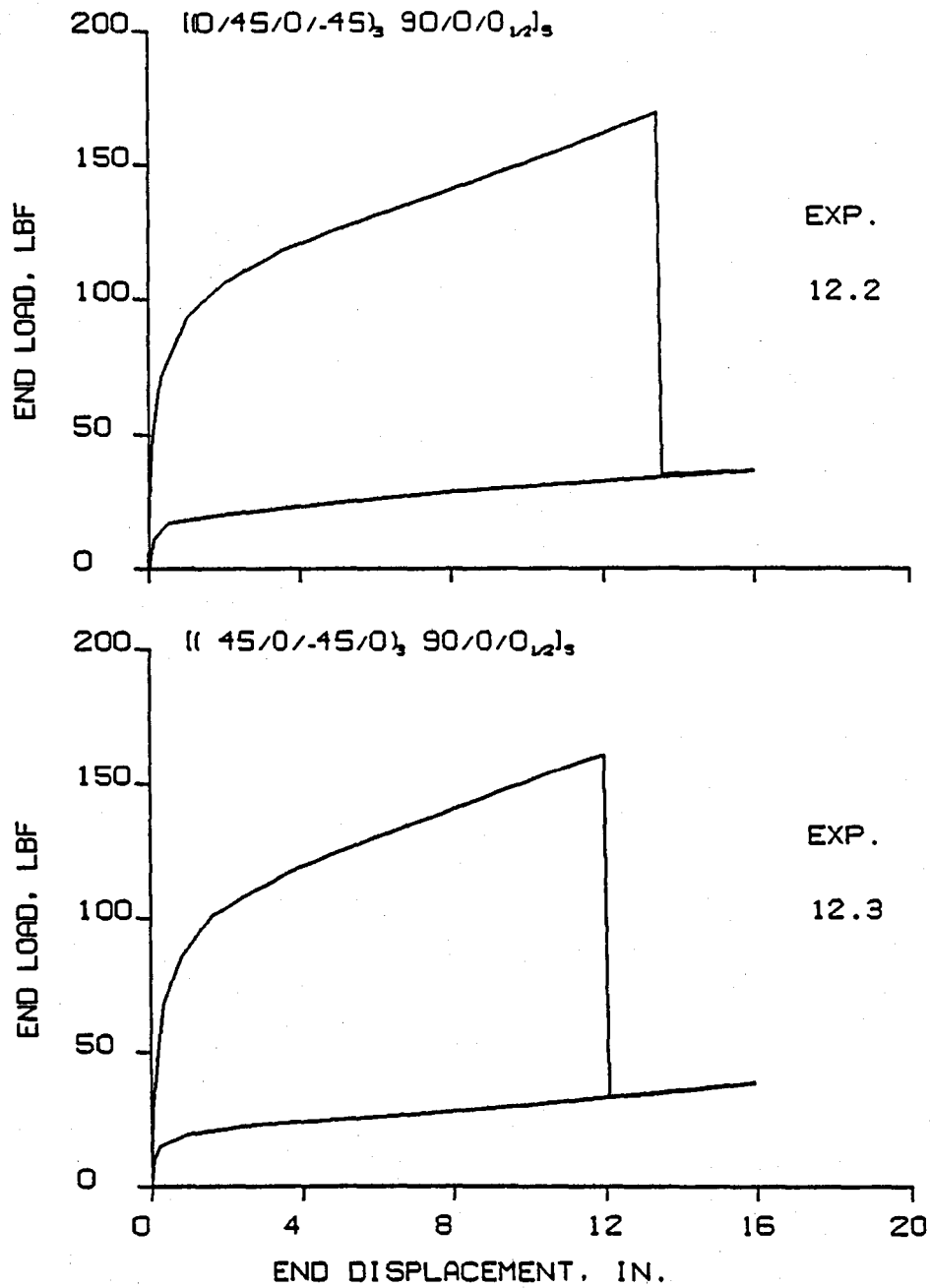
Figure 0.16   Static Load-Displacement Relation for Specimens
12.2 and 12.3

Appendix E

DYNAMIC LOAD-TIME DATA

This appendix presents the dynamic load-time relation for all the laminate types tested, with the exception of laminate type 2.
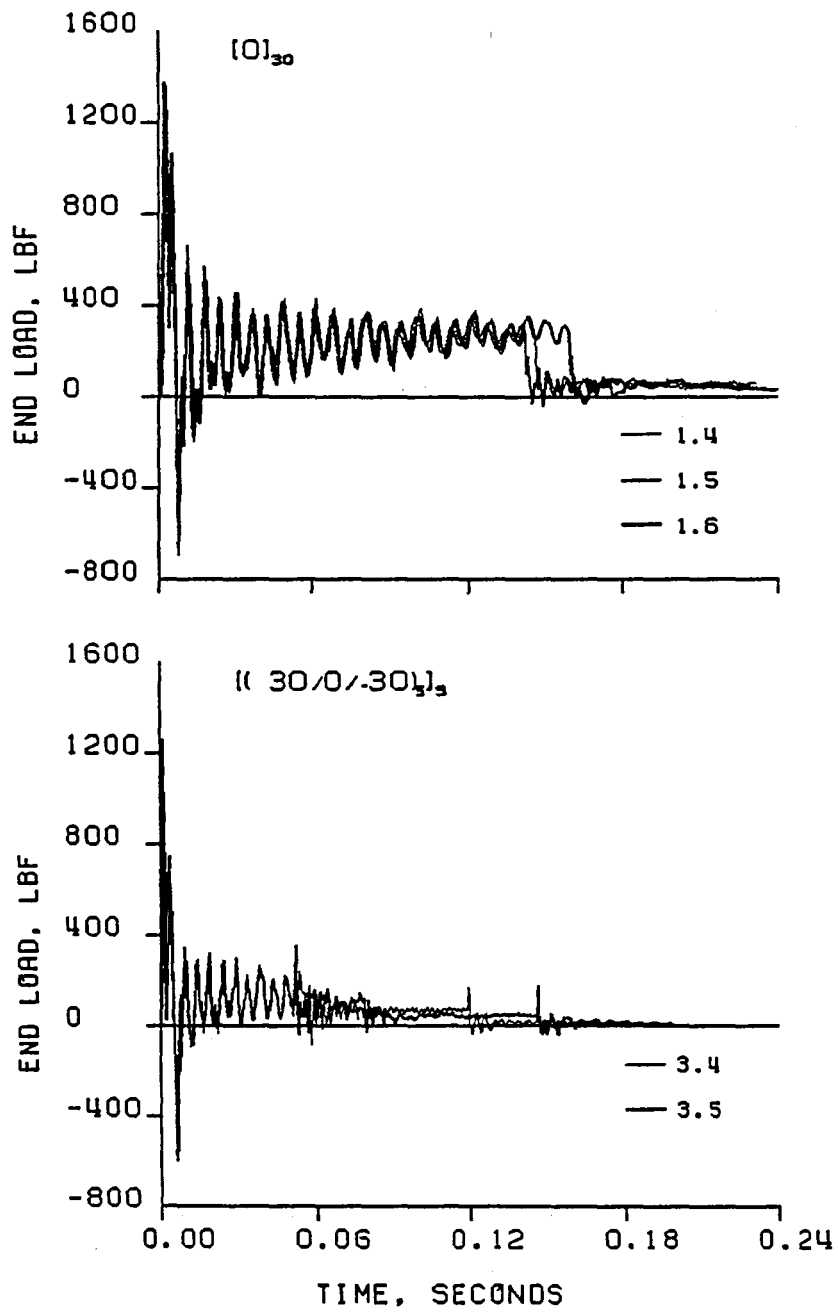
Figure E.1   Dynamic Load vs. Time for the $[0]_{30}$ and $[(30/0/-30)_5]_s$ Laminates
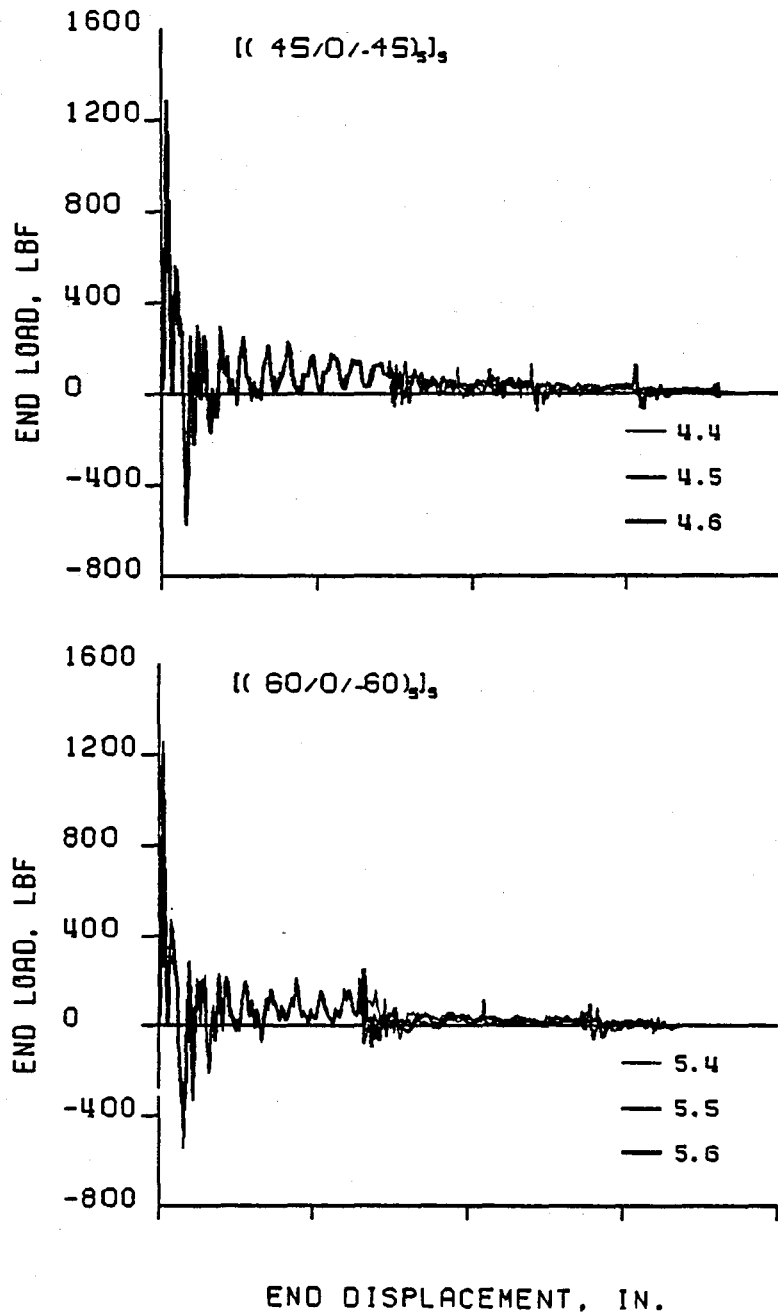
Figure E.2   Dynamic Load vs. Time for the $[(45/0/-45)_5]_s$ and $[(60/0/-60)_5]_s$ Laminates
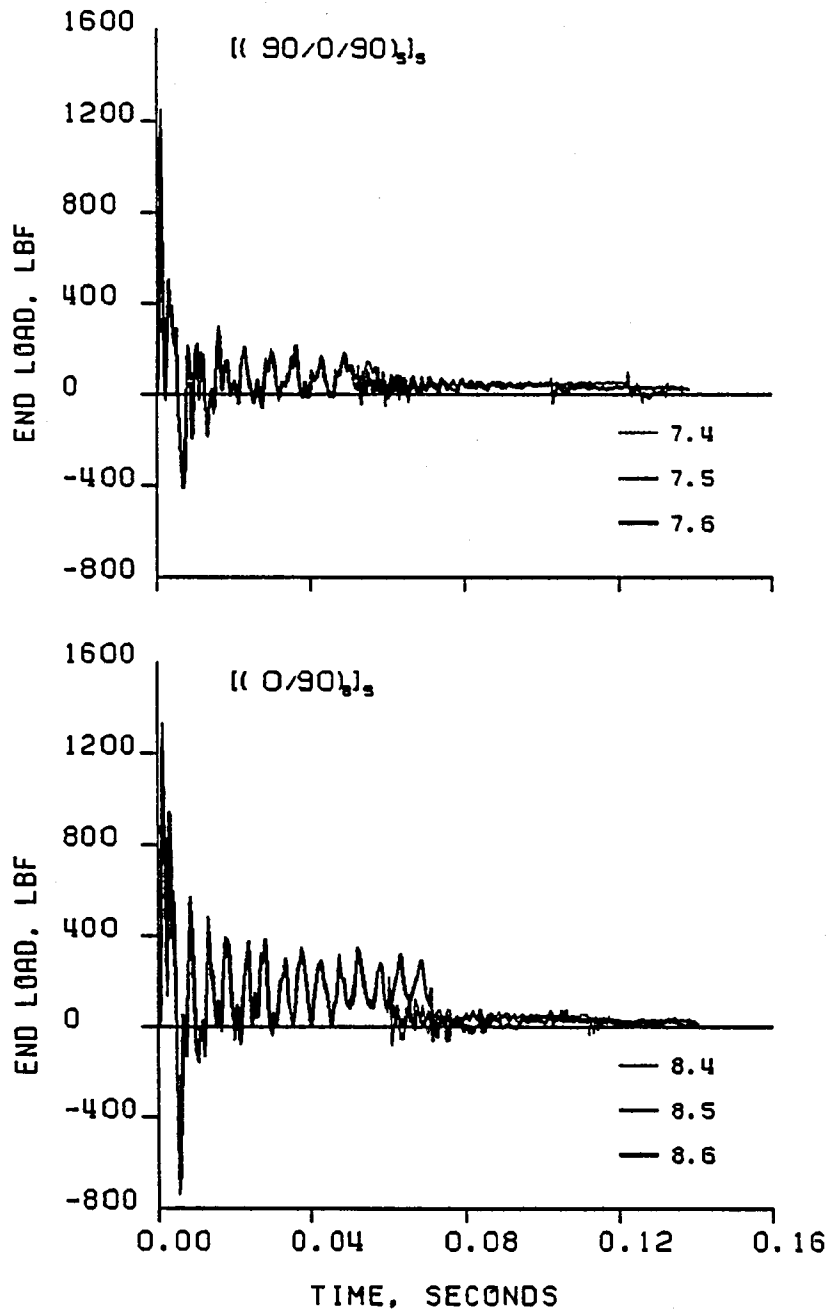
Figure E.3   Dynamic Load vs. Time for the $[(90/0/90)_5]_s$ and $[(0/90)_8]_s$ Laminates
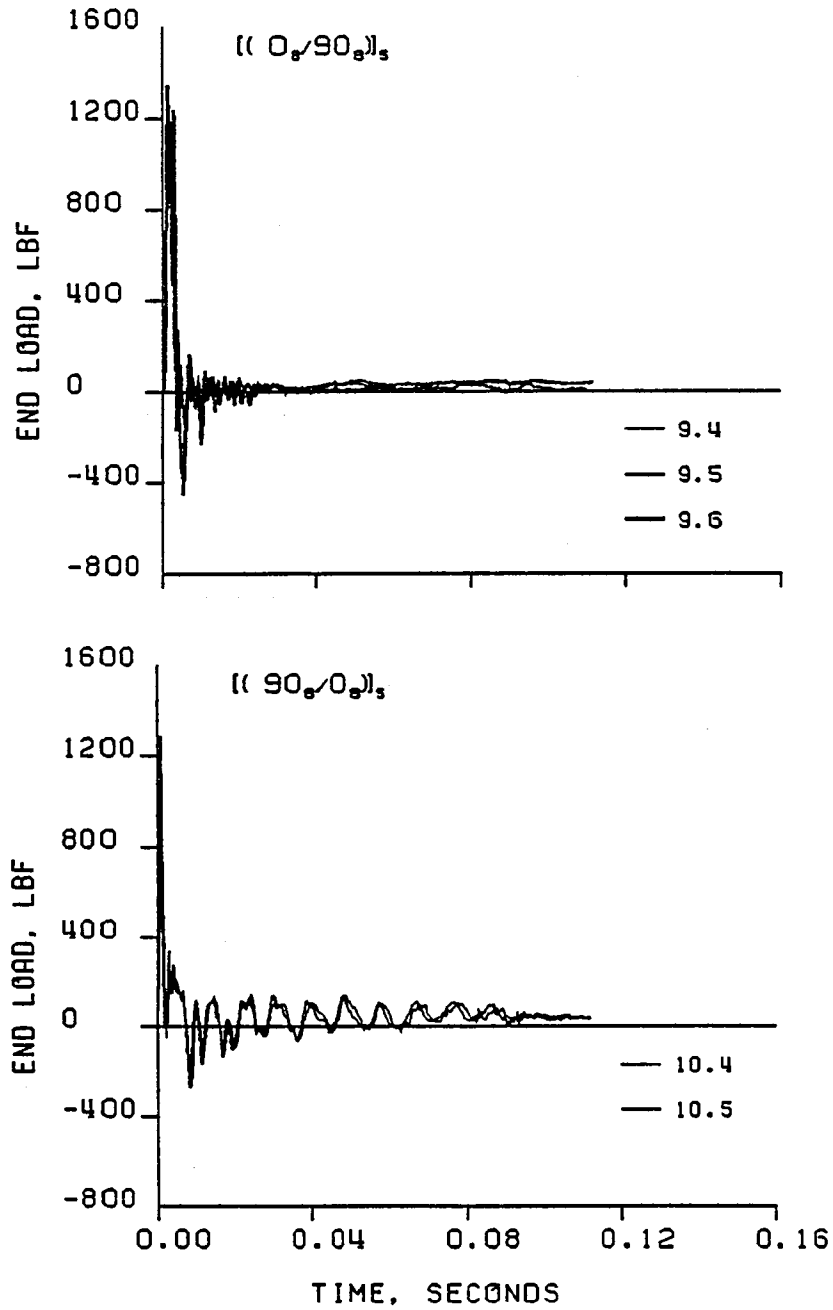
Figure E.4   Dynamic Load vs. Time for the $[(0_8/90_8)]_s$ and $[(90_8/0_80]_s$ Laminates
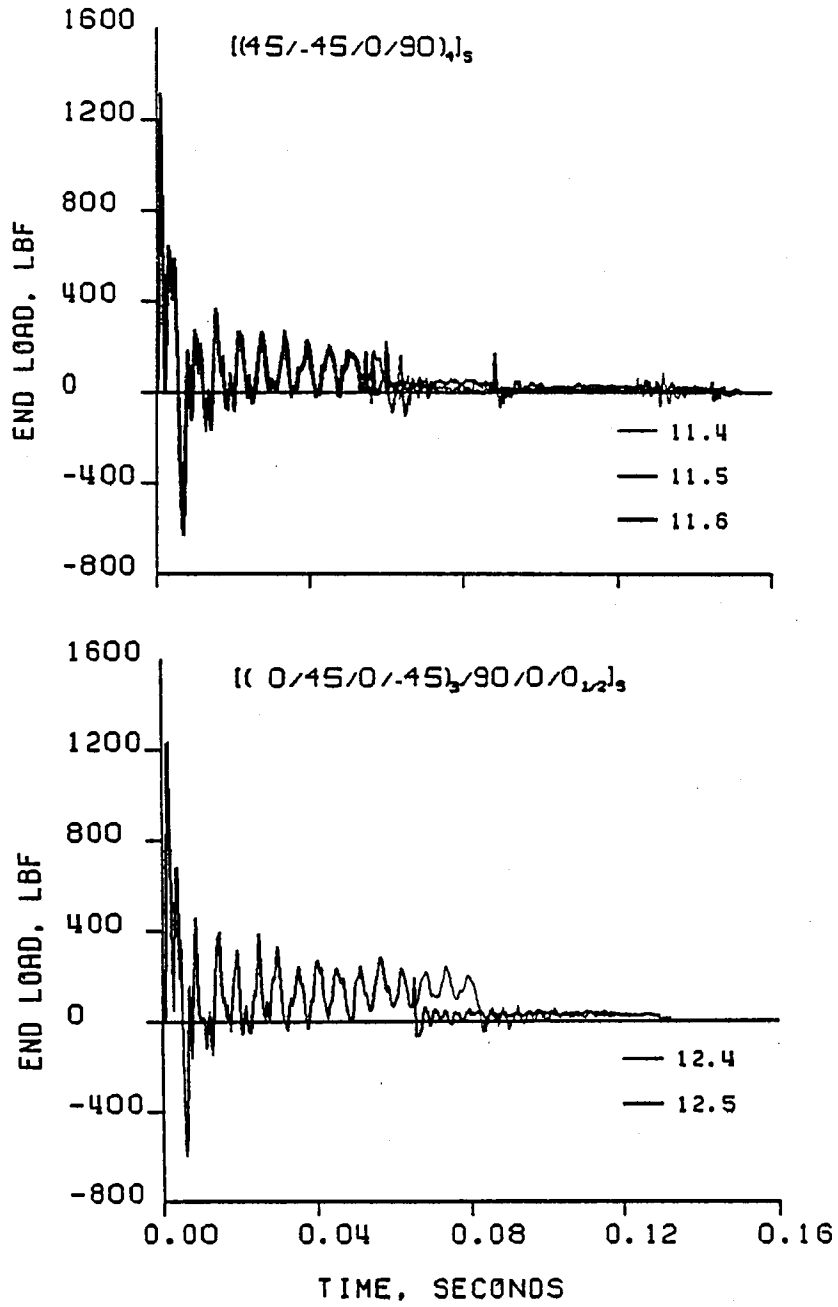
Figure E.5   Dynamic Load vs. Time for the $[(45/-45/0/90)_4]_s$ and $[(0/45/0/-45)_3 90/0/0_{1/2}]_s$ Laminates

Appendix F

ULTIMATE FAILURE STRAINS

This appendix presents the ultimate longitudinal strains for all of the static and dynamic specimens tested. The results are presented in Table F.1. The compressive side strain and the tensile side strains are recorded in the table.

TABLE F.1
FAILURE STRAINS

Laminate Number	Specimen		ε^t_{Ult}	ε^c_{Ult}
1				
	Static	1.1	.0169	0.189
		1.2	.0153	.0174
		1.3	(not strain guaged)	
	Dynamic	1.4	.0153	.0168
		1.5	.0146	.0171
		1.6	.0152	.0170
2				
	Static	2.1	.0086	.0101
		2.2	.0084	.0096
		2.3	(not strain guaged)	
	Dynamic	2.4	.0075	.0088
		2.5	.0075	.0088
		2.6	(not tested)	
3				
	Static	3.1	.0100	.0140
		3.2	.0104	.0136
		3.3	.0104	.0135
	Dynamic	3.4	.0091	.0128
		3.5	.0093	.0127
		3.6	(not tested)	
4				
	Static	4.1	.0110	.0150
		4.2	.0110	.0152
		4.3	.0112	.0155
	Dynamic	4.4	.0099	.0140
		4.5	.0100	.0140
		4.6	.0100	.0141
5				
	Static	5.1	.0122	.0146
		5.2	.0111	.0134
		5.3	.0121	.0148
	Dynamic	5.4	.0098	.0118
		5.5	.0097	.0116
		5.6	.0103	.0124

TABLE F.1 (continued)

Laminate Number	Specimen		ε^t_{Ult}	ε^c_{Ult}
7				
	Static	7.1	(instrumentation problems)	
		7.2	.0134	.0140
		7.3	(instrumentation problems)	
	Dynamic	7.4	.012	0.130
		7.5	.0125	.0135
		7.6	.012	.0135
8				
	Static	8.1	.0154	.0170
		8.2	.0156	.0174
		8.3	.0162	.0177
	Dynamic	8.4	.0141	.0156
		8.5	.0141	.0156
		8.6	.0150	.0168
9				
	Static	9.1	.0137	.0170
		9.2	.0116	.0132
		9.3	.0144	.0176
	Dynamic	9.4	(no meaningful data)	
		9.5		
		9.6		
10				
	Static	10.1	(no meaningful data)	
		10.2		
		10.3		
	Dynamic	10.4	(no meaningful data)	
		10.4		
		10.6		
11				
	Static	11.1	(instrumentation problems)	
		11.2	(instrumentation problems)	
		11.3	.0138	.0170
	Dynamic	11.4	.0120	.0150
		11.5	.0123	.0153
		11.6	.0120	.0150

TABLE F.1 (continued)

Laminate Number	Specimen		ε_{Ult}^{t}	ε_{Ult}^{c}
12				
	Static	12.1	.0127	.0160
		12.2	.0142	.0176
		12.3	.0132	.0161
	Dynamic	12.4	.0123	.0160
		12.5	.0135	.0174
		12.6	(not tested)	

Appendix G

FLEXURAL MODULI DATA

This appendix presents the data used to calculate the bending tensile and compressive moduli of the laminates. Tabulated are the axial displacement of the end of the beam, the lateral deflection of the center of the beam, the axial load, and the tensile and compressive strains. To compute the distance D used in the computation of the moduli, 0.725 in. must be subtracted from the lateral displacement. Then the distance from the compressive surface to the neutral surface must be added to this difference. (The 0.725 in. represents the offset of the vertical reference bar).

Table G.1
FLEXURAL DATA FOR LAMINATE 1

Axial Disp. (in.)	Lateral Disp. (in.)	Axial Load (lbF)	Tensile Strain (ε^t) ($\mu\varepsilon$)	Compressive Strain (ε^c) ($\mu\varepsilon$)
0.50	2.72	135	1812.	1922.
1.00	3.58	162	3000.	3225.
1.50	4.22	176	3940.	4282.
2.00	4.76	186	4750.	5200.
2.50	5.22	193	5470.	6020.
3.00	5.65	199	6140.	6780.
3.50	6.02	204	6760.	7490.
4.00	6.35	209	7350.	8170.
4.50	6.67	213	7910.	8810.
5.00	6.95	218	8440.	9430.
5.50	7.21	222	8970.	10030.
6.00	7.48	226	9470.	10610.
6.50	7.70	230	9960.	11180.
7.00	7.90	233	10440.	11740.
7.50	8.10	237	10910.	12280.
8.00	8.30	241	11370.	12820.
8.50	8.48	245	11830.	13380.
9.00	8.65	249	12270.	13940.
9.50	8.80	252	12730.	14470.
10.00	8.95	256	13170.	15000.
10.50	9.10	260	13600.	15520.
11.00	9.20	264	14030.	16040.

TABLE G.2
FLEXURAL DATA FOR LAMINATE 2

Axial Disp. (in.)	Lateral Disp. (in.)	Axial Load (lbF)	Tensile Strain (ε^t) ($\mu\varepsilon$)	Compessive Strain (ε^C) ($\mu\varepsilon$)
0.50	2.73	129	1820.	2020.
1.00	3.60	153	2940.	3350.
1.50	4.25	166	3830.	4430.
2.00	4.76	175	4580.	5350.
2.50	5.25	181	5270.	6170.
3.00	5.65	187	5900.	6920.
3.50	6.02	192	6500.	7630.

TABLE G.3
FLEXURAL DATA FOR LAMINATE 3

Axial Disp. (in.)	Lateral Disp. (in.)	Axial Load (lbF)	Tensile Strain (ε^t) ($\mu\varepsilon$)	Compressive Strain (ε^C) ($\mu\varepsilon$)
0.50	2.75	78	1710.	1980.
1.00	3.60	93	2730.	3340.
1.50	4.25	101	3530.	4460.
2.00	4.80	107	4200.	5440.
2.50	5.25	112	4790.	6320.
3.00	5.68	116	5340.	7150.
3.50	6.02	120	5860.	7900.
4.00	6.35	123	6350.	8631.
4.50	6.68	127	6830.	9320.
5.00	6.96	130	7280.	9980.
5.50	7.20	133	7730.	10620.
6.00	7.48	136	8170.	11230.
6.50	7.72	138	8600.	11830.
7.00	7.92	141	9020.	12420.
7.50	8.12	144	9450.	12990.

Table G.4
FLEXURAL DATA FOR LAMINATE 4

Axial Disp. (in.)	Lateral Disp. (in.)	Axial Load (lbF)	Tensile Strain (ε^t) ($\mu\varepsilon$)	Compressive Strain (ε^c) ($\mu\varepsilon$)
0.50	2.75	57	1850.	1950.
1.00	3.60	67	2940.	3270.
1.50	4.25	73	3790.	4360.
2.00	4.80	76	4490.	5310.
2.50	5.25	79	5100.	6200.
3.00	5.69	82	5650.	7020.
3.50	6.04	84	6160.	7780.
4.00	6.40	86	6640.	8520.
4.50	6.70	88	7090.	9230.
5.00	6.99	90	7530.	9900.
5.50	7.25	92	7940.	10560.
6.00	7.50	94	8340.	11200.
6.50	7.71	96	8730.	11830.
7.00	7.95	98	9110.	12440.
7.50	8.15	100	9480.	13050.
8.00	8.30	102	9850.	13650.
8.50	8.50	103	10200.	14250.
9.00	8.67	105	10500.	14830.

TABLE G.5
FLEXURAL DATA FOR LAMINATE 5

Axial Disp. (in.)	Lateral Disp. (in.)	Axial Load (lbF)	Tensile Strain (ε^t) ($\mu\varepsilon$)	Compressive Strain (ε^c) ($\mu\varepsilon$)
0.50	2.78	46	1760.	1830.
1.00	3.60	56	2900.	3080.
1.50	4.25	60	3800.	4120.
2.00	4.80	63	4570.	5030.
2.50	5.25	65	5250.	5850.
3.00	5.68	68	5880.	6620.
3.50	6.02	69	6470.	7350.
4.00	6.40	71	7020.	8030.
4.50	6.70	72	7530.	8700.
5.00	6.98	74	8030.	9340.
5.50	7.25	75	8510.	9960.
6.00	7.50	76	8950.	10570.
6.50	7.72	78	9400.	11120.
7.00	7.93	79	9830.	11750.
7.50	8.125	80	10250.	12330.
8.00	8.30	82	10670.	12900.

TABLE G.6
FLEXURAL DATA FOR LAMINATE 6

Axial Disp. (in.)	Lateral Disp. (in.)	Axial Load (lbF)	Tensile Strain (ε^t) ($\mu\varepsilon$)	Compressive Strain (ε^c) ($\mu\varepsilon$)
0.50	2.75	53	1770.	1930.
1.00	3.60	62	2920.	3200.
1.50	4.25	66	3830.	4220.
2.00	4.80	69	4610.	5110.
2.50	5.25	70	5310.	5900.
3.00	5.68	72	5960.	6660.
3.50	6.03	74	6540.	7340.
4.00	6.38	78	7100.	8000.
4.50	6.70	77	7640.	8640.
5.00	6.98	78	8140.	9260.
5.50	7.25	80	8710.	9880.
6.00	7.50	80	9340.	10490.
6.50	7.75	81	9820.	11060.
7.00	7.95	82	10250.	11590.
7.50	8.15	83	10670.	12140.
8.00	8.35	84	11100.	12360.

TABLE G.7
FLEXURAL DATA FOR LAMINATE 7

Axial Disp. (in.)	Lateral Disp. (in.)	Axial Load (lbF)	Tensile Strain (ϵ^t) ($\mu\epsilon$)	Compressive Strain (ϵ^c) ($\mu\epsilon$)
0.50	2.75	53	1800.	1920.
1.00	3.60	62	2930.	3110.
1.50	4.25	67	3830.	4040.
2.00	4.80	71	4610.	4840.
2.50	5.25	73	5310.	5560.
3.00	5.68	76	5960.	6220.
3.50	6.03	78	6560.	6840.
4.00	6.38	79	7130.	7440.
4.50	6.70	81	7680.	8010.
5.00	6.98	83	8190.	8560.
5.50	7.25	85	8690.	9090.
6.00	7.50	86	9180.	9610.
6.50	7.75	88	9680.	10110.
7.00	7.95	89	10130.	10610.
7.50	8.15	91	10530.	11110.
8.00	8.35	92	10970.	11580.
8.50	8.50	94	11370.	12060.
9.00	8.68	95	11830.	12550.

TABLE G.8
FLEXURAL DATA FOR LAMINATE 11

Axial Disp. (in.)	Lateral Disp. (in.)	Axial Load (lbF)	Tensile Strain (ε^t) ($\mu\varepsilon$)	Compressive Strain (ε^c) ($\mu\varepsilon$)
0.50	2.72	72	2080.	2140.
1.00	3.55	83	3320.	3480.
1.50	4.22	88	4310.	4580.
2.00	4.78	92	5150.	5550.
2.50	5.20	95	5890.	6430.
3.00	5.65	98	6560.	7250.
3.50	6.01	100	7180.	8020.
4.00	6.35	102	7760.	8750.
4.50	6.70	104	8310.	9460.
5.00	6.98	106	8830.	10140.
5.50	7.25	107	9330.	10810.
6.00	7.50	109	9810.	11450.
6.50	7.72	111	10290.	12100.
7.00	7.95	112	10730.	12700.
7.50	8.14	114	11170.	13310.
8.00	8.31	116	11590.	13920.
8.50	8.50	118	12020.	14520.
9.00	8.66	119	12450.	15110.

Appendix H

EFFECT OF TRACKING THE LOCATION OF THE NEUTRAL SURFACE
ON THE LOAD-DISPLACEMENT RESPONSE

As described in ch. 4, the laminates exhibited bimodular properties. With different tensile and compressive flexural moduli, the neutral surface of the beam was no longer coincident with the midplane. For the analysis performed in ch. 6, the neutral surface and the midplane were assumed to be coincident. The effect of that assumption on the static load-displacement response is examined here.

To examine this effect, laminates 1 and 3 were studied. Laminate 3 showed the greatest bimodularity. The compressive flexural modulus was 50% less than the tensile flexural modulus, and hence, this laminate should show the largest effect of the shifting of the neutral surface. Laminate 1 showed a more moderate bimodularity with the compressive moduli being 23% less than the tensile moduli. Figures H.1 and H.2 show the load-displacement relation for laminates 3 and 1, respectively. In the upper curve the analysis assumes the neutral surface to be at the midplane. In the lower curve the analysis tracks the location of the neutral surface. For laminate 3 the error is significant. At 150 lb of force, there is a difference of 2 in. in the predicted axial deflection. This is a 25% error. For laminate 1 the error is much less. At 300 lb of force, there is a difference of 0.25 in. in the predicted axial deflection. This is an error of only 2%.
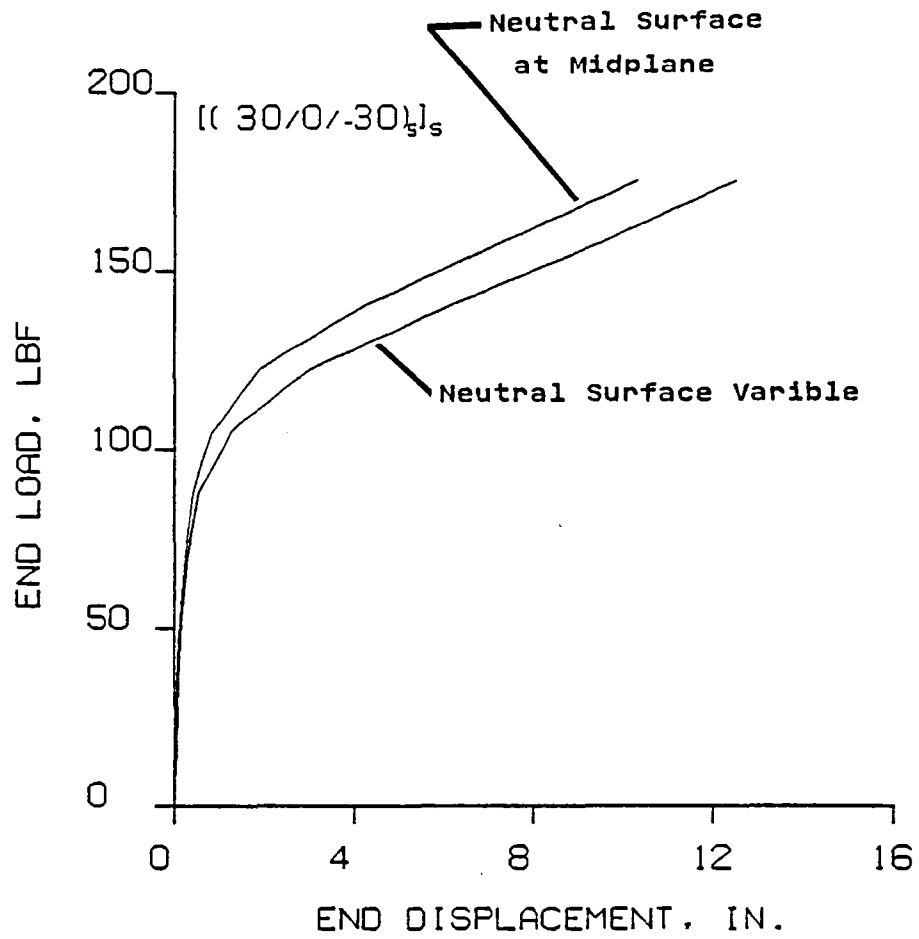
Figure H.1   Effect of Shift in Neutral Surface on the Load-
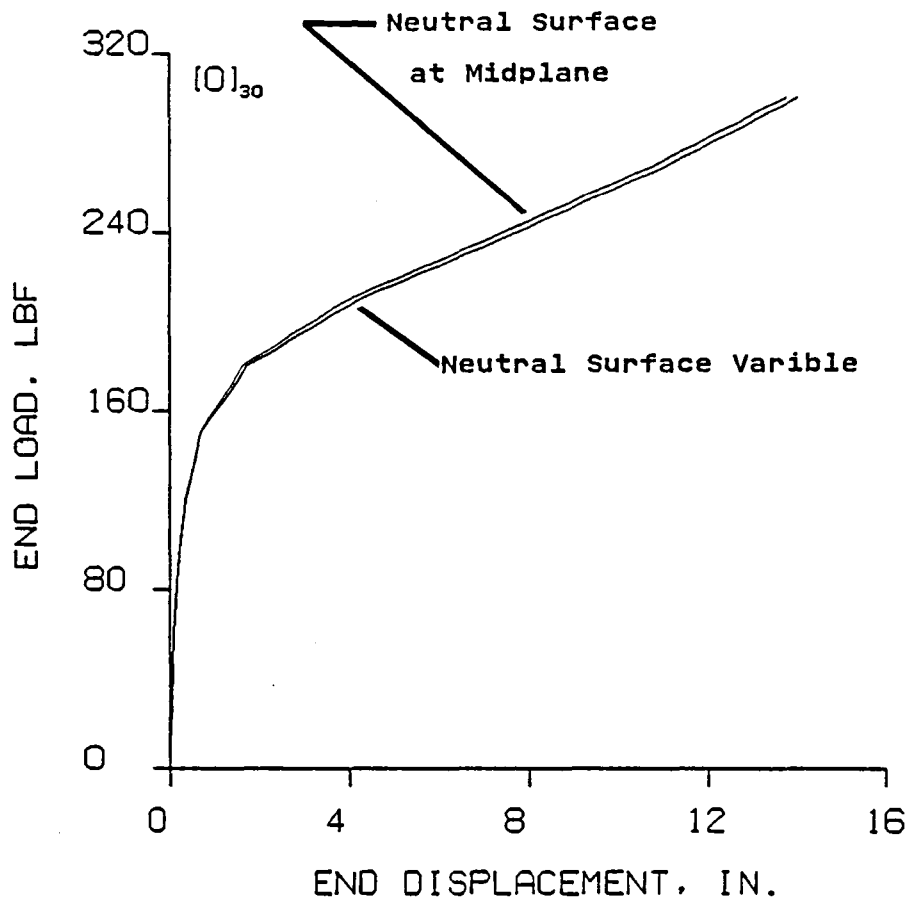Displacement Relation for the [(30/0/-30)$_5$]$_s$ Laminate

Figure H.2   Effect of Shift in Neutral Surface on the Load-
              Displacement Relation for the $[0]_{30}$ Laminate

Appendix I

EFFECT OF UNCERTAINTY IN THE MODULI ON THE
LOAD-DISPLACEMENT RELATION

As mentioned in ch. 5 the uncertainty in the empirical moduli calculations was about ±1 MSI. This is one factor which could account for the deviation between the analytical results and the experimental data. To examine the effect of the uncertainty in the moduli on the load-displacement relation, the finite element analysis was employed.

Figure I.1 shows the load-displacement relation for 3 unidirectional beams. The center curve has the flexural properties taken from Table 6.1. The other two curves represent the range of the uncertainty in the flexural properties. Uncertainty in the modulus of ±1 MSI results in a uncertainty in the displacement of ±1.65 in., at the 12 in. displacement level. This represents a 13% deviation in the predicted response.
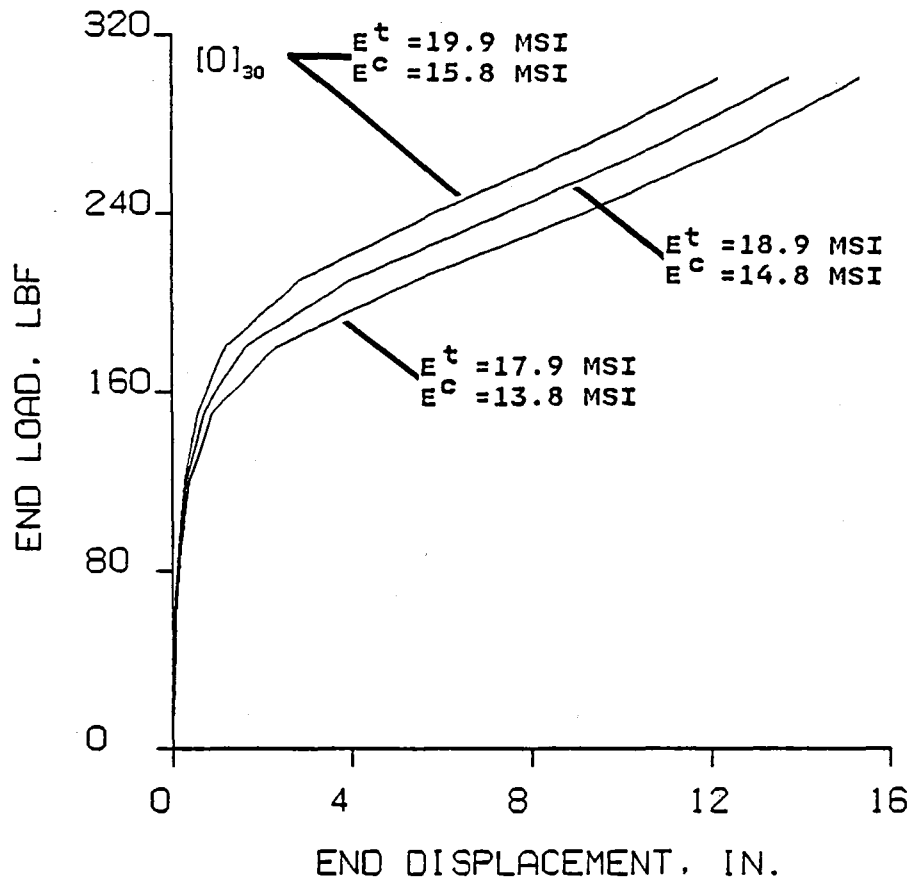
Figure I.1   Effect on the Uncertainty in the Moduli on the Load-
Displacement Relation

1. Report No. NASA CR-4006	2. Government Accession No.	3. Recipient's Catalog No.
4. Title and Subtitle Large Deformation Dynamic Bending of Composite Beams		5. Report Date August 1986
		6. Performing Organization Code
7. Author(s) E. J. Derian and M. W. Hyer		8. Performing Organization Report No.
		10. Work Unit No.
9. Performing Organization Name and Address Department of Engineering Science and Mechanics Virginia Polytechnic Institute and State University Blacksburg, VA 24061		11. Contract or Grant No. NAG1-343
		13. Type of Report and Period Covered Contractor Report Interim 9/83-4/86
12. Sponsoring Agency Name and Address National Aeronautics and Space Administration Washington, DC 20546		14. Sponsoring Agency Code 505-63-41-01

15. Supplementary Notes

16. Abstract

Studies were conducted on the large deformation response of composite beams subjected to a dynamic axial load. The beams were loaded with a moderate eccentricity to promote bending. The study was primarily experimental but some finite element results were obtained. Both the deformation and the failure of the beams were of interest. The static response of the beams was also studied to determine potential differences between the static and dynamic failure. Twelve different laminate types were tested. The beams tested were 23 in. by 2 in. and generally 30 plies thick. The beams were loaded dynamically with a gravity-driven impactor traveling at 19.6 ft/sec and quasi-static tests were conducted on identical beams in a displacement controlled manner. For laminates of practical interest, the failure modes under static and dynamic loadings were identical. Failure in most of the laminate types occurred in a single event involving 40% to 50% of the plies. However, failure in laminates with 30° or 15° off-axis plies occurred in several events. All laminates exhibited bimodular elastic properties. The compressive flexural moduli in some laminates was measured to be 1/2 the tensile flexural modulus. No simple relationship could be found among the measured ultimate failure strains of the different laminate types. Using empirically determined flexural properties, a finite element analysis was reasonably accurate in predicting the static and dynamic deformation response.

17. Key Words (Suggested by Author(s)) Composite materials Dynamic response Failure of composites Bimodular behavior	18. Distribution Statement Unclassified - Unlimited Subject Category 39

19. Security Classif. (of this report) Unclassified	20. Security Classif. (of this page) Unclassified	21. No. of Pages 220	22. Price A10

End of Document